CLINICAL PHARMACOKINETICS AND PHARMACOCYNAMICS OF ANTICANCER AGENTS DELIVERED VIA PEGYLATED LIPOSOMES

Huali Wu

A dissertation submitted to the faculty of the University of North Carolina at Chapel Hill in partial fulfillment of the requirements for the degree of Doctor of Philosophy in the School of Pharmacy.

Chapel Hill
2010

Approved by

Advisor: William C. Zamboni, Pharm.D., Ph.D.

Chairman: Howard McLeod, Pharm.D.

Reader: Marie Davidian, Ph.D.

Reader: Craig R. Lee, Pharm.D., Ph.D.

Reader: Christine M. Walko, Pharm.D.

.

ABSTRACT

HUALI WU: Clinical Pharmacology of Anticancer Agents Delivered via PEGylated Liposomes
(Under the direction of William C. Zamboni, Pharm.D., Ph.D.)

PEGylated liposome is one of the most useful nanocarriers for cancer therapy. Studies described in this dissertation provide new knowledge about (1) the nature of nonlinear PK of PEGylated liposomal anticancer agents, (2) the role of the bi-directional interaction between PEGylated liposomes and the monocytes/macrophages in the PK/PD of these agents, and (3) patient factors that significantly influence the PK/PD of PEGylated liposomal anticancer agents.

The PK disposition of encapsulated CPT-11, released CPT-11, and SN-38 after IHL-305 (PEGylated liposomal CPT-11) in cancer patients was evaluated using noncompartmental, individual-based compartmental and population PK analysis. The PK of IHL-305 was characterized by a prolonged circulation time, a reduced volume of distribution and saturable clearance. The high inter-patient variability in the PK and PD of IHL-305 was associated with age, body composition, gender, and monocyte function.

The PK disposition of S-CKD602 (PEGylated liposomal CKD-602) was evaluated using population PK analysis. PK of encapsulated CKD-602 was described by 1-compartment model with nonlinear clearance and PK of released CKD-602 was described by a 2-compartment model with linear clearance for all patients. The release rate of CKD-602

from S-CKD602 was influenced by age and clearance of encapsulated CKD-602 was influenced by presence of tumors in liver.

A mechanism-based PK-PD model was also developed that described the relationship between PEGylated liposomal anticancer drug and monocyte in cancer patients treated with S-CKD602 and IHL-305. In this model, an irreversible uptake of liposomal drug to monocyte was used account for the bi-directional interaction between PEGylated liposomal anticancer drug and monocyte. The degradation of liposomes through routes other than uptake by monocytes was included. The estimated half-life and baseline value of monocytes were close to the published data. The mechanism-based PK-PD model was compared with a published PK-PD model used for neutropenia and leukocytopenia. Both of these two models adequately described the PK and PD of S-CKD602 and IHL-305.

Overall, this work helped to explain the nonlinear PK and high interpatient variability in PK of PEGylated liposomal anticancer agents and defined the role of the bi-directional interaction between PEGylated liposomes and the monocytes in the PK/PD of these agents.

ACKNOWLEDGEMENTS

I would like to express my great appreciation to my advisor, Dr. William C. Zamboni, for his guidance, scientific training, and mentorship during the course of my graduate education.

I am deeply indebted to all my committee members, Drs. Howard McLeod, Marie Davidian, Craig Lee and Christine Walko for their valuable guidance and suggestions.

I would also like to express my deepest appreciation to my husband, Xin Ming, and daughters, May and Joycelyn, for their continued support, love, and for all the good and bad times we've been through.

I am especially grateful to my parents, Wenbin Wu and Shufen Gao, and parents in law, Chengzhong Ming and Yuanli Deng, for providing me with the encouragement and support to pursue higher education.

TABLE OF CONTENTS

Page

LIST OF TABLES x

LIST OF FIGURES xii

LIST OF ABBREVIATIONS xv

Chapter

1. INTRODUCTION 1

A. Introduction 2

B. Classification of Liposome Formulations 3

C. PK Characteristics of Liposomal Agents 3

C.1. Distribution 3

C.2. Elimination 4

C.3. Release of Drug from Liposome 5

C.4. PK Nomenclature 6

D. Factors Affecting PK of Liposomal Agents 6

D.1. Liposome Associated Factors 6

D.2. Host Associated Factors 12

D.3. Effect of Dose Schedule 16

D.4. Drug-drug Interaction 17

E. Factors Affecting PD of Liposomal Agents 17

E.1. Efficacy 17

E.2. Toxicity 18

F. Conclusion 21

G. Rationale and Overview of Proposed Research 23

H. References 27

2. PHARMACOKINETIC (PK) STUDY OF PEGYLATED LIPOSOMAL IRINOTECAN (IHL-305) IN PATIENTS WITH ADVANCED SOLID TUMORS 47

A. Introduction 48

B. Patients and Methods 51

C. Results 55

D. Discussion 58

E. References 61

3. FACTORS AFFECTING THE PHARMACOKINETICS (PK) AND PHARMACODYNAMICS (PD) OF PEGYLATED LIPOSOMAL IRINOTECAN (IHL-305) IN PATIENTS WITH ADVANCED SOLID TUMORS 74

A. Introduction 75

B. Patients and Methods 78

C. Results 83

D. Discussion 87

E. References 90

4. POPULATION PHARMACOKINETICS OF PEGYLATED LIPOSOMAL CKD-602 (S-CKD602) IN PATIENTS WITH ADVANCED MALIGNANCIES 102

A. Introduction 103

B. Patients and Methods 106

C. Results 115

D. Discussion 119

E. References 122

5. POPULATION PHARMACOKINETICS OF PEGYLATED LIPOSOMAL CPT-11 (IHL-305) IN PATIENTS WITH ADVANCED SOLID TUMORS 138

A. Introduction 139

B. Patients and Methods 143

C. Results 151

D. Discussion 154

E. References 157

6. MECHANISM-BASED PHARMACOKINETIC-PHARMACODYNAMIC MODEL CHARACTERIZING BI-DIRECTIONAL INTERACTION BETWEEN PEGYLATED LIPOSOMAL CKD-602 (S-CKD602) AND MONOCYTES IN PATIENTS WITH ADVANCED MALIGNANCIES 167

A. Introduction 168

B. Patients and Methods 173

C. Results 179

D. Discussion 182

E. References 188

7. MECHANISM-BASED PHARMACOKINETIC-PHARMACODYNAMIC MODEL CHARACTERIZING BI-DIRECTIONAL INTERACTION BETWEEN PEGYLATED LIPOSOMAL CPT-11 (IHL-305) AND MONOCYTES IN PATIENTS WITH ADVANCED MALIGNANCIES 201

A. Introduction 202

B. Patients and Methods 207

C. Results 213

D. Discussion 216

E. References 222

8. MECHANISM-BASED PHARMACOKINETIC-PHARMACODYNAMIC MODEL CHARACTERIZING BI-DIRECTIONAL INTERACTION BETWEEN LIPIDS AND MONOCYTES IN PATIENTS WITH ADVANCED MALIGNANCIES .. 235

A. Introduction 236

B. Patients and Methods 239

C. Results 244

D. Discussion 246

E. References 248

9. CONCLUSIONS 255

LIST OF TABLES

Table 1.1 Selected Liposomal Drugs Approved for Clinical Application or Undergoing Clinical Evaluation..... 38

Table 1.2 Selected Liposomal Drugs with Conjugated Ligands to Achieve Active Targeting..... 39

Table 2.1 The Total Form of Sum Total CPT-11, Released CPT-11, SN-38, SN-38G, and APC Area Under the Concentration Verses Time Curves (AUC) after Administration of IHL-305 at Each Dose..... 64

Table 2.2 The Ratio of Released CPT-11 AUC to Sum Total CPT-11 AUC, SN-38 AUC to Released CPT-11 AUC, SN-38G AUC to SN-38 AUC, and APC AUC to Released CPT-11 AUC after Administration of IHL-305 at Each Dose..... 66

Table 2.3 The Nadir and Percentage Decrease at Nadir in ANC, Platelets, RBC, and Monocytes on Cycles 1, 2, 3, and 4..... 68

Table 3.1 Compartmental Pharmacokinetic Parameters of Sum Total CPT-11 after IHL-305 in Patients with Linear and Non-Linear Disposition..... 93

Table 3.2 Summary of ANC and Monocytes Parameters After Administration of IHL-305 95

Table 4.1 A Summary of Patient Demographics and Covariates Included in The Analysis 126

Table 4.2 Population Pharmacokinetic Parameters Obtained from the Final Covariate Model for Encapsulated CKD-602 127

Table 4.3 Population Pharmacokinetic Parameters Obtained from the Final Model for CKD-602 after Administration of Non-liposomal CKD-602..... 128

Table 4.4 Population Pharmacokinetic Parameters Obtained From the Final Covariate Model for Encapsulated and Released CKD-602 in Patients with Linear Clearance of Encapsulated CKD-602 129

Table 4.5 Population Pharmacokinetic Parameters Obtained From the Final Model for Encapsulated and Released CKD-602 in Patients with Nonlinear Clearance of Encapsulated CKD-602 130

Table 5.1 A Summary of Patient Demographics and Covariates Included in The Analysis 161

Table 5.2 Population PK Parameters Obtained from the Final Covariate Model for Encapsulated CPT-11, Released CPT-11 and SN-38 162

Table 6.1 A Summary of Patient Demographics. 193

Table 6.2 Population PK-PD Parameters Obtained From the Myelosuppression-Based Model for Encapsulated CKD-602 and Monocytes. 194

Table 6.3 Population PK-PD Parameters Obtained From the Mechanism-Based Model for Encapsulated CKD-602 and Monocytes 195

Table 7.1 A Summary of Patient Demographics. 227

Table 7.2 Population PK-PD Parameters Obtained From the Myelosuppression-Based Model for Encapsulated CPT-11 and Monocytes. 228

Table 7.3 Population PK-PD Parameters Obtained From the Mechanism-Based Model for Encapsulated CPT-11 and Monocytes 229

Table 8.1 Population PK-PD Parameters Obtained From the Myelosuppression-Based Model for Lipids and Monocytes. 250

LIST OF FIGURES

Figure 1.1 Clearance of Stabilized and Non-Stabilized Liposomes 40

Figure 1.2 Scheme of PEGylated Liposomes 41

Figure 1.3 The Relationship Between Age and Encapsulated CKD-602 AUC/dose After S-CKD602..... 42

Figure 1.4 Relationship Between the Ratio of Total Body Weight to Ideal Body Weight (TBW/IBW) and S-CKD602 Encapsulated AUC/dose 45

Figure 1.5 The Clearance of Sum Total (Encapsulated + Released) PEGylated Liposomal Doxorubicin (Doxil® Within Patients on Cycles 1, 2, and 3 46

Figure 2.1 Concentrations Versus Time Profiles of Sum Total CPT-11, Released CPT-11 and SN-38 in All Patients Treated with IHL-305 at The Maximum Tolerated Dose 69

Figure 2.2 Relationship Between Dose of IHL-305 and AUC of Sum Total CPT-11, Released CPT-11, SN-38, SN-38G, and APC. 71

Figure 3.1 Relationship Between The Ratio of Total Body Weight to Ideal Body Weight (TBW/IBW) and Dose Normalized IHL-305 Sum Total AUC. 96

Figure 3.2 Relationship Between Two factors, Age and The Ratio of Total Body Weight to Ideal Body Weight (TBW/IBW), and Ratio of Released CPT-11 AUC to Sum Total CPT-11 AUC..... 97

Figure 3.3 Relationship between % decrease in monocytes and dose normalized CPT-11 AUC. 98

Figure 3.4 The relationship between % decrease in monocytes and age in all patients with dose $\geq$ 50 mg/m^2. 99

Figure 3.5 The clearance of total IHL-305 and dose normalized sum total CPT-11 AUC (AUC/Dose) in male and female patients. 100

Figure 4.1 The Final Structural Pharmacokinetic Model for Encapsulated Alone in All Patients (A), Encapsulated and Released CKD-602 in Patients With Linear Clearance of Encapsulated CKD-602 (B), and Encapsulated and Released CKD-602 in Patients With Nonlinear Clearance of Encapsulated CKD-602 (C). 131

Figure 4.2 Representative Individual Plots of Observed, Population Predicted, and Individual Predicted Values of Plasma Concentrations of Encapsulated CKD-602. 132

Figure 4.3 Goodness-of-fit Plots for The Final Model of Encapsulated CKD-602 133

Figure 4.4 Goodness-of-fit Plots for The Final Model of CKD-602 After Administration of Non-liposomal CKD-602. 134

Figure 4.5 Representative Individual Plots of Observed, Population Predicted, and Individual Predicted Values of Plasma Concentrations of Encapsulated and Released CKD-602 in Patients with Linear Clearance of Encapsulated CKD-602 (a) and in Patients with Nonlinear Clearance of Encapsulated CKD-602 (b). 135

Figure 4.6 Observed Versus Population Model-Predicted Encapsulated and Released Plasma Concentrations for The Final Models in Patients with Linear Clearance of Encapsulated CKD-602 (a) and in Patients with Nonlinear Clearance of Encapsulated CKD-602 (b) 136

Figure 5.1 The Final Structural PK model for Encapsulated CPT-11, Released CPT-11 and SN-38. 164

Figure 5.2 Goodness-of-fit Plots for The Final Model of Encapsulated CPT-11, Released CPT-11, and SN-38. 165

Figure 5.3 Representative Individual Plots of Observed and Individual Predicted Values of Plasma Concentrations of Encapsulated CPT-11, Released CPT-11, and SN-38 in Patients 166

Figure 6.1 The Myelosuppression-Based PK-PD Model for (A) and The Mechanism -Based PK-PD Model (B) for Encapsulated CKD-602 and Monocytes 196

Figure 6.2 Goodness-of-fit Plots for The Myelosuppression-Based Model of Encapsulated CKD-602 and Monocytes. 197

Figure 6.3 Representative Individual Plots of Observed and Individual Predicted Values from Myelosuppression-Based Model for The Plasma Concentrations of Encapsulated CKD-602 and Monocyte Count 198

Figure 6.4 Goodness-of-fit Plots for The Mechanism-Based Model of Encapsulated CKD-602 and Monocytes. 199

Figure 6.5 Representative Individual Plots of Observed and Individual Predicted Values from Mechanism-Based Model for The Plasma Concentrations of Encapsulated CKD-602 and Monocyte Count 200

Figure 7.1 The Myelosuppression-Based PK-PD Model for (A) and The Mechanism -Based PK-PD Model (B) for Encapsulated CPT-11 and Monocytes 230

Figure 7.2 Goodness-of-fit Plots for The Myelosuppression-Based Model of Encapsulated CPT-11 and Monocytes. 231

Figure 7.3 Representative Individual Plots of Observed and Individual Predicted Values from Myelosuppression-Based Model for The Plasma Concentrations of Encapsulated CPT-11 and Monocyte Count 232

Figure 7.4 Goodness-of-fit Plots for The Mechanism-Based Model of Encapsulated CPT-11 and Monocytes. 233

Figure 7.5 Representative Individual Plots of Observed and Individual Predicted Values from Mechanism-Based Model for The Plasma Concentrations of Encapsulated CPT-11 and Monocyte Count 234

Figure 8.1 The Mechanism-Based PK-PD Model for Liposome Membrane Lipids and Monocytes 251

Figure 8.2 Goodness-of-fit Plots for The Mechanism-Based Model of Liposome Membrane Lipids and Monocytes. 252

Figure 8.3 Representative Individual Plots of Observed and Individual Predicted Values from Mechanism-Based Model for The Plasma Concentrations of Liposome Membrane Lipids and Monocyte Count in All Patients After Administration of S-CKD602 (A) and IHL-305 (B) 254

LIST OF ABBREVIATIONS

AIC	Akaike's information criterion
ANC	Absolute neutrophil count
AUC	Area under the curve
DLT	Dose-limiting toxicities
FOCE	First order conditional estimation
HPLC	High Pressure Liquid Chromatography
IIV	Interindividual variability
K_m	Michaelis-Menten Constant
MTD	Maximum tolerated dose
OFV	Objective function value
PD	Pharmacodynamics
PEG	Polyethylene Glycol
PK	Pharmacokinetics
PLD	PEGylated liposomal doxorubicine
MPS	Mononuclear phagocytic system
RBC	Red blood cells
RES	Reticuloendothelial system
V_{max}	Maximum velocity

CHAPTER 1

INTRODUCTION

A. INTRODUCTION

Liposomal drug delivery systems have been studied extensively to increase the solubility and therapeutic index of chemotherapeutic agents (1). A variety of agents such as conventional drugs, proteins, genes and oligonucleotides can be delivered via liposomes because of their attractive biological properties including biocompatibility, improved solubility of hydrophobic compounds, increased stability of large molecules, improved efficacy and reduced toxicity. Current applications of the liposomes are in the immunology, dermatology, vaccine adjuvant, eye disorders, brain targeting, infective disease and in tumour therapy (2) (**Table 1.1**).

A liposome is an artificial microscopic vesicle consisting of an aqueous core surrounded by one or more phospholipid layers. Drugs with widely varying lipophilicities can be encapsulated in liposomes, either in the phospholipid bilayer, in the entrapped aqueous volume or at the bilayer interface (3). As drugs are encapsulated in liposome, the pharmacokinetic (PK) disposition of the liposomal drugs is dependent upon the liposome and not the parent-drug until the drug is released from the carrier (4). The drug that remains encapsulated in liposomes is an inactive-prodrug and thus the drug must be released from the carrier to be active (5, 6). The PK disposition of liposome and the encapsulated drug are often different. Therefore, it is very important to understand the PK of liposomes to predict the efficacy and toxicity of liposomal drugs.

In this introduction, we will briefly describe the characteristics of liposome formulations and discuss the effect of various factors including liposome associated factors, host associated factors and dose schedules on the PK and pharmacodynamics (PD) of liposomal agents.

B. Classification of Liposome formulations

Liposomes are micro-particulates or colloidal carriers, usually 0.05 to 5.0 μm in diameter which form spontaneously when certain lipids are hydrated in aqueous media (3). Vesicle formulations are usually based on natural and synthetic phospholipids and cholesterol. There are a number of different types of liposomes. Liposomes can be classified according to different aspects, such as physiocochemical properties, surface modification, method of preparation and application. From the point of PK, liposomes can be classified as mononuclear phagocytic system (MPS) or reticuloendothelial system (RES) targeting liposomes and MPS or RES avoiding liposomes, which have significantly different PK properties. The physicochemical properties of liposomes such as lipid composition, structure (lamellarity), size, stability and surface characteristics, membrane fluidity can affect liposome behavior in biological systems and influence the biodistribution, efficacy and safety of liposome loaded with therapeutic agents (3).

C. PK Characteristics of Liposomal Drugs

Depending on the specific application, liposomal drugs can be administered in a number of different routes including intravenous, intraperitoneal, subcutaneous, intramuscular, oral, inhalational and topical (ocular). Intravenous injection is the most commonly-used administration route for liposomal drugs.

C.1 Distribution.

Following administration, unlike small molecule drugs, the distribution of liposomes is greatly limited because they are larger than the holes or gaps of the endothelial walls of

most normal tissues. Tissues surrounded by endothelial wall with larger holes or gaps such as liver, spleen, and bone marrow usually are the major deposition sites of liposomes (7, 8). The enhanced uptake in the liver, spleen, and bone marrow is largely attributed to the macrophages residing in the tissues, which are responsible for clearing particulates and macromolecules circulating in the blood (9). The abnormal and leaky vasculature of tumor results in enhanced permeability of liposomal drugs in tumors. Moreover, tumor tissues usually lack effective lymphatic drainage. Therefore, liposomes, other nanoparticles, or macromolecules can be drained through the leaky blood vessels and be retained which results in an increased accumulation of liposomal anticancer agents in tumors. This phenomenon was called the enhanced permeation and retention (EPR) effect (10, 11).

C.2 Elimination.

Unlike small molecular drugs which are cleared by enzymes and secretion in the liver and filtration and secretion in the kidneys, the clearance of liposomes is via the MPS or RES which includes monocytes, macrophages and dendritic cells located primarily in the liver and spleen (12) (**Figure 1.1**). Uptake by the MPS usually results in irreversible sequestering of the encapsulated drug in the MPS, where it can be degraded. Moreover, the capture of the liposomes by the MPS can result in acute impairment of the mononuclear phagocyte system and toxicity. There are two sides to the interaction between liposomes and macrophages in MPS. This is beneficial for the treatment of macrophage-associated diseases such as infectious disease, autoimmune disease, transplantation, neurological disorders, gene therapy and cancer. However, this is an unfavorable for the treatment of disease not involving the MPS and the target site is outside of liver, spleen, and bone marrow such as cancer. MPS

avoiding liposomes were developed to treat the diseases not involving the MPS. These liposomes can evade the immune system and prolong the duration of exposure (**Figure 1.1**)

C.3 Release of Drug from Liposomes.

There are two potential mechanisms of release of drug from liposomes. The encapsulated drug can diffuse out of the liposome. The encapsulated drug can also be released from the carrier as the liposome carrier is cleared. The rate of in vivo drug release is an extremely important parameter since it can influence the rate of clearance of the drug from the general circulation, the bioavailability and thus the activity of the drug at its site of action, the targetability of the drug, and the observed toxicities (13-15). After the drug is released from the carrier, the PK disposition of the drug will be the same as after administration of the non-carrier form of the drug. Delivery of drugs to their target site is an important step for desired therapeutic effect. Release of drug at the target site is an equally important step since only released drug is active and the accumulation of active drug at the target site depends on the rate of drug release. The term 'drug release' refers to the desired process of the release of drugs from liposomes, which is necessary to enable drug-target interaction. The term 'drug leakage' implies the unwanted loss of the drug caused by instability or destruction of the liposomal carrier (16). The uptake of liposome by MPS is a desired process of the release of liposomal drugs for the treatment of macrophage-associated diseases such as infectious disease, autoimmune disease, transplantation, neurological disorders, gene therapy and cancer. While for the treatment of disease not involving MPS and the target site is outside of liver, spleen, and bone marrow, such as cancer, the uptake of liposome by MPS is an

unwanted loss of drug. Decreasing the uptake of liposome by MPS while increasing drug release at the target site is the goal.

C.4 PK Nomenclature

The nomenclature used to describe the PK disposition of carrier-mediated drugs are termed encapsulated or conjugated (drug within or bound to the carrier), released (the active-drug released from the carrier), and sum total (encapsulated or conjugated drug plus released drug) (5). The released drug has also been called the legacy drug, regular drug, or warhead (5, 17). Released drug consists of drug that is protein bound and unbound or free drug. The ability to evaluate the various forms (encapsulated, released, unbound) of the drug after administration of liposome or nanoparticle formulation is dependent upon specific sample processing methods (18).

D. Factors Affecting PK of Liposomal Agents

There are two major sources of factors that influence the PK and PD of liposomal drugs. One is liposome associated factors including the physiochemical properties of liposomes, such as size, surface charge and membrane composition. The other is host associated factors. In addition, dose schedule and drug-drug interaction also play a role in the PK disposition of liposomal agents.

D.1 Liposome Associated Factors

D.1.1 Particle Size.

When a liposomal drug is introduced into the body, where it can go mainly depends on its particle size. Unlike conventional small molecule drugs which can diffuse freely through the endothelial wall, the diffusion of intact liposomes is dependent on both particle size and the anatomical structure of the tissue. The tissues can be classified as non-endocrine organs (heart, lung, kidney, muscle and fat tissue), endocrine tissues (liver and adrenocortical), and spleen and lymphatics according to their capillaries and extracellular matrices. The accessibility of liposome to these tissues is in this order: spleen and lymphatics > endocrine tissues (liver and adrenocortical) > non-endocrine organs (heart, lung, kidney, muscle and fat tissue) (7).

The effect of particle size on the tumor uptake of liposomes has been demonstrated by different groups. In one study, liposomes with a size between 100 nm and 200 nm showed a 4-fold higher rate of uptake in the tumor compared to the liposomes with a size less than 50 nm or greater than 300 nm (19). In another study, liposomes with a size ranged between 80 and 160 nm resulted in a significantly greater accumulation in tumor compared to liposomes with a size of 241 nm (20). The lower uptake of larger liposome in tumor may be explained by the sized limited permeability of tumor vascular. The lower accumulation of very small liposomes (< 20-30 nm in diameter) may be explained by their high permeability but low retention because they can easily pass through the leaky capillary wall in the tumor but can also be returned to circulating blood by diffusion (21).

Particle size also affects the uptake of liposomes by monocytes. The effect of liposome size on inactivation or depletion of monocytes was investigated by Golomb group (22). In this study, larger liposomes were internalized faster by monocytes compared to smaller liposomes. Following 30-min incubation of human monocytes with empty liposomes

and the liposomes containing alendronate, human monocytes internalized 49 ± 5, 61 ± 4, 72 ± 3 and 80 ± 5% of empty liposomes, and liposomes containing alendronate with a size of 85 ± 20, 190 ± 24, 400 ± 64 and 654 ± 124 nm, respectively (22). In addition, the increased cellular internalization capacity of larger liposomes resulted in an increased effect of monocyte/macrophage inhibition. The in vivo depletion of monocytes following iv administration of liposomal bisphosphonates was examined using rabbits. Depletion of rabbit monocytes after treatments with small liposomes with a size of 55 nm (40±5%) was significantly less than that after treatments with larger liposomes (>67%) (22).

D.1.2 Surface Charge

In general, uncharged liposomes were cleared from the circulation slower than either positively or negatively charged liposomes (15). The reduced clearance of uncharged liposomes is thought to be the result of reduced opsonisation followed by the decreased MPS uptake. Surface charge can also affect the biodistribution of liposomes. For example, high concentrations of anionic lipids increase accumulation of liposomes in the liver and spleen (13, 23, 24). Cationic liposomes often exhibit a rapid blood clearance phase with a large dose accumulating primarily in the liver, spleen, and lung (24, 25) In addition, cationic liposomes were found to be selectively delivered to tumor vascular endothelial cell because of the natural affinity of cationic carrier molecules for the tumor microvasculature (25, 26). Although utilization of cationic liposome for gene delivery and cancer therapy gains increasing interests, the toxic effect of positively charged compounds in cationic liposomes should be taken into consideration (27, 28). Large amounts of cationic liposomes may cause a tissue inflammatory response (29). However, even cationic liposomes can be made stable

and long circulating by reducing the content of cationic lipid and inclusion of PEG-lipid stabilizers (27).

D.1.3 Lipid Composition

The effect of lipid composition on the PK of liposomal drug lies in two aspects. Firstly, it can affect the drug release rate as the permeability of drug against lipid bilayer is controlled by lipid composition. Secondly, it is important in determining the PK fate of liposomal drug since the property of lipid bilayer is also controlled by lipid composition.

The permeability of solute against lipid bilayer is dependent on the species of phospholipids and lipid composition. For instance, if the acyl chains and unsaturated phospholipid is included in the lipid bilayer, the permeability is relatively higher because of lower phase transition temperature and high membrane fluidity (30). Thus, permeability and phase transition temperature is determined from the lipid molecule structure. In general, the lipid with a higher phase transition temperature than body temperature (35 to 37ºC) is preferably used for the main membrane component since it can prevent the unwanted leakage of drug from the liposome during the storage.

pH sensitive liposomes, which are made of pH-sensitive phospholipids such as 1,2-dioleoyl-sn-glycero-3-phosphoethanolamine with cholesteryl hemisuccinate, can fuse with the endosomal membrane as a result of the lower pH inside the endosome, and release their content into the cytoplasm following endocytotic uptake (16). pH-sensitive liposomes are used to deliver highly polar drugs, such as DNA, RNA or siRNA molecules to the cytosol or nucleus of cells and thus the degradation of the drug by lysosome is avoided.

The synthesis of novel lipids with desired properties made a major progress in liposomal drug delivery. PEGylated lipids are an example of such lipids. PEGylated liposomes have a lipid bilayer membrane like conventional liposomes, but the surface contains surface-grafted linear segments of PEG extending 5 nm from the surface (31, 32). The presence of PEG on the surface of the liposome can prevent protein adsorption on outer leaflet of liposomes and reduce MPS uptake of liposome (**Figure 1.1**). As a result, PEGylated liposomes can remain in the circulation for prolonged periods after IV injection. In addition to prolonged plasma exposure, the PEGylated liposomes help to achieve better passive targeting effect because longer circulation time will allow more drugs reach the target site before they are removed out of the body.

Currently, there are two types of PEGylated liposome as shown in **Figure 1.2**. One has PEG tether projected on both the inside and outside of liposome. This is the PEGylated liposome used for like Doxil and S-CKD602. Doxil is a PEGylated liposomal formulation of doxorubicin which is approved for the treatment of refractory ovarian cancer, Kaposi sarcoma, and multiple myeloma (33, 34). S-CKD602 is a PEGylated liposomal formulation of CKD-602, a camptothecin analogue which inhibits topoisomerase I (5). The other type has PEG tether only localized on the outer leaflet. This PEGylated liposome has been used for IHL-305. IHL-305 is a PEGylated liposomal formulation of irinotecan (CPT-11), also a camptothecin analogue.

Thus, there are several aspects of the liposomal formulation to consider that are major factors that influence the PK and PD of liposomal agents. The coverage amount and consistency of PEG lipid on the surface might be the most important of these factors. As described above PEGylated liposomes have significant advantages compared with non-

PEGylated or non-stabilized liposomes. PEGylated lipids are widely used to improve PK properties of other liposomal delivery systems, such as cationic liposomes and pH-sensitive liposomes.

D.1.4 Ligand Conjugation

The conjugation of a targeting ligand to the surface of a liposome can affect its PK and biodistribution (15). The targeting ligands for liposomes include peptides, growth factors, proteins, antibodies or antibody fragments, and small molecules such as folate that can recognize cancer cells (35-37). A summary of some of the targeting ligands that have been used in liposomal carriers to achieve active targeting is listed in **Table 1.2**. In theory, the presence of targeting ligands promotes the accumulation of liposomes or other nanoparticles within certain tissues or cells in the body as a result of highly specific interactions between the ligands and the target (38). Estrone conjugated PEGylated liposome doxorubicin (ES-SL-DOX) was reported to have an increased accumulation in the tumor tissue compared to non-conjugated PEGylated liposome doxorubicin (39). Additionally, the half-life of estrone conjugated liposomes was also increased compared to non-conjugated liposomes (39).

D.1.5 Environment Factors

Environment factors can affect the release of drug from liposomes. There are two types of environment factors. The first type of environment factors is the factors inside the body such as the presence of particular chemicals and enzymes. These internal environment factors trigger release of drug from specially designed liposomes. For example, glucose-

triggered release from pH-sensitive liposomes with surface-bound glucose oxidase has been reported (40). Novel liposomes modified with surface-bound substrate (GPOn) of matrix metalloproteases (MMP) rapidly released their content in the presence of cell-secreted MMP9 (41). The second type of environment factors is the factors outside the body (external stimuli) such as heat or ultrasound (42-45). Use of external stimuli has attracted much attentions for targeted drug delivery in the clinic (16). Release from thermosensitive liposomes (TSL) occurs at temperatures close to the Tm (solid gel to liquid disordered phase transition temperature) of the membrane lipids because of the increased the membrane permeability at Tm. The Tm of the TSLs can be adjusted to the clinical attainable temperatures (Tm = 40 to 42°C) by altering the lipid composition (43, 46). ThermoDox (TSL doxorubicin; Celsion Corp Yakult Honsha KK) was the first TSL formulation to enter clinical trials, and is in phase III clinical trials for the treatment of patients with hepatocellular carcinoma (ClinicalTrials.gov Identifier: NCT00617981) (16). Ultrasound was also demonstrated to trigger drug release from TSL in vivo (44).

D.2 Host associated factors

As discussed above, PK properties of different formulations of liposomal drugs are affected by the formulation-related factors. Inter-individual variabilities in PK of a liposomal drug are affected by host associated factors. There is significant interpatient variability in the PK disposition of liposomal encapsulated agents (5, 47, 48). It appears that the PK variability of the carrier formulation of a drug is several-fold higher compared with the non-liposomal formulation of the drug (5, 48, 49). For example, the inter-patient PK variability of PEGylated liposomal CKD-602 (S-CKD602) was approximately 100-fold at lower doses

and 10- to 25-fold at higher doses (47). However, certain PEGylated liposomal agents, such as PEGylated liposomal irinotecan (IHL-305) appear to have less PK variability (47, 50, 51). Thus, there is a need to identify factors associated with the significant PK variability. A few factors have been reported to be associated with the significant PK variability of liposomal drugs.

D.2.1 Age

Age was reported to be associated with PK of S-CKD602 and Doxil. In a phase I and PK study of S-CKD602, patients ≥ 60 years of age have a 2.7-fold higher exposure of S-CKD602 compared with patients < 60 years of age ($P = 0.02$) (**Figure 1.3a** and 1.**3b**) (48, 52). In phase I and II studies of Doxil in patients with solid tumors (n = 23) and in patients with AIDS-related Kaposi's sarcoma (KS) (n = 37) , mean ± SD Doxil clearance in patients with solid tumors that were < 60 yo and ≥ 60 yo were 48.2 ±19.9 and 27.2 ± 10.4 L/h/m2, respectively ($P = 0.001$) (53). Gender and age effect were reported in PK studies of PEGylated liposomal drugs including Doxil, S-CKD602, and IHL-305. Male patients < 60 years of age have a 2.2-fold higher clearance of Doxil compared with male patients ≥ 60 years of age (54). Male patients < 60 years of age have a 2.1-fold higher clearance of S-CKD602 compared with male patients ≥ 60 years of age (54). Age appeared to affect the clearance of Doxil and S-CKD602 in male patients but not female patients (54).

D.2.2 Gender

Gender was found to be a factor affecting the PK of a PEGylated liposomal drug. The effect of gender on clearance with and without stratification by age was evaluated. Female

patients had lower clearance of Doxil (P <0.001), IHL-305 (P = 0.068), and SCKD-602 (P = 0.67) as compared with male patients overall and also when stratified by age (54). The gender effect on PK of TLI (Optisomal Topotecan) and S-CKD602 in rats was also reported (55). In this study, clearance of TLI and S-CKD602 was 1.2-fold (P = 0.14) and 1.4-fold (P = 0.009) lower in female rats compared with male rats, respectively. The difference in PK of PEGylated liposomal agents in male and female subjects may be related to age, body composition, and reticuloendothalial system activity (54).

D.2.3 Body composition

Body composition was a factor associated with PK of S-CKD602. Patients with a lean body composition have an increased plasma exposure of S-CKD602 (P = 0.02) (**Figure 1.4**) (48, 52). However, there was no relationship between Doxil clearance and body composition as measure by TBW/IBW or BMI. In a PK study of liposomal daunorubicin in pediatric patients, body weight was found to be an significant covariate on clearance and volume of distribution of liposomal daunorubicin through population PK analysis (56). The effect of body weight on clearance of volume of distribution was also demonstrated in a PK study of liposomal amphotericin B in pediatric patients (57).

D.2.4 Estrous Cycle Stage

The estrous cycle comprises the recurring physiologic changes that are induced by reproductive hormones in most mammalian placental females. The dynamic balance among reproductive hormones modulates cellular proliferation in many organs, such as ovary, uterus, and breast. The rhythmic fluctuation of sex hormones during the estrous cycle also

controls breast cancer angiogenesis and/or tumor vascular permeability. There are four estrous stages – diestrus, proestrus, estrus, and medestrus. The estrous cycle stage of 4T1 tumor-bearing mice altered the retention of Doxil in transplanted murine mammary tumors (58). In this study, Doxil was administered at certain time point during the mouse estrous cycle. A significant higher (5.6 fold) drug concentration were detected in the tumor tissues when Doxil was injected during the diestrus stage compared to when drug was administered at all other estrous stages. The effect of estrous cycle on the plasma PK of Doxil was not evaluated in this study. The altered retention of drug may be explained by the changes in breast cancer capillary permeability resulting from the changing sex hormone milieus during the estrous cycle.

D.2.5 Prior treatment

Prior treatment can also affect the PK of liposomal drugs. In a phase I and PK study of S-CKD602, patients receiving prior PEGylated liposomal doxorubicin (PLD) had a 2.2-fold higher exposure of S-CKD602 compared with patients not receiving PLD ($P = 0.045$).

Gabizon and colleagues reported that the clearance of sum total (encapsulated + released doxorubicin) decreased by approximately 25 to 50% from cycle 1 to 3 in patients with ovarian cancer (**Figure 1.5**) (59). In addition, La and colleagues reported that this reduction in clearance of Doxil from cycle 1 to cycle 3 was associated with a reduction in pre-cycle monocyte count (60). These studies suggest that there is a reduction in the clearance of liposomes over time that is associated with a reduction in MPS function. Thus, dose reductions may be needed in subsequent cycles to minimize the risk of toxicity (59). Interestingly, repeat dose studies of PEGylated liposomal doxorubicin in mice and rats did

not report accumulation of drug in plasma suggesting that these preclinical models may not accurately reflect the disposition of PEGylated liposomal agents after repeated dosing (61, 62). Thus, there is a need to develop better preclinical animal models for pharmacology and toxicology studies of liposomal and nanoparticle agents.

D.3 Effect of Dose Schedules

Conventional liposome formulations show a dose-dependent clearance (12, 13). Circulation time of conventional liposomes increase proportionately with increasing lipid dose. The decreased clearance of conventional liposomes may due to a combination of saturation of MPS (63) and due to depletion of serum opsonins at high lipid doses (64, 65). PK of drug-free pegylated liposomes has been reported to be independent of dose within a certain range. However, inhibition of MPS-mediated liposome clearance by PEGylated liposomal doxorubicine (PLD) but not drug-free liposomes or non-liposomal doxorubicin was reported in murine model. In this study, treatment with PLD followed one day later by injection of drug-free radio-labeled liposomes or repeated treatment with PLD every 4 days for a total of four injections have been shown to cause a delay in liposome and liposomal drug clearance. In addition, clinical PK analysis of Doxil suggests a dose-dependent clearance and saturation of clearance phenomenon when a broad range of doses are examined (66). Dose-dependent clearance was also observed in a phase I PK study of S-CKD602 (47, 48).

The dose-dependent PK not only is reflected in saturation of clearance but also changed the biodistribution of Doxil. In murine model, dose escalation results in a disproportional increase of the amount of liposomal drug accumulating in tumor (66). The

enhancement of tumor drug levels with liposomal delivery is much more prominent at higher doses than at lower doses. In addition, decreased amounts of liposomes in liver and increased amounts of liposomes in spleen and blood were observed with increasing liposome dose (67, 68).

D.4 Drug-Drug Interaction

Drug-drug interactions were also reported for the PK of liposomal drugs. Pazopanib is a small-molecue inhibitor of vascular endothelial growth factor (VEGF) and platelet-derived growth factor (PDGF) receptors. Coadministration of Pazopanib and Doxil resulted in a significantly reduced penetration of Doxil from microvessels of tumor. No significant difference in doxorubicin concentration normalized by tumor weight between Pazopanib treated and control tumor was observed (69). The effect of Pazopanib on distribution of Doxil may be explained by the altered vessel permeability and oncotic pressure gradients which play an important role in the liposomal drug delivery to tumor. In addition, cisplatin has been shown to increase the clearance of Doxil; however, the mechanism of this interaction is unclear (70).

E. Factors Affecting PD of Liposomal Agents

Liposome drug delivery systems have been widely used to reduce the drug toxicity while at the same time improve or maintain the drug efficacy. Like conventional drugs, efficacy and toxicity of liposomal drugs can be accounted for to a great extent by its PK disposition. The factors that affect PK of liposomal drugs may also have an effect on the PD of liposomal drugs.

E.1 Efficacy

Liposomal delivery system improved efficacy of drugs by changing the PK disposition and biodistribution of encapsulated drugs. The improved efficacy of liposomal drugs has been repeatedly demonstrated. In addition to the improved biodistribution, the interaction between liposome and blood cells including platelets provided a PK-independent enhancement in efficacy of hemophilia treatment. Recombinant FVIII formulated in PEG-ylated liposomes (rFVIII-PEG-Lip) was reported to increase the bleed-free days from 7 to 13 days (at 35 IU/kg rFVIII) in severe hemophilia A patients (71). The efficacy of rFVIII-PEG-Lip represents an approximately 2.5-fold higher "apparent" FVIII activity, which is not accounted for by its modestly increased (13%) half-life (72). PEG-Lip associates with the majority of platelets and monocytes in vivo, and results in increased P-selectin surface expression on platelets in response to collagen (72).

Family history of ovarian cancer was reported to be a factor on the efficacy of PEGylated liposomal doxorubicin (PLD). The median time to progression was 11.5 months for high-risk patients versus 6.5 months for patients with sporadic cancer ($P = 0.0188$) and the median overall survival for high-risk patients was 48.7 months (95% CI, 21.2-) compared with 16.2 months (95% CI, 11.8 - 24.0) for the patients with sporadic cancer ($P = 0.0032$) (73). Patients with hereditary ovarian cancer were more sensitive to PLD. This observation may be related to a high incidence of a *BRCA1* or *BRCA2* germ-line mutation in these patients.

E.2 Toxicity

Liposomal formulations can also modify the toxicity profile of a drug (e.g., Ambisome) (74). Amphotericin B is a polyene antibiotic used in the treatment of systemic fungal infection. The use of non-liposomal amphotericin B is associated with extensive renal toxicity (75). The toxicity of this compound is due to non specific binding to the mammalian cell cholesterol (75). The liposome formulation of amphotericin B (AmBisome) reduces the renal and general toxicity of amphotericin B by passively targeting the liver and spleen (6, 12, 76). The cardiotoxicity of Doxil is significantly less than non-liposomal doxorubicin, whereas, the efficacy of Doxil is comparable to non-liposomal doxorubicin. Histologic examination of cardiac biopsies from patients who received cumulative doses of Doxil from 440 mg/m^2 to 840 mg/m^2, and had no prior exposure to anthracyclines, revealed significantly less cardiac toxicity than in matched doxorubicin controls ($P < 0.001$) (77). These results suggest that the decreased cardiotoxicity of Doxil may be due to reduced accumulation of doxorubicin in heart. However, a new adverse event called hand-foot syndrome (HFS) also known as palmar-plantar erythrodysesthesia (PPE) and stomatitis commonly occurs after Doxil treatment (78). PPE/HFS can be dose limiting in some patients. This has not been reported with non-liposomal doxorubicin at standard doses (79). The exact mechanisms associated with these toxicities are unknown, but these toxicities are schedule and dose dependent. The relationship between PK of Doxil and HFS incidence was studied by Lyass et al. It was found that HFS incidence correlated with elimination half-life, but not with drug dose, maximum plasma concentration, or area under the concentration curve (AUC) (70, 80, 81). These findings suggested that prolonged exposure and that longer dosing interval may decrease the risk of HFS. Doxil is generally well tolerated and its side-effect profile compares favorably with other chemotherapy used in the treatment of refractory ovarian

cancer. Proper dosing and monitoring may further enhance tolerability while preserving efficacy; however, these is still a need to identify factors associated with PPE (79).

In general, drug toxicity is reduced using liposomal delivery system due to their limited distribution to normal tissue and organs. Although liposome toxicity appears to be minimal, potential toxicity should be considered for tissues such as the liver, spleen, and lungs because of macrophage ingestion of liposomes. The interaction between liposome and MPS may cause toxicity to MPS after administration of liposomal agents. Our group performed the first study evaluating the PK and PD relationships between a liposomal anticancer agent and monocytes, a primary cell of the MPS, in patients (52). In this study, the relationship between monocyte count and absolute neutrophil count (ANC) in the blood and PK disposition of S-CKD602 and non-liposomal CKD-602 (NL-CKD602) in patients were evaluated. For S-CKD602 in patients <60 years, the percent decrease in ANC and monocytes were 43 ± 31 and 58 ± 26%, respectively (P = 0.001). For S-CKD602 in patients >= 60, the percent decrease in ANC and monocytes were 41 ± 31 and 45 ± 36%, respectively (P = 0.50). For NL-CKD602 (n = 42), the percent decrease in ANC and monocytes were similar (P > 0.05). The results of our study suggest that monocytes are more sensitive to S-CKD602 as compared with neutrophils and that the increased sensitivity is related to the liposomal formulation and not the encapsulated CKD-602. The relationship between changes in monocytes and the PK disposition of S-CKD602 suggest that monocytes engulf liposomal anticancer agents which cause the release of CKD-602 from the liposome and toxicity to the monocytes (82). Our study also suggests that there are age-related factors associated with the PD interaction between S-CKD602 and monocytes with a decrease in the function of monocytes in older patients.

Interestingly, the interaction between liposomes and small molecule drugs may be used to reduce toxicity of the drugs. Pretreatment with empty liposomes reduced acute toxicity of non-liposomal amphotericin B in mice (83). The protective effect of liposomes from the erythrocyte membrane damage induced by non-liposomal amphotericin B may be due to an altered structure of amphotericin B after interacting with the liposomes (84).

Positively charged liposomes are associated with pulmonary toxicity. The pulmonary toxicity of liposome depends on dose and charge (85). The toxicities of differently charged liposomes were evaluated after pulmonary administration in mice. It was found that multivalent cationic liposome LipofectAMINE was much more toxic than the monovalent cationic liposome DOTAP, and that neutral and negative liposomes were not toxic at similar concentrations (85).

F. CONCLUSION

Liposomes have been used to increase the therapeutic index of a wide range of drugs because of their unique PK properties. Liposomal properties such as particle size, charge and lipid composition have been extensively investigated for their influence on the PK of liposomal drugs in preclinical studies. Based on the understanding of the role of these factors along with the advanced liposomal technology, it is now possible to engineer a wide range of liposomes of different physicochemical properties suitable for a wide range of applications. However, the clinical use of liposomal drugs is complicated by large intra- and inter-individual variabilities in their PK and PD. Although several physiological factors such as age, body composition, and gender have been reported to affect the fate of liposomal drugs,

much work is still needed to identify factors and validate the identified factors in clinical studies of liposomal drugs.

Liposomal drugs generally have comparable or greater activity than conventional drugs while at the same time reducing toxicity of conventional drugs. Factors associated with PK of liposomal drugs are of great importance in driving the PD of liposomal drugs. In addition, understanding of the interaction between liposome and organ systems, such as MPS, provides stronger basis to predict efficacy and safety of liposomal drugs.

Future studies need to evaluate the mechanism of clearance of liposomal agents and identify the factors associated with PK and PD variability of liposomes and nanoparticle anticancer agents in patients and specifically in tumors (86, 87). Future studies also need to develop phenotypic probes that can be used to predict this variability and individualize therapy with liposomal agents. In addition, to advance the science and the translational development of liposomal agents it is of the utmost importance to determine the most appropriate animal model for the pharmacology, toxicology and efficacy studies of liposomal agents and all carrier-mediated agents.

G. RATIONALE AND OVERVIEW OF PROPOSED RESEARCH

The PK disposition of carrier-mediated agents, such as, nanoparticles, liposomes, and conjugated agents, is dependent upon the carrier until the drug is released from the carrier. Thus, the pharmacology of a particular liposomal drug is significantly affected by the PK, biodistribution, and drug release rates of the liposomal carrier. Physiochemical properties of liposomal formulations and environment factors affecting the PK of liposomal drugs have been extensively evaluated in preclinical studies. However, nonlinear and highly variable PK property of the PEGylated liposomal anticancer agents has been observed in the clinical studies. The nonlinear PK of Doxil may be explained by the saturation of MPS. The factors associated with the PK/PD variability of these agents remain unclear, but most likely include the MPS.

PEGylated liposomes are mainly cleared by the MPS which includes monocytes in the blood circulation and macrophages in the tissue. The clearance of PEGylated liposomal anticancer agents by monocytes causes the release of anticancer agents and acute cytotoxicity to the monocytes. This toxicity to the monocytes in turn decreases clearance of the PEGylated liposomal anticancer agents and affects the PD of PEGylated liposomal anticancer agents. PK of PEGylated liposomal anticancer agents has been evaluated by empirical modeling approach. However, mechanistic models based on physiology and pharmacology have not been developed for PEGylated liposomal anticancer agents to date. The goals of this dissertation work is to understand the role of bi-directional interaction between the PEGylated liposomal anticancer agents and monocytes in determining the PK and PD of PEGylated liposomal anticancer agents, and identify patient factors associated with the significant PK/PD variability of PEGylated liposomal anticancer agents. A

population PK/PD modeling approach will be used to characterize the PK/PD of PEGylated liposomal anticancer agents.

The central hypothesis of this project is that the bi-directional interaction between the PEGylated liposomal anticancer agents and cells of the MPS, such as monocytes, macrophages, and dendritic cells, drives the PK/PD of PEGylated liposomal anticancer agents. Therefore, this interaction can be monitored and utilized to optimize the treatment with PEGylated liposomal anticancer agents. S-CKD602 and IHL-305 were selected as representative PEGylated liposomal anticancer agents for this work.

S-CKD602 is a PEGylated liposomal formulation of CKD-602, a camptothecin analogue which inhibits topoisomerase I (5). The PEGylated liposomal formulation consists of phospholipids covalently bound to methoxypolyethylene glycol (mPEG) on the outside of the lipid bilayer. Non-liposomal CKD-602 administered IV at 0.5 mg/m^2/day for 5 consecutive days repeated every 21 days is approved in Korea for the treatment of newly diagnosed small cell lung cancer and relapsed ovarian cancer (88-91). The results of a phase I study of S-CKD602 administered IV x1 over 1 hour every 21 days reported that S-CKD602 was associated with high interpatient variability in the PK disposition of encapsulated and released CKD-602 (48). There was a 100-fold range at lower dose and a 10-fold to 20-fold range at higher dose in encapsulated CKD-602 AUC (47). We were the first to report a reduced clearance of the liposomal encapsulated forms of Doxil and S-CKD602 in patients ≥ 60 years of age (92, 93). We have also reported that patients with a lean body composition may have a reduced tissue distribution and an increased plasma exposure of S-CKD602 (92, 93). In addition, we have reported an age related decrease in the function of monocytes

which may be associated with a reduced clearance of liposomes and reduced cytotoxicity to the monocytes (52, 94, 95).

IHL-305 is a PEGylated liposomal formulation of irinotecan (CPT-11), also a camptothecin analogue. CPT-11 has been approved for the treatment of metastatic colorectal cancer (5, 96-98). Unlike S-CKD602, CPT-11, the encapsulated drug in IHL-305, is a prodrug that requires activation to the active metabolite, 7-ethyl-10-hydroxy-camptothecin (SN-38). SN-38 is approximately 100- to 1000-fold more active than the parent CPT-11. IHL-305 is currently in phase I clinical studies (99). The PEGylated liposomes of S-CKD602 and IHL-305 were made using two different methods. The PEGylated liposome of S-CKD602 was made by adding the PEG lipid before the process of liposomal formation which results PEG tether being projected on both the inside and outside of liposome. The PEGylated liposome of IHL-305 is made by adding the PEG lipids after the process of liposomal formation which results in PEG tether only being localized on the outer leaflet (100).

The major goals of this research plan are:

Aim 1. To identify important patient factors affecting the PK of PEGylated liposomal anticancer agents.

1a) Evaluate the influence of patient characteristics on PK parameters using noncompartmenal PK analysis.

1b) Evaluate the influence of patient characteristics on PK parameters using individual-based PK analysis.

1c) Evaluate the influence of patient characteristics on PK parameters using population-based PK analysis.

Aim 2. To develop a mechanism-based population PK/PD model for the representative PEGylated liposomal anticancer agents by incorporating the bi-directional interaction between the PEGylated liposomal anticancer agents and the monocytes as a component.

2a) Investigate the nature of nonlinear PK of these agents

2b) Evaluate the role of the bi-directional interaction between these agents and the monocytes in the PK and PD of these agents.

In this dissertation, various PK analyses were performed for S-CKD602 and IHL-305 to define role of bi-directional interaction between the PEGylated liposomal anticancer agents and monocytes in determining the PK and PD of PEGylated liposomal anticancer agents. In addition, this work identified patient factors affecting the PK/PD of these agents. Non-compartmental analysis was performed as part of a phase I study of IHL-305 in patients with advanced solid tumors to evaluate the PK disposition of sum total (encapsulated + released) and released CPT-11, and its metabolites, and the PD of IHL-305. Conventional PK analysis based on individual patient data was performed to evaluate the factors associated with the inter-patient variability in the PK and PD of IHL-305 in patients with advanced solid tumors. A population PK analysis of IHL-305 based on a conventional (empirical) PK model was performed to describe the population PK of the encapsulated CPT-11, released CPT-11 and the active metabolite SN-38 after administration of the PEGylated liposomal form of the drug. This model was also used to characterize clinical covariates that influence IHL-305 PK. A mechanism-based population PK-PD model was developed to investigate the nature of nonlinear PK of IHL-305 and to increase our understanding of the bi-directional interaction between PEGylated liposomal anticancer agents and monocytes in cancer patients.

Results of non-compartmental PK analysis and conventional PK analysis based on individual patient data of a phase I study of S-CKD602 have been published (47, 48). A population PK analysis of S-CKD602 based on conventional (empirical) PK model was performed to describe the population PK of the encapsulated CKD-602 and released CKD-602 after administration of the PEGylated liposomal form of the drug and to characterize clinical covariates that influence S-CKD602 PK. A mechanism-based population PK-PD model was developed to investigate the nature of nonlinear PK of S-CKD602 and to increase our understanding of the bi-directional interaction between PEGylated liposomal anticancer agents and monocytes in cancer patients.

Finally, we developed a mechanism-based population PK-PD model for PEGylated liposome membrane lipids to evaluate the bi-directional interaction between PEGylated liposome membrane lipids and monocytes. This model was used to test if PEGylated liposome membrane lipids alone can explain the toxicity associated with monocytes after administration of PEGylated liposomal anticancer agents.

This project will generate new knowledge about: (1) the nature of the nonlinear PK of PEGylated liposomal anticancer agents; (2) the role of the bi-directional interaction between PEGylated liposomes and the monocytes in the PK/PD of these agents; and (3) patient factors that significantly affect the PK/PD of PEGylated liposomal anticancer agents.

H. REFERENCES

1. Torchilin VP. Recent advances with liposomes as pharmaceutical carriers. Nat Rev Drug Discov 2005; 4:145-60.

2. Samad A, Sultana Y, Aqil M. Liposomal drug delivery systems: an update review. Curr Drug Deliv 2007; 4:297-305.

3. Wang J, Sui M, Fan W. Nanoparticles for tumor targeted therapies and their pharmacokinetics. Curr Drug Metab; 11:129-41.

4. Laginha K, Mumbengegwi D, Allen T. Liposomes targeted via two different antibodies: assay, B-cell binding and cytotoxicity. Biochim Biophys Acta 2005; 1711:25-32.

5. Zamboni WC. Liposomal, nanoparticle, and conjugated formulations of anticancer agents. Clin Cancer Res 2005; 11:8230-4.

6. Zamboni WC, Gervais AC, Egorin MJ, et al. Systemic and tumor disposition of platinum after administration of cisplatin or STEALTH liposomal-cisplatin formulations (SPI-077 and SPI-077 B103) in a preclinical tumor model of melanoma. Cancer Chemother Pharmacol 2004; 53:329-36.

7. Igarashi E. Factors affecting toxicity and efficacy of polymeric nanomedicines. Toxicol Appl Pharmacol 2008; 229:121-34.

8. Fujita T. A scanning electron microscope study of the human spleen. Arch Histol Jpn 1974; 37:187-216.

9. Li SD, Huang L. Pharmacokinetics and biodistribution of nanoparticles. Mol Pharm 2008; 5:496-504.

10. Yuan F, Dellian M, Fukumura D, et al. Vascular permeability in a human tumor xenograft: molecular size dependence and cutoff size. Cancer Res 1995; 55:3752-6.

11. Maeda H, Bharate GY, Daruwalla J. Polymeric drugs for efficient tumor-targeted drug delivery based on EPR-effect. Eur J Pharm Biopharm 2009; 71:409-19.

12. Allen TM, Hansen C. Pharmacokinetics of stealth versus conventional liposomes: effect of dose. Biochim Biophys Acta 1991; 1068:133-41.

13. Drummond DC, Meyer O, Hong K, Kirpotin DB, Papahadjopoulos D. Optimizing liposomes for delivery of chemotherapeutic agents to solid tumors. Pharmacol Rev 1999; 51:691-743.

14. Allen TM, Cheng WW, Hare JI, Laginha KM. Pharmacokinetics and pharmacodynamics of lipidic nano-particles in cancer. Anticancer Agents Med Chem 2006; 6:513-23.

15. Drummond DC, Noble CO, Hayes ME, Park JW, Kirpotin DB. Pharmacokinetics and in vivo drug release rates in liposomal nanocarrier development. J Pharm Sci 2008; 97:4696-740.

16. Lindner LH, Hossann M. Factors affecting drug release from liposomes. Curr Opin Drug Discov Devel; 13:111-23.

17. Yurkovetskiy AV, Hiller A, Syed S, et al. Synthesis of a macromolecular camptothecin conjugate with dual phase drug release. Mol Pharm 2004; 1:375-82.

18. Zamboni WC, Edwards RP, Mountz JM. The Development of Liposomal and Nanoparticle Anticancer Agents: Methods to Evaluate the Encapsulated and Released Drug in Plasma and Tumor and Phenotypic Probes for Pharmacokinetic (PK) and Pharmacodynamic (PD) Disposition. NSTI Nanotechnology Conference; 2007; 2007.

19. Liu D, Mori A, Huang L. Role of liposome size and RES blockade in controlling biodistribution and tumor uptake of GM1-containing liposomes. Biochim Biophys Acta 1992; 1104:95-101.

20. Charrois GJ, Allen TM. Rate of biodistribution of STEALTH liposomes to tumor and skin: influence of liposome diameter and implications for toxicity and therapeutic activity. Biochim Biophys Acta 2003; 1609:102-8.

21. Noguchi Y, Wu J, Duncan R, et al. Early phase tumor accumulation of macromolecules: a great difference in clearance rate between tumor and normal tissues. Jpn J Cancer Res 1998; 89:307-14.

22. Epstein-Barash H, Gutman D, Markovsky E, et al. Physicochemical parameters affecting liposomal bisphosphonates bioactivity for restenosis therapy: internalization, cell inhibition, activation of cytokines and complement, and mechanism of cell death. J Control Release; 146:182-95.

23. Chonn A, Semple SC, Cullis PR. Association of blood proteins with large unilamellar liposomes in vivo. Relation to circulation lifetimes. J Biol Chem 1992; 267:18759-65.

24. Gregoriadis G, Senior J. Control of fate and behaviour of liposomes in vivo. Prog Clin Biol Res 1982; 102 pt A:263-79.

25. Schmitt-Sody M, Strieth S, Krasnici S, et al. Neovascular targeting therapy: paclitaxel encapsulated in cationic liposomes improves antitumoral efficacy. Clin Cancer Res 2003; 9:2335-41.

26. Campbell RB, Fukumura D, Brown EB, et al. Cationic charge determines the distribution of liposomes between the vascular and extravascular compartments of tumors. Cancer Res 2002; 62:6831-6.

27. Campbell RB, Ying B, Kuesters GM, Hemphill R. Fighting cancer: from the bench to bedside using second generation cationic liposomal therapeutics. J Pharm Sci 2009; 98:411-29.

28. Conwell CC, Huang L. Recent Advances in Non-viral Gene Delivery. Adv Genet 2005; 53PA:1-18.

29. Scheule RK, St George JA, Bagley RG, et al. Basis of pulmonary toxicity associated with cationic lipid-mediated gene transfer to the mammalian lung. Hum Gene Ther 1997; 8:689-707.

30. Dos Santos N, Mayer LD, Abraham SA, et al. Improved retention of idarubicin after intravenous injection obtained for cholesterol-free liposomes. Biochim Biophys Acta 2002; 1561:188-201.

31. Papahadjopoulos D, Allen TM, Gabizon A, et al. Sterically stabilized liposomes: improvements in pharmacokinetics and antitumor therapeutic efficacy. Proc Natl Acad Sci U S A 1991; 88:11460-4.

32. Woodle MC, Lasic DD. Sterically stabilized liposomes. Biochim Biophys Acta 1992; 1113:171-99.

33. Markman M, Gordon AN, McGuire WP, Muggia FM. Liposomal anthracycline treatment for ovarian cancer. Semin Oncol 2004; 31:91-105.

34. Krown SE, Northfelt DW, Osoba D, Stewart JS. Use of liposomal anthracyclines in Kaposi's sarcoma. Semin Oncol 2004; 31:36-52.

35. Federman N, Denny CT. Targeting liposomes toward novel pediatric anticancer therapeutics. Pediatr Res; 67:514-9.

36. Noble CO, Kirpotin DB, Hayes ME, et al. Development of ligand-targeted liposomes for cancer therapy. Expert Opin Ther Targets 2004; 8:335-53.

37. Sapra P, Allen TM. Ligand-targeted liposomal anticancer drugs. Prog Lipid Res 2003; 42:439-62.

38. Alexis F, Pridgen E, Molnar LK, Farokhzad OC. Factors affecting the clearance and biodistribution of polymeric nanoparticles. Mol Pharm 2008; 5:505-15.

39. Paliwal SR, Paliwal R, Mishra N, Mehta A, Vyas SP. A novel cancer targeting approach based on estrone anchored stealth liposome for site-specific breast cancer therapy. Curr Cancer Drug Targets; 10:343-53.

40. Jo SM, Lee HY, Kim JC. Glucose-sensitive liposomes incorporating hydrophobically modified glucose oxidase. Lipids 2008; 43:937-43.

41. Banerjee J, Hanson AJ, Gadam B, et al. Release of liposomal contents by cell-secreted matrix metalloproteinase-9. Bioconjug Chem 2009; 20:1332-9.

42. Needham D, Anyarambhatla G, Kong G, Dewhirst MW. A new temperature-sensitive liposome for use with mild hyperthermia: characterization and testing in a human tumor xenograft model. Cancer Res 2000; 60:1197-201.

43. Lindner LH, Eichhorn ME, Eibl H, et al. Novel temperature-sensitive liposomes with prolonged circulation time. Clin Cancer Res 2004; 10:2168-78.

44. Dromi S, Frenkel V, Luk A, et al. Pulsed-high intensity focused ultrasound and low temperature-sensitive liposomes for enhanced targeted drug delivery and antitumor effect. Clin Cancer Res 2007; 13:2722-7.

45. Schroeder A, Kost J, Barenholz Y. Ultrasound, liposomes, and drug delivery: principles for using ultrasound to control the release of drugs from liposomes. Chem Phys Lipids 2009; 162:1-16.

46. Hossann M, Wiggenhorn M, Schwerdt A, et al. In vitro stability and content release properties of phosphatidylglyceroglycerol containing thermosensitive liposomes. Biochim Biophys Acta 2007; 1768:2491-9.

47. Zamboni WC, Ramalingam S, Friedland DM, et al. Phase I and pharmacokinetic study of pegylated liposomal CKD-602 in patients with advanced malignancies. Clin Cancer Res 2009; 15:1466-72.

48. Zamboni WC, Strychor S, Maruca L, et al. Pharmacokinetic study of pegylated liposomal CKD-602 (S-CKD602) in patients with advanced malignancies. Clin Pharmacol Ther 2009; 86:519-26.

49. Sidone BJ, Edwards RP, Zamboni BA. Evaluation of body surface area (BSA) based dosing, age, and body composition as factors affecting the pharmacokinetic (PK) variability of PEGYLATED liposomal doxorubicin (Doxil). AACR-NCI-EORTC; 2007; 2007.

50. Jones SF, Zamboni WC, Burris III HA, et al. Phase I and pharmacokinetic (PK) study of IHL-305 (pegylated liposomal irinotecan) in patients with advanced solid tumors. ASCO; 2009 Jun, 2009; Orlando, FL; 2009.

51. Wu H, Infante JR, Jones SF, et al. Factors affecting the pharmacokinetics (PK) and pharmacodynamics (PD) of PEGylated liposomal irinotecan (IHL-305) in patients with advanced solid tumors AACR-NCI-EORTC; 2009; 2009.

52. Zamboni WC, Maruca LJ, Strychor S, et al. Bidirectional pharmacodynamic interaction between pegylated liposomal CKD-602 (S-CKD602) and monocytes in patients with refractory solid tumors. J Liposome Res.

53. Zomorodi K, Gupta S. Population Pharmacokinetic Analysis of DOXIL in Adult Patients. AAPS; 1999; 1999.

54. La-Beck NM, Wu H, Infante JR, et al. The evaluation of gender on the pharmacokinetics (PK) of pegylated liposomal anticancer agents. ASCO Annual Meeting; 2010; 2010. p. e13003.

55. Song G, Wu H, La-Beck N, Zamboni BA, Strychor S, Zamboni WC. Effect of Gender on Pharmacokinetic Disposition of Pegylated Liposomal CKD-602 (S-CKD602) and Optisomal Topotecan (TLI) in Rats. AACR 2009.

56. Hempel G, Reinhardt D, Creutzig U, Boos J. Population pharmacokinetics of liposomal daunorubicin in children. Br J Clin Pharmacol 2003; 56:370-7.

57. Hong Y, Shaw PJ, Nath CE, et al. Population pharmacokinetics of liposomal amphotericin B in pediatric patients with malignant diseases. Antimicrob Agents Chemother 2006; 50:935-42.

58. You S, Zuo L, Li W. Optimizing the time of Doxil injection to increase the drug retention in transplanted murine mammary tumors. Int J Nanomedicine; 5:221-9.

59. Gabizon A, Isacson R, Rosengarten O, Tzemach D, Shmeeda H, Sapir R. An open-label study to evaluate dose and cycle dependence of the pharmacokinetics of pegylated liposomal doxorubicin. Cancer Chemother Pharmacol 2008; 61:695-702.

60. La-Beck NM, Zamboni BA, Tzemach D, et al. Evaluation of the relationship between patient factors and the reduction in clearance of pegylated liposomal doxorubicin. ASCO Annual Meeting; 2009 Dec 15; 2009. p. abstr 2548.

61. Charrois GJ, Allen TM. Multiple injections of pegylated liposomal Doxorubicin: pharmacokinetics and therapeutic activity. J Pharmacol Exp Ther 2003; 306:1058-67.

62. Park JW, Kirpotin DB, Hong K, et al. Tumor targeting using anti-her2 immunoliposomes. J Control Release 2001; 74:95-113.

63. Allen TM, Smuckler EA. Liver pathology accompanying chronic liposome administration in mouse. Res Commun Chem Pathol Pharmacol 1985; 50:281-90.

64. Oja CD, Semple SC, Chonn A, Cullis PR. Influence of dose on liposome clearance: critical role of blood proteins. Biochim Biophys Acta 1996; 1281:31-7.

65. Cullis PR, Chonn A, Semple SC. Interactions of liposomes and lipid-based carrier systems with blood proteins: Relation to clearance behaviour in vivo. Adv Drug Deliv Rev 1998; 32:3-17.

66. Gabizon A, Tzemach D, Mak L, Bronstein M, Horowitz AT. Dose dependency of pharmacokinetics and therapeutic efficacy of pegylated liposomal doxorubicin (DOXIL) in murine models. J Drug Target 2002; 10:539-48.

67. Ellens H, Morselt HW, Dontje BH, Kalicharan D, Hulstaert CE, Scherphof GL. Effects of liposome dose and the presence of lymphosarcoma cells on blood clearance and tissue distribution of large unilamellar liposomes in mice. Cancer Res 1983; 43:2927-34.

68. Abra RM, Hunt CA. Liposome disposition in vivo. III. Dose and vesicle-size effects. Biochim Biophys Acta 1981; 666:493-503.

69. Tailor TD, Hanna G, Yarmolenko PS, et al. Effect of pazopanib on tumor microenvironment and liposome delivery. Mol Cancer Ther; 9:1798-808.

70. Lyass O, Hubert A, Gabizon AA. Phase I study of doxil-cisplatin combination chemotherapy in patients with advanced malignancies. Clin Cancer Res 2001; 7:3040-6.

71. Spira J, Plyushch OP, Andreeva TA, Andreev Y. Prolonged bleeding-free period following prophylactic infusion of recombinant factor VIII reconstituted with pegylated liposomes. Blood 2006; 108:3668-73.

72. Pan J, Liu T, Kim JY, et al. Enhanced efficacy of recombinant FVIII in noncovalent complex with PEGylated liposome in hemophilia A mice. Blood 2009; 114:2802-11.

73. Nicoletto MO, Bertorelle R, Borgato L, et al. Family history of cancer rather than p53 status predicts efficacy of pegylated liposomal doxorubicin and oxaliplatin in relapsed ovarian cancer. Int J Gynecol Cancer 2009; 19:1022-8.

74. Veerareddy PR, Vobalaboina V. Lipid-based formulations of amphotericin B. Drugs Today (Barc) 2004; 40:133-45.

75. Laniado-Laborin R, Cabrales-Vargas MN. Amphotericin B: side effects and toxicity. Rev Iberoam Micol 2009; 26:223-7.

76. Newman MS, Colbern GT, Working PK, Engbers C, Amantea MA. Comparative pharmacokinetics, tissue distribution, and therapeutic effectiveness of cisplatin encapsulated in long-circulating, pegylated liposomes (SPI-077) in tumor-bearing mice. Cancer Chemother Pharmacol 1999; 43:1-7.

77. Berry G, Billingham M, Alderman E, et al. The use of cardiac biopsy to demonstrate reduced cardiotoxicity in AIDS Kaposi's sarcoma patients treated with pegylated liposomal doxorubicin. Ann Oncol 1998; 9:711-6.

78. Ewer MS, Martin FJ, Henderson C, Shapiro CL, Benjamin RS, Gabizon AA. Cardiac safety of liposomal anthracyclines. Semin Oncol 2004; 31:161-81.

79. Rose PG. Pegylated liposomal doxorubicin: optimizing the dosing schedule in ovarian cancer. Oncologist 2005; 10:205-14.

80. Lyass O, Uziely B, Ben-Yosef R, et al. Correlation of toxicity with pharmacokinetics of pegylated liposomal doxorubicin (Doxil) in metastatic breast carcinoma. Cancer 2000; 89:1037-47.

81. Hubert A, Lyass O, Pode D, Gabizon A. Doxil (Caelyx): an exploratory study with pharmacokinetics in patients with hormone-refractory prostate cancer. Anticancer Drugs 2000; 11:123-7.

82. Zamboni WC, Friedland DM, Ramalingam S, et al. Relationship between the plasma and tumor disposition of STEALTH liposomal CKD-602 and macrophages/dendritic cells (MDC) in mice bearing human tumor xenografts. American Association for Cancer Research; 2006; 2006. p. 1280.

83. Pisarik L, Joly V, Jullien S, Carbon C, Yeni P. Reduction of free amphotericin B acute toxicity in mice after intravenous administration of empty liposomes. J Infect Dis 1990; 161:1042-4.

84. Janoff AS, Boni LT, Popescu MC, et al. Unusual lipid structures selectively reduce the toxicity of amphotericin B. Proc Natl Acad Sci U S A 1988; 85:6122-6.

85. Dokka S, Toledo D, Shi X, Castranova V, Rojanasakul Y. Oxygen radical-mediated pulmonary toxicity induced by some cationic liposomes. Pharm Res 2000; 17:521-5.

86. Dark GG, Calvert AH, Grimshaw R, et al. Randomized trial of two intravenous schedules of the topoisomerase I inhibitor liposomal lurtotecan in women with relapsed epithelial ovarian cancer: a trial of the national cancer institute of Canada clinical trials group. J Clin Oncol 2005; 23:1859-66.

87. Giles FJ, Tallman MS, Garcia-Manero G, et al. Phase I and pharmacokinetic study of a low-clearance, unilamellar liposomal formulation of lurtotecan, a topoisomerase 1 inhibitor, in patients with advanced leukemia. Cancer 2004; 100:1449-58.

88. Crul M. CKD-602. Chong Kun Dang. Curr Opin Investig Drugs 2003; 4:1455-9.

89. Lee JH, Lee JM, Lim KH, et al. Preclinical and phase I clinical studies with Ckd-602, a novel camptothecin derivative. Ann N Y Acad Sci 2000; 922:324-5.

90. Yu NY, Conway C, Pena RL, Chen JY. STEALTH liposomal CKD-602, a topoisomerase I inhibitor, improves the therapeutic index in human tumor xenograft models. Anticancer Res 2007; 27:2541-5.

91. Lee DH, Kim SW, Suh C, et al. Belotecan, new camptothecin analogue, is active in patients with small-cell lung cancer: results of a multicenter early phase II study. Ann Oncol 2008; 19:123-7.

92. Zamboni WC, Maruca LJ, Strychor S, et al. Age and body composition related-effects on the pharmacokinetic disposition of STEALH liposomal CKD-602 (S-CKD602) in patients with advanced solid tumors. 2007; 2007.

93. Sidone BJ, Edwards RP, Zamboni BA, Strychor S, Maruca LJ, Zamboni WC. Evaluation of body surface area (BSA) based dosing, age, and body composition as factors

affecting the pharmacokinetic (PK) variability of STEALTH liposomal doxorubicin (Doxil). AACR-NCI-EORTC; 2007; 2007.

94. Zamboni WC, Strychor S, Maruca L, et al. Pharmacokinetic Study of Pegylated Liposomal CKD-602 (S-CKD602) in Patients With Advanced Malignancies. Clin Pharmacol Ther 2009.

95. De Martinis M, Modesti M, Ginaldi L. Phenotypic and functional changes of circulating monocytes and polymorphonuclear leucocytes from elderly persons. Immunol Cell Biol 2004; 82:415-20.

96. Zamboni WC. Concept and clinical evaluation of carrier-mediated anticancer agents. Oncologist 2008; 13:248-60.

97. Innocenti F, Kroetz DL, Schuetz E, et al. Comprehensive pharmacogenetic analysis of irinotecan neutropenia and pharmacokinetics. J Clin Oncol 2009; 27:2604-14.

98. Slatter JG, Schaaf LJ, Sams JP, et al. Pharmacokinetics, metabolism, and excretion of irinotecan (CPT-11) following I.V. infusion of [(14)C]CPT-11 in cancer patients. Drug Metab Dispos 2000; 28:423-33.

99. Jones SF, Zamboni WC, Burris III HA, et al. Phase I and pharmacokinetic (PK) study of IHL-305 (pegylated liposomal irinotecan) in patients with advanced solid tumors. ASCO Annual meeting; 2009 Feb 15; 2009.

100. Zamboni WC, Yoshino K. Formulation and physiological factors affecting the pharmacokinetics and pharmacodynamics of liposomal anticancer agents. Japan DDS 2010; 25:58-70.

101. Gabizon A, Shmeeda H, Barenholz Y. Pharmacokinetics of pegylated liposomal Doxorubicin: review of animal and human studies. Clin Pharmacokinet 2003; 42:419-36.

102. Batist G, Barton J, Chaikin P, Swenson C, Welles L. Myocet (liposome-encapsulated doxorubicin citrate): a new approach in breast cancer therapy. Expert Opin Pharmacother 2002; 3:1739-51.

103. Fassas A, Anagnostopoulos A. The use of liposomal daunorubicin (DaunoXome) in acute myeloid leukemia. Leuk Lymphoma 2005; 46:795-802.

104. Blau IW, Fauser AA. Review of comparative studies between conventional and liposomal amphotericin B (Ambisome) in neutropenic patients with fever of unknown origin and patients with systemic mycosis. Mycoses 2000; 43:325-32.

105. Phuphanich S, Maria B, Braeckman R, Chamberlain M. A pharmacokinetic study of intra-CSF administered encapsulated cytarabine (DepoCyt) for the treatment of neoplastic meningitis in patients with leukemia, lymphoma, or solid tumors as part of a phase III study. J Neurooncol 2007; 81:201-8.

106. Booser DJ, Esteva FJ, Rivera E, et al. Phase II study of liposomal annamycin in the treatment of doxorubicin-resistant breast cancer. Cancer Chemother Pharmacol 2002; 50:6-8.

107. Duffaud F, Borner M, Chollet P, et al. Phase II study of OSI-211 (liposomal lurtotecan) in patients with metastatic or loco-regional recurrent squamous cell carcinoma of the head and neck. An EORTC New Drug Development Group study. Eur J Cancer 2004; 40:2748-52.

108. Fedier A, Poyet C, Perucchini D, Boulikas T, Fink D. MLH1-deficient tumor cells are resistant to lipoplatin, but retain sensitivity to lipoxal. Anticancer Drugs 2006; 17:315-23.

109. Ravaioli A, Papi M, Pasquini E, et al. Lipoplatin monotherapy: A phase II trial of second-line treatment of metastatic non-small-cell lung cancer. J Chemother 2009; 21:86-90.

110. Veal GJ, Griffin MJ, Price E, et al. A phase I study in paediatric patients to evaluate the safety and pharmacokinetics of SPI-77, a liposome encapsulated formulation of cisplatin. Br J Cancer 2001; 84:1029-35.

111. Seetharamu N, Kim E, Hochster H, Martin F, Muggia F. Phase II study of liposomal cisplatin (SPI-77) in platinum-sensitive recurrences of ovarian cancer. Anticancer Res; 30:541-5.

112. Wu H, Ramanathan RK, Strychor S, et al. Population Pharmacokinetics of PEGylated Liposomal CKD-602 (S-CKD602) in Patients with Advanced Malignancies. ASCO; 2009; 2009.

113. Rudin CM, Marshall JL, Huang CH, et al. Delivery of a liposomal c-raf-1 antisense oligonucleotide by weekly bolus dosing in patients with advanced solid tumors: a phase I study. Clin Cancer Res 2004; 10:7244-51.

114. Stathopoulos GP, Boulikas T, Kourvetaris A, Stathopoulos J. Liposomal oxaliplatin in the treatment of advanced cancer: a phase I study. Anticancer Res 2006; 26:1489-93.

115. Sangha R, Butts C. L-BLP25: a peptide vaccine strategy in non small cell lung cancer. Clin Cancer Res 2007; 13:s4652-4.

116. Hassan M, Nilsson C, Hassan Z, et al. A phase II trial of liposomal busulphan as an intravenous myeloablative agent prior to stem cell transplantation: 500 mg/m(2) as a optimal total dose for conditioning. Bone Marrow Transplant 2002; 30:833-41.

117. Nardin A, Lefebvre ML, Labroquere K, Faure O, Abastado JP. Liposomal muramyl tripeptide phosphatidylethanolamine: Targeting and activating macrophages for adjuvant treatment of osteosarcoma. Curr Cancer Drug Targets 2006; 6:123-33.

118. Meyers PA, Schwartz CL, Krailo M, et al. Osteosarcoma: a randomized, prospective trial of the addition of ifosfamide and/or muramyl tripeptide to cisplatin, doxorubicin, and high-dose methotrexate. J Clin Oncol 2005; 23:2004-11.

119. Yoo GH, Hung MC, Lopez-Berestein G, et al. Phase I trial of intratumoral liposome E1A gene therapy in patients with recurrent breast and head and neck cancer. Clin Cancer Res 2001; 7:1237-45.

120. Gabizon A, Tzemach D, Gorin J, et al. Improved therapeutic activity of folate-targeted liposomal doxorubicin in folate receptor-expressing tumor models. Cancer Chemother Pharmacol; 66:43-52.

121. Shmeeda H, Tzemach D, Mak L, Gabizon A. Her2-targeted pegylated liposomal doxorubicin: retention of target-specific binding and cytotoxicity after in vivo passage. J Control Release 2009; 136:155-60.

122. Chang DK, Lin CT, Wu CH, Wu HC. A novel peptide enhances therapeutic efficacy of liposomal anti-cancer drugs in mice models of human lung cancer. PLoS One 2009; 4:e4171.

123. Eavarone DA, Yu X, Bellamkonda RV. Targeted drug delivery to C6 glioma by transferrin-coupled liposomes. J Biomed Mater Res 2000; 51:10-4.

124. Uyama I, Kumai K, Yasuda T, et al. Improvement of therapeutic effect by using Fab' fragment in the treatment of carcinoembryonic antigen-positive human solid tumors with adriamycin-entrapped immunoliposomes. Jpn J Cancer Res 1994; 85:434-40.

125. Drummond DC, Noble CO, Guo Z, et al. Development of a highly stable and targetable nanoliposomal formulation of topotecan. J Control Release; 141:13-21.

126. Xiong XB, Huang Y, Lu WL, et al. Intracellular delivery of doxorubicin with RGD-modified sterically stabilized liposomes for an improved antitumor efficacy: in vitro and in vivo. J Pharm Sci 2005; 94:1782-93.

127. Garg A, Tisdale AW, Haidari E, Kokkoli E. Targeting colon cancer cells using PEGylated liposomes modified with a fibronectin-mimetic peptide. Int J Pharm 2009; 366:201-10.

128. Soni V, Kohli DV, Jain SK. Transferrin-conjugated liposomal system for improved delivery of 5-fluorouracil to brain. J Drug Target 2008; 16:73-8.

129. Kobayashi T, Ishida T, Okada Y, Ise S, Harashima H, Kiwada H. Effect of transferrin receptor-targeted liposomal doxorubicin in P-glycoprotein-mediated drug resistant tumor cells. Int J Pharm 2007; 329:94-102.

Table 1.1

Selected Liposomal Drugs Approved for Clinical Application or Undergoing Clinical Evaluation

Active drug	Product name	PEGylated liposome	Indication	Trial Phase	Reference
Doxorubicin	Doxil/ Caelyx	yes	Refractory ovarian cancer	Approved	(101)
Doxorubicin	Myocet	no	Metastatic breast cancer	Approved	(102)
Daunorubicin	DaunoXome	no	Advanced HIV-associated Kaposi's sarcoma	Approved	(103)
Amphotericin B	AmBisome	no	Fungal infections	Approved	(104)
Cytarabine	Depocyt	no	Lymphomatous meningitis	Approved	(105)
Annamycin	L-AN	no	Doxorubicin-resistant tumours	Phase II	(106)
Lurtotecan	NX211 OSI-211	no	Hematologic malignancies	Phase II	(107)
Cisplatin	Lipoplatin	no	Advanced non-small cell lung cancer	Phase III	(108, 109)
Cisplatin	SPI-77	yes	Ovarian cancer	Phase II	(110, 111)
CKD-602	S-CKD602	yes	Solid tumors	Phase I	(47)
CPT-11	IHL-305	yes	Solid tumors	Phase I	(112)
c-raf-1 antisense oligonucleotide	LErafAON	NA[a]	cancer	Phase I	(113)
Oxaliplatin	Lipoxal	NA[a]	cancer	Phase I	(114)
Vaccine BLP25	L-BLP25	no	Non-small cell lung cancer	Phase II	(115)
Busulphan	LBu	no	Myeloablative agent for stem cell transplantation	Phase II	(116)
MTP-PE	L-MTP-PE	no	Osteosarcoma	Phase III	(117, 118)
E1A gene	E1A gene liposome	no	Recurrent Breast and Head and Neck Cancer	Phase I	(119)

[a] Not reported.

Table 1.2

Selected Liposomal Drugs with Conjugated Ligands to Achieve Active Targeting

Active drug	Targeting ligand	Ligand class	PEGylated liposome	Reference
Doxorubicin	Folic acid	Organic compound	Yes	(120)
Doxorubicin Topotecan	Anti-Her2 (ErbB2) mAb, and ScFv fragment	Antibody	Yes	(121)
Doxorubicin	Tryptophan, threonine, and tyrosine (WTY)	Peptide	Yes	(122)
Doxorubicin	Transferrin	Glycoprotein	Yes	(123)
Doxorubicin	Anti-CEA mAb and Fab fragment	Antibody	Yes	(124)
Topotecan	Anti-EGFR mAb ScFv, and Fab	Antibody	Yes	(125)
Doxorubicin	RGD	Peptide	Yes	(126)
Doxorubicin	PRβ	Peptide	Yes	(127)
Doxorubicin	Estrone	Hormone	Yes	(39)
5-FU	Transferrin	Protein	no	(128)
Doxorubicin	Transferrin	Protein	no	(129)

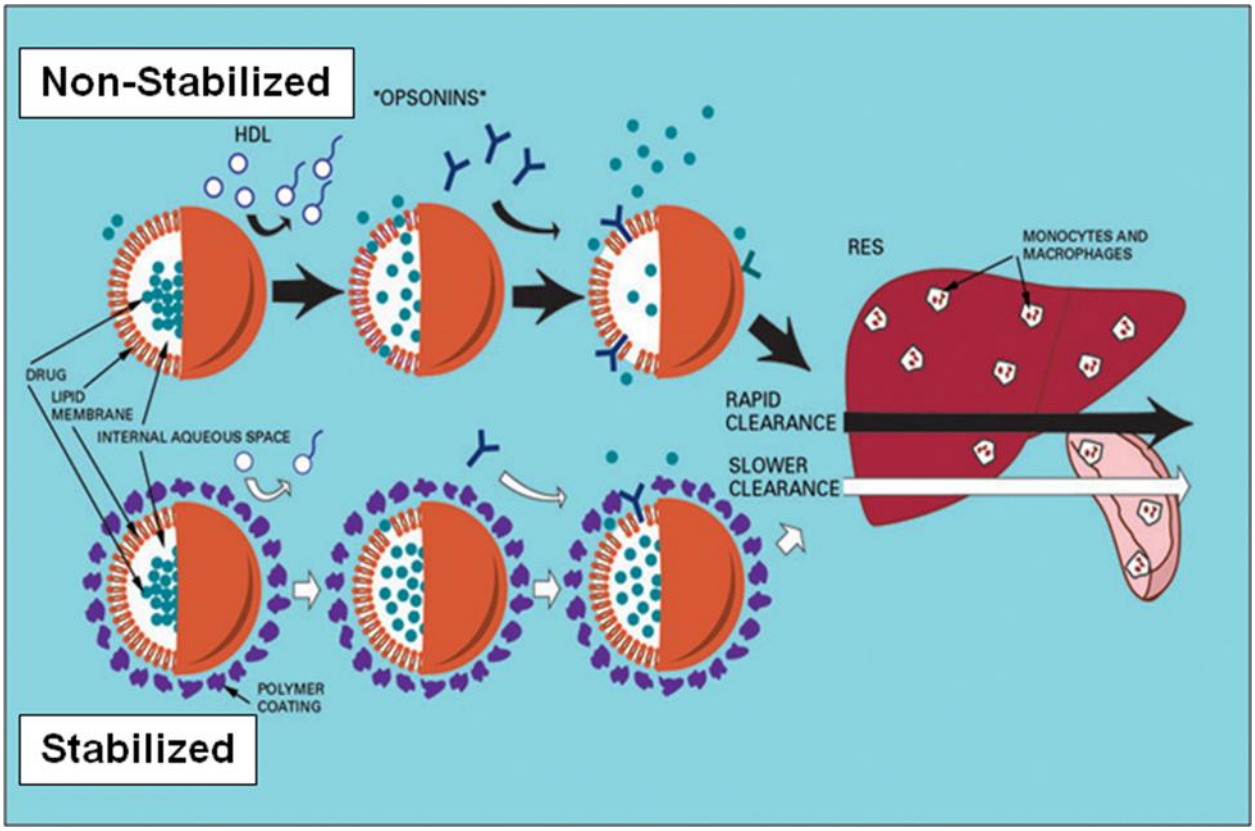

Figure 1.1. Clearance of stabilized and non-stabilized liposomes.

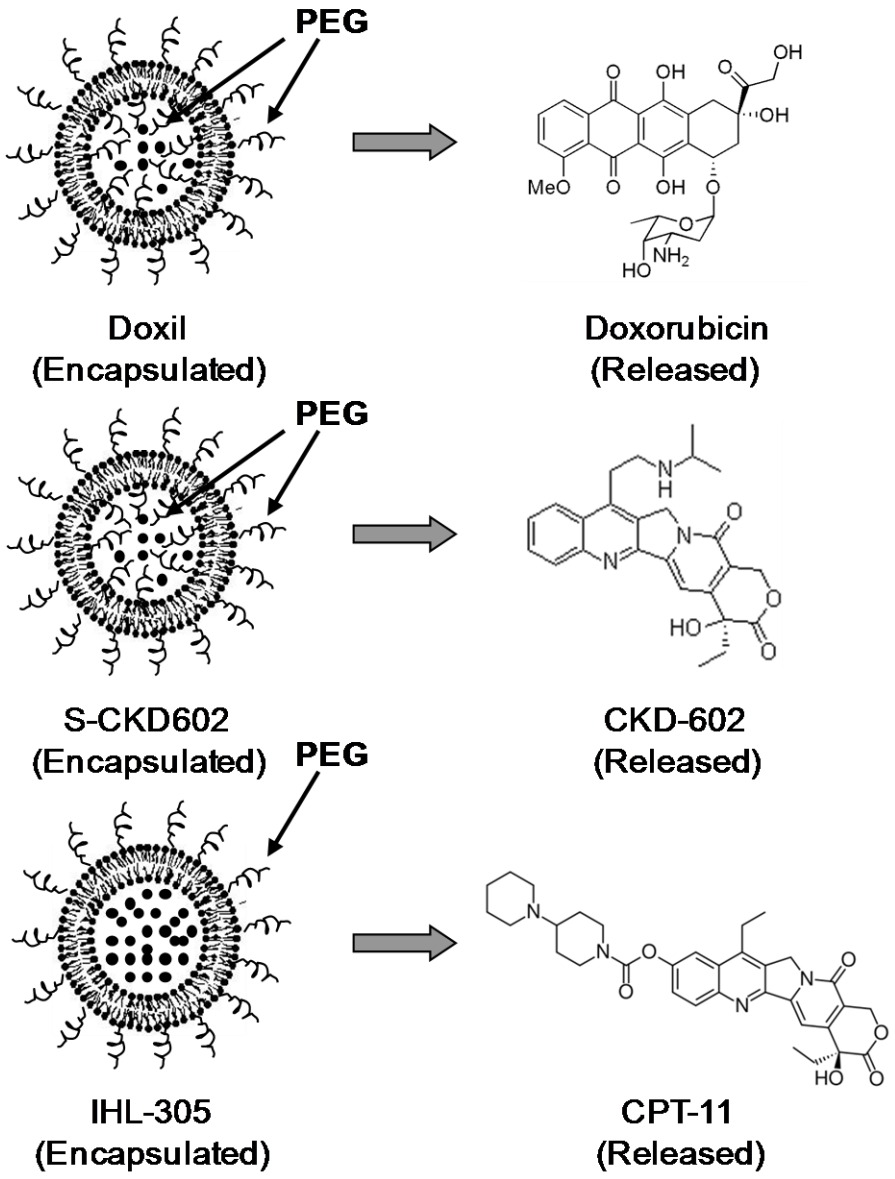

Figure 1.2. Structure of PEGylated liposomes. PEG tether are projected on both the inside and outside of liposome for Doxil and S-CKD602. PEG tether are only localized on the outside of liposome for IHL-305.

Figure 1.3a. Age vs Encapsulated AUC / Dose

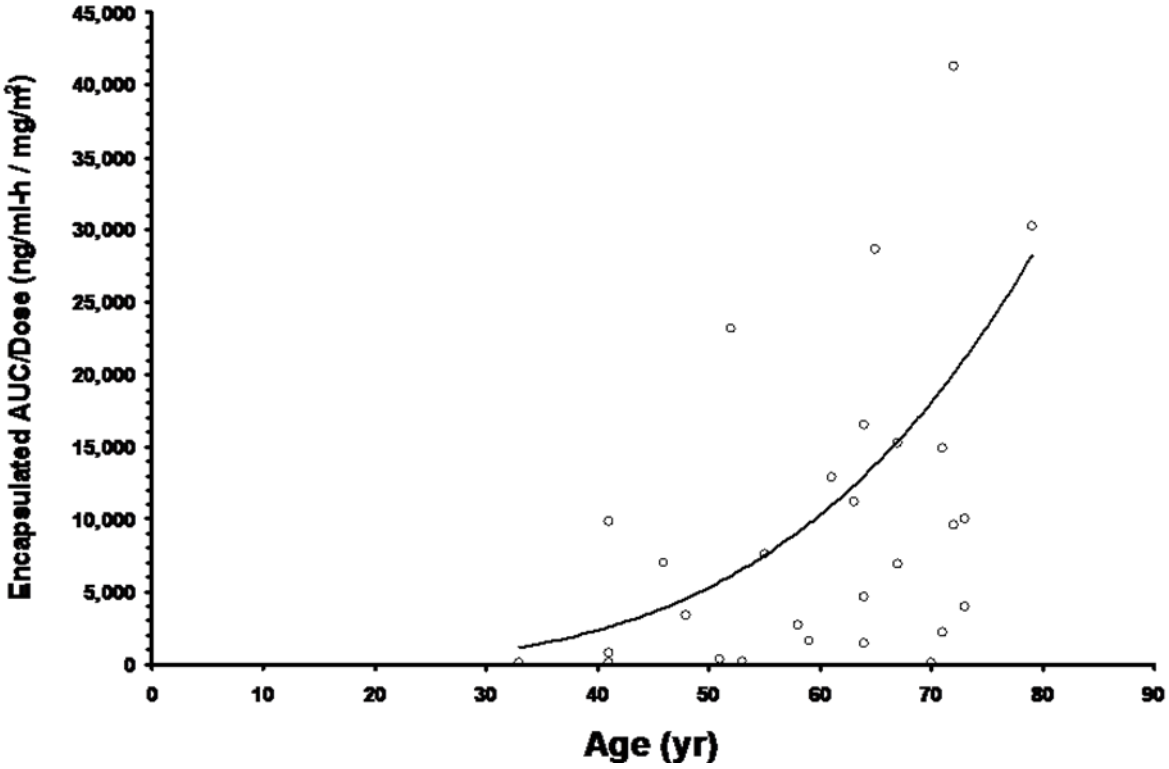

Figure 1.3b. Age vs Encapsulated AUC / Dose

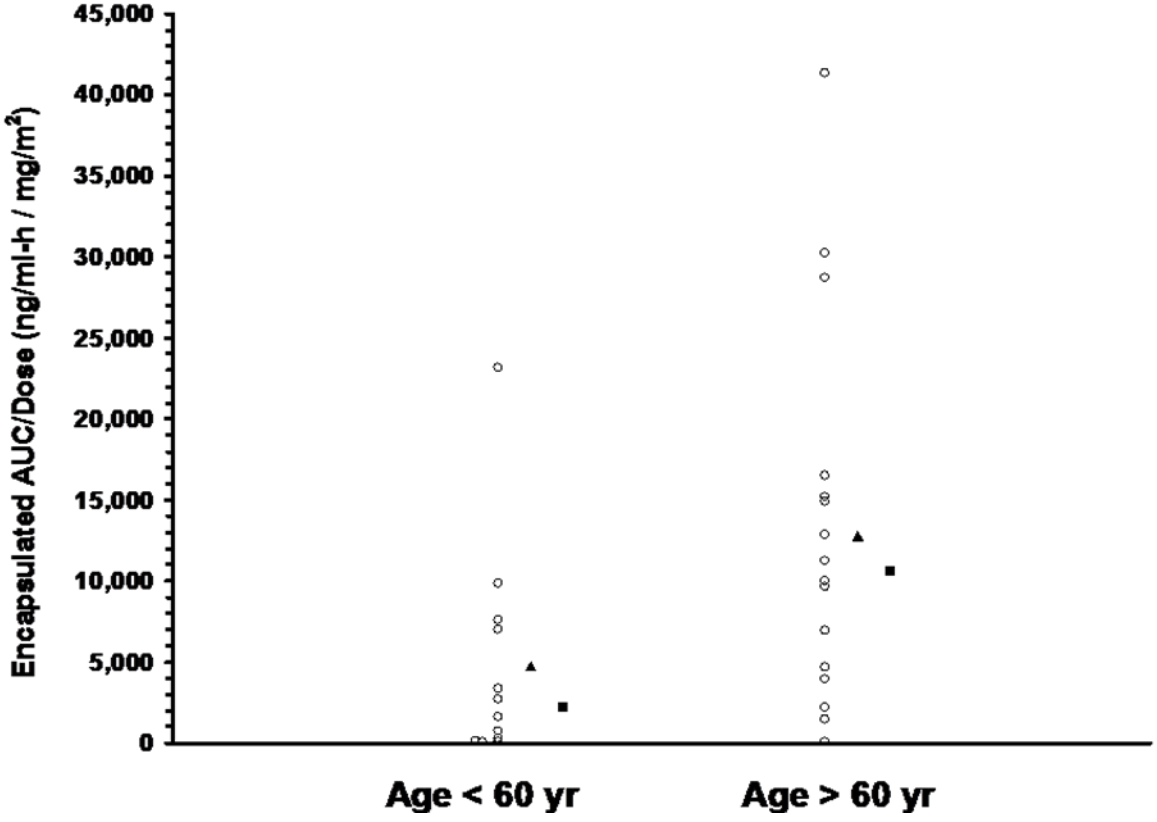

Figure 1.3a and 1.3b. The relationship between age and encapsulated CKD-602 AUC/dose after S-CKD602. **Figure 1.3a** represents the continuous relationship between age and the encapsulated CKD-602 AUC/dose. Individual patients AUC/Dose are represented by the ○. The best fit line of the data is represented by the curved-solid line ($R^2 = 0.2$). There was a statistically significant ($P = 0.01$) relationship between age and CKD-602 encapsulated AUC/dose where a high age was associated with high AUC/dose. **Figure 1.3b** represents the encapsulated CKD-602 AUC/Dose for patients < 60 and ≥ 60 years of age. Individual patients AUC/Dose are represented by the ○. The mean and median AUC/Dose for each group is represented by the ▲ and ■, respectively. Mean ± SD sum total CKD-602

AUC/dose for patients < 60 and ≥ 60 years of age were 3,941 ± 5,283 and 9,644 ± 10,876 (ng/mL)/(mg/m^2), respectively (P = 0.02; CI = 9.7, 89.4).

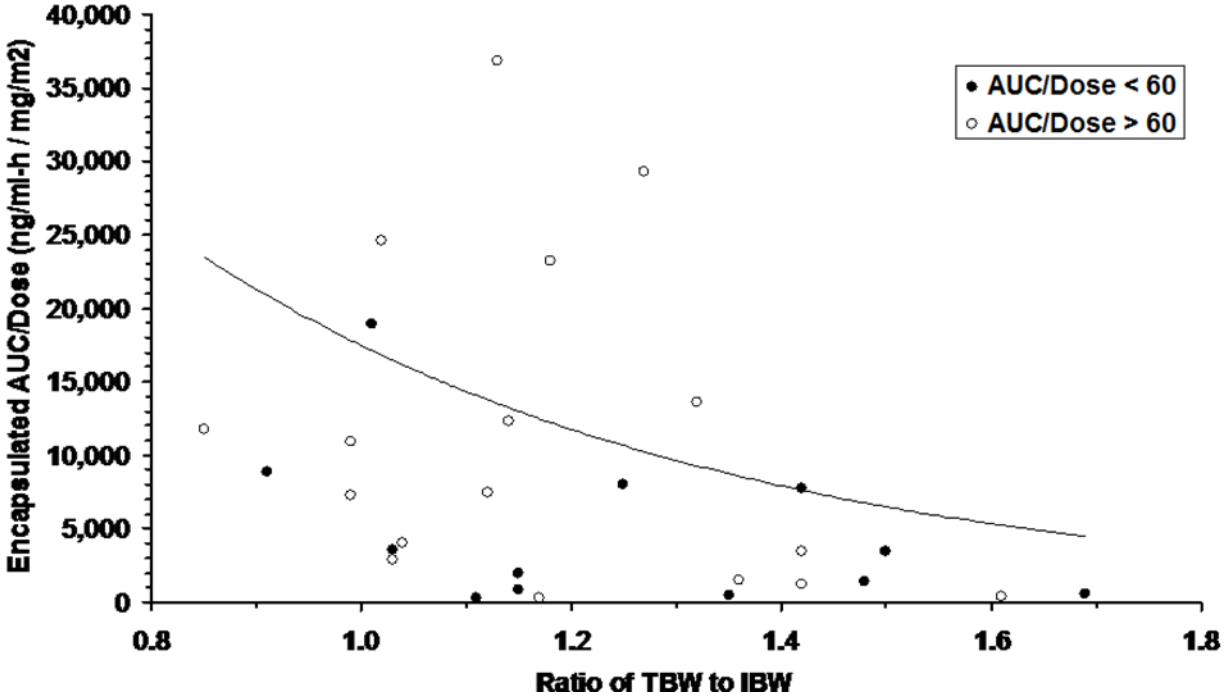

Figure 1.4. Relationship between the ratio of total body weight to ideal body weight (TBW/IBW) and S-CKD602 encapsulated AUC/dose. Encapsulated AUC/dose in patients < 60 and ≥ 60 years of age are represented by • and ○, respectively. The best fit line of the data is represented by the curved-solid line ($R^2 = 0.2$). Controlling for age, there was a statistically significant ($P = 0.02$) inverse relationship between TBW/IBW and AUC/dose where low TBW/IBW was associated with high AUC/dose in both age groups.

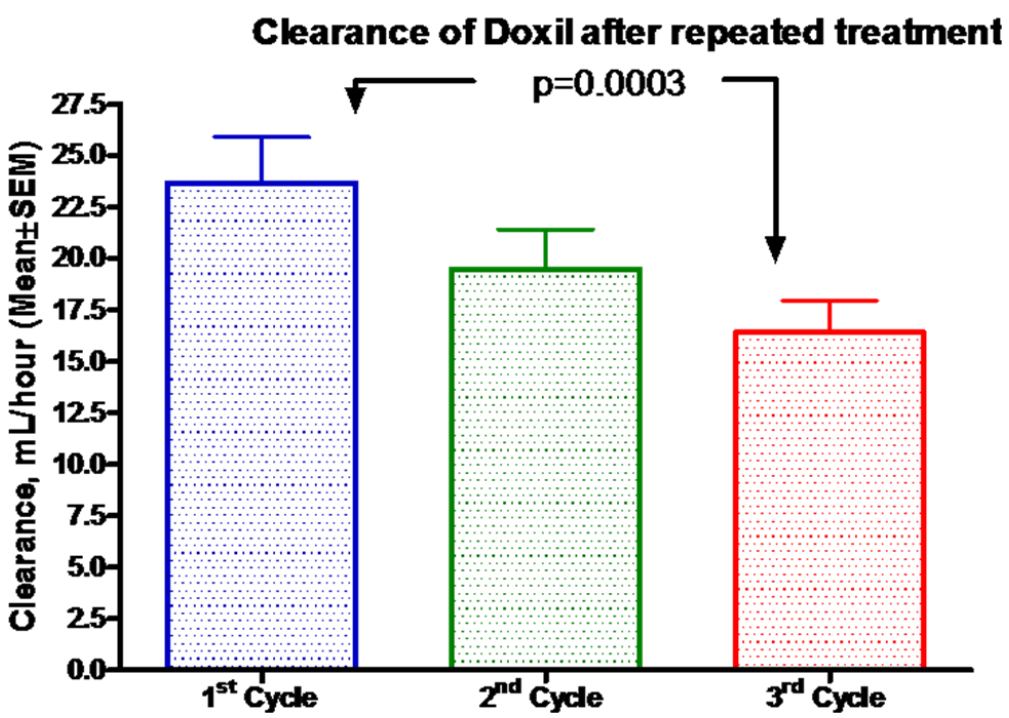

Figure 1.5. The clearance of sum total (encapsulated + released) PEGylated liposomal doxorubicin (Doxil) within patients on cycles 1, 2 and 3. There was a statistically significant reduction in the clearance of Doxil from cycle 1 to 3 ($P < 0.0003$).

CHAPTER 2

PHARMACOKINETIC (PK) STUDY OF PEGYLATED LIPOSOMAL IRINOTECAN (IHL-305) IN PATIENTS WITH ADVANCED SOLID TUMORS

A. INTRODUCTION

IHL-305 is a PEGylated liposomal formulation of irinotecan (CPT-11), a camptothecin analogue which inhibits topoisomerase I and has been approved worldwide for the treatment of metastatic colorectal cancer (1-4). The PEGylated liposomal formulation consists of phospholipids covalently bound to polyethylene glycol (PEG) on the outside of the lipid bilayer. CPT-11 is a prodrug that requires activation to the active metabolite, 7-ethyl-10-hydroxy-camptothecin (SN-38), which is approximately 100- to 1000-fold more active than the parent drug. SN-38 is further conjugated to an inactive glucuronide (SN-38G) by uridine diphosphate glucuronosyltransferases (UGTs), primarily the UGT1A1 isoform. Other identified CPT-11 metabolites are 7-ethyl-10-[4-N-(5-aminopentanoic acid)-1-piperidino]-carbonyloxycamptothecin (APC) and 7-ethyl-10-[4-amino-1-piperidino]-carbonyloxycamptothecin (NPC) (3, 5).

The development of PEGylated liposomes was based on the discovery that incorporation of methoxyPEG-lipids into liposomes yields preparations with prolonged plasma exposure and superior tumor delivery compared to conventional liposomes composed of natural phospholipids (4, 6, 7). PEGylated liposomal doxorubicin (Doxil®) is approved for the treatment of refractory ovarian cancer, Kaposi sarcoma, and multiple myeloma (8, 9). The PEGylated liposomes of Doxil and IHL-305 were made using two different methods. The PEGylated liposome of Doxil was made by adding the PEG lipid before the process of liposomal formation which results PEG tether being projected on both the inside and outside of liposome. The PEGylated liposome of IHL-305 is made by adding the PEG lipids after the process of liposomal formation which results in PEG tether only being localized on the outer leaflet (10). Encapsulation of the CPT-11 in the acidic core of a PEGylated liposome should also protect the active-lactone form of the drug from being converted to the inactive-

hydroxy acid form in the blood and allow for release of the active-lactone form into the tumor over a protracted period of time, which is ideal for a cell cycle-specific drug (1-4, 11, 12). The clearance of non-PEGylated and PEGylated liposomes is via the mononuclear phagocytotic system (MPS), which has also been called the reticuloendothelial system (RES) (4, 6, 7, 13, 14). Once the drug is released from the liposome the pharmacokinetic (PK) disposition will be the same as after administration of the non-liposomal formulation of the drug (4, 6, 7, 13, 14).

The nomenclature used to describe the PK disposition of carrier-mediated drugs includes encapsulated or conjugated (drug within or bound to the carrier), released (the active drug released from the carrier), and sum total (encapsulated or conjugated drug plus released drug). The ability to evaluate the various forms (encapsulated and released) of the drug after administration of nanosome or nanoparticle formulations is dependent upon specific sample processing methods (15). The factors affecting the PK and pharmacodynamic variability of these agents remain unclear, but most likely include the MPS. S-CKD602 is a PEGylated liposomal formulation of CKD-602, a semi-synthetic camptothecin analogue. The PK disposition of liposomal encapsulated and released CKD-602 in plasma was evaluated as part of a phase I study in patients (16). The interpatient variability in the disposition of encapsulated CKD-602 was 10-fold greater than for non-nanoparticle CKD-602. We also have reported that the PK variability of S-CKD602 was related to the age, body composition and monocyte function of patients (13, 17, 18).

Studies of the PK of IHL-305 compared to CPT-11 in mice, rats, and dogs showed a marked increase in the concentrations of CPT-11 and its metabolites in the

plasma, liver, kidney, spleen, and tumor tissue after administration of IHL-305 as compared with

non-liposomal CPT-11 administration. The plasma exposure of IHL-305 at 16.7 mg/kg IV x 1 was approximately 302-fold greater than non-liposomal CPT-11 at the same dose in tumor-bearing mice (19). In mice bearing human tumor xenografts, the exposures of CPT-11 and SN-38 in tumor were 9.0 and 3.9-fold higher and the mean residence time of CPT-11 and SN-38 in plasma was 4.4 and 4.7-fold longer for IHL-305 compared with non-liposomal CPT-11 (20). In addition, the antitumor response was greater for IHL-305 compared with non-liposomal CPT-11 (20). These results are consistent with reports that the antitumor response to camptothecin analogues is enhanced by prolonged duration of exposures in tumors (11, 12, 14, 21, 22).

We performed the first study evaluating the PK disposition of IHL-305 as part of a phase I study in patients with advanced solid tumors. The objectives of this study were to evaluate the PK disposition of sum total (encapsulated + released) and released CPT-11, and its metabolites, and evaluate the pharmacodynamics of IHL-305.

B. PATIENTS AND METHODS

Patients

Written informed consent, approved by the Institutional Review board of the Sarah Cannon Research Institute and Vanderbilt University Medical Center, was obtained from all patients prior to study entry. Patients ≥ 18 years of age with a histologically confirmed malignant solid tumor for which no effective therapy was available or a conventional therapy have failed to treat or a conventional therapy does not exist were eligible for this study. Patients must have recovered from all acute adverse effects of prior therapies, excluding alopecia. Pertinent eligibility criteria included a Eastern Cooperative Oncology Group (ECOG) performance status of 0, 1, or 2, adequate bone marrow, hepatic, and renal function as evidenced by the following: absolute neutrophil count (ANC) ≥ 1500/μL, platelets ≥ 100,000/μL, total bilirubin within normal institutional limits, aspartate aminotransferase (AST) ≤ 2.5 x institutional upper limit of normal (ULN) if liver metastases were not present and ≤ 5.0 x ULN if liver metastases were present, plasma creatinine ≤ 1.5 x the institutional ULN or creatinine clearance ≥ 60 ml/min/1.73 m^2 for patients with creatinine levels above institutional normal. Patients must have the ability to understand and the willingness to sign a written informed consent document. Patient were excluded from the study for any of the following: prior treatment with CPT-11; chemotherapy or radiotherapy within 4 weeks (6 weeks for nitrosoureas or mitomycin C); treatment with any other investigational agent during study; brain metastases; a history of allergic reactions to compounds of similar chemical composition to IHL-305; concurrent serious infections; pregnancy or breastfeeding; uncontrolled intercurrent illness including ongoing or active infection, unstable angina pectoris or psychiatric illness/social situations; significant cardiac disease including heart

failure that meets New York Heart Association (NYHA) class III and IV definitions, history of myocardial infarction within one year of study entry, uncontrolled dysrhythmias or poorly controlled angina; a history of serious ventricular arrhythmia, QTc $\geq$ 450 msec for men and 470 msec for women, or LVEF $\leq$ 40% by MUGA. Prior treatment with camptothecin analogues other than IHL-305 or CPT-11 was permitted.

Dosage and Administration

IHL-305 is a formulation of CPT-11 encapsulated in long-circulating PEGylated liposome. In IHL-305, the PEGylated liposome bilayer is composed of cholesterol and hydrogenated soybean phosphatidylcholine (HSPC), and the surface of liposomes is modified with PEG. The mean particle diameter is approximately 100 nm and the ratio of CPT-11 to lipid is 1:4. The PEGylated liposomal formulation was generated by Terumo Corporation (Tokyo, Japan). IHL-305 was supplied by Yakult Honsha Corporation in sterile 10 mL light-resistant, single-use glass vials as a translucent white to pale yellow liquid with a nominal total CPT-11 concentration of 5 mg/mL. IHL-305 was diluted 25-fold in 5% dextrose or normal saline prior to administration. Prior to administration of the study drug, patients were premedicated with ondansetron (or other 5-HT3 inhibitor should circumstances require) and dexamethasone, according to each institution's standard of care.

IHL-305 was administered IVx1 over 60 minutes every 4 weeks. Doses administrated (expressed in mg of CPT-11) were 3.5, 7, 10.5, 14, 28, 33.5, 37, 50, 67, 80, 88, 120, 160, and 210 mg/m^2. This phase I study followed a standard dose escalation design with patients enrolled in cohorts of 3, with the possibility of extending the cohort up to 6 patients depending on the number of dose-limiting toxicities (DLT) (18). No intra-patient dose

escalation was permitted. The maximum tolerated dose (MTD) was defined based on standard criteria.

Patient Assessment

Response and progression was measured by the Response Evaluation Criteria in Solid Tumors (RECIST) after receiving at least two cycles of study therapy (23). Toxicity was assessed according to the National Cancer Institute Common Terminology Criteria for Adverse Events version 3.0 (CTCAE version 3.0) and by relationship to study drug. Dose limiting toxicities (DLT) on this study were defined as treatment-related events experienced during cycle 1 for patients with UGT1A1*28 genotype (*wt/wt* and *wt/*28). Hematologic DLT's were defined as: grade 4 hematologic toxicity which lasts at least 5 days; grade 3 or 4 febrile neutropenia or grade 4 thrombocytopenia of any duration; grade 3 or greater non-hematologic toxicities (except alopecia and nausea/vomiting well-controlled with anti-emetics) irrespective of clinical significance attributed by the investigator or baseline lab values; ≥ grade 3 prolonged QTc (QTc > 500 msec) as defined in CTCAEv.3.0; any toxicity resulting in a treatment delay beyond 1 week. Complete blood counts were obtained weekly and as medically indicated. The nadir and percentage decrease at nadir for the absolute neutrophil count (ANC), platelets, red blood cells (RBC), and monocytes were estimated using standard methods (24, 25).

Sample Collection, Processing, Analytical Studies, and Pharmacokinetic Analysis

Plasma samples for PK assessment were obtained from all patients. On cycle 1, blood (5 mL) was collected in tubes containing sodium heparin at prior to administration, at

end of the infusion (approximately 1 h), and at 1.5 h, 2 h, 3 h, 5 h, 9 h, 13 h, and 25 h after the start of the infusion for patients treated at < 67 mg/m^2 and the first three patients treated at 67 mg/m^2. Additional samples at 49 h, 73 h, 97 h, 169 h (day 7), 192 h (day 8), and 216 h (day 9) after the start of the infusion were also collected for patients treated at > 67 mg/m^2 and the last three patients treated at 67 mg/m^2.

The blood samples were centrifuged at 3,000 x g for 15 min at 4ºC to separate plasma samples. Plasma samples were processed to measure sum total (encapsulated + released) CPT-11 and released CPT-11, SN-38, SN-38G, APC, and NPC as previously described (26). The sum total CPT-11, released CPT-11, SN-38, SN-38G, APC, and NPC concentrations were measured by a high-performance liquid chromatography (HPLC) as previously described (26). The total (lactone + hydroxy acid) form of camptothecin was measured for sum total CPT-11, released CPT-11, SN-38, SN-38G, and APC samples. The lower limit of quantitation (LLQ) of the total form sum total CPT-11, released CPT-11, SN-38, SN-38G, APC, and NPC were 100, 2, 2, 2, 2, and 2 ng/mL, respectively.

The area under the sum total CPT-11, released CPT-11, SN-38, SN-38G, APC, and NPC plasma concentration versus time curve from 0 to last measurable sample (AUC_{0-t}) and 0 to infinity ($AUC_{0-\infty}$) were calculated using the log trapezoidal method (27). The ratio of released CPT-11 AUC to sum total CPT-11 AUC for each patient was calculated.

Statistical Analysis

Comparisons between the nadir and percent decrease at nadir for ANC, platelets, RBC, and monocytes on cycles 1 and 2 were performed using analysis of variance (28). The statistical analysis was performed using SAS software (Cary, NC).

RESULTS

42 patients were enrolled on this study from December 14, 2006 to December 15, 2008 at Sarah Cannon Research Institute and Vanderbilt University Medical Center. All patients received at least one dose of drug and were evaluable for toxicity. A total of 112 cycles were administered. The mean (range) number of cycles administered was 2.9 (1 to 4). PK sampling was initiated in 39 patients enrolled on the study.

Pharmacokinetics

The plasma concentrations versus time profiles of sum total CPT-11, released CPT-11 and SN-38 in all patients treated with IHL-305 at the maximum tolerated dose (160 mg/m2) are presented in Figure 2.1. There was significant variability in the plasma concentrations of sum total CPT-11, released CPT-11 and SN-38. The sum total CPT-11 plasma concentrations declined monoexponentially. The maximum levels of released CPT-11 and SN-38 were observed 0 h to 72 h and 2 to 48 h after the end of infusion, respectively. The mean plasma concentrations of sum total CPT-11 was 30-fold to 600-fold higher than that of released CPT-11, whereas the mean plasma concentrations of released CPT-11 was 14-fold to 237-fold higher than that of SN-38.

The relationship between IHL-305 dose and sum total CPT-11 AUC is presented in **Figures 2.2A** . There was significant variability in the sum total CPT-11 AUC at higher dose of IHL-305 and a roughly linear relationship between dose and sum total CPT-11 AUC. At the MTD of 160 mg/m^2, there was a 2.7-fold range in sum total CPT-11 AUC.

The relationship between IHL-305 dose and released CPT-11 AUC is presented in **Figures 2.2B**. There was significant variability in the released CPT-11 AUC at each dose of

IHL-305 and a poor linear relationship between dose and released CPT-11 AUC. At the MTD of 160 mg/m^2, there was a 4.0-fold range in released CPT-11 AUC. The released CPT-11 AUCs were similar from 3.5 to 14 mg/m^2, from 37 to 50 mg/m^2, and from 120 to 160 mg/m^2. However, the mean released CPT-11 AUC increased 8.6-fold from 14 to 28 mg/m^2 and 2.0-fold from 50 to 67 mg/m^2, and 3.0-fold from 88 to 120 mg/m^2.

The relationship between IHL-305 dose and SN-38 AUC is presented in **Figures 2.2C**. There was significant variability in the SN-38 AUC at each dose of IHL-305 and a poor linear relationship between dose and SN-38 AUC. At the MTD of 160 mg/m^2, there was a 12.5-fold range in SN-38 AUC. The SN-38 AUCs were similar from 37 to 50 mg/m^2 and from 120 to 210 mg/m^2. However, the mean SN-38 AUC increased 1.5-fold from 50 to 67 mg/m^2, and 2.5-fold from from 88 to 160 mg/m^2, whereas it decreased 2.0-fold from 67 to 88 mg/m^2.

The relationship between IHL-305 dose and SN-38G AUC is presented in **Figures 2.2D**. The relationship between IHL-305 dose and APC AUC is presented in **Figures 2.2E**. There were significant variability in the SN-38G and APC AUCs at each dose of IHL-305 and a poor linear relationship between dose and SN-38G and APC AUCs. Plasma samples were also evaluated for NPC but were not detectable in most patients.

The sum total CPT-11, released CPT-11, SN-38, SN-38G, and APC AUCs at each IHL-305 dose are presented in **Table 2.1**. The sum total CPT-11 AUC was significantly greater than the released CPT-11, SN-38, SN-38G, and APC AUCs at all doses. In addition, released CPT-11 AUC was higher than SN-38G and APC AUCs; whereas, SN-38 AUC was lower than SN-38G and APC AUCs at all doses. The ratio of released CPT-11 AUC to sum

total CPT-11 AUC, SN-38 AUC to released CPT-11 AUC, SN-38G AUC to SN-38 AUC, and APC AUC to released CPT-11 AUC at each IHL-305 dose are presented in **Table 2.2**.

Pharmacodynamics

The cumulative toxicity of IHL-305 as related to ANC, platelets, red blood cells (RBC), and monocytes was evaluated. The nadir and % decrease at nadir for ANC, platelets, RBC, and monocytes are presented in **Table 2.3**. The nadir and % decrease at nadir for ANC, platelets, RBC, and monocytes were similar on cycles 1, 2, 3, and 4 ($P > 0.05$). The mean ± SD for intrapatient ratio of % decrease at nadir for ANC, platelets, RBC, and monocytes from cycle 1 to cycle 4 was 3.53 ± 4.9, 0.98 ± 2.1, 2.94 ± 6.0, and 1.04 ± 0.37, respectively.

C. DISCUSSION

Major advances in the use of liposomes, conjugates, and nanoparticles as vehicles to deliver drugs have occurred the past 10 years (4, 6, 7). PEGylated liposomal doxorubicin (Doxil®) and albumin stabilized nanoparticle formulation of paclitaxel (Abraxane®) are now FDA approved (8, 9, 29). In addition, there are greater than 100 liposomal and nanoparticle formulations of anticancer agents currently in development (4). This is the first PK study of a PEGylated-liposomal formulation of CPT-11 that evaluates the PK disposition of the released drug from a liposomal carrier. Evaluation of the PK disposition of the liposomal encapsulated verses released drug is of the utmost importance because the liposomal encapsulated drug is an inactive prodrug and thus only the released drug is active (1, 4).

The prolonged plasma exposure of released CPT-11 over 1 week after administration of IHL-305 is consistent with PEGylated liposomes and provides extended exposure compared with non-liposomal CPT-11 (1-4). The PK disposition of IHL-305 is consistent with the PEGylated concept (4, 6, 7, 13, 14). After a single dose of IHL-305 at the MTD of 160 mg/m^2, the plasma exposure of sum total CPT-11 was 252-fold higher compared with a single dose of non-liposomal CPT-11 at the MTD of 150 mg/m^2 (30). Patients treated at doses of IHL-305 $\geq$ 67 mg/m^2 had quantifiable plasma concentrations of released CPT-11 from 4 to 8 days after administration of a single dose of IHL-305. The sum total CPT-11 AUC was significantly greater than the released CPT-11 AUC at all doses. At the MTD of 160 mg/m^2, the mean ± SD ratio of released CPT-11 AUC to sum total CPT-11 AUC was 0.0065 ± 0.0036. This data suggests that most of the CPT-11 remains encapsulated in the plasma after administration of IHL-305. These results are also consistent with previous studies of IHL-305 in mice (19, 20).

The PK profiles of released CPT-11, SN-38, and SN-38G were prolonged compared with results reported for non-liposomal CPT-11. The mean ratio of SN-38 AUC to released CPT-11 AUC and APC AUC to released CPT-11 AUC after administration of IHL-305 ranged from 0.02 to 0.06 and from 0.09 to 0.55, respectively, which are similar to that after administration of non-liposomal CPT-11 (30, 31). After a single dose of IHL-305 at the MTD of 160 mg/m^2, the plasma exposure of released SN-38G was 3.5-fold higher compared with a single dose of non-liposomal CPT-11 at the MTD of 150 mg/m^2, whereas the plasma exposure of CPT-11 and SN-38 were similar to that of non-liposomal CPT-11 (30, 31). This data suggest that the PK of the released CPT-11 after administration of IHL-305 is consistent with that after administration of non-liposomal CPT-11.

The inter-patient variability in the PK disposition of sum total and released CPT-11 after administration of IHL-305 is lower than that of sum total and released CKD-602 after administration of S-CKD602. At the MTD of IHL-305 (160 mg/m^2), there was a 2.7-fold range in sum total CPT-11 AUC and 4-fold range in released CPT-11 AUC. At the MTD of of S-CKD602 (2.1 mg/m^2), there was a 13-fold range in encapsulated CKD-602 AUC and 17-fold range in released CKD-602 AUC (16). The encapsulated CKD-602 AUC was similar to the sum total AUC at all doses (16). Additionally, there is greater PK variability in released CPT-11 compared with sum total CPT-11, whereas, there is smaller PK variability in released CKD-602 compared with sum total CKD-602. The difference in the PK between IHL-305 and S-CKD602 may be related to the difference in liposomal formulations and pegylation between these two agents. There was also a poor relationship between the dose of IHL-305 and the AUC of released CPT-11. At high doses of IHL-305 the variability of sum

total CPT-11 were greater than at lower doses. The high inter-patient variability in the PK disposition of IHL-305 is consistent with other liposomal anticancer agents (5, 26-28).

The clinical significance of these differences and the factors associated with the PK variability need to be evaluated for IHL-305 and other liposomal and nanoparticle anticancer agents (4). IHL-305 exhibits all of the pharmacologic, antitumor, and cytotoxic advantages of a long acting, liposomal anticancer agent (1-4, 11, 12).

D. REFERENCE

1. Zamboni WC. Concept and clinical evaluation of carrier-mediated anticancer agents. Oncologist 2008;13: 248-60.

2. Innocenti F, Kroetz DL, Schuetz E, *et al.* Comprehensive pharmacogenetic analysis of irinotecan neutropenia and pharmacokinetics. J Clin Oncol 2009;27: 2604-14.

3. Slatter JG, Schaaf LJ, Sams JP, *et al.* Pharmacokinetics, metabolism, and excretion of irinotecan (CPT-11) following I.V. infusion of [(14)C]CPT-11 in cancer patients. Drug Metab Dispos 2000;28: 423-33.

4. Zamboni WC. Liposomal, nanoparticle, and conjugated formulations of anticancer agents. Clin Cancer Res 2005;11: 8230-4.

5. Xie R, Mathijssen RH, Sparreboom A, Verweij J, Karlsson MO. Clinical pharmacokinetics of irinotecan and its metabolites in relation with diarrhea. Clin Pharmacol Ther 2002;72: 265-75.

6. Papahadjopoulos D, Allen TM, Gabizon A, *et al.* Sterically stabilized liposomes: improvements in pharmacokinetics and antitumor therapeutic efficacy. Proc Natl Acad Sci U S A 1991;88: 11460-4.

7. Maeda H, Wu J, Sawa T, Matsumura Y, Hori K. Tumor vascular permeability and the EPR effect in macromolecular therapeutics: a review. J Control Release 2000;65: 271-84.

8. Markman M, Gordon AN, McGuire WP, Muggia FM. Liposomal anthracycline treatment for ovarian cancer. Semin Oncol 2004;31: 91-105.

9. Krown SE, Northfelt DW, Osoba D, Stewart JS. Use of liposomal anthracyclines in Kaposi's sarcoma. Semin Oncol 2004;31: 36-52.

10. Zamboni WC, Yoshino K. Formulation and physiological factors affecting the pharmacokinetics and pharmacodynamics of liposomal anticancer agents. Japan DDS 2010;25: 58-70.

11. Zamboni WC, Stewart CF, Thompson J, *et al.* Relationship between topotecan systemic exposure and tumor response in human neuroblastoma xenografts. J Natl Cancer Inst 1998;90: 505-11.

12. Stewart CF, Zamboni WC, Crom WR, *et al.* Topoisomerase I interactive drugs in children with cancer. Invest New Drugs 1996;14: 37-47.

13. Zamboni WC, Strychor S, Maruca L, *et al.* Pharmacokinetic Study of Pegylated Liposomal CKD-602 (S-CKD602) in Patients With Advanced Malignancies. Clin Pharmacol Ther 2009.

14. Zamboni WC, Strychor S, Joseph E, *et al.* Plasma, tumor, and tissue disposition of STEALTH liposomal CKD-602 (S-CKD602) and nonliposomal CKD-602 in mice bearing A375 human melanoma xenografts. Clin Cancer Res 2007;13: 7217-23.

15. Zamboni WC, Edwards RP, Mountz JM, *et al.* The Development of Liposomal and Nanoparticle Anticancer Agents: Methods to Evaluate the Encapsulated and Released Drug in Plasma and Tumor and Phenotypic Probes for Pharmacokinetic (PK) and Pharmacodynamic (PD) Disposition. In: NSTI Nanotechnology; 2007; 2007.

16. Zamboni WC, Ramalingam S, Friedland DM, *et al.* Phase I and pharmacokinetic study of pegylated liposomal CKD-602 in patients with advanced malignancies. Clin Cancer Res 2009;15: 1466-72.

17. Zamboni WC, Maruca LJ, Strychor S, *et al.* Age and body composition related-effects on the pharmacokinetic disposition of STEALH liposomal CKD-602 (S-CKD602) in patients with advanced solid tumors. In: ASCO; 2007; 2007.

18. Maruca LJ, Ramanathan RK, Strychor S, *et al.* Age-related effects on the pharmacodynamic (PD) relationship between STEALTH liposomal CKD-602 (S-CKD602) and monocytes in patients with refractory solid tumors. In: ASCO; 2007; 2007.

19. Kurita A, Furuta T, Kaneda N, al. e. Pharmacokinetics of irinotecan and its metabolites after iv administration of IHL-305, a novel pegylated liposome containing irinotecan, to tumor-bearing mice. In: the 2007 American Association for Cancer Research–National Cancer Institute–European Organization for Research and Treatment of Cancer AACR-NCI-EORTC Conference; 2007 November 2007; San Francisco, CA; 2007.

20. Takagi A, Matsuzaki T, Furuta T, al e. Antitumor activity of IHL-305, a novel pegylated liposome containing irinotecan, in human xenograft models. In: the 2007 American Association for Cancer Research–National Cancer Institute–European Organization for Research and Treatment of Cancer AACR-NCI-EORTC Conference; 2007 November 2007; San Francisco, CA; 2007.

21. Yu NY, Conway C, Pena RL, Chen JY. STEALTH liposomal CKD-602, a topoisomerase I inhibitor, improves the therapeutic index in human tumor xenograft models. Anticancer Res 2007;27: 2541-5.

22. Zamboni WC, Gajjar AJ, Mandrell TD, *et al.* A four-hour topotecan infusion achieves cytotoxic exposure throughout the neuraxis in the nonhuman primate model: implications for treatment of children with metastatic medulloblastoma. Clin Cancer Res 1998;4: 2537-44.

23. Miller AB, Hoogstraten B, Staquet M, Winkler A. Reporting results of cancer treatment. Cancer 1981;47: 207-14.

24. Rowinsky EK, Kaufmann SH, Baker SD, *et al.* A phase I and pharmacological study of topotecan infused over 30 minutes for five days in patients with refractory acute leukemia. Clin Cancer Res 1996;2: 1921-30.

25. Jung LL, Zamboni WC. Cellular, pharmacokinetic, and pharmacodynamic aspects of response to camptothecins: can we improve it? Drug Resist Updat 2001;4: 273-88.

26. Kurita A, Kaneda N. High-performance liquid chromatographic method for the simultaneous determination of the camptothecin derivative irinotecan hydrochloride, CPT-11, and its metabolites SN-38 and SN-38 glucuronide in rat plasma with a fully automated on-line solid-phase extraction system, PROSPEKT. J Chromatogr B Biomed Sci Appl 1999;724: 335-44.

27. Rowland M, Tozer T. Clinical pharmacokinetics: concepts and applications. Philadelphia: Lea and Febiger; 1989.

28. Rosner G. Fundamentals of Biostatistics. 5th Edition ed. Pacific Grove, CA: Duxbury; 2000.

29. Gradishar WJ, Tjulandin S, Davidson N, *et al.* Phase III trial of nanoparticle albumin-bound paclitaxel compared with polyethylated castor oil-based paclitaxel in women with breast cancer. J Clin Oncol 2005;23: 7794-803.

30. Rothenberg ML, Kuhn JG, Burris HA, 3rd, *et al.* Phase I and pharmacokinetic trial of weekly CPT-11. J Clin Oncol 1993;11: 2194-204.

31. Rothenberg ML, Kuhn JG, Schaaf LJ, *et al.* Phase I dose-finding and pharmacokinetic trial of irinotecan (CPT-11) administered every two weeks. Ann Oncol 2001;12: 1631-41.

Table 2.1. The Total Form of Sum total CPT-11, Released CPT-11, SN-38, SN-38G, and APC Area Under the Concentration Verses Time Curves (AUC) after Administration of IHL-305 at Each Dose

Dose (mg/m^2)	Number of Patients	Sum Total CPT-11 [a,g] AUC (μg/mL•h)	Released CPT-11 [g] AUC (μg/mL•h)	SN-38 AUC_{last} (μg/mL•h)	SN-38G AUC_{last} (μg/mL•h)	APC AUC_{last} (μg/mL•h)
3.5 [b]	1	32	0.060	N/A [e]	0.052	0.050
7.0 [b]	3	78 ± 18 (62 – 97)	0.21 ± 0.066 (0.14 – 0.27)	0.019 [h]	0.19 ± 0.18 (0.032 – 0.38)	0.083 [f] (0.070 – 0.097)
14.0 [b]	3	198 ± 34 (168 – 234)	0.43 ± 0.14 (0.34 – 0.58)	N/A [e]	0.21 ± 0.15 (0.075 – 0.38)	0.084 [f] (0.053 – 0.12)
28.0 [b]	2	403 (332 – 474)	3.69 (0.98 – 6.40)	N/A [e]	0.21 (0.18 – 0.23)	0.077 (0.072 – 0.083)
33.5 [b]	1	405	0.45	0.060	0.13	0.082
37.0 [b]	3	549 ± 118 (444 – 677)	1.74 ± 1.39 (0.77 – 3.34)	0.070 [h]	0.26 ± 0.065 (0.21 – 0.33)	0.10 ± 0.030 (0.077 – 0.14)
50.0 [b]	3	624 ± 76 (542 – 691)	1.26 ± 0.42 (1.00 – 1.75)	0.070 [i] (0.056 – 0.085)	0.30 ± 0.14 (0.21 – 0.46)	0.28 ± 0.20 (0.12 – 0.50)
67.0 [c, d]	6	767 ± 179 [c] (567 – 1,039) [c] 1,158 ± 235 [d] (944 – 1,410) [d]	2.53 ± 2.79 [c] (0.77 – 8.13) [c] 4.59 ± 1.19 [d] (3.26 – 5.53) [d]	0.078 ± 0.045 [c] (0.058 – 0.31) [c] 0.21 ± 0.095 [d] (0.12 – 0.31) [d]	0.54 ± 0.32 [c] (0.23 – 1.05) [c] 2.79 ± 2.29 [d] (1.41 – 5.44) [d]	0.32 ± 0.13 [c] (0.20 – 0.55) [c] 1.63 ± 0.70 [d] (1.22 – 2.44) [d]
80.0	2	1,698 (1,165 – 2,231)	8.69 (7.83 – 9.54)	0.16 (0.080 – 0.24)	1.67 (0.24 – 3.09)	0.79 (0.21 – 1.37)
88.0	3	1,388 ± 396 (932 – 1,644)	4.04 ± 1.79 (2.94 – 6.04)	0.10 ± 0.048 (0.061 – 0.16)	1.16 ± 0.21 (0.94 – 1.35)	0.97 ± 0.88 (0.36 – 1.98)
120.0	4	1,744 ± 738	11.93 ± 9.73	0.17 ± 0.23	3.43 ± 1.97	2.27 ± 0.93

		(936 – 2,675)	(4.27 – 25.67)	(0.047 – 0.51)	(1.67 – 5.38)	(1.45 – 3.42)
160.0	6	2,123 ± 893 (1,299 – 3,502)	12.63 ± 7.52 (6.73 – 27.45)	0.25 ± 0.22 (0.053 – 0.66)	3.90 ± 1.53 (1.70 – 5.57)	5.98 ± 7.44 (1.76 – 20.90)
210.0	2	3,488 (1,738 – 5,238)	7.93 (7.69 – 8.16)	0.16 (0.050 – 0.26)	2.56 (1.29 – 3.82)	1.07 (0.70 – 1.44)

[a] The sum total (encapsulated + released) CPT-11 AUC was based on measured concentrations in plasma and was not calculated based on adding the encapsulated + released concentrations.

[b] At dose < 67 mg/m^2, all patients had PK samples obtained from 0 to 24 hours after end of infusion. Thus, the sum total CPT-11, released CPT-11, SN-38, SN-38G, and APC AUC for these patients is from 0 to 25 h because the percent of the AUC from 0 to infinity that was extrapolated was > 15%.

[c] The first three patients at 67 mg/m^2 had PK samples obtained from 0 to 24 hours after end of infusion and the percent of the AUC from 0 to infinity that was extrapolated was > 15%. So the AUCs from 0 to 25 h of sum total CPT-11, released CPT-11, SN-38, SN-38G, and APC for all the six patients in this dose group were calculated.

[d] The last three patients at 67 mg/m^2 had PK samples obtained from 0 to 192 hours after end of infusion. Thus, the sum total CPT-11, released CPT-11, SN-38, SN-38G, and APC AUC for these patients is from 0 to infinity.

[e] Every patient in each dose level treated at 3.5, 14, and 28 mg/m^2 had no quantifiable concentrations of SN-38.

[f] One patient in each dose level treated at 7.0 and 14.0 mg/m^2 had no quantifiable concentrations of SN-38G.

[g] The total (lactone + hydroxyl acid) form of sum total (encapsulated + released) and released CPT-11 AUCs are presented.

[h] Two patients in each dose level treated at 7.0 and 37.0 mg/m^2 had no quantifiable concentrations of SN-38.

[i] One patient at 50 mg/m^2 had 1 quantifiable concentrations of SN-38 and thus an accurate SN-38 AUC could not be calculated for this patient.

Table 2.2. The Ratio of Released CPT-11 AUC to Sum Total CPT-11 AUC, SN-38 AUC to Released CPT-11 AUC, SN-38G AUC to SN-38 AUC, and APC AUC to Released CPT-11 AUC after Administration of IHL-305 at Each Dose

Dose (mg/m2)	Number of Patients	Ratio Released CPT-11 AUC to Sum total CPT-11 AUC [a,e]	Ratio SN-38 AUC to Released CPT-11 AUC [b,e]	Ratio SN-38G AUC to SN-38 AUC [b,e]	Ratio APC AUC to Released CPT-11 AUC [b,e]
3.5	1	0.0019	N/A	N/A	0.83
7.0	3	0.0027 ± 0.0007 (0.0022 – 0.0036)	0.072	1.65	0.46 (0.42 – 0.50)
14.0	3	0.0023 ± 0.0011 (0.0015 – 0.0035)	N/A	N/A	0.24 (0.15 – 0.34)
28.0	2	0.0082 (0.0030 – 0.014)	N/A	N/A	0.048 (0.011 – 0.085)
33.5	1	0.0011	0.13	2.13	0.18
37.0	3	0.0029 ± 0.0017 (0.0017 – 0.0049)	0.021	3.49	0.092 ± 0.077 (0.030– 0.18)
50.0	3	0.0021 ± 0.0010 (0.0014 – 0.0032)	0.057 (0.032 – 0.082)	4.58 (3.74 – 5.42)	0.25 ± 0.21 (0.071 – 0.48)
67.0 [c,d]	6	0.0031 ± 0.0029 [c] (0.0013 – 0.0087) [c] 0.0040 ± 0.0008 [d] (0.0034 – 0.0049) [d]	0.038 ± 0.020 [c] (0.019 – 0.073) [c] 0.049 ± 0.018 [d] (0.035 – 0.069) [d]	8.17 ± 3.60 [c] (5.00 – 14.12) [c] 12.42 ± 4.77 [d] (8.14 – 17.56) [d]	0.19 ± 0.078 [c] (0.067 – 0.25) [c] 0.40 ± 0.16 [d] (0.22 – 0.54) [d]
80.0	2	0.0055 (0.0043 – 0.0067)	0.018 (0.011 – 0.026)	7.92 (3.02 – 12.82)	0.087 (0.028 – 0.14)
88.0	3	0.0030 ± 0.0010 (0.0018 – 0.0037)	0.027 ± 0.0068 (0.020 – 0.034)	13.48 ± 6.91 (6.05 – 19.73)	0.32 ± 0.35 (0.061 – 0.72)

120.0	4	0.010 ± 0.012 (0.0016 – 0.027)	0.018 ± 0.018 (0.0022 – 0.044)	38.69 ± 31.86 (10.45 – 83.93)	0.25 ± 0.094 (0.13 – 0.35)
160.0	6	0.0065 ± 0.0036 (0.0026 – 0.0124)	0.023 ± 0.025 (0.0091 – 0.073)	23.17 ± 10.56 (5.37 – 34.46)	0.55 ± 0.72 (0.21 – 2.01)
210.0	2	0.0030 (0.0016 – 0.0044)	0.022 (0.0071 – 0.036)	40.44 (4.93 – 75.95)	0.15 (0.097 – 0.20)

[a] The ratio of released CPT-11 AUC to sum total CPT-11 AUC was calculated as released CPT-11 AUC from 0 to 25 h divided by sum total CPT-11 AUC from 0 to 25 h for dose lower than 67 mg/m^2 and released CPT-11 AUC from 0 to infinity divided by sum total CPT-11 AUC from 0 to infinity for dose higher than 67 mg/m^2.

[b] The ratios of SN-38 AUC to released CPT-11 AUC, SN-38G AUC to SN-38 AUC, and APC AUC to released CPT-11 AUC were calculated based on AUC from 0 to 25 h for dose lower than 67 mg/m^2 and from 0 to 193 h for dose higher than 67 mg/m^2.

[c] The first three patients at 67 mg/m^2 had PK samples obtained from 0 to 24 hours after end of infusion and the percent of the AUC from 0 to infinity that was extrapolated was > 15%. So the ratios of released CPT-11 AUC to sum total CPT-11 AUC, SN-38 AUC to released CPT-11 AUC, SN-38G AUC to SN-38 AUC, and APC AUC to released CPT-11 AUC were calculated based on AUC from 0 to 25 h for all the six patients in this dose group.

[d] The last three patients at 67 mg/m^2 had PK samples obtained from 0 to 192 hours after end of infusion. Thus, the ratio of SN-38 AUC to released CPT-11 AUC, SN-38G AUC to SN-38 AUC, and APC AUC to released CPT-11 AUC for these patients were calculated based on AUC from 0 to 193 h and from 0 to infinity for the ratio of released CPT-11 AUC to sum total CPT-11 AUC,.

[e] The ratios of released CPT-11 AUC to sum total CPT-11 AUC, SN-38 AUC to released CPT-11 AUC, SN-38G AUC to SN-38 AUC, and APC AUC to released CPT-11 AUC were calculated for individual patient values and not the mean of the cohort.

Table 2.3. The Nadir and Percentage Decrease at Nadir in ANC, Platelets, RBC, and Monocytes on Cycles 1, 2, 3, and 4

	Cycle 1		**Cycle 2**		**Cycle 3**		**Cycle 4**	
Blood Cells	% Decrease Mean ± SD (Range) [n = 42]	Nadir (cells x $10^3/\mu L$) Mean ± SD (Range) [n = 42]	% Decrease Mean ± SD (Range) [n = 32]	Nadir (cells x $10^3/\mu L$) Mean ± SD (Range) [n = 32]	% Decrease Mean ± SD (Range) [n = 19]	Nadir (cells x $10^3/\mu L$) Mean ± SD (Range) [n = 19]	% Decrease Mean ± SD (Range) [n = 19]	Nadir (cells x $10^3/\mu L$) Mean ± SD (Range) [n = 19]
ANC	28.8 ± 20.3 (0.0 – 84.8)	3.9 ± 1.7 (1.3 – 8.0)	19.4 ± 20.6 (0.0 – 64.0)	3.2 ± 1.4 (0.8 – 7.3)	27.8 ± 21.8 (0.0 – 68.2)	3.2 ± 1.6 (0.8 – 7.2)	22.4 ± 22.8 (0.0 – 87.7)	3.6 ± 1.7 (0.3 – 6.7)
Platelets	17.3 ± 19.8 (0.0 – 74.1)	252.6 ± 97.9 (88.8 – 518.0)	12.7 ± 20.1 (0.0 – 81.6)	239.2 ± 100.2 (47.6 – 567.0)	10.7 ± 9.3 (0.0 – 27.3)	239.4 ± 80.5 (115 – 388)	16.6 ± 22.0 (0.0 – 82.3)	237.7 ± 99.1 (35.8 – 375.0)
RBC	9.2 ± 6.2 (0.0 – 25.6)	3.8 ± 0.53 (2.6 – 4.7)	6.8 ± 5.6 (0.0 – 18.6)	3.7 ± .58 (2.7 – 4.7)	5.0 ± 4.6 (0.0 – 17.7)	4.1 ± .42 (3.1 – 4.8)	5.7 ± 4.2 (0.0 – 12.7)	3.9 ± .47 (3.0 – 4.8)
Mono	42.0 ± 23.9 (0.0 – 80.1)	0.45 ± 0.35 (0.08 - 1.89)	38.9 ± 25.8 (0.0 – 97.9)	0.36 ± .17 (0.02 - 0.88)	36.9 ± 28.6 (0.0 – 99.1)	0.33 ± .14 (0.01 - 0.52)	40.0 ± 21.5 (4.26 – 81.6)	0.36 ± .12 (0.16 - 0.54)

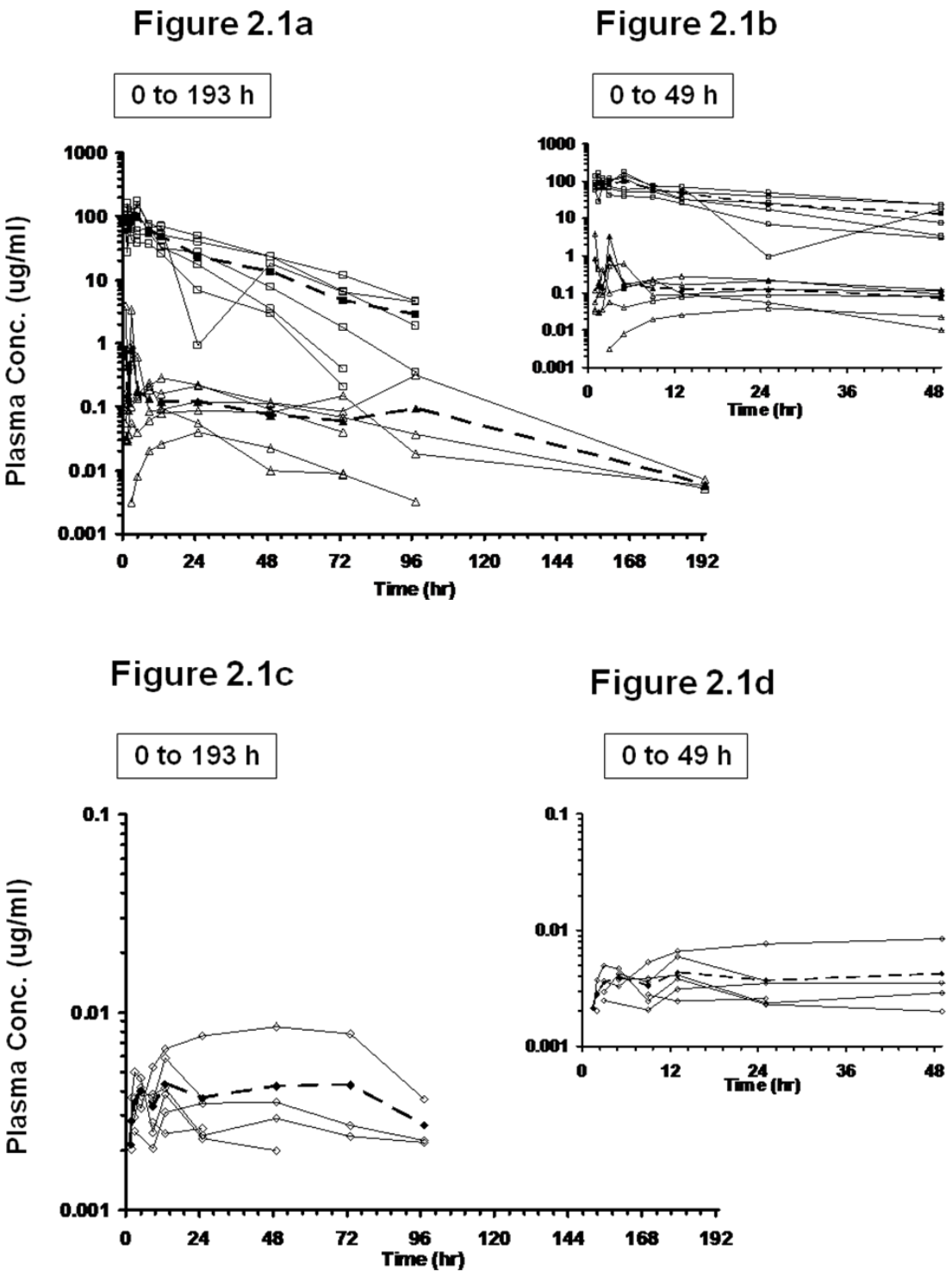

Figure 2.1a, 2.1b, 2.1c, and 2.1d. Concentrations versus time profiles of sum total CPT-11, released CPT-11 and SN-38 in all patients treated with IHL-305 at the maximum tolerated

dose (160 mg/m^2). Figure 2.1a and 2.1c represent the concentration versus time profile from 0 to 193 hour. Figure 2.1b and 2.1d represent the concentration versus time profile from 0 to 49 hour. The sum total (□,—) and released (Δ,—) CPT-11 concentrations for each patient and the average sum total (■, ----) and released (▲,----) CPT-11 concentrations are presented. The SN-38 (◊,—) for each patient and the average SN-38 (♦, ----) concentrations are presented. The average sum total CPT-11, released CPT-11, and SN-38 AUCs were 2,123, 12.63, and 0.25 μg/mL•h, respectively.

Figure 2.2A

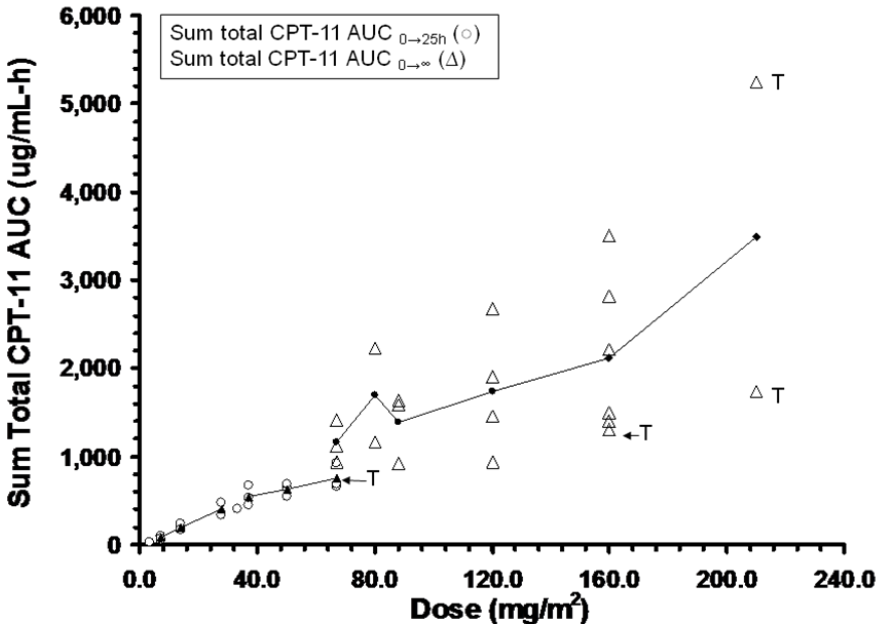

Figure 2.2B

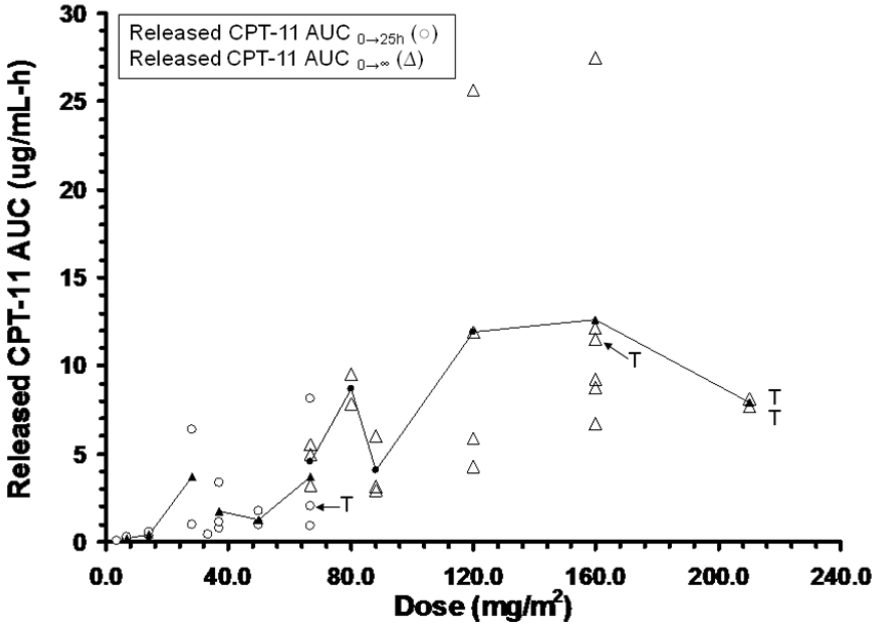

Figure 2.2C

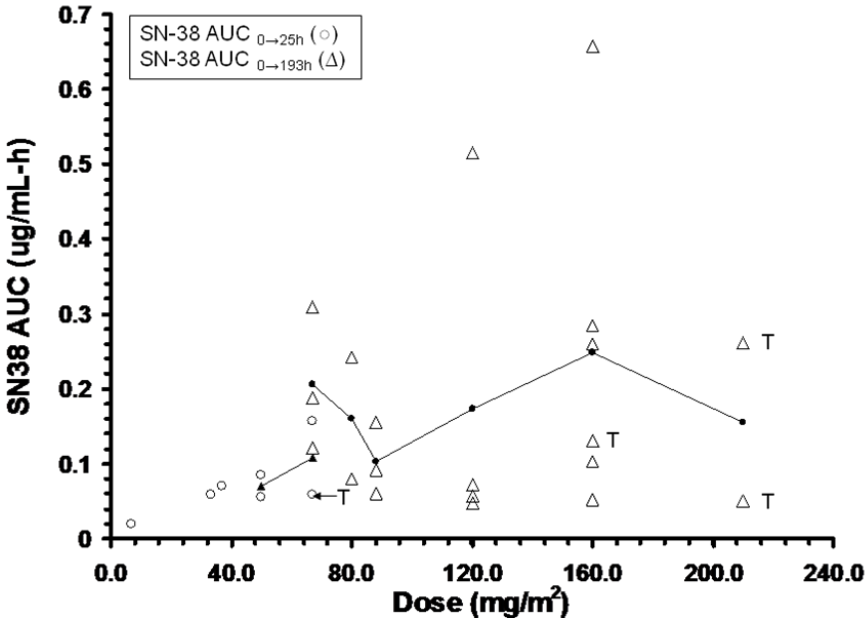

Figure 2.2D

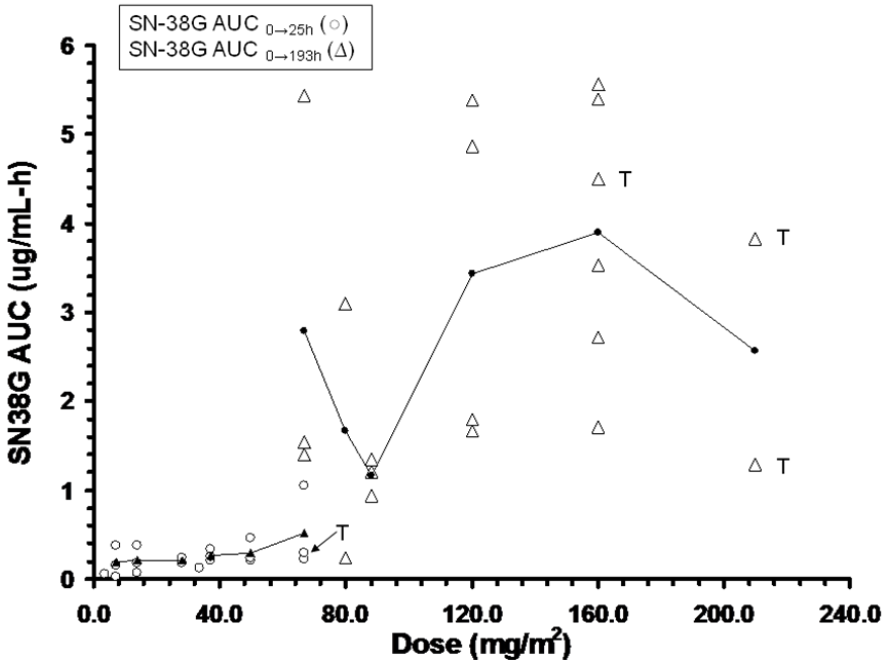

Figure 2.2E

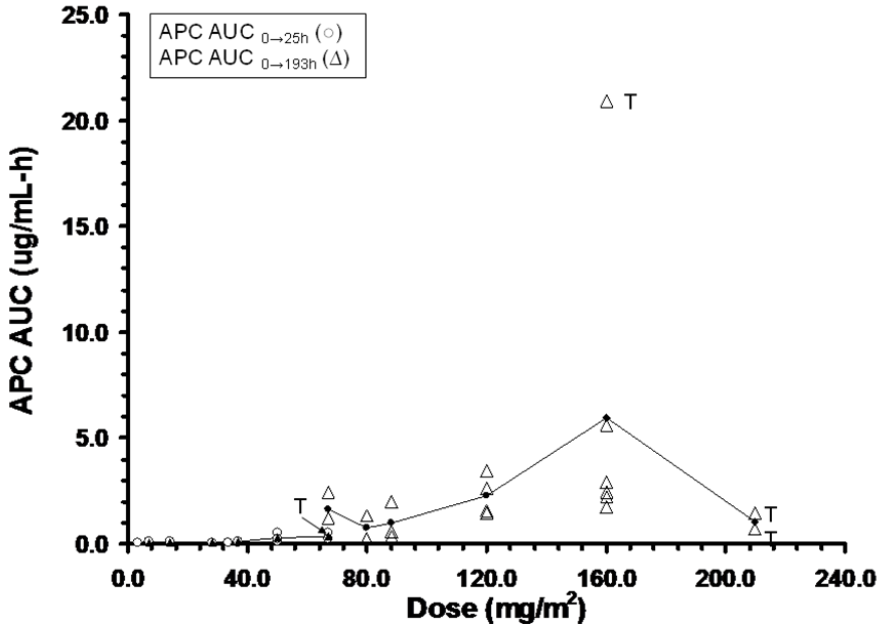

Figure 2.2A, 2.2B, 2.2C, 2.2D, and 2.2E. Relationship between dose of IHL-305 and AUC of sum total CPT-11, released CPT-11, SN-38, SN-38G, and APC. Figures 2.2A, 2.2B, 2.2C, 2.2D, and 2E represent the AUC of sum total CPT-11, released CPT-11, SN-38, SN-38G, and APC, respectively. IHL-305 was administered at 3.5, 7, 10.5, 14, 28, 33.5, 37, 50, 67, 80, 88, 120, 160, and 210 mg/m2. The patients with DLT are represented by the T. The AUC for patients treated at dose of 3.5 to 50 mg/m^2 was calculated from 0 to 25 h and for patients treated at dose of 80 to 210 mg/m^2 was calculated from 0 to 193 h. The AUC for the first three patients treated at dose of 67 mg/m^2 was calculated from 0 to 25 h and for the last three patients treated at dose of 67 mg/m^2 was calculated from 0 to 193 h.

CHAPTER 3

FACTORS AFFECTING THE PHARMACOKINETICS (PK) AND PHARMACODYNAMICS (PD) OF PEGYLATED LIPOSOMAL IRINOTECAN (IHL-305) IN PATIENTS WITH ADVANCED SOLID TUMORS

A. INTRODUCTION

IHL-305 is a PEGylated liposomal formulation of irinotecan (CPT-11), a camptothecin analogue which inhibits topoisomerase I and has been approved for the treatment of metastatic colorectal cancer (1-4). The PEGylated liposomal formulation consists of phospholipids covalently bound to polyethylene glycol (PEG) only on the outside of the lipid bilayer. CPT-11 is a prodrug that requires activation to the active metabolite, 7-ethyl-10-hydroxy-camptothecin (SN-38), which is approximately 100- to 1000-fold more active than the parent drug. SN-38 is further conjugated to form an inactive glucuronide (SN-38G) by uridine diphosphate glucuronosyltransferases (UGTs), primarily the UGT1A1 isoform. Other identified CPT-11 metabolites are 7-ethyl-10-[4-N-(5-aminopentanoic acid)-1-piperidino]-carbonyloxycamptothecin (APC) and 7-ethyl-10-[4-amino-1-piperidino]-carbonyloxycamptothecin (NPC) (3, 5).

The development of PEGylated liposomes, such as PEGylated liposomal doxorubicin (Doxil), CKD-602 (S-CKD602), and CPT-11 (IHL-305) was based on the discovery that incorporation of PEG-lipids into liposomes yields preparations with prolonged plasma exposure and superior tumor delivery compared to conventional liposomes composed of natural phospholipids (4, 6, 7). Doxil® is approved for the treatment of refractory ovarian cancer, Kaposi sarcoma, and multiple myeloma (8, 9). The PEGylated liposomes of Doxil and IHL-305 were made using two different methods. The PEGylated liposome of Doxil was made by adding the PEG lipid before the process of liposomal formation which results PEG tether being projected on both the inside and outside of liposome. The PEGylated liposome of IHL-305 is made by adding the PEG lipids after the process of liposomal formation which results in PEG tether only being localized on the outer leaflet (10). Encapsulation of the CPT-

11 allow for release of the active-lactone form into the tumor over a protracted period of time, which is ideal for a cell cycle-specific drug (1-4, 11, 12).

The pharmacokinetic (PK) disposition of carrier-mediated agents, such as, nanoparticles, nanosomes, and conjugated agents, is dependent upon the carrier until the drug is released from the carrier. Unlike traditional anticancer agents which are cleared by the liver and kidneys, the clearance of non-PEGylated and PEGylated liposomes is via the mononuclear phagocytic system, which has also been called the reticuloendothelial system (RES) which include monocytes, macrophages and dendritic cells located primarily in the liver and spleen (13). Uptake by the MPS usually results in sequestering of the encapsulated drug in the MPS, where it can be degraded. In addition, the uptake of the liposomes by the MPS may result in acute impairment of the MPS and toxicity. PEGylated liposomes are cleared much slower via MPS compared to non-PEGylated liposomes (6). Once the drug is released from the carrier, the PK disposition of the drug will be the same as after administration of the non-carrier form of the drug (4, 13). Thus, the PK of liposomes are complex.

The nomenclature used to describe the PK disposition of carrier-mediated drugs includes encapsulated or conjugated (drug within or bound to the carrier), released (the active drug released from the carrier), and sum total (encapsulated or conjugated drug plus released drug). The ability to evaluate the various forms (encapsulated and released) of the drug after administration of nanosome or nanoparticle formulations is dependent upon specific sample processing methods (14). The drug that remains encapsulated within nanosomes or nanoparticles, or linked to a conjugate or polymer is an inactive prodrug, thus the drug must be released from the carrier to be active.

Nanoparticle agents have higher variability in PK (drug clearance, systemic exposure, distribution, etc.) disposition with potentially higher variability in pharmacodynamic (PD) (antitumor response and toxicity) disposition as compared with traditional small molecule chemotherapy. However, the factors affecting the PK and pharmacodynamic variability of encapsulated and released forms of conventional and PEGylated liposomes remain unclear, but most likely include the MPS (1). We have evaluated factors affecting the PK and PD of liposomal anticancer agents. We were the first to report a reduced clearance of the liposomal encapsulated forms of Doxil and S-CKD602 in patients ≥ 60 years of age (15, 16). We have also reported that patients with a lean body composition may have a reduced tissue distribution and an increased plasma exposure of S-CKD602. In addition, we have reported an age related decrease in the function of monocytes which may be associated with a reduced clearance of liposomes and reduced cytotoxicity to the monocytes (17, 18).

The clinical results of the phase I study and limited PK results were previously published (19). IHL-305 was associated with higher interpatient variability in the PK disposition of sum total (encapsulated + released) and released CPT-11 (19). The objectives of this study were to evaluate the factors associated with the inter-patient variability in the PK and PD of IHL-305 in patients with advanced solid tumors.

B. PATIENTS AND METHODS

Patients

Written informed consent, approved by the Institutional Review board of the Sarah Cannon Research Institute and Vanderbilt University Medical Center, was obtained from all patients prior to study entry. All other eligibility criteria were previously reported.

Dosage and Administration

IHL-305 is a formulation of CPT-11 encapsulated in long-circulating PEGylated liposome. In IHL-305, the PEGylated liposome bilayer is composed of cholesterol and hydrogenated soybean phosphatidylcholine (HSPC), and the surface of liposomes is modified with PEG. The mean particle diameter is approximately 100 nm and the ratio of CPT-11 to lipid is 1:4. The PEGylated liposomal formulation was generated by Terumo Corporation (Tokyo, Japan). IHL-305 was supplied by Yakult Honsha Corporation in sterile 10 mL light-resistant, single-use glass vials as a translucent white to pale yellow liquid with a nominal total CPT-11 concentration of 5 mg/mL. IHL-305 was diluted 25-fold in 5% dextrose or normal saline prior to administration. Prior to administration of the study drug, patients were premedicated with ondansetron (or other 5-HT3 inhibitor should circumstances require) and dexamethasone, according to each institution's standard of care.

IHL-305 was administered IVx1 over 60 minutes every 4 weeks. Doses administrated (expressed in mg of CPT-11) were 3.5, 7, 10.5, 14, 28, 33.5, 37, 50, 67, 80, 88, 120, 160, and 210 mg/m^2. This phase I study followed a standard dose escalation design with patients enrolled in cohorts of 3, with the possibility of extending the cohort up to 6 patients depending on the number of dose-limiting toxicities (DLT) (18). No intra-patient dose escalation was permitted. The MTD was defined based on standard criteria.

Blood Counts

ANC and monocyte counts were obtained at least once per week on cycle 1 of the IHL-305 study. Additional counts were obtained as clinically required. The % decrease in ANC and monocytes at nadir was calculated using the standard formula [(Pre value – nadir) / Pre-value] x 100.

Sample Collection, Processing and Analytical Studies

Plasma samples for PK assessment were obtained from all patients. On cycle 1, blood (5 mL) was collected in tubes containing sodium heparin at prior to administration, at end of the infusion (approximately 1 h), and at 1.5 h, 2 h, 3 h, 5 h, 9 h, 13 h, and 25 h after the start of the infusion for patients treated at < 67 mg/m^2 and the first three patients treated at 67 mg/m^2. Additional samples at 49 h, 73 h, 97 h, 169 h (day 7), 192 h (day 8), and 216 h (day 9) after the start of the infusion were also collected for patients treated at > 67 mg/m^2 and the last three patients treated at 67 mg/m^2.

The blood samples were centrifuged at 3,000 x g for 15 min at 4ºC to separate plasma samples. Plasma samples were processed to measure sum total (encapsulated + released) CPT-11 and released CPT-11, SN-38, SN-38G, APC, and NPC as previously described (20). The sum total CPT-11, released CPT-11, SN-38, SN-38G, APC, and NPC concentrations were measured by a high-performance liquid chromatography (HPLC) as previously described (20). The total (lactone + hydroxy acid) form of camptothecin was measured for sum total CPT-11, released CPT-11, SN-38, SN-38G, and APC samples. The lower limit of

quantitation (LLQ) of the total form sum total CPT-11, released CPT-11, SN-38, SN-38G, APC, and NPC were 100, 2, 2, 2, 2, and 2 ng/mL, respectively.

Compartmental Pharmacokinetic Analysis

Compartmental PK analysis of sum total CPT-11 after administration of IHL-305 was performed using WinNonlin (version 5.0.1; Pharsight Corp., Mountain View, Calif.) (21). Different PK model structures were considered to characterize the disposition of IHL-305 in plasma. In the model development, one- and two-compartment models with linear and non-linear (Michaelis-Menten) clearance were evaluated to describe the plasma disposition of IHL-305. The final model structure used for the PK analysis produced identifiable parameters in all patients except one patient.

PK model parameters for sum total CPT-11 after administration of IHL-305 included the volume of the central compartment (V_c) and intercompartment rate constants, (k_{12}, k_{21}) (21). The elimination rate constant from the central compartment (k_{10}) was used to represent linear clearance. For the non-linear clearance, the maximum rate (velocity, V_{max}) and a Michaelis constant (Km) were estimated using the standard Michaelis Menten Equation described below where X_1 represents the amount remaining.

$$\frac{dX_1}{dt} = -\frac{V_{max} \bullet X_1}{K_m \bullet V_1 + X_1}$$

Using standard equations, clearance (CL) and elimination half life ($t_{1/2}$) were calculated using parameter estimates from the models. The area under the IHL-305 plasma concentration versus time curve from 0 to infinity ($AUC_{0-\infty}$) were calculated using the log

trapezoidal method by simulating the concentration versus time data from each patient using patient-specific parameters (21). The AUC was also normalized by dose (AUC/Dose).

The evaluation of the goodness of fit and the estimated parameters was based on the Akaike information criterion, the precision of the parameter estimates, the random distribution of weighted residuals between measured and predicted concentrations with respect to time, and the absence of a significant correlation between independent model parameters (<0.95) (21).

Evaluation of the Factors

The patient's age, gender, the ratio of total body weight to ideal body weight (TBW/IBW), and % decrease in monocytes at nadir were evaluated as potential factors associated with the PK variability of IHL-305. The ratio of total body weight to ideal body weight (TBW/IBW) was calculated using standard equations and was used as measure of body composition. These same factors were evaluated as a potential factor associated with the PD variability of IHL-305.

Statistical Analysis

The relationship between TBW/IBW and AUC/Dose was analyzed using multiple linear regressions controlling for age. The relationship between clearance and the % decrease in monocytes was analyzed using simple linear regression. The relationship between dose normalized sum total CPT-11 AUC and the % decrease in monocytes was analyzed using simple linear regression. The relationship between the % decrease in monocytes and age was analyzed using multiple linear regressions controlling for dose. The % decrease in

monocytes and ANC at nadir within a patient were compared using the Wilcoxon signed ranked test. The % decrease in monocytes and ANC at nadir in patients < 60 and ≥ 60 years of age were compared using the Two Sample T-test. The influence of gender on PK values was assessed using Two Sample T-test and ANCOVA by incorporating body surface area as a covariate. The statistical analysis was performed using SAS software (Cary, NC) (22).

C. RESULTS

Patient Characteristics

Patient characteristics were described previously (19). 42 patients were enrolled on this study from 14 December 2006 to 15 December 2008 at Sarah Cannon Research Institute and Vanderbilt University Medical Center. The numbers of male and female patients evaluated in the phase I study were 13 and 26, respectively. The mean (median, range) age of the patients was 59.3 years (60 years, 41 to 75 years). PK studies of IHL-305 were performed in 39 patients.

Linear and Non-Linear Pharmacokinetic Disposition of IHL-305

The variability in the PK disposition of sum total CPT-11 was related to linear and non-linear (saturable) clearance of IHL-305 in patients. The occurrence of linear and non-linear clearance was associated with the dose of IHL-305. At doses from 3.5 to 50 mg/m^2, the IHL-305 sum total CPT-11 plasma concentration versus time profiles were best described using a model with linear clearance in all patients (n = 14). At doses from 67 to 210 mg/m^2, the IHL-305 sum total CPT-11 plasma concentration versus time profiles were best described using a model with linear (n = 16) and non-linear clearance (n = 8). The dose of IHL-305 was significantly higher in patients with linear clearance than patients with nonlinear clearance (P =0.01). The dose normalized sum total CPT-11 AUC in patients with linear clearance and patients with nonlinear clearance are presented in **Table 3.1**.

Relationship between Age and Body Composition, and the Pharmacokinetic Disposition of IHL-305

Based on our previous studies reporting both age and the ratio of total body weight to ideal body weight (TBW/IBW) affecting the PK disposition of S-CKD602, we evaluated the relationship between these two factors and the PK disposition of IHL-305. The relationship between TBW/IBW and dose normalized CPT-11 AUC (AUC/Dose) in all the patients is presented in **Figure 3.1.** Controlling for age, there was an inverse relationship between TBW/IBW and AUC/Dose ($R^2 = 0.12$) where low TBW/IBW was associated with high AUC/Dose in patients < 60 years of age. The effect of age and TBW/IBW together on ratio of released CPT-11 AUC to sum total CPT-11 AUC in all the patients was evaluated using bubble chart and presented in **Figure 3.2**. Patients whose age and TBW/IBW were greater than the median of the study had a 1.7- to 2.6- fold higher ratio of released CPT-11 AUC to sum total CPT-11 AUC.

Relationship between % Decrease in Monocytes and the Pharmacokinetic Disposition of IHL-305

Based on our prior studies, the % decrease in monocytes at nadir on cycle 1 was used as a measure of monocytes function. The relationship between the % decrease in monocytes and dose normalized CPT-11 AUC in patients with linear clearance and nonlinear clearance are presented in **Figures 3.3a** and **Figure 3.3b, respectively**. There was a statistically significant linear relationship in patients with linear clearance between % decrease in monocytes and AUC/Dose ($P = 0.008$, $R^2 = 0.49$), where high % decrease in monocytes was associated with low AUC/Dose. However, the relationship between the % decrease in monocytes and dose normalized CPT-11 AUC in patients with nonlinear clearance was not

significant ($P = 0.37$, $R^2 = 0.20$) which may be due to the saturation of interaction between IHL-305 and monocytes.

Neutropenia and Monocytopenia Associated with IHL-305

To evaluate differential effects of IHL-305 on neutrophils and monocytes we evaluated the % decrease of ANC and monocytes at nadir in the blood of patients administered IHL-305 on cycle 1. The mean ± SD day of ANC and monocyte nadir after administration of IHL-305 was 18.7 ± 7.4 days and 11.2 ± 6.1 days, respectively ($P = 0.0006$). The parameters describing the neutropenia and monocytopenia administration of IHL-305 are summarized in **Table 3.2**. After administration of IHL-305 in all patients, the % decrease in ANC and monocytes at nadir were 29 ± 20% and 42 ± 24 %, respectively ($P = 0.19$). After administration of IHL-305 in all patients, the ratio of % decrease in monocytes to ANC at nadir within a patient was 1.4 ± 1.0.

To evaluate age-related effects on the relationship between neutropenia and monocytopenia after administration of IHL-305 we evaluated the % decrease of ANC and monocytes in the blood of patients < 60 and ≥ 60 years of age. Categorizing patients as < 60 or ≥ 60 years of age was based on our previous studies reporting a reduced clearance of PEGylated liposomal anticancer agents in patients ≥ 60 years of age compared with patients < 60 years of age (27,28). The mean ± SD age of patients in groups < 60 and ≥ 60 years of age were 51.4 ± 4.8 years and 67.3 ± 5.2 years, respectively ($P < 0.001$). The parameters describing the neutropenia and monocytopenia administration of IHL-305 in patients < 60 and ≥ 60 years of age are summarized in **Table 3.2**. The % decrease in ANC and monocytes in patients < 60 years of age were 30 ± 23 % and 45 ± 30 %, respectively ($P = 0.46$). The ratio of % decrease in monocytes to ANC within a patient < 60 years of age was 1.7 ± 1.4.

The % decrease in ANC and monocytes ≥ 60 years of age were 28 ± 19 % and 40 ± 20 %, respectively (P = 0.30). The ratio of % decrease in monocytes to ANC within a patient ≥ 60 years of age was 1.2 ± 0.7.

Relationship between Age and the Pharmacodynamics of IHL-305

The relationship between age and % decrease in monocytes in all patients with dose ≥ 50 mg/m^2 is presented in **Figure 3.4**. There was a linear relationship between the % decrease in monocytes and age in all patients (R^2 = 0.32), patients with dose ≤ 88 mg/m^2 (R^2 = 0.49), and in patients with dose ≥ 120 mg/m^2 (R^2 = 0.43) where younger patients have higher % decrease in monocytes. Additionally, the % decrease in monocytes is lower in patients with dose ≤ 88 mg/m^2 compared to patients with dose ≥ 120 mg/m^2.

Relationship between Gender and the Pharmacokinetic Disposition of IHL-305

The relationship between the gender and clearance in patients with linear clearance is presented in **Figure 3.5a**. There was a statistically significant (P < 0.05) difference in clearance between female and male patients with linear clearance. The clearance of sum total CPT-11 was 1.7-fold lower in female patients compared to male patients. The relationship between the gender and clearance in patients with linear clearance was evaluated by incorporating BSA as a covariate which is presented in **Figure 3.5b**. The clearance of sum total CPT-11 was 1.6-fold lower in female patients compared to male patients with linear clearance. There was a statistically significant linear relationship (R^2 = 0.29) between BSA and clearance where high BSA was associated with high clearance.

D. DISCUSSION

Major advances in the use of liposomes, conjugates, and nanoparticles as vehicles to deliver drugs have occurred the past 10 years (4, 6, 7). Doxil® and albumin stabilized nanoparticle formulation of paclitaxel (Abraxane®) are now FDA approved (8, 9, 23). In addition, there are greater than 100 liposomal and nanoparticle formulations of anticancer agents currently in development (4). This is the first study to identify age, body composition, and monocyte counts as factors associated with the PK variability of a PEGylated-liposomal CPT-11. These results are consistant with our prior studies of Doxil® and S-CKD602 (15-17).

The % decrease in monocytes was significantly correlated with clearance of sum total CPT-11 where patients with a higher % decrease in monocytes at nadir have an increased clearance of sum total CPT-11. The relationship between changes in monocytes and the PK disposition of IHL-305 suggests that the monocytes engulf liposomal anticancer agents via their phagocytic function as part of the MPS which causes the release of drug from the liposome and cytotoxicity to the monocytes (24). Additionally, monocytes are more sensitive to IHL-305 as compared with neutrophils in our study. This is consistant with our previous study that the increased sensitivity is related to the liposomal formulation and not the encapsulated drug (25). The overall difference in monocyte and neutrophil sensitivity to IHL-305 is less than reported for S-CKD602. This may be due to CPT-11 being less potent than CKD-602 or due to the different liposomal formulations used in each product.

The non-linear clearance of IHL-305 was associated with doses of IHL-305 $\geq$ 67 mg/m^2. The nonlinear clearance of sum total CPT-11 after administration of IHL-305 and other nanoparticle agents may be related to the saturation in the clearance capacity of the

MPS. Age and body composition are not associated with the PK variability of patients with non-linear clearance which is consistent with our prior studies (26).

In patients < 60 years of age with a lean body composition have an increased plasma exposure of IHL-305. The relationship between body composition and plasma exposure of IHL-305 in patients is consistent with our prior studies of S-CKD602 which showed that patients with a lean body composition have a higher plasma exposure of S-CKD602 (17).

The influence of gender on the PK of liposomal agents has been reported. Pardue et al. reported that clearance of liposomal ampicillin was higher in female rats compared to male rats (27). In contrast, we found that clearance of total CPT-11 was lower in female patients compared to male patients. We also found that the clearance of TLI and S-CKD602 was lower in female rats compared to male rats (32). These results indicate that gender is an influential factor on the PK disposition of liposomal agents. Gender-related differences in monocyte function may account for the differences in clearance of liposomal agents. The influence of gender needs to be investigated further.

The influence of age on the PD of PEGylated liposomal agents have been reported by our group. There was an inverse relationship between patients age and % decrease in monocytes at nadir with younger patients having a higher % decrease in monocytes. This is consistant with our study of S-CKD602 (PEGylated liposomal CKD-602), indicating that an age related decrease in the function of monocytes may account for the reduced uptake and clearance of PEGylated liposomes and cytotoxicity to the monocytes (25).

IHL-305 exhibits all of the pharmacologic, antitumor, and cytotoxic advantages of a long acting, liposomal anticancer agent (4, 28-30). The high inter-patient variability in the PK and PD of sum total IHL-305 was associated with age, body composition, gender,

saturable clearance and monocyte function. Our data also suggests that IHL-305 undergoes non-linear or saturable clearance at higher doses (28). The clinical significance of these differences and the factors associated with them need to be evaluated for IHL-305 and other liposomal and nanoparticle anticancer agents. Ultimately, the best predictor of the PK and PD variability of IHL-305 and other liposomal and nanoparticle agents may be a phenotypic probe that measures the clearance capacity of liposomes in individual patients (31). This phenotypic probe can then be used to individualize the dosages of liposomal and nanoparticle agents for each patient to achieve a target exposure and thus reduce the PD variability of these agents (31).

E. REFERENCE

1. Zamboni WC. Concept and clinical evaluation of carrier-mediated anticancer agents. Oncologist 2008; 13:248-60.

2. Innocenti F, Kroetz DL, Schuetz E, et al. Comprehensive pharmacogenetic analysis of irinotecan neutropenia and pharmacokinetics. J Clin Oncol 2009; 27:2604-14.

3. Slatter JG, Schaaf LJ, Sams JP, et al. Pharmacokinetics, metabolism, and excretion of irinotecan (CPT-11) following I.V. infusion of [(14)C]CPT-11 in cancer patients. Drug Metab Dispos 2000; 28:423-33.

4. Zamboni WC. Liposomal, nanoparticle, and conjugated formulations of anticancer agents. Clin Cancer Res 2005; 11:8230-4.

5. Xie R, Mathijssen RH, Sparreboom A, Verweij J, Karlsson MO. Clinical pharmacokinetics of irinotecan and its metabolites in relation with diarrhea. Clin Pharmacol Ther 2002; 72:265-75.

6. Papahadjopoulos D, Allen TM, Gabizon A, et al. Sterically stabilized liposomes: improvements in pharmacokinetics and antitumor therapeutic efficacy. Proc Natl Acad Sci U S A 1991; 88:11460-4.

7. Maeda H, Wu J, Sawa T, Matsumura Y, Hori K. Tumor vascular permeability and the EPR effect in macromolecular therapeutics: a review. J Control Release 2000; 65:271-84.

8. Markman M, Gordon AN, McGuire WP, Muggia FM. Liposomal anthracycline treatment for ovarian cancer. Semin Oncol 2004; 31:91-105.

9. Krown SE, Northfelt DW, Osoba D, Stewart JS. Use of liposomal anthracyclines in Kaposi's sarcoma. Semin Oncol 2004; 31:36-52.

10. Zamboni WC, Yoshino K. Formulation and physiological factors affecting the pharmacokinetics and pharmacodynamics of liposomal anticancer agents. Japan DDS 2010; 25:58-70.

11. Zamboni WC, Stewart CF, Thompson J, et al. Relationship between topotecan systemic exposure and tumor response in human neuroblastoma xenografts. J Natl Cancer Inst 1998; 90:505-11.

12. Stewart CF, Zamboni WC, Crom WR, et al. Topoisomerase I interactive drugs in children with cancer. Invest New Drugs 1996; 14:37-47.

13. Allen TM, Hansen C. Pharmacokinetics of stealth versus conventional liposomes: effect of dose. Biochim Biophys Acta 1991; 1068:133-41.

14. Zamboni WC, Edwards RP, Mountz JM, et al. The Development of Liposomal and Nanoparticle Anticancer Agents: Methods to Evaluate the Encapsulated and Released Drug

in Plasma and Tumor and Phenotypic Probes for Pharmacokinetic (PK) and Pharmacodynamic (PD) Disposition. NSTI Nanotechnology; 2007; 2007.

15. Zamboni WC, Maruca LJ, Strychor S, et al. Age and body composition related-effects on the pharmacokinetic disposition of STEALH liposomal CKD-602 (S-CKD602) in patients with advanced solid tumors. 2007; 2007.

16. Sidone BJ, Edwards RP, Zamboni BA, Strychor S, Maruca LJ, Zamboni WC. Evaluation of body surface area (BSA) based dosing, age, and body composition as factors affecting the pharmacokinetic (PK) variability of STEALTH liposomal doxorubicin (Doxil). AACR-NCI-EORTC; 2007; 2007.

17. Zamboni WC, Strychor S, Maruca L, et al. Pharmacokinetic Study of Pegylated Liposomal CKD-602 (S-CKD602) in Patients With Advanced Malignancies. Clin Pharmacol Ther 2009.

18. De Martinis M, Modesti M, Ginaldi L. Phenotypic and functional changes of circulating monocytes and polymorphonuclear leucocytes from elderly persons. Immunol Cell Biol 2004; 82:415-20.

19. Jones SF, Zamboni WC, Burris III HA, et al. Phase I and pharmacokinetic (PK) study of IHL-305 (pegylated liposomal irinotecan) in patients with advanced solid tumors. ASCO; 2009 Jun, 2009; Orlando, FL; 2009.

20. Kurita A, Kaneda N. High-performance liquid chromatographic method for the simultaneous determination of the camptothecin derivative irinotecan hydrochloride, CPT-11, and its metabolites SN-38 and SN-38 glucuronide in rat plasma with a fully automated on-line solid-phase extraction system, PROSPEKT. J Chromatogr B Biomed Sci Appl 1999; 724:335-44.

21. Gabrielsson JL, Weiner DL. Pharmacokinetic and pharmacodynamic data analysis: concepts and applications. 3 ed: Taylor & Francis; 2000.

22. Rosner G. Fundamentals of Biostatistics. 5th Edition ed. Pacific Grove, CA: Duxbury; 2000.

23. Roy V, LaPlant BR, Gross GG, Bane CL, Palmieri FM. Phase II trial of weekly nab (nanoparticle albumin-bound)-paclitaxel (nab-paclitaxel) (Abraxane) in combination with gemcitabine in patients with metastatic breast cancer (N0531). Ann Oncol 2009; 20:449-53.

24. Zamboni WC, Eiseman JE, Strychor S, et al. Relationship between the plasma and tumor disposition of STEALTH liposomal CKD-602 and macrophages/dendritic cells (MDC) in mice bearing human tumor xenografts. AACR; 2006; 2006. p. 5449.

25. Zamboni WC, Maruca LJ, Strychor S, et al. Bi-Directional Pharmacodynamic Interaction between STEALTH Liposomal CKD-602 (S-CKD602) and Monocytes in Patients with Refractory Solid Tumors. Clin Cancer Res; Submitted.

26. Zamboni WC, Strychor S, Maruca L, et al. Pharmacokinetic study of pegylated liposomal CKD-602 (S-CKD602) in patients with advanced malignancies. Clin Pharmacol Ther 2009; 86:519-26.

27. Pardue RL, White CA. Pharmacokinetic evaluation of liposomal encapsulated ampicillin in male and female rats. Biopharm Drug Dispos 1997; 18:279-92.

28. Jones SF, Zamboni WC, Burris III HA, et al. Phase I and pharmacokinetic (PK) study of IHL-305 (pegylated liposomal irinotecan) in patients with advanced solid tumors. ASCO; 2009; 2009.

29. Sparreboom A, Zamboni WC. Cancer Chemotherapy and Biotherapy: Principles and Practice. 4th Edition ed: Lippincott Williams & Wilkins; 2005.

30. Stewart CF, Zamboni WC, Crom WR, et al. Topoisomerase I interactive drugs in children with cancer. Investigational New Drugs 1996; 14:37-47.

31. Zamboni WC, Edwards RP, Mountz JM, et al. The Development of Liposomal and Nanoparticle Anticancer Agents: Methods to Evaluate the Encapsulated and Released Drug in Plasma and Tumor and Phenotypic Probes for Pharmacokinetic (PK) and Pharmacodynamic (PD) Disposition. NSTI Nanotechnology Conf; 2007; 2007.

32. Song G, Wu H, La-Beck N, Zamboni BA, Strychor S, Zamboni WC. Effect of Gender on Pharmacokinetic Disposition of Pegylated Liposomal CKD-602 (S-CKD602) and Optisomal Topotecan (TLI) in Rats. AACR 2009.

Table 3.1.

Compartmental Pharmacokinetic Parameters of Sum Total CPT-11 after IHL-305 in Patients with Linear and Non-Linear Disposition

		Linear Pharmacokinetic Disposition		Non-Linear Pharmacokinetic Disposition
Parameters	Units	Age < 60 Mean ± SD (Range) n = 15	Age ≥ 60 Mean ± SD (Range) n = 15	All Ages Mean ± SD (Range) n = 8
k_{10}	(h^{-1})	0.031 ± 0.0098 (0.016 – 0.046)	0.034 ± 0.0077 (0.019 – 0.047)	---
t½ [a]	(h)	24.9 ± 8.1 (15.0 – 43.7)	21.3 ± 5.6 (14.8 – 35.8)	11.6 ± 3.8 (7.8 – 17.0)
V_{c1}	(L/m^2)	1.6 ± 0.45 (0.90 – 2.70)	1.6 ± 0.55 (1.14 – 2.86)	1.6 ± 0.36 (1.08 – 2.12)
CL	($L/h/m^2$)	0.048 ± 0.024 (0.021 – 0.12)	0.055 ± 0.027 (0.023 – 0.12)	---
k_{12}	(h^{-1})	---	---	0.15 ± 0.070 [b] (0.10 – 0.20)
k_{21}	(h^{-1})	---	---	0.095 ± 0.040 [b] (0.066 – 0.12)
K_m	(ng/mL)	---	---	32.8 ± 31.3 (0.93 – 92.7)
V_{max}	(ng/h)	---	---	4.54 ± 3.39 (1.72 – 11.3)
Sum Total AUC/Dose[e]	(μg/mL•h) /(mg/m^2)	12.9 ± 4.9 [c,d] (8.19 – 27.5)	14.5 ± 4.6 [c,d] (8.29 – 25.1)	14.8 ± 5.3 [d] (7.79 – 23.6)

[a] t½ is the terminal half life

[b] Estimates are from 2 patients.

[c] The sum total CPT-11 AUC normalized by dose in patients with linear disposition was not significantly different between patients ≥ 60 years of age and patients < 60 years of age ($P > 0.05$).

[d] The sum total CPT-11 AUC normalized by dose was not significantly different between patients with non-linear disposition and patients with linear disposition that were ≥ 60 and < 60 years of age ($P > 0.05$).

[e] Sum total AUC was calculated from 0 to the last sampling time point.

Table 3.2.
Summary of ANC and Monocytes Parameters
After Administration of IHL-305

		IHL-305		
	Units	Monocytes	ANC	Ratio Monocytes to ANC
		Mean ± SD (Range)	Mean ± SD (Range)	Mean ± SD (Range)
All Patients				
% Decrease	%	[a] 42.0 ± 23.9 (0.0 – 80.1)	[a] 28.8 ± 20.3 (0.0 – 84.8)	1.40 ± 0.98 (0.067 – 4.28)
Patients < 60 yo				
% Decrease	%	[b, d] 44.7 ± 29.9 (0.0 – 80.1)	[b, e] 29.6 ± 22.6 (0.0 – 84.8)	1.65 ± 1.36 (0.22 – 4.28)
Patients ≥ 60 yo				
% Decrease	%	[c, d] 40.2 ± 20.3 (4.35 – 71.6)	[c, e] 28.1 ± 18.9 (0.0 – 65.3)	1.24 ± 0.68 (0.067 – 2.35)

[a] $P > 0.05$
[b] $P > 0.05$
[c] $P > 0.05$
[d] $P > 0.05$
[e] $P > 0.05$

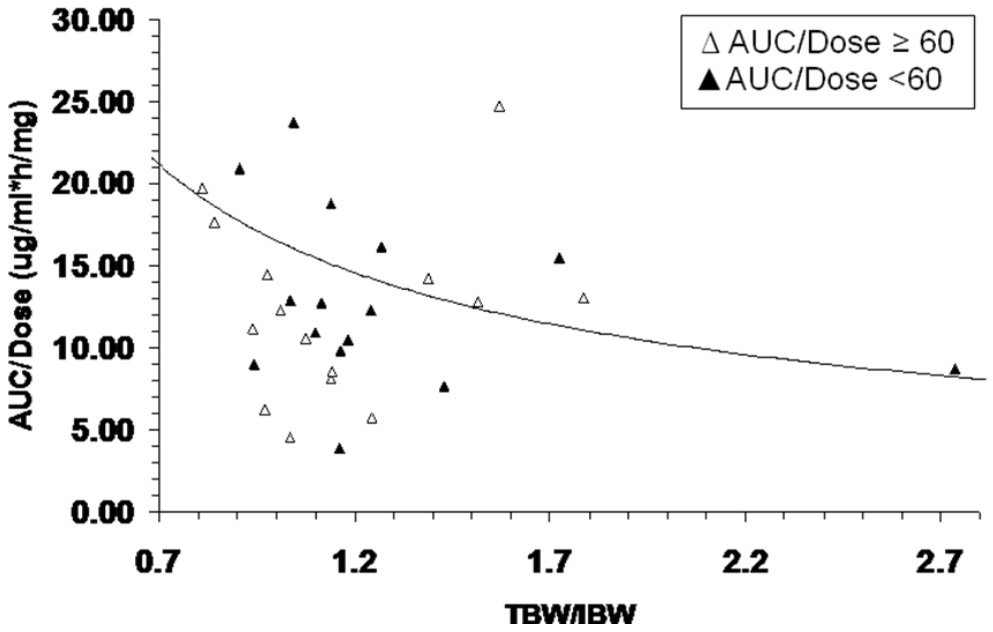

Figure 3.1. Relationship between the ratio of total body weight to ideal body weight (TBW/IBW) and dose normalized IHL-305 sum total AUC (AUC/Dose). AUC/Dose in patients < 60 and ≥ 60 years of age are represented by the solid triangles and the open triangles, respectively. The best-fit line of the data is represented by the curved solid line (R^2 = 0.12). After controlling for age, there was an inverse relationship between TBW/IBW and AUC/Dose, with a low TBW/IBW being associated with high AUC/Dose in paitents < 60 years of age.

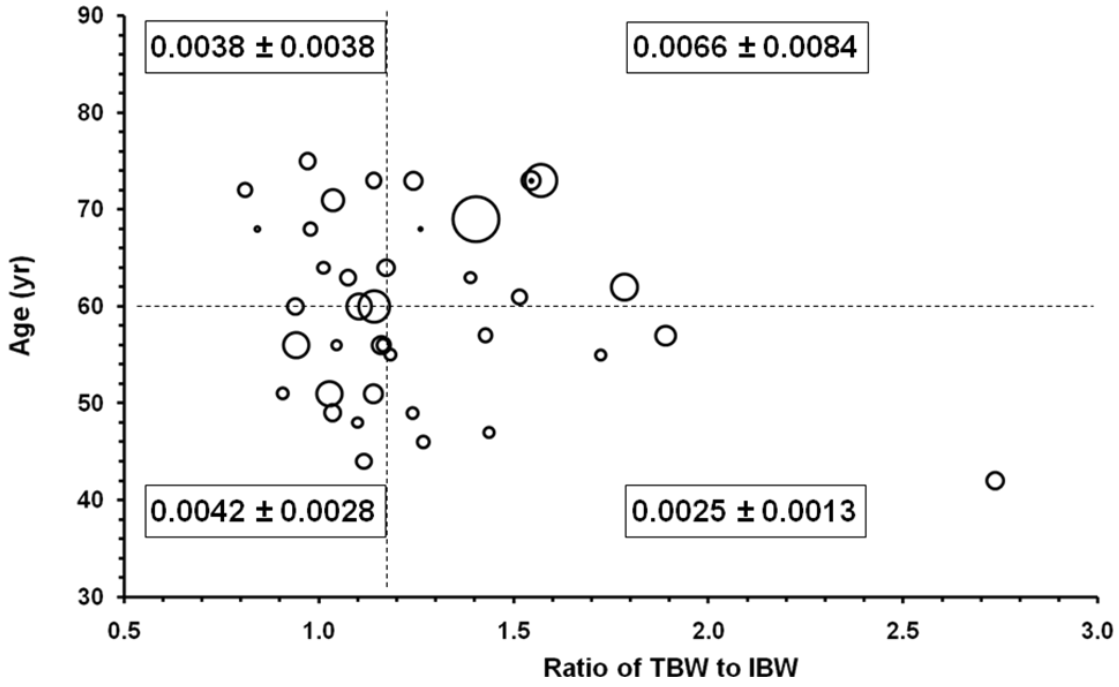

Figure 3.2. Relationship between two factors, age and the ratio of total body weight to ideal body weight (TBW/IBW), and ratio of released CPT-11 AUC to sum total CPT-11 AUC. Patients are divided into four groups according to the median value of age and TBW/IBW. In Figure 3.2, mean value ± SD of ratio of released CPT-11 AUC to sum total CPT-11 AUC were 0.0042 ± 0.0028, 0.0038 ± 0.0038, 0.0066 ± 0.0084, and 0.0025 ± 0.0013 in patients < 60 years of age and TBW/IBW < 1.16, patients ≥ 60 years of age and TBW/IBW < 1.16, patients ≥ 60 years of age and TBW/IBW ≥ 1.16, and patients < 60 years of age and TBW/IBW ≥ 1.16, respectively.

Figure 3.3a

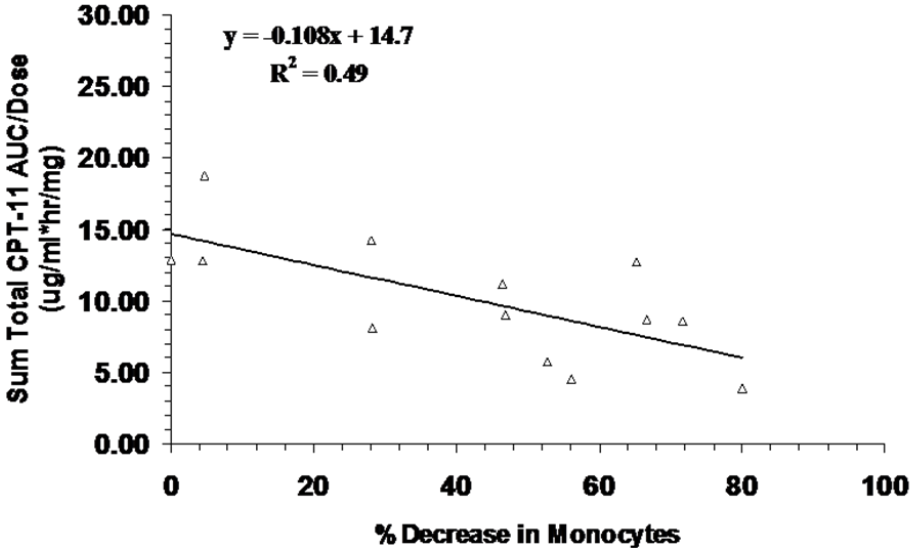

Figure 3.3b

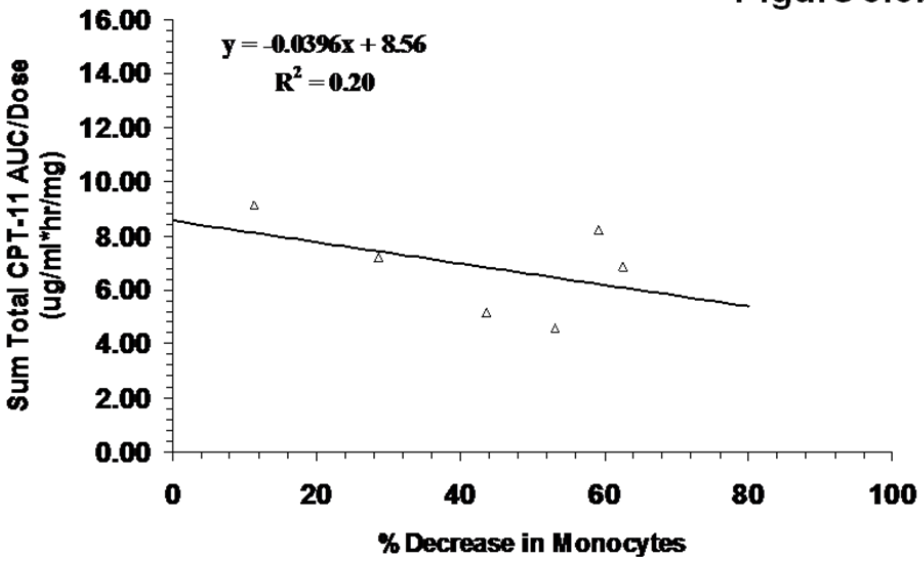

Figures 3.3. Relationship between % decrease in monocytes and dose normalized CPT-11 AUC (AUC/Dose). Figures 3.3a and 3.3b represent the relationship between % decrease in monocytes and AUC/Dose in patients with linear clearance and nonlinear clearance, respectively. The relationship between AUC/Dose and % decrease in monocytes was best described by a linear relationship in patients with linear clearance ($P = 0.008$, $R^2 = 0.49$).

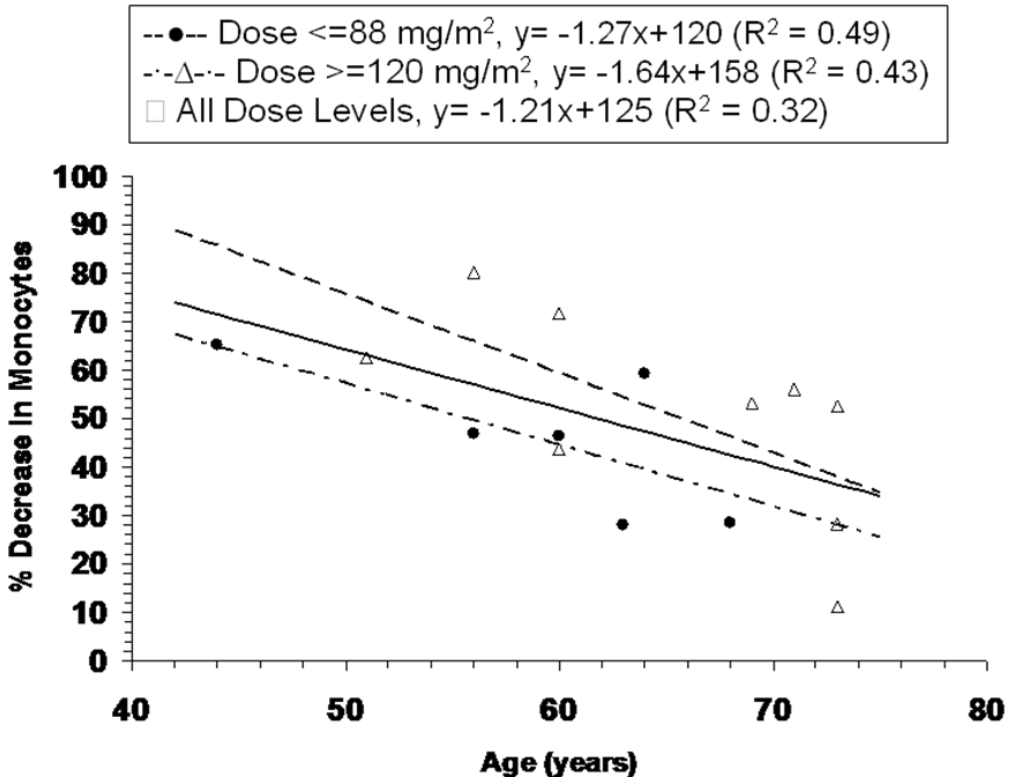

Figure 3.4. The relationship between % decrease in monocytes and age in all patients with dose ≥ 50 mg/m^2. For patients with dose ≥ 50 mg/m^2 and ≤ 88 mg/m^2, individual values are represented by the solid circles. For patients with dose ≥ 120 mg/m^2, individual values are represented by the open triangles. There was a linear relationship between the % decrease in monocytes and age in all patients ($R^2 = 0.32$), patients with dose ≤ 88 mg/m^2 ($R^2 = 0.49$), and in patients with dose ≥ 120 mg/m^2 ($R^2 = 0.43$).

Figure 3.5a

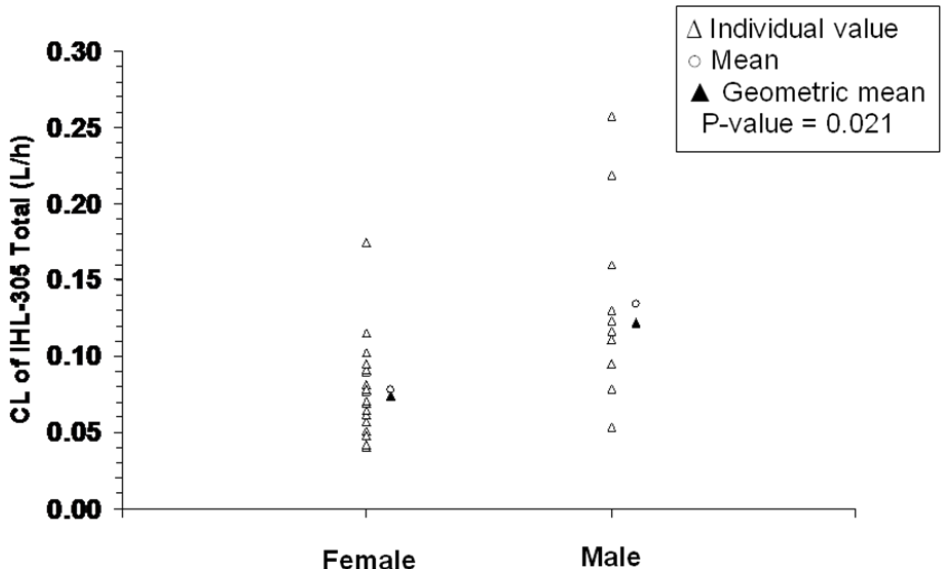

Figure 3.5b

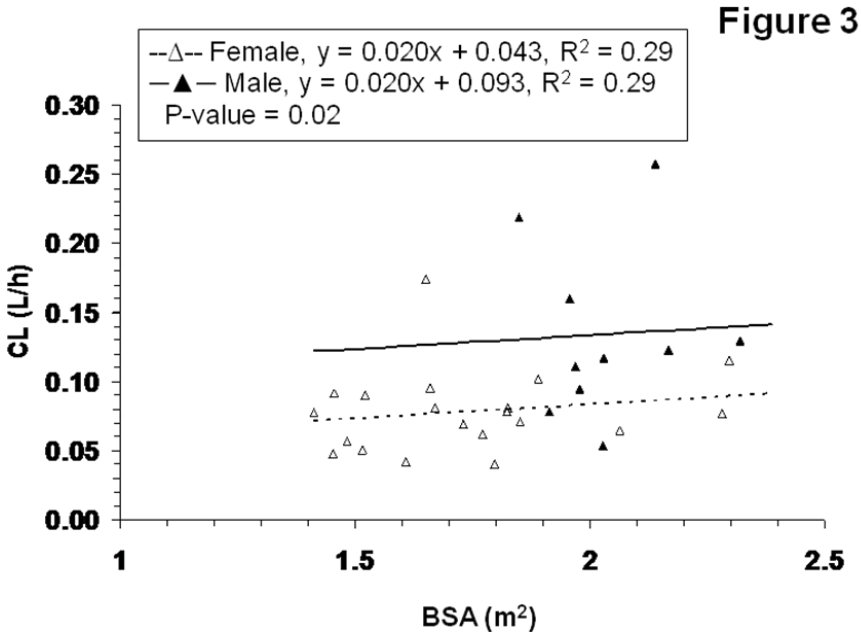

Figure 3.5. The clearance of total IHL-305 and dose normalized sum total CPT-11 AUC (AUC/Dose) in male and female patients. The clearance of total IHL-305 for male and female patients with linear clearance is presented in Figure 3.5a. The clearance values of individual patients are represented by the open triangles. The mean and geometric mean of

for each group is represented by the open circles and the solid triangles, respectively. Mean value ± SD clearance of total IHL-305 for male and female patients were 0.134 ± 0.063 and 0.0783 ± 0.030 (L/h), respectively (P = 0.02). The effect of gender on clearance of total IHL-305 with body surface area (BSA) as a covariate is presented in Figures 3.5b. The clearance of individual female and male patients is represented by the open triangles and solid triangles, respectively. Regression lines for data from female patients and male patients are represented by dashed line and solid line, respectively. There is a significant difference in clearance of total IHL-305 (P = 0.02) between male and female patients with linear clearance after adjust the effects of BSA.

CHAPTER 4

POPULATION PHARMACOKINETICS OF PEGYLATED LIPOSOMAL CKD-602 (S-CKD602) IN PATIENTS WITH ADVANCED MALIGNANCIES

This chapter has been published by the *Journal of Clinical Pharmacology* and is presented in the style of that journal.

A. INTRODUCTION

S-CKD602 is a STEALTH® liposomal formulation of CKD-602, a camptothecin analogue which inhibits topoisomerase I. [1-3] The STEALTH liposomal formulation consists of phospholipids covalently bound to methoxypolyethylene glycol (mPEG) on the outside of the lipid bilayer. Non-liposomal CKD-602 administered IV at 0.5 mg/m^2/day for 5 consecutive days repeated every 21 days is approved in Korea for the treatment of newly diagnosed small cell lung cancer and relapsed ovarian cancer. [4-7]

The development of STEALTH liposomes was based on the discovery that incorporation of mPEG-lipids into liposomes yields preparations with prolonged plasma exposure and superior tumor delivery compared to conventional liposomes composed of natural phospholipids.[3, 8, 9] STEALTH liposomal doxorubicin (Doxil®) is approved for the treatment of refractory ovarian cancer, Kaposi sarcoma, and multiple myeloma.[10, 11] The generation of a liposomal formulation of a camptothecin analogue, such as CKD-602, has specific advantages such as protecting the lactone form and providing prolonged exposure in tumors which is associated with greater antitumor effect of camptothecines.[3, 12-16] The STEALTH® liposomal formulation is expected to have an enhanced therapeutic ratio compared to free CKD-602 (non-liposomal), as well as a more convenient schedule of administration.

In mice, the plasma exposure of S-CKD602 at 1 mg/kg i.v. × 1 was ~25-fold greater than the plasma exposure of nonliposomal CKD-602 at 30 mg/kg i.v. × 1.[6, 17] In the plasma of mice, ~82% of CKD-602 was encapsulated inside the liposome after administration of S-CKD602.[17] The duration of exposure of CKD-602 in the tumor was threefold longer with S-CKD602 than with nonliposomal CKD-602 in mice bearing human tumor xenografts.[17] The

improved pharmacokinetics of S-CKD602 resulted in greater therapeutic index compared to free CKD-602. In human tumor xenograft models, the therapeutic index (TI) of S-CKD602 was estimated to be approximately 6-fold greater than that of free CKD-602 in ES-2 ovarian and approximately 3-fold greater in H82 SCLC tumors.[6] These results are consistent with the antitumor response to camptothecin analogs, which is related to the duration of time for which the drug concentration is above a critical threshold.[6, 15-18]

The pharmacokinetic disposition of carrier-mediated agents, such as, nanoparticles, nanosomes, and conjugated agents, is dependent upon the carrier until the drug is released from the carrier. Unlike traditional anticancer agents which are cleared by the liver and kidneys, the clearance of non-PEGylated and PEGylated liposomes is via the mononuclear phagocytic system, which has also been called the reticuloendothelial system (RES) which include monocytes, macrophages and dendritic cells located primarily in the liver and spleen.[19] Uptake by the MPS usually results in sequestering of the encapsulated drug in the MPS, where it can be degraded. In addition, the uptake of the liposomes by the MPS may result in acute impairment of the MPS and toxicity. PEGylated liposomes are cleared much slower via MPS compared to non-PEGylated liposomes.[8, 20] Once the drug is released from the carrier, the pharmacokinetic disposition of the drug will be the same as after administration of the non-carrier form of the drug.[19, 21] Thus, the pharmacokinetics of liposomes are complex.

Nanoparticle agents have higher variability in pharmacokinetic (drug clearance, systemic exposure, distribution, etc.) disposition with potentially higher variability in pharmacodynamic (antitumor response and toxicity) disposition as compared with traditional small molecule chemotherapy. However, the factors affecting the pharmacokinetic and

pharmacodynamic variability of encapsulated and released forms of conventional and PEGylated liposomes remain unclear, but most likely include the MPS.[12] We have evaluated factors affecting the pharmacokinetics and pharmacodynamics of liposomal anticancer agents. We were the first to report a reduced clearance of the liposomal encapsulated forms of Doxil and S-CKD602 in patients ≥ 60 years of age.[22, 23] We have also reported that patients with a lean body composition may have a reduced tissue distribution and an increased plasma exposure of S-CKD602. In addition, we have reported an age related decrease in the function of monocytes which may be associated with a reduced clearance of liposomes and reduced cytotoxicity to the monocytes.[20, 24, 25]

S-CKD602 was associated with high interpatient variability in the pharmacokinetic disposition of encapsulated and released CKD-602.[26] Population pharmacokinetic analysis is a useful tool for identification of sources of pharmacokinetic variability and can aid in the design of alternative dosing regimens to enhance efficacy and safety. The objectives of this study was to describe the population pharmacokinetics of both encapsulated CKD-602 and released CKD-602 after administration of the PEGylated liposomal form of the drug and to characterize clinical covariates that influence S-CKD602 pharmacokinetics.

B. METHODS

Patients

Patients ≥ 18 years of age with a histologically or cytologically confirmed malignancy for which no effective therapy was available were eligible for this study. Pertinent eligibility criteria included a Eastern Cooperative Oncology Group (ECOG) performance status of 0 to 2, adequate bone marrow, hepatic, and renal function as evidenced by the following: absolute neutrophil count (ANC) ≥ 1500/μL, platelets ≥ 100,000/μL, total bilirubin ≤ 1.5 x upper limit of the institutional normal range (ULN), aspartate aminotransferase (AST) ≤ 1.5 x the ULN if liver metastases were not present and ≤ 4 x the ULN if liver metastases were present, and absence of microscopic hematuria (18). Prior treatment with camptothecin analogues other than S-CKD602 or non-liposomal CKD-602 was permitted. Written informed consent, approved by the Institutional Review board of the University of Pittsburgh Medical Center, was obtained from all patients prior to study entry.

Study Design

This was a phase I, dose escalation study in patients with advanced solid tumors.[26, 27] The study design and clinical results have been reported elsewhere.[26, 27] This phase I study followed a standard dose escalation design with patients enrolled in cohorts of 3 initially, with the possibility of extending the cohort up to 6 patients depending on the number of dose-limiting toxicities (DLT) (18). No intra-patient dose escalation was permitted. The MTD was defined as the dose below the dose at which two out of up to six patients experienced a DLT. At the 2.5 mg/m^2 dose level, two out of three patients experienced a

DLT. Because the next lower dose (1.7 mg/m^2) dose level was associated with minimal toxicity, an additional intermediate dose level of 2.1 mg/m^2 was investigated.

Dosage and Administration

S-CKD602 is a formulation of CKD-602 encapsulated in long-circulating STEALTH® liposomes. In S-CKD602, the STEALTH® liposome bilayer is composed of N-(carbonyl-methoxypolyethylene glycol 2000)-1,2-distearoyl-*sn*-glycero-phosphoethanolamine (MPEG-DSPE) and 1,2-distearoyl-*sn*-glycero-phosphocholine (DSPC) in a molar ratio of approximately 5:95. The mean particle diameter is approximately 100 nm, and CKD-602 encapsulation inside the liposomes exceeds 85%. S-CKD602 was supplied by ALZA Corporation in sterile 10 mL single-use amber vials as a clear to slightly opalescent suspension with a nominal total CKD-602 concentration of 0.1 mg/mL. S-CKD602 was diluted 3-fold in 5% dextrose prior to administration. No pre-medications were administered prior to S-CKD602.

S-CKD602 was administered IV over approximately 1 hour every 3 weeks. Doses administrated, expressed in mg of CKD-602 per m^2, were 0.10, 0.15, 0.20, 0.25, 0.30, 0.35, 0.40, 0.45, 0.50, 0.65, 0.85, 1.1, 1.7, 2.1, and 2.5 mg/m^2.

Sample Collection, Processing, and Analytical Studies

Plasma samples for pharmacokinetic assessment were obtained from all patients. On cycle 1, blood (7 mL) was collected in EDTA (purple top) tubes prior to administration, at end of the infusion (approximately 1 h), and at 3 h , 5 h , 7 h , 24 h , 48 h , 72 h, 96 h, 168 h (day 8), and 336 h (day 15) after the start of the infusion. The blood samples were

centrifuged at 1,380 x g for 6 min. The plasma for the determination of the encapsulated and released CKD-602 was immediately placed in regrigerator at 4°C and kept refrigerated until separatation by solid-phase separation (SPS).[17, 27] The encapsulated CKD-602 and released CKD-602 was fully eluted and separated by SPS as previously described.[17, 27] The encapsulated and released CKD-602 concentrations were then measured by a specific liquid chromatographic tandem mass spectrometric assay (LC-MS/MS) as previously described.[17, 27] The total (lactone + hydroxy acid) form of CKD-602 was measured for encapsulated and released samples. The lower limit of quantitation (LLQ) of the total form encapsulated and released CKD-602 were 2 and 0.05 ng/mL, respectively.[17, 27]

Population Pharmacokinetic Analysis

Encapsulated CKD-602 and released CKD-602 concentration-time data were analyzed using the nonlinear mixed effects modeling approach as implemented in NONMEM (version 6; University of California, San Francisco, CA). Both the first order approximation method and first order conditional estimation (FOCE) method were used in analyses. S-PLUS 8.0 (Version 8.0, Insightful Corporation, Seattle, Washington) was used for graphical diagnostics and covariate screen. The population pharmacokinetic model of S-CKD602 was developed in two steps: (a) basic (structural) model development and (b) covariate model development.

Mean population pharmacokinetic variables, interindividual variability, and residual error were assessed in the model development. Interindividual variability for each pharmacokinetic variable was modeled with an exponential function. Residual error models of the additive, proportional, exponential, and combination methods were evaluated for the

best structural pharmacokinetic model. Individual pharmacokinetic variables were obtained by posterior Bayesian estimation.

Model selection for nonhierarchical models (i.e., linear and nonlinear elimination models) was guided by goodness-of-fit plots (e.g., observed versus predicted plasma concentrations, weighted residuals versus predicted concentrations, and weighted residuals versus time), Akaike information criterion (AIC), and precision of parameter estimates. AIC was calculated as AIC = OFV + 2 x p, where OFV is the NONMEM objective function value and p is the number of pharmacokinetic variables. The model was chosen on the basis of smaller values of AIC, better precision of estimates, and superior goodness-of-fit plots.

Model Development

The structural model of encapsulated CKD-602 and released CKD-602 was built sequentially. Firstly, the best model for encapsulated CKD-602 was selected from all the possible models. Then based on the best model for encapsulated CKD-602, simultaneous modeling of the encapsulated and the released CKD-602 were attempted for data from all patients. In this modeling process, one-compartment model, two-compartment model and three-compartment model with first-order elimination were tested to fit released plasma concentration data. However, the estimation of pharmacokinetic parameters for released drug proved to be unsatisfactory because no successful minimization with successful covariance step could be achieved. Therefore, the mean value of pharmacokinetic parameters associated with distribution and elimination of released CKD-602 were determined from a CKD-602 pharmacokinetic model after administration of non-liposomal CKD-602 and fixed in the final population pharmacokinetic model of encapsulated and

released CKD-602. The inter-individual variability of pharmacokinetic parameters associated with distribution and elimination of released CKD-602 were not fixed and allowed to be estimated in the final population pharmacokinetic model of encapsulated and released CKD-602. The ability to fix the mean value of pharmacokinetic parameters of the released drug using the estimated mean value of pharmacokinetic parameters from non-liposomal drugs is based on our studies reporting the pharmacokinetic disposition of released drug is the same as non-liposomal drugs.[28]

Encapsulated Drug Model

The structural model was built to fit encapsulated CKD-602 plasma concentration-time profiles from all 45 patients. One-compartment model and two-compartment model with first-order elimination or nonlinear elimination characterized by Michaelis-Menten kinetics described as below were tested to fit encapsulated plasma concentration data.

The pharmacokinetic model used to characterize the disposition of encapsulated CKD-602 in all patients is shown in **Figure 4.1A**. The differential equation describing the pharmacokinetic model of encapsulated CKD-602 is as follows:

$$\frac{dA_{Encap}}{dt} = k_0 - \frac{V_{max} \bullet A_{Encap}}{K_m \bullet V_{Encap} + A_{Encap}} \quad , \quad A_{Encap}(0) = 0,$$

$$C_{Encap} = \frac{A_{Encap}}{V_{Encap}}$$

dA_{Encap}/dt is the elimination rate, V_{max} is the maximum elimination rate or maximum velocity, K_m is the concentration at which half-maximum elimination rate is achieved, V_{Encap} is the volume of distribution, A_{Encap} is the encapsulated CKD-602 amount in plasma, C_{Encap} is

the plasma concentration of encapsulated CKD-602, k_0 is the infusion rate and k_0 is 0 after stop of infusion.

CKD-602 Model after Administration of Non-liposomal CKD-602

CKD-602 pharmacokinetic data were from a phase I and pharmacokinetic study of CKD-602 in patients with advanced solid malignancies.[5] The study design and clinical results have been reported elsewhere.[5] Sixteen patients received CKD-602 (0.5 to 0.9 mg/m^2/day) IV x 1 over thirty-minute daily for 5 consecutive days. Frequent plasma sampling was performed prior to administration and at 0.25 h , 0.5 h , 1 h , 1.5 h, 2 h, 3 h, 4 h , 6 h , 8 h, 12 h and 24 h after the start of the infusion for all the patients. The structural model was built to fit CKD-602 plasma concentration versus time profiles from all 16 patients. Two-compartment and three-compartment models with first-order elimination were tested to fit CKD-602 pharmacokinetic profiles.

Encapsulated and Released Drug Model

Based on the best model for encapsulated CKD-602 and the best model for CKD-602 after administration of nonliposomal CKD-602, one-compartment model with Michaelis-Menten kinetics for encapsulated drug and two-compartment model with first-order elimination for released drug was used to fit combined data of encapsulated and released CKD-602 after administration of S-CKD602. In this model developing, in addition to fixing mean value of pharmacokinetic parameters [volume of distribution for central compartment (V_{Rel1}), volume of distribution for peripheral compartment (V_{Rel2}), systemic clearance (CL_{Rel}) and distribution clearance (CL_{Rel-d})] of released drug, patients were further subdivided as

linear and nonlinear patients according to the clearance of encapsulated drug from our previous pharmacokinetic analysis.[26] As most of the CKD-602 remains encapsulated in the plasma after administration of S-CKD602 and the plasma concentration of released CKD-602 is only 1% of encapsulated CKD-602, the amount or concentration of CKD-602 existing in the non-encapsulated form in the dosage (infusion bag) is important in order to capture the relative high concentration of released CKD-602 at earlier time points. Thus, estimates of the non-encapsulated CKD-602 in the formulation were included in models for encapsulated and released CKD-602 after administration of S-CKD602.

The pharmacokinetic model used to characterize the disposition of encapsulated and released CKD-602 in patients with linear clearance of encapsulated CKD-602 is shown in **Figure 4.1B**. The differential equations describing the pharmacokinetic model of encapsulated and released CKD-602 are as follows:

$$\frac{dA_{Encap}}{dt} = k_0 \bullet E\% - \frac{CL_{Encap}}{V_{Encap}} \bullet A_{Encap} - \frac{CL_{Encap-Rel}}{V_{Encap}} \bullet A_{Encap} \quad , \ A_{Encap}(0) = 0$$

$$\frac{dA_{Rel1}}{dt} = k_0 \bullet (1-E\%) + \frac{CL_{Encap-Rel}}{V_{Encap}} \bullet A_{Encap} + \frac{CL_{Rel-d}}{V_{Rel2}} \bullet A_{Rel2} - \frac{CL_{Rel}}{V_{Rel1}} \bullet A_{Rel1} - \frac{CL_{Rel-d}}{V_{Rel1}} \bullet A_{Rel1}, \ A_{Rel1}(0) = 0$$

$$\frac{dA_{Rel2}}{dt} = -\frac{CL_{Rel-d}}{V_{Rel2}} \bullet A_{Rel2} + \frac{CL_{Rel-d}}{V_{Rel1}} \bullet A_{Rel1}, \ A_{Rel2}(0) = 0$$

$$C_{Rel} = \frac{A_{Rel1}}{V_{Rel1}}$$

The CL_{Encap} is the clearance of encapsulated CKD-602, $CL_{Encap-Rel}$ is the clearance of release CKD-602 from S-CKD602, and E% is the encapsulation percent of CKD602 in the formulation. A_{Rel1} is the released CKD-602 amount in central compartment, A_{Rel2} is the

released CKD-602 amount in peripheral compartment and C_{Rel} is the plasma concentration of released CKD-602.

The pharmacokinetic model used to characterize the disposition of encapsulated and released CKD-602 in patients with nonlinear clearance of encapsulated CKD-602 is shown in **Figure 4.1C**. The differential equations describing the pharmacokinetic model of encapsulated and released CKD-602 are as follows:

$$\frac{dA_{Encap}}{dt} = k_0 \bullet E\% - \frac{V_{\max, Encap} \bullet A_{Encap}}{K_m \bullet V_{Encap} + A_{Encap}} - \frac{V_{\max, Encap-Rel} \bullet A_{Encap}}{K_m \bullet V_{Encap} + A_{Encap}}, \; A_{Encap}(0) = 0$$

$$\frac{dA_{Rel1}}{dt} = k_0 \bullet (1 - E\%) + \frac{V_{\max, Encap-Rel} \bullet A_{Encap}}{K_m \bullet V_{Encap} + A_{Encap}} + \frac{CL_{Rel-d}}{V_{Rel2}} \bullet A_{Rel2} - \frac{CL_{Rel}}{V_{Rel1}} \bullet A_{Rel1} - \frac{CL_{Rel-d}}{V_{Rel1}} \bullet A_{Rel1}, \; A_{Rel1}(0) = 0$$

$$\frac{dA_{Rel2}}{dt} = -\frac{CL_{Rel-d}}{V_{Rel2}} \bullet A_{Rel2} + \frac{CL_{Rel-d}}{V_{Rel1}} \bullet A_{Rel1}, \; A_{Rel2}(0) = 0$$

$$C_{Rel} = \frac{A_{Rel1}}{V_{Rel1}}$$

The $V_{max, Encap}$ is the maximum velocity of encapsulated CKD-602, $V_{max, Encap-Rel}$ is the maximum velocity of release CKD-602 from S-CKD602, and K_m is the concentration at which half-maximum elimination rate is achieved.

Covariate Analysis

The covariate model building was a stepwise process. A screen for potential significant covariates was done using S-PLUS 8.0 (Version 8.0, Insightful Corporation, Seattle, Washington). The potential covariates as listed in **Table 4.1** were tested for

influence on the structural pharmacokinetic variables that describe the pharmacokinetics of encapsulated and released CKD-602. The potential significant covariates selected from screen were introduced into the covariate model as linear, exponential, or power function, and assessed in the population pharmacokinetic models. A significant covariate was selected to be retained in the final model if addition of the covariate resulted in a decrease in OFV >3.875 ($P < 0.05$) during the forward full covariate model building, and removal of the covariate resulted in an increase in OFV >10.828 ($P < 0.001$) during the stepwise backward model reduction. In addition, the increase in precision of the variable estimate (% relative SE of prediction) and reduction in interindividual variability were used as another indicator of the improvement of the goodness of fit.

Model Evaluation

Bootstrap analyses were performed to evaluate the stability of the final models and estimate the confidence interval (CI) of the parameters using the bootstrap option in the software package Perl-speaks-NONMEM (M. Karlsson and A. Hooker, Version 3.1.0, Dec 2009). One thousand replicate bootstrap data sets were obtained by resampling with the replacement from the original data set and fitted with the same model to obtain parameter estimates for each replicate. The median and 2.5th and 97.5th values for the population parameters were obtained.

C. RESULTS

Patient demographics

Forty-five patients were enrolled on this study from September 29, 2003 to October 17, 2005 at University of Pittsburgh Cancer Institute. Pharmacokinetic studies of encapsulated and released CKD-602 were performed in all 45 patients. Patient characteristics are listed in **Table 4.1**. The numbers of male and female patients evaluated in the phase I study were 21 and 24, respectively. The mean (median, range) age of the patients was 60.6 years (62 years, 33 to 79 years). Twenty-six patients had tumor in liver and nineteen patients did not have tumor in liver. A total of 292 plasma concentrations of encapsulated CKD-602 and 268 plasma concentrations of released CKD-602 were used to develop the population pharmacokinetic model.

Population Pharmacokinetic Model of S-CKD602

Encapsulated Drug Model

Both linear and nonlinear pharmacokinetic models were evaluated for encapsulated CKD-602. A one-compartment model with Michaelis-Menten kinetics (AIC = 2246) better described the data than either nonlinear plus linear (AIC = 2257) or linear kinetics (AIC = 2313). The distribution of residual variability was best described by a proportional plus additive error model. During the covariate screen, tumor in liver was identified as a significant covariate for maximum velocity of encapsulated CKD-602. The pharmacokinetic parameter estimates obtained from the final covariate model and the 95% CI from bootstrap analysis are provided in **Table 4.2**. The observed bootstrap medians were consistent with the population mean estimates in general. In the final model, the mean (interindividual

variability, CV%) values for the distribution volume is 3.46 L (70.9%) and is very close to plasma volume in humans. The mean Michaelis-Menten constant (Km) were estimated to be 992 μg/L. The inclusion of tumor in liver as a covariate in the final model decreased the inter-individual variability (IIV) of the maximum velocity (Vmax) of encapsulated CKD-602 by 29%. Vmax in patients with tumor in liver and patients without tumor in liver were estimated to be 150 (IIV 205%) and 97.4 (IIV 205%) μg/h, respectively ($P < 0.001$). Vmax showed the most inter-individual variability, with IIV for Vmax was estimated to be 205% even after the incorporation of tumor in liver as a covariate.

Selected individual pharmacokinetic time profiles of encapsulated CKD-602 in patients with and without tumors in their livers are shown in **Figure 4.2**. The final pharmacokinetic model well characterized the nonlinear pharmacokinetic of encapsulated CKD-602. Goodness-of-fit plots from the final pharmacokinetic model are given in **Figure 4.3**. The plots indicated a reasonable fit of the model to the data.

CKD-602 Model after Administration of Non-liposomal CKD-602

Two-compartment and three-compartment models with first-order elimination were tested to fit CKD-602 pharmacokinetic profiles. A two-compartment model with first-order elimination resulted in a similar model fit but better precision of parameter estimates compared to a three-compartment model with first-order elimination. The distribution of residual variability was best described by a proportional error model. No significant covariates were found. The pharmacokinetic parameter estimates from the final model are provided in **Table 4.3**. The population mean (IIV, CV%) values of volume of central compartment (Vc), elimination clearance (CL), volume of peripheral compartment (Vp), and

distribution clearance (CLd) for non-liposomal CKD-602 were 9.72 L, 7.9 L/ h (IIV 27%) , 27.7 L (IIV 21.8%), and 5.07 L/h. Goodness-of-fit plots from the final pharmacokinetic model are given in **Figure 4.4**. The plots indicated a reasonable fit of the model to the data.

Encapsulated and Released Drug Model

Combined data of the encapsulated and released CKD-602 were modeled separately for patients with linear clearance and nonlinear clearance of encapsulated CKD-602. Pharmacokinetic parameters [volume of central compartment (V_{Rel1}), volume of peripheral compartment (V_{Rel2}), systemic clearance (CL_{Rel}), and distribution clearance (CL_{Rel-d})] of released CKD-602 were determined from CKD-602 pharmacokinetic model after administration of non-liposomal CKD-602 and fixed in the final population pharmacokinetic model of encapsulated and released CKD-602. Results of the final covariate model for patients with linear clearance of encapsulated CKD-602 are summarized in **Table 4.4**. V_{Encap} and CL_{Encap} of encapsulated CKD-602 for patients with linear clearance of encapsulated CKD-602 were estimated to be 4.69 L (IIV 53%) and 0.089 L/h (IIV 151%), respectively. The population mean of encapsulation of CKD-602 in the formulation was estimated to be 96%. The inclusion of age decreased IIV in the release of CKD-602 from S-CKD602 by 33%. The population mean of release rate of CKD-602 from S-CKD602 in patients < 60 years old (yo) and patients ≥ 60 yo were 0.130 and 0.048 L/h, respectively ($P < 0.001$).

The results of final model for patients with nonlinear clearance of encapsulated CKD-602 are summarized in **Table 4.5.** No covariates were identified for these patients. V_{Encap}, $V_{max, Encap}$ and Km of encapsulated CKD-602 were estimated to be 3.36 L (IIV 12.6%), 36.1 μg/h (IIV 28.8%) and 1450 μg/L, respectively. The ratio of $V_{max, Encap-Rel}$ to Km for the

release of CKD-602 from S-CKD602 was 0.063 L/h. The population mean of encapsulation of CKD-602 in the formulation was estimated to be 96%.

Selected individual pharmacokinetic time profiles of encapsulated and released CKD-602 in patients with linear clearance and nonlinear clearance of encapsulated CKD-602 are shown in **Figure 4.5a** and **Figure 4.5b**, respectively. In general, the observed data of encapsulated and released CKD-602 were well described by the final model. Goodness-of-fit plots from the final pharmacokinetic model in patients with linear clearance and nonlinear clearance of encapsulated CKD-602 are given in **Figure 4.6a** and **Figure 4.6b**, respectively. The model adequately describes the pharmacokinetic profile of encapsulated CKD-602 in both groups of patients. Although the pharmacokinetic data of released CKD-602 were variable, the observed and model predicted data agreed relatively well. Bootstrap CIs for pharmacokinetic parameters were not obtained because of the computational intensity of the parameter estimation.

D. DISCUSSION

Major advances in the use of liposomes, conjugates, and nanoparticles as vehicles to deliver drugs have occurred the past 10 years.[3, 8, 9] Doxil® and albumin stabilized nanoparticle formulation of paclitaxel (Abraxane®) are now FDA approved.[10, 11, 29] In addition, there are greater than 200 liposomal and nanoparticle formulations of anticancer agents currently in development.[3] This is the first study where population pharmacokinetic modeling was applied to assess the pharmacokinetics of the encapsulated and released drug after administration of a pegylated liposomal formulation of a camptothecin analogue.[30, 31] This is also the first study identify tumor in liver as a factor associated with the pharmacokinetic variability of liposomal agents. Evaluation of the pharmacokinetic disposition of the liposomal encapsulated verses released drug is of the utmost importance because the liposomal encapsulated drug is an inactive prodrug and thus only the released drug is active.[3, 17]

Pegylated-liposomal CKD-602 displayed nonlinear pharmacokinetics best described by a one-compartment structural model. The volume of distribution for encapsulated CKD-602 was 3.46 L (70.9%) and is very close to plasma volume in humans. The limited volume of distribution of encapsulated-CKD602 is consistent with other liposomal anticancer agents since the size of liposome limited their distribution to the normal tissue.[32] Saturation of clearance has been reported for both Doxil® and S-CKD602 and the nonlinear pharmacokinetics of these two drugs have been modeled using Michaelis-Menten kinetics.[26, 33-35]

The interpatient variability in the disposition of S-CKD602 can be explained in part by the presence of primary or metastatic tumor(s) located in the liver. Vmax in patients with

tumor(s) in the liver is 1.5-fold higher compared with patients without tumor(s) in the liver. This data suggest that patients with tumor in liver may have 35% lower plasma exposure and are at risk of having a lower response potential. Most studies show a decrease in clearance of small molecule drugs in patients with tumors in the liver.[36-38] This is the first study reporting an increased clearance of drug in patients with tumor involvement in the liver. The exact mechanism of this phenomenon is unknown. Recruitment of various populations of phagocytic cells (monocytes, macrophages and dendritic cells) of the MPS is involved in the immune response against tumor cell deposits in liver.[39, 40] Since liposomes are mainly cleared by MPS and liver is an important functional center of MPS, the increased clearance of encapsulated CKD-602 may due to enhanced MPS activity in patients with tumor in liver.

In patients with linear clearance of encapsulated CKD-602, patients $\geq$ 60 years of age have a reduced release rate of CKD-602 from S-CKD602 compared with patients < 60 years. This is consistent with our prior studies which showed that a reduced clearance of the liposomal encapsulated form of S-CKD-602 in patients $\geq$ 60 years of age and that the release of drug from liposome is related to clearance of liposome.[22, 23] Aging related decrease in the function of monocytes may account for the reduced clearance of liposomal agents.[24, 25] Tumor in liver is not significantly associated with the pharmacokinetic variability of patients with linear clearance of encapsulated CKD-602. This may due to the lower number of patients in the group of patients with linear clearance of encapsulated CKD-602 (n = 20) compared to the patients included in the encapsulated CKD-602 pharmacokinetic analysis (n = 39). Age is not associated with the pharmacokinetic variability of patients with nonlinear clearance of encapsulated CKD-602. The results in patients with non-linear clearance may

be associated with the overall low number of patients in this group and the number of patients with complete concentration versus time profiles.

The developed model did not take into account the lactone and carboxylate forms of CKD-602 since only total (lactone + hydroxy acid) drug concentrations were available on our study. Only the lactone form of CKD-602 has antitumor activity, and they undergo a pH-dependent equilibrium with carboxylate forms. Thus, the model of encapsulated and released CKD-602 can only be used to predict total CKD-602 exposure in the encapsulated and released forms. However, the pharmacokinetics of encapsulated CKD-602 is not affected by this limitation as the drug that remains encapsulated is all in the lactone form because the pH of the core solution is around 5.4.

In conclusion, a population pharmacokinetic model was developed for encapsulated and released CKD-602 in patients with advanced solid tumors. The release rate of CKD-602 from S-CKD602 was influenced by age and clearance of encapsulated CKD-602 was influenced by presence of tumor in liver. The development of phenotypic probes of MPS function in the liver of patients with and without tumors in the liver is needed to further evaluate these effects. The application of the population pharmacokinetic model in optimal dosing of pegylated liposomal agents needs to be further investigated to achieve a target exposure for each patient with malignant diseases.

E. REFERENCES

1. Zamboni WC, Friedland DM, Ramalingam S, et al. Relationship between the plasma and tumor disposition of STEALTH liposomal CKD-602 and macrophages/dendritic cells (MDC) in mice bearing human tumor xenografts. Paper presented at: American Association for Cancer Research2006.

2. Zamboni WC, Strychor S, Joseph E, et al. Plasma and tumor disposition of STEALTH Liposomal CKD-602 (S-CKD602) and non-liposomal CKD-602, a camptothecin analogue, in mice bearing A375 human melanoma xenograft. . Paper presented at: American Association for Cancer Research; Nov, 2006.

3. Zamboni WC. Liposomal, nanoparticle, and conjugated formulations of anticancer agents. Clin Cancer Res. Dec 1 2005;11(23):8230-8234.

4. Crul M. CKD-602. Chong Kun Dang. Curr Opin Investig Drugs. Dec 2003;4(12):1455-1459.

5. Lee JH, Lee JM, Lim KH, et al. Preclinical and phase I clinical studies with Ckd-602, a novel camptothecin derivative. Ann N Y Acad Sci. 2000;922:324-325.

6. Yu NY, Conway C, Pena RL, Chen JY. STEALTH liposomal CKD-602, a topoisomerase I inhibitor, improves the therapeutic index in human tumor xenograft models. Anticancer Res. Jul-Aug 2007;27(4B):2541-2545.

7. Lee DH, Kim SW, Suh C, et al. Belotecan, new camptothecin analogue, is active in patients with small-cell lung cancer: results of a multicenter early phase II study. Ann Oncol. Jan 2008;19(1):123-127.

8. Papahadjopoulos D, Allen TM, Gabizon A, et al. Sterically stabilized liposomes: improvements in pharmacokinetics and antitumor therapeutic efficacy. Proc Natl Acad Sci U S A. Dec 15 1991;88(24):11460-11464.

9. Maeda H, Wu J, Sawa T, Matsumura Y, Hori K. Tumor vascular permeability and the EPR effect in macromolecular therapeutics: a review. J Control Release. Mar 1 2000;65(1-2):271-284.

10. Markman M, Gordon AN, McGuire WP, Muggia FM. Liposomal anthracycline treatment for ovarian cancer. Semin Oncol. Dec 2004;31(6 Suppl 13):91-105.

11. Krown SE, Northfelt DW, Osoba D, Stewart JS. Use of liposomal anthracyclines in Kaposi's sarcoma. Semin Oncol. Dec 2004;31(6 Suppl 13):36-52.

12. Zamboni WC. Concept and clinical evaluation of carrier-mediated anticancer agents. Oncologist. Mar 2008;13(3):248-260.

13. Innocenti F, Kroetz DL, Schuetz E, et al. Comprehensive pharmacogenetic analysis of irinotecan neutropenia and pharmacokinetics. J Clin Oncol. Jun 1 2009;27(16):2604-2614.

14. Slatter JG, Schaaf LJ, Sams JP, et al. Pharmacokinetics, metabolism, and excretion of irinotecan (CPT-11) following I.V. infusion of [(14)C]CPT-11 in cancer patients. Drug Metab Dispos. Apr 2000;28(4):423-433.

15. Zamboni WC, Stewart CF, Thompson J, et al. Relationship between topotecan systemic exposure and tumor response in human neuroblastoma xenografts. J Natl Cancer Inst. Apr 1 1998;90(7):505-511.

16. Stewart CF, Zamboni WC, Crom WR, et al. Topoisomerase I interactive drugs in children with cancer. Invest New Drugs. 1996;14(1):37-47.

17. Zamboni WC, Strychor S, Joseph E, et al. Plasma, tumor, and tissue disposition of STEALTH liposomal CKD-602 (S-CKD602) and nonliposomal CKD-602 in mice bearing A375 human melanoma xenografts. Clin Cancer Res. Dec 1 2007;13(23):7217-7223.

18. Zamboni WC, Gajjar AJ, Mandrell TD, et al. A four-hour topotecan infusion achieves cytotoxic exposure throughout the neuraxis in the nonhuman primate model: implications for treatment of children with metastatic medulloblastoma. Clin Cancer Res. Oct 1998;4(10):2537-2544.

19. Allen TM, Hansen C. Pharmacokinetics of stealth versus conventional liposomes: effect of dose. Biochim Biophys Acta. Sep 30 1991;1068(2):133-141.

20. Zamboni WC, Maruca LJ, Strychor S, et al. Bidirectional pharmacodynamic interaction between pegylated liposomal CKD-602 (S-CKD602) and monocytes in patients with refractory solid tumors. J Liposome Res. Jul 14.

21. Zamboni WC. Liposomal, nanoparticle, and conjugated formulations of anticancer agents. Clin Cancer Res. 2005;11:8230-8234.

22. Zamboni WC, Maruca LJ, Strychor S, et al. Age and body composition related-effects on the pharmacokinetic disposition of STEALH liposomal CKD-602 (S-CKD602) in patients with advanced solid tumors2007.

23. Sidone BJ, Edwards RP, Zamboni BA, Strychor S, Maruca LJ, Zamboni WC. Evaluation of body surface area (BSA) based dosing, age, and body composition as factors affecting the pharmacokinetic (PK) variability of STEALTH liposomal doxorubicin (Doxil). Paper presented at: AACR-NCI-EORTC2007.

24. Zamboni WC, Strychor S, Maruca L, et al. Pharmacokinetic Study of Pegylated Liposomal CKD-602 (S-CKD602) in Patients With Advanced Malignancies. Clin Pharmacol Ther. Aug 12 2009.

25. De Martinis M, Modesti M, Ginaldi L. Phenotypic and functional changes of circulating monocytes and polymorphonuclear leucocytes from elderly persons. Immunol Cell Biol. Aug 2004;82(4):415-420.

26. Zamboni WC, Strychor S, Maruca L, et al. Pharmacokinetic study of pegylated liposomal CKD-602 (S-CKD602) in patients with advanced malignancies. Clin Pharmacol Ther. Nov 2009;86(5):519-526.

27. Zamboni WC, Ramalingam S, Friedland DM, et al. Phase I and pharmacokinetic study of pegylated liposomal CKD-602 in patients with advanced malignancies. Clin Cancer Res. Feb 15 2009;15(4):1466-1472.

28. Jones SF, Zamboni WC, Burris III HA, et al. Phase I and pharmacokinetic (PK) study of IHL-305 (pegylated liposomal irinotecan) in patients with advanced solid tumors. Paper presented at: ASCO; Jun, 2009, 2009; Orlando, FL.

29. Roy V, LaPlant BR, Gross GG, Bane CL, Palmieri FM. Phase II trial of weekly nab (nanoparticle albumin-bound)-paclitaxel (nab-paclitaxel) (Abraxane) in combination with gemcitabine in patients with metastatic breast cancer (N0531). Ann Oncol. Mar 2009;20(3):449-453.

30. Giles FJ, Tallman MS, Garcia-Manero G, et al. Phase I and pharmacokinetic study of a low-clearance, unilamellar liposomal formulation of lurtotecan, a topoisomerase 1 inhibitor, in patients with advanced leukemia. Cancer. Apr 1 2004;100(7):1449-1458.

31. Gelmon K, Hirte H, Fisher B, et al. A phase 1 study of OSI-211 given as an intravenous infusion days 1, 2, and 3 every three weeks in patients with solid cancers. Invest New Drugs. Aug 2004;22(3):263-275.

32. Allen TM, Cullis PR. Drug delivery systems: entering the mainstream. Science. Mar 19 2004;303(5665):1818-1822.

33. Gabizon A, Isacson R, Rosengarten O, Tzemach D, Shmeeda H, Sapir R. An open-label study to evaluate dose and cycle dependence of the pharmacokinetics of pegylated liposomal doxorubicin. Cancer Chemother Pharmacol. Apr 2008;61(4):695-702.

34. Gabizon A, Shmeeda H, Barenholz Y. Pharmacokinetics of pegylated liposomal Doxorubicin: review of animal and human studies. Clin Pharmacokinet. 2003;42(5):419-436.

35. Gabizon A, Tzemach D, Mak L, Bronstein M, Horowitz AT. Dose dependency of pharmacokinetics and therapeutic efficacy of pegylated liposomal doxorubicin (DOXIL) in murine models. J Drug Target. Nov 2002;10(7):539-548.

36. Robieux I, Sorio R, Borsatti E, et al. Pharmacokinetics of vinorelbine in patients with liver metastases. Clin Pharmacol Ther. Jan 1996;59(1):32-40.

37. Twelves CJ, O'Reilly SM, Coleman RE, Richards MA, Rubens RD. Weekly epirubicin for breast cancer with liver metastases and abnormal liver biochemistry. Br J Cancer. Dec 1989;60(6):938-941.

38. Wilson WH, Berg SL, Bryant G, et al. Paclitaxel in doxorubicin-refractory or mitoxantrone-refractory breast cancer: a phase I/II trial of 96-hour infusion. J Clin Oncol. Aug 1994;12(8):1621-1629.

39. Heuff G, van der Ende MB, Boutkan H, et al. Macrophage populations in different stages of induced hepatic metastases in rats: an immunohistochemical analysis. Scand J Immunol. Jul 1993;38(1):10-16.

40. Gulubova M, Manolova I, Cirovski G, Sivrev D. Recruitment of dendritic cells in human liver with metastases. Clin Exp Metastasis. 2008;25(7):777-785.

Table 4.1.

A summary of Patient Demographics and Covariates Included in the Analysis

Characteristics	Number of patients	Mean ± SD	Median (Range)
Age (years)		60.6 ± 12.2	62 (33.– 79)
Body Surface Area (m2)		1.91 ± 0.30	1.86 (1.36 – 2.76)
Body Weight (kg)		78.7 ± 21.4	75.5 (44.0 – 148)
Body Mass Index (kg/m2)		27.4 ± 5.60	26.7 (18.8 – 45.7)
Creatinine Clearance (ml/min)		98.4 ± 46.6	84.7 (33.2 – 277)
Height (cm)		169 ± 11.9	170 (142 – 196)
Ratio of Body Weight to Ideal Body Weight		1.27 ± 0.28	1.22 (0.83 – 2.13)
Sex			
Male	24		
Female	21		
Primary tumor type			
Colorectal Adenocarcinoma	17		
Ovarian Cancer	5		
Sarcoma	5		
Non-Small Cell Lung Cancer	4		
Pancreatic Adenocarcinoma	3		
Hepatocellular Carcinoma	2		
Prostate Carcinoma	2		
Esophageal, Metastatic Breast, Mesothelioma, Renal Cell Carcinoma, Thyroid, Appendix, Unknown Primary	1 patient for each type		
Patients with Tumors in liver	26		
Patients without tumors in liver	19		

Table 4.2.

Population Pharmacokinetic Parameters Obtained from the Final Covariate Model for Encapsulated CKD-602

Parameter	Definition	Population Mean RSE[a] (%)	Bootstrap Median (95% CI[f])	IIV, CV%[b] RSE[a] (%)
V_{Encap} (L)	Volume of distribution	3.63 (9)	3.78 (3.32-6.00)	72 (48)
V_{max} (μg/h)	Maximum velocity			
w/ tumor in liver[c]		150 (19)	163 (102 - 345)	205 (51)
w/o tumor in liver[d]		97.4 (32)	99.7 (52.3 – 186)	
K_m (μg/L)	Michaelis-Menten constant	992 (17)	985 (558-1250)	NE[e]
Residual variability				
Proportional error (variability as %)		14.4 (57)	14.8 (9.4-31.9)	NA[g]
Additive error (μg/L)		10.9 (65)	10.3 (1.65-28.5)	

[a] Relative standard error for estimate.

[b] Coefficient of variation.

[c] The estimated maximum velocity for patients with tumor in liver.

[d] The estimated maximum velocity for patients without tumor in liver.

[e] Negligible.

[f] Confidence interval calculated from 910 bootstrap resamplings.

[g] Not estimated.

Table 4.3.

Population Pharmacokinetic Parameters Obtained from the Final Model for CKD-602 after Administration of Non-liposomal CKD-602

Parameter	Definition	Population Mean RSE (%)	Bootstrap Median (95% CI)	IIV, CV% RSE (%)
V_c (L)	Volume of distribution for central compartment	9.72 (9)	9.57 (7.62-11.84)	NE
CL (L/h)	Systemic clearance	7.90 (13)	7.84 (5.77-10.05)	27.0 (38)
V_p (L)	Volume of distribution for peripheral compartment	27.7 (15)	27.8 (20.2-35.2)	21.8 (39)
CL_d (L/h)	Distribution clearance	5.07 (17)	5.17 (2.90-7.26)	NE
Residual variability				
Proportional error (variability as %)		31.3 (9.5)	40.1 (24.3-54.8)	NA

Table 4.4.

Population Pharmacokinetic Parameters Obtained From the Final Covariate Model for Encapsulated and Released CKD-602 in Patients with Linear Clearance of Encapsulated CKD-602

Parameter	Definition	Population Mean RSE (%)	IIV, CV% RSE (%)
V_{Encap} (L)	Volume of distribution for encapsulated	4.69 (2.2)	53 (26)
V_{Rel1} (L)	Volume of distribution for central compartment of released	9.72 (NA[c])	369 (46)
V_{Rel2} (L)	Volume of distribution for peripheral compartment of released	27.7 (NA[c])	180 (103)
CL_{Encap} (L/h)	Clearance of encapsulated	0.089 (6.5)	151 (27)
$CL_{Encap-Rel}$ (L/h)	Clearance of release CKD-602 from S-CKD602		
Age < 60 yo[a]		0.130 (17)	58 (65)
Age ≥ 60 yo[b]		0.048 (14)	
E%, %	Encapsulation percent of CKD-602 in the formulation	96.3 (28)	NA[c]
CL_{Rel-d} (L/h)	Distribution clearance for released	5.07 (NA[c])	126 (55)
CL_{Rel} (L/h)	Systemic clearance for released	7.90 (NA[c])	NA[c]
Residual variability			
Proportional error (variability as %)		19.8 (26)	
Additive error for encapsulated (μg/L)		7.82 (31)	NA[c]
Additive error for released (μg/L)		0.019 (38)	

[a] The clearance of release CKD-602 from S- CKD602 for patients younger than 60 years old.

[b] The clearance of release CKD-602 from S- CKD602 for patients older than 60 years old.

[c] Not estimated.

Table 4.5.

Population Pharmacokinetic Parameters Obtained From the Final Model for Encapsulated and Released CKD-602 in Patients with Nonlinear Clearance of Encapsulated CKD-602

Parameter	Definition	Population Mean RSE (%)	IIV, CV% RSE (%)
V_{Encap} (L)	Volume of distribution for encapsulated	3.36 (4.6)	12.6 (44)
V_{Rel1} (L)	Volume of distribution for central compartment of released	9.72 (NA)	115 (104)
V_{Rel2} (L)	Volume of distribution for peripheral compartment of released	27.7 (NA)	130 (89)
$V_{max, Encap}$ (μg/h)	Maximum velocity of encapsulated	36.1 (81)	28.8 (32)
$V_{max, Encap-Rel}$ (μg/h)	Maximum velocity of release CKD-602 from S-CKD602	90.9 (81)	28.8 (32)
K_m (μg/L)	Michaelis-Menten constant	1450 (16)	NA
E%, %	Encapsulation percent of CKD-602 in the formulation	96.3 (31)	NA
CL_{Rel-d} (L/h)	Distribution clearance for released	5.07 (NA)	NA
CL_{Rel} (L/h)	Systemic clearance for released	7.90 (NA)	89 (59)
Residual variability			
Proportional error for encapsulated (variability as %)		11.7 % (43)	
Proportional error for released (variability as %)		26.2 % (29)	NA[a]
Additive error for released (μg/L)		0.632 (69)	

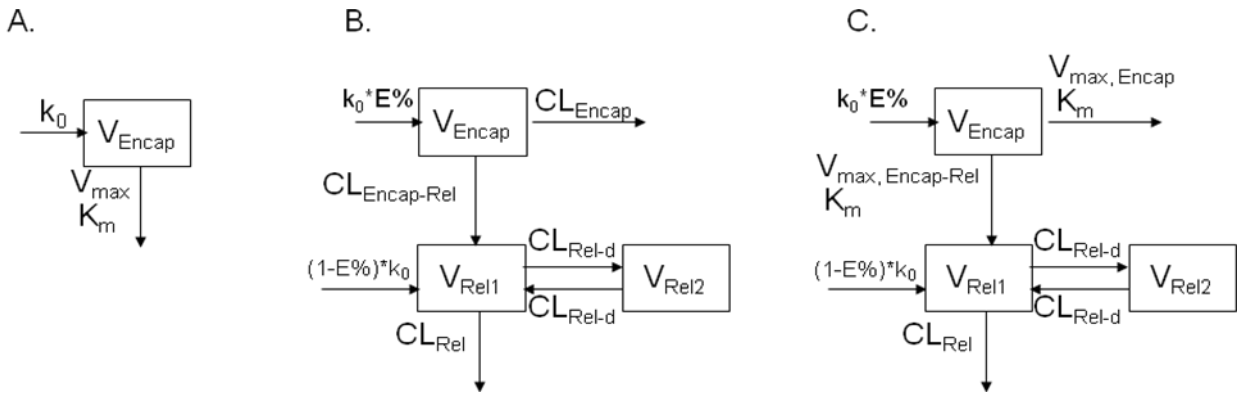

Figure 4.1. The final structural pharmacokinetic model for encapsulated alone (one compartment with nonlinear clearance) in all patients (A), encapsulated (one compartment with linear clearance) and released CKD-602 (two compartments with linear clearance) in patients with linear clearance of encapsulated CKD-602 (B), and encapsulated (one compartment with nonlinear clearance) and released CKD-602 (two compartments with linear clearance) in patients with nonlinear clearance of encapsulated CKD-602 (C). A fraction of dose which was administered in the form of non-liposomal CKD-602 was included. E% is encapsulation percent of CKD-602 in the formulation. V_{Rel1}, V_{Rel2}, CL_{Rel}, and CL_{Rel-d} in Figure 4.1B and 4.1C were fixed based on non-liposomal CKD-602 pharmacokinetic data.

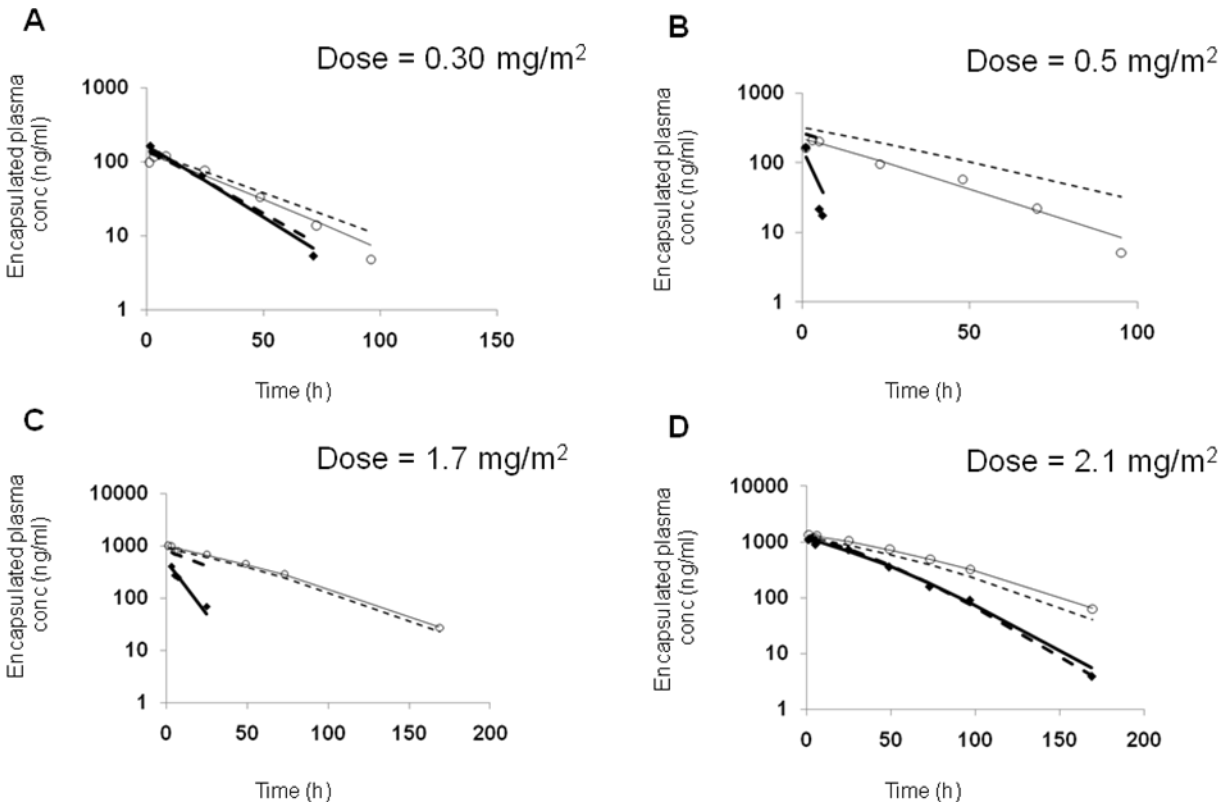

Figure 4.2. Representative individual plots of observed, population predicted, and individual predicted values of plasma concentrations of encapsulated CKD-602. Figure 4.2A, 4.2B, 4.2C, and 4.2D represent the concentration versus time profile in patients treated with dose of 0.30 mg/m^2, 0.5 mg/m^2, 1.7 mg/m^2 and 2.1 mg/m^2 respectively. The observed (○), population predicted (- - -), and individual predicted (—) values of encapsulated CKD-602 in patients without tumor in liver are presented. The observed (♦), population predicted (**- - -**), and individual predicted (**——**) values of encapsulated CKD-602 in patients with tumor in liver are presented.

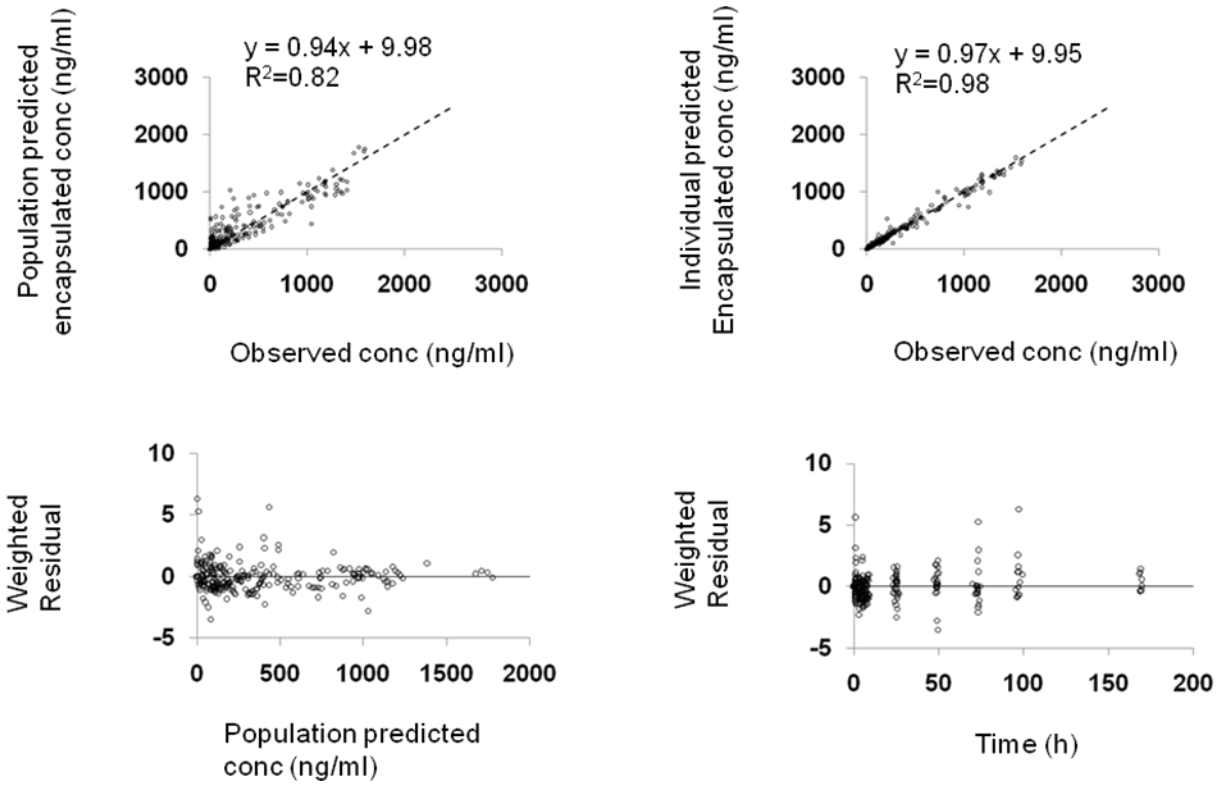

Figure 4.3. Goodness-of-fit plots for the final model of encapsulated CKD-602. The dashed lines in the upper left and right panels are lines of identity . The solid lines in the lower left and right panels represent the line y=0. .

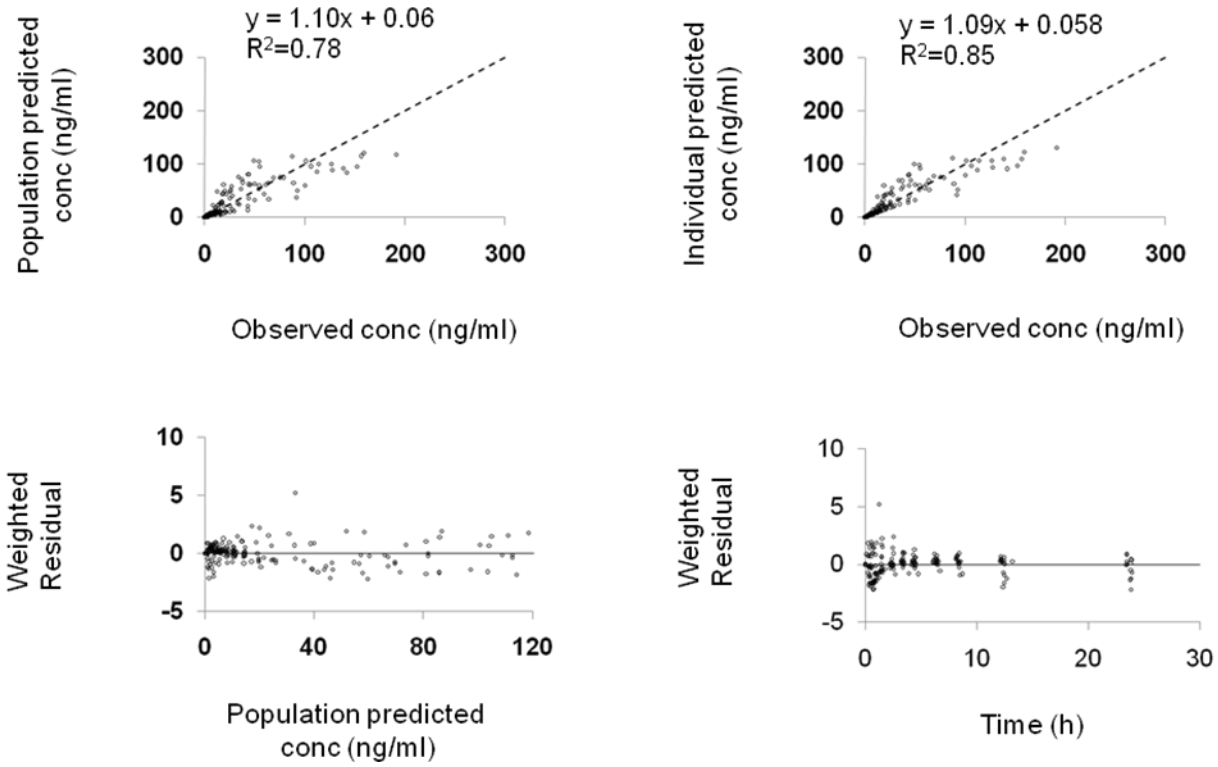

Figure 4.4. Goodness-of-fit plots for the final model of CKD-602 after administration of non-liposomal CKD-602. The dashed lines in the upper left and right panels are lines of identity. The solid lines in the lower left and right panels represent the line y=0.

Figure 4.5a **Figure 4.5b**

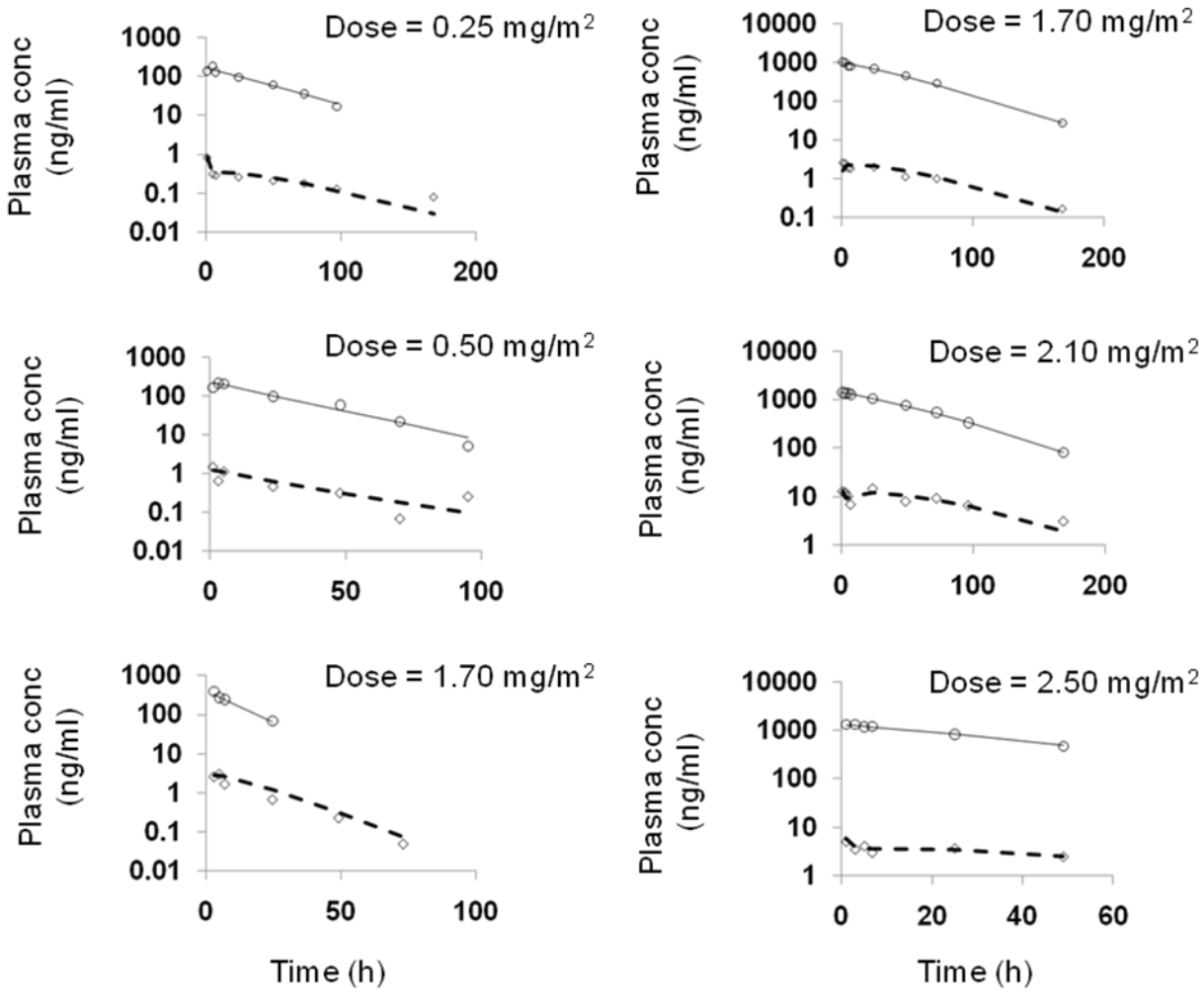

Figures 4.5a and 4.5b. Representative individual plots of observed (○), and individual predicted (—) values of plasma concentrations of encapsulated and the observed (◊) and individual predicted (- - -) values of plasma concentrations of released CKD-602 in patients with linear clearance of encapsulated CKD-602 (5a) and in patients with nonlinear clearance of encapsulated CKD-602 (5b).

Figure 4.6a

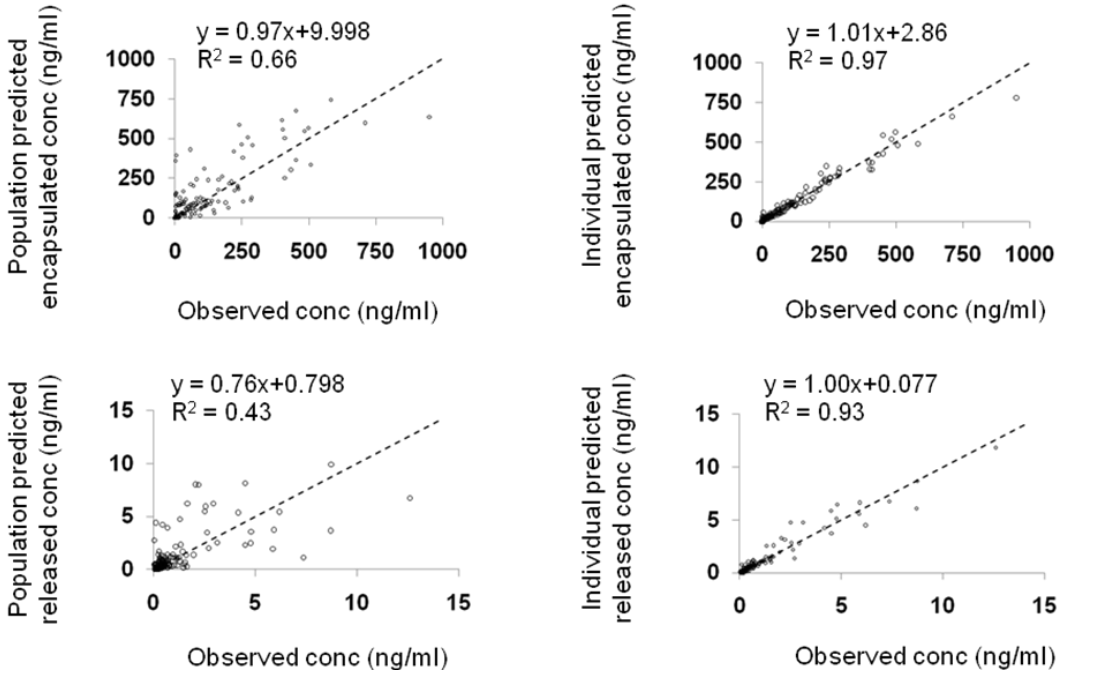

Figure 4.6b

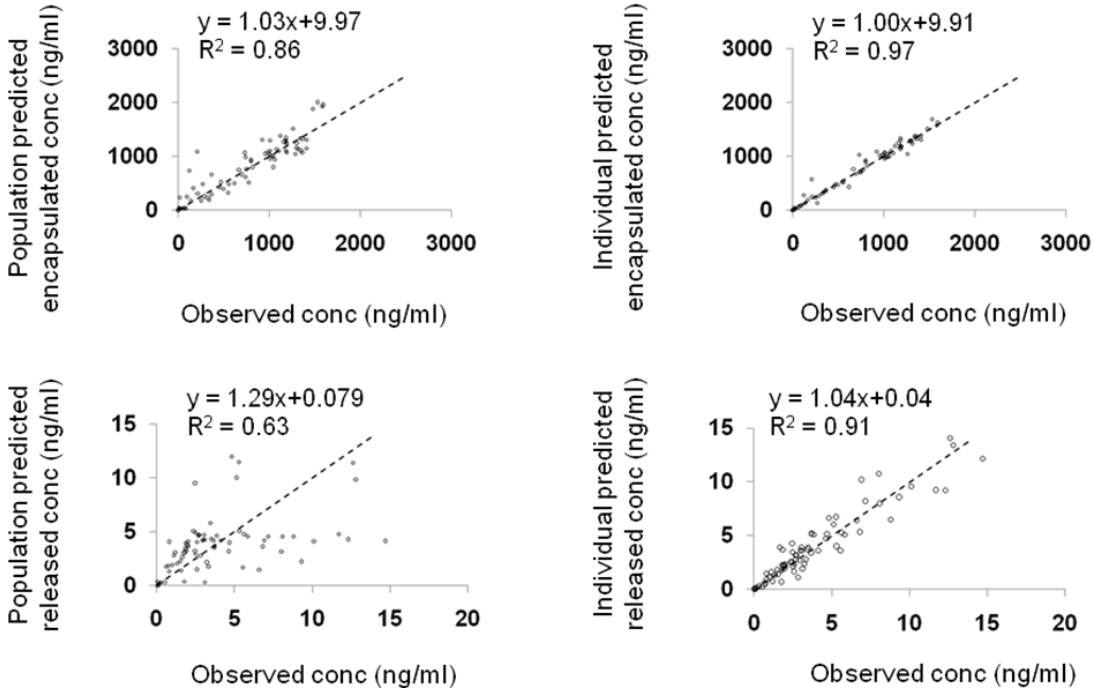

Figures 4.6a and 4.6b. Observed versus population model-predicted encapsulated and released plasma concentrations for the final models in patients with linear clearance of encapsulated CKD-602 (4.6a) and in patients with nonlinear clearance of encapsulated CKD-602 (4.6b). The dashed lines are lines of identity.

CHAPTER 5

POPULATION PHARMACOKINETICS OF PEGYLATED LIPOSOMAL CPT-11 (IHL-305) IN PATIENTS WITH ADVANCED SOLID TUMORS

A. INTRODUCTION

IHL-305 is a PEGylated liposomal formulation of irinotecan (CPT-11), a camptothecin analogue which inhibits topoisomerase I and has been approved for the treatment of metastatic colorectal cancer (1-4). The PEGylated liposomal formulation consists of phospholipids covalently bound to polyethylene glycol (PEG) only on the outside of the lipid bilayer. CPT-11 is a prodrug that requires activation to the active metabolite, 7-ethyl-10-hydroxy-camptothecin (SN-38), which is approximately 100- to 1000-fold more active than the parent drug. SN-38 is further conjugated to form an inactive glucuronide (SN-38G) by uridine diphosphate glucuronosyltransferases (UGTs), primarily the UGT1A1 isoform. Other identified CPT-11 metabolites are 7-ethyl-10-[4-N-(5-aminopentanoic acid)-1-piperidino]-carbonyloxycamptothecin (APC) and 7-ethyl-10-[4-amino-1-piperidino]-carbonyloxycamptothecin (NPC) (3, 5).

The development of PEGylated liposomes, such as PEGylated liposomal doxorubicin (Doxil), CKD-602 (S-CKD602), and CPT-11 (IHL-305) was based on the discovery that incorporation of PEG-lipids into liposomes yields preparations with prolonged plasma exposure and superior tumor delivery compared to conventional liposomes composed of natural phospholipids (4, 6, 7). Doxil® is approved for the treatment of refractory ovarian cancer, Kaposi sarcoma, and multiple myeloma (8, 9). The PEGylated liposomes of Doxil and IHL-305 were made using two different methods. The PEGylated liposome of Doxil was made by adding the PEG lipid before the process of liposomal formation which results PEG tether being projected on both the inside and outside of liposome. The PEGylated liposome of IHL-305 is made by adding the PEG lipids after the process of liposomal formation which results in PEG tether only being localized on the outer leaflet (10). Encapsulation of the CPT-

11 allow for release of the active-lactone form into the tumor over a protracted period of time, which is ideal for a cell cycle-specific drug (1-4, 11, 12). The PEGylated liposomal formulation is expected to have an enhanced therapeutic ratio compared to non-liposomal CPT-11.

Studies of the pharmacokinetics (PK) of IHL-305 compared to CPT-11 in mice, rats, and dogs showed a marked increase in the concentrations of CPT-11 and its metabolites in the plasma, liver, kidney, spleen, and tumor tissue after administration of IHL-305 as compared with non-liposomal CPT-11 administration. The plasma exposure of IHL-305 at 16.7 mg/kg IV x 1 was approximately 302-fold greater than non-liposomal CPT-11 at the same dose in tumor-bearing mice (13). In mice bearing human tumor xenografts, the exposures of CPT-11 and SN-38 in tumor were 9.0 and 3.9-fold higher and the mean residence time of CPT-11 and SN-38 in plasma was 4.4 and 4.7-fold longer for IHL-305 compared with non-liposomal CPT-11 (14). In addition, the antitumor response was greater for IHL-305 compared with non-liposomal CPT-11 (14). These results are consistent with reports that the antitumor response to camptothecin analogues is enhanced by prolonged duration of exposures in tumors (11, 12, 15-17).

The PK disposition of carrier-mediated agents, such as, nanoparticles, nanosomes, and conjugated agents, is dependent upon the carrier until the drug is released from the carrier. Unlike traditional anticancer agents which are cleared by the liver and kidneys, the clearance of non-PEGylated and PEGylated liposomes is via the mononuclear phagocytic system (MPS) which include monocytes, macrophages and dendritic cells located primarily in the liver and spleen (18). Uptake by the MPS usually results in sequestering of the encapsulated drug in the MPS, where it can be degraded. In addition, the uptake of the

liposomes by the MPS may result in acute impairment of the MPS and toxicity. PEGylated liposomes are cleared much slower via MPS compared to non-PEGylated liposomes (6, 19). Once the drug is released from the carrier, the PK disposition of the drug will be the same as after administration of the non-carrier form of the drug (4, 18). Thus, the PK of liposomes are complex.

The nomenclature used to describe the PK disposition of carrier-mediated drugs includes encapsulated or conjugated (drug within or bound to the carrier), released (the active drug released from the carrier), and sum total (encapsulated or conjugated drug plus released drug). The ability to evaluate the various forms (encapsulated and released) of the drug after administration of nanosome or nanoparticle formulations is dependent upon specific sample processing methods (20). The drug that remains encapsulated within nanosomes or nanoparticles, or linked to a conjugate or polymer is an inactive prodrug, thus the drug must be released from the carrier to be active.

Nanoparticle agents have higher variability in PK (drug clearance, systemic exposure, distribution, etc.) disposition with potentially higher variability in pharmacodynamic (PD) (antitumor response and toxicity) disposition as compared with traditional small molecule chemotherapy. However, the factors affecting the PK and PD variability of encapsulated and released forms of conventional and PEGylated liposomes remain unclear, but most likely include the MPS (1). We have evaluated factors affecting the PK and PD of liposomal anticancer agents. We were the first to report a reduced clearance of the liposomal encapsulated forms of Doxil and S-CKD602 in patients $\geq$ 60 years of age (21, 22). We have also reported that patients with a lean body composition may have a reduced tissue distribution and an increased plasma exposure of S-CKD602. In addition, we have reported

an age related decrease in the function of monocytes which may be associated with a reduced clearance of liposomes and reduced cytotoxicity to the monocytes (19, 23, 24).

The clinical results of the phase I study and limited PK results were previously published (25). IHL-305 was associated with high interpatient variability in the PK disposition of sum total (encapsulated + released) and released CPT-11 (25). Population PK analysis is a useful tool for identification of sources of PK variability and can aid in the design of alternative dosing regimens to enhance efficacy and safety. The objectives of this study were to describe the population PK of the encapsulated CPT-11, released CPT-11 and the active metabolite SN-38 after administration of the PEGylated liposomal form of the drug and to characterize clinical covariates that influence IHL-305 PK.

B. METHODS

Patients

Written informed consent, approved by the Institutional Review board of the Sarah Cannon Research Institute and Vanderbilt University Medical Center, was obtained from all patients prior to study entry. Patients ≥ 18 years of age with a histologically confirmed malignant solid tumor for which no effective therapy was available or a conventional therapy have failed to treat or a conventional therapy does not exist were eligible for this study. Patients must have recovered from all acute adverse effects of prior therapies, excluding alopecia. Pertinent eligibility criteria included a Eastern Cooperative Oncology Group (ECOG) performance status of 0, 1, or 2, adequate bone marrow, hepatic, and renal function as evidenced by the following: absolute neutrophil count (ANC) ≥ 1500/μL, platelets ≥ 100,000/μL, total bilirubin within normal institutional limits, aspartate aminotransferase (AST) ≤ 2.5 x institutional upper limit of normal (ULN) if liver metastases were not present and ≤ 5.0 x ULN if liver metastases were present, plasma creatinine ≤ 1.5 x the institutional ULN or creatinine clearance ≥ 60 ml/min/1.73 m^2 for patients with creatinine levels above institutional normal. Patients must have the ability to understand and the willingness to sign a written informed consent document. Patient were excluded from the study for any of the following: prior treatment with CPT-11; chemotherapy or radiotherapy within 4 weeks (6 weeks for nitrosoureas or mitomycin C); treatment with any other investigational agent during study; brain metastases; a history of allergic reactions to compounds of similar chemical composition to IHL-305; concurrent serious infections; pregnancy or breastfeeding; uncontrolled intercurrent illness including ongoing or active infection, unstable angina pectoris or psychiatric illness/social situations; significant cardiac disease including heart

failure that meets New York Heart Association (NYHA) class III and IV definitions, history of myocardial infarction within one year of study entry, uncontrolled dysrhythmias or poorly controlled angina; a history of serious ventricular arrhythmia, QTc $\geq$ 450 msec for men and 470 msec for women, or LVEF $\leq$ 40% by MUGA. Prior treatment with camptothecin analogues other than IHL-305 or CPT-11 was permitted.

Dosage and Administration

IHL-305 is a formulation of CPT-11 encapsulated in long-circulating PEGylated liposome. In IHL-305, the PEGylated liposome bilayer is composed of cholesterol and hydrogenated soybean phosphatidylcholine (HSPC), and the surface of liposomes is modified with PEG. The mean particle diameter is approximately 100 nm and the ratio of CPT-11 to lipid is 1:4. The PEGylated liposomal formulation was generated by Terumo Corporation (Tokyo, Japan). IHL-305 was supplied by Yakult Honsha Corporation in sterile 10 mL light-resistant, single-use glass vials as a translucent white to pale yellow liquid with a nominal total CPT-11 concentration of 5 mg/mL. IHL-305 was diluted 25-fold in 5% dextrose or normal saline prior to administration. Prior to administration of the study drug, patients were premedicated with ondansetron (or other 5-HT3 inhibitor should circumstances require) and dexamethasone, according to each institution's standard of care.

IHL-305 was administered IV x 1 over 60 minutes every 4 weeks. Doses administrated (expressed in mg of CPT-11) were 3.5, 7, 10.5, 14, 28, 33.5, 37, 50, 67, 80, 88, 120, 160, and 210 mg/m^2. This phase I study followed a standard dose escalation design with patients enrolled in cohorts of 3, with the possibility of extending the cohort up to 6 patients depending on the number of dose-limiting toxicities (DLT) (18). No intra-patient dose

escalation was permitted. The maximum tolerated dose (MTD) was defined based on standard criteria.

Sample Collection, Processing, and Analytical Studies

Plasma samples for PK assessment were obtained from all patients. On cycle 1, blood (5 mL) was collected in tubes containing sodium heparin at prior to administration, at end of the infusion (approximately 1 h), and at 1.5 h, 2 h, 3 h, 5 h, 9 h, 13 h, and 25 h after the start of the infusion for patients treated at < 67 mg/m^2 and the first three patients treated at 67 mg/m^2. Additional samples at 49 h, 73 h, 97 h, 169 h (day 7), 192 h (day 8), and 216 h (day 9) after the start of the infusion were also collected for the last three patients treated at 67 mg/m^2 and patients treated at > 67 mg/m^2.

The blood samples were centrifuged at 3,000 x g for 15 min at 4ºC to separate plasma samples. Plasma samples were processed to measure sum total (encapsulated + released) CPT-11 and released CPT-11, and SN-38 as previously described (26). The sum total CPT-11, released CPT-11, and SN-38 concentrations were measured by a high-performance liquid chromatography (HPLC) as previously described (26). The total (lactone + hydroxy acid) form of camptothecin was measured for sum total CPT-11, released CPT-11, and SN-38 samples. The lower limit of quantitation (LLQ) of the total form sum total CPT-11, released CPT-11, and SN-38 were 100, 2, and 2 ng/mL, respectively. The encapsulated concentration of CPT-11 was calculated as difference between sum total and released CPT-11.

Population PK Analysis

Encapsulated CPT-11, released CPT-11 and SN-38 concentration-time data were analyzed using the nonlinear mixed effects modeling approach as implemented in NONMEM (version 6; University of California, San Francisco, CA). The first order conditional estimation (FOCE) method were used in analyses. S-PLUS 8.0 (Version 8.0, Insightful Corporation, Seattle, Washington) was used for graphical diagnostics and covariate screen. The population PK model of IHL-305 was developed in two steps: (a) basic (structural) model development and (b) covariate model development.

Mean population PK variables, interindividual variability, and residual error were assessed in the model development (27, 28). Interindividual variability for each PK variable was modeled with an exponential function. Residual error models of the additive, proportional, exponential, and combination methods were evaluated for the best structural PK model. Individual PK variables were obtained by posterior Bayesian estimation (27, 28). Model selection for nonhierarchical models (i.e., linear and nonlinear elimination models) was guided by goodness-of-fit plots (e.g., observed versus predicted plasma concentrations, weighted residuals versus predicted concentrations, and weighted residuals versus time), Akaike information criterion (AIC), and precision of parameter estimates. AIC was calculated as AIC = OFV + 2 x p, where OFV is the NONMEM objective function value and p is the number of PK variables. The model was chosen on the basis of smaller values of AIC, better precision of estimates, and superior goodness-of-fit plots.

Encapsulated Drug, Released Drug and Active Metabolite Model

The structural model of encapsulated CPT-11, released CPT-11, and SN-38 was built sequentially. Firstly, the best model for encapsulated CPT-11 was selected from all the

possible models. Then based on the best model for encapsulated CPT-11, simultaneous modeling of the encapsulated and the released CPT-11 were performed for data from all patients, in which various compartment models for released drug were tested. Finally, based on the best model for encapsulated and released CPT-11, simultaneous modeling of the encapsulated CPT-11, released CPT-11 and SN-38 were attempted for data from all patients.

Encapsulated Drug Model. The structural model was built to fit encapsulated CPT-11 plasma concentration-time profiles from all 39 patients. One-compartment model and two-compartment model with first-order elimination or nonlinear elimination characterized by Michaelis-Menten kinetics were tested to fit encapsulated plasma concentration data.

Released Drug Model. Based on the best model for encapsulated CPT-11, one-compartment model, two-compartment model and three-compartment model with first-order elimination were tested to fit released plasma concentration data in the simultaneous modeling of the encapsulated and the released drug. As most of the CPT-11 remains encapsulated in the plasma after administration of IHL-305 and the plasma concentration of released CPT-11 is only 1% of encapsulated CPT-11, the amount or concentration of CPT-11 that is non-encapsulated in the dosage (infusion bag) is important to capture relative to the high concentrations of released CPT-11 at earlier time points. Thus, estimates of the non-encapsulated CPT-11 in the formulation were included in models for encapsulated and released CPT-11 after administration of IHL-305.

Active Metabolite Model. Base on the best model for encapsulated and released CPT-11, one-compartment model, two-compartment model and three-compartment model with first-order elimination (Eq. A) were tested to fit SN-38 plasma concentration data in the simultaneous modeling of the encapsulated CPT-11, released CPT-11 and SN-38. However,

the estimation of PK parameters for the released CPT-11 and SN-38 proved to be unsatisfactory because no successful termination with covariance step could be achieved. Therefore, in this modeling process, the PK parameters associated with distribution and elimination of encapsulated and released CPT-11 were determined from PK model of the encapsulated and released CPT-11 and fixed in the population PK model of encapsulated CPT-11, released CPT-11, and SN-38. In addition to fixing PK parameters of encapsulated and released CPT-11, two-compartment model with linear clearance was used and the initial estimate range of parameter estimates was set according to a published PK model for SN-38 (29).

The PK model used to characterize the disposition of encapsulated CPT-11, released CPT-11 and SN-38 is shown in **Figure 5.1**. The differential equations describing the PK model of encapsulated CPT-11, released CPT-11 and SN-38 are as follows:

$$\frac{dA_{Encap}}{dt} = k_0 \bullet E\% - \frac{V_{\max,Encap} \bullet A_{Encap}}{K_m \bullet V_{Encap} + A_{Encap}} - \frac{V_{\max,Encap} \bullet F_{Rel} \bullet A_{Encap}}{K_m \bullet V_{Encap} + A_{Encap}}, \; A_{Encap}(0) = 0$$

$$\frac{dA_{Rel}}{dt} = k_0 \bullet (1 - E\%) + \frac{V_{\max,Encap} \bullet F_{Rel} \bullet A_{Encap}}{K_m \bullet V_{Encap} + A_{Encap}} - \frac{CL_{Rel}}{V_{Rel}} \bullet A_{Rel}, \; A_{Rel}(0) = 0$$

$$\frac{dA_{SN-38-1}}{dt} = \frac{CL_{Rel}}{V_{Rel}} \bullet A_{Rel} + \frac{CL_{SN-38-d}}{V_{SN-38-2}} \bullet A_{SN-38-2} - \frac{CL_{SN-38}}{V_{SN-38-1}} \bullet A_{SN-38-1} - \frac{CL_{SN-38-d}}{V_{SN-38-1}} \bullet A_{SN-38-1}, \; A_{SN-38-1}(0) = 0$$

$$\frac{dA_{SN-38-2}}{dt} = -\frac{CL_{SN-38-d}}{V_{SN-38-2}} \bullet A_{SN-38-2} + \frac{CL_{SN-38-d}}{V_{SN-38-1}} \bullet A_{SN-38-1}, \; A_{SN-38-2}(0) = 0$$

$$C_{Encap} = -\frac{A_{Encap}}{V_{Encap}}$$

$$C_{\mathrm{Re}\,l} = -\frac{A_{\mathrm{Re}\,l}}{V_{\mathrm{Re}\,l}}$$

$$C_{SN-38} = -\frac{A_{SN-38-1}}{V_{SN-38-1}}$$

dA_{Encap}/dt is the elimination rate, $V_{max,\ Encap}$ is the maximum velocity of encapsulated CPT-11, F_{Rel} is the fraction of encapsulated CPT-11 released from IHL-305, and K_m is the concentration at which half-maximum elimination rate is achieved, V_{Encap} is the volume of distribution of encapsulated CPT-11, CL_{Rel} is the clearance of the released CPT-11, V_{Rel} is the volume of distribution of released CPT-11, E% is the encapsulation percent of CKD602 in the formulation, CL_{SN-38} is the apparent systemic clearance of SN-38, $CL_{SN-38-d}$ is the apparent distribution clearance of SN-38, V_{SN-3-1} is the apparent volume of distribution for the central compartment of SN-38, $V_{SN-38-2}$ is the apparent volume of distribution for the peripheral compartment of SN-38. A_{Encap} is encapsulated CPT-11 amount in plasma, C_{Encap} is the plasma concentration of encapsulated CPT-11, A_{Rel} is released CPT-11 amount in plasma, C_{Rel} is the plasma concentration of released CPT-11, $A_{SN-38-1}$ is SN-38 amount in plasma, C_{SN-38} is the plasma concentration of SN-38. k_0 is the infusion rate and k_0 is 0 after stop of infusion.

Covariate Analysis

The covariate model building was a stepwise process. A screen for potential significant covariates was done using S-PLUS 8.0 (Version 8.0, Insightful Corporation, Seattle, Washington). The potential covariates as listed in **Table 5.1** were tested for influence on the structural PK variables. The potential significant covariates selected from screen were introduced into the covariate model as linear, exponential, or power function,

and assessed in the population PK models. A significant covariate was selected to be retained in the final model if addition of the covariate resulted in a decrease in OFV >3.875 ($P < 0.05$) during the forward full covariate model building, and removal of the covariate resulted in an increase in OFV >10.828 ($P < 0.001$) during the stepwise backward model reduction (30). In addition, the increase in precision of the variable estimate (% relative SE of prediction) and reduction in interindividual variability were used as another indicator of the improvement of the goodness of fit.

C. RESULTS

Patient demographics

Fourty-two patients were enrolled on this study from 14 December 2006 to 15 December 2008 at Sarah Cannon Research Institute and Vanderbilt University Medical Center. PK studies of encapsulated CPT-11, released CPT-11 and SN-38 were performed in 39 patients. Patient characteristics are listed in **Table 5.1**. The numbers of male and female patients evaluated in the phase I study were 13 and 26, respectively. The mean (median, range) age of the patients was 59.3 years (60 years, 41 to 75 years). A total of 392 plasma concentrations of encapsulated CPT-11, 322 plasma concentrations of released CPT-11 and 123 plasma concentrations of SN-38 were used to develop the population PK model. The PK model used to characterize the disposition of encapsulated CPT-11, released CPT-11, and SN-38 is shown in **Figure 5.1**.

Population PK Model of IHL-305

Encapsulated and Released Drug Model. The encapsulated and released CPT-11 were modeled simultaneously for all patients. For encapsulated CPT-11, both linear and nonlinear PK models were evaluated. A one-compartment model with Michaelis-Menten kinetics (AIC = 1616) better described the data than either nonlinear plus linear (AIC = 1619) or linear kinetics (AIC = 1630). For released CPT-11, a one-compartment model with linear kinetics (AIC = -913) best described the data than either two-compartment model with linear kinetics (AIC = -911) or three-compartment model with linear kinetics (AIC = -877). The distribution of residual variability was best described by a proportional error model. During the covariate screen, gender was identified as a significant covariate for volume of

distribution of encapsulated CPT-11 (V_{encap}) and maximum velocity of encapsulated CPT-11 ($V_{max, encap}$). The PK parameter estimates obtained from the final covariate model are provided in **Table 5.2**. The inclusion of gender as a covariate in the final model decreased the inter-individual variability (IIV) of V_{encap} and $V_{max, encap}$ by 5.7%, and 4.3%, respectively. V_{encap} in female patients and male patients were estimated to be 2.4 L (IIV 22.4%) and 3.6 L (IIV 22.4%), respectively ($P < 0.001$). The estimated V_{encap} for both female and male patients are very close to plasma volume in humans. $V_{max, encap}$ in female and male patients was estimated to be 13.2 mg/h (IIV 40.8%) and 19.2 mg/h (IIV 40.8%), respectively ($P < 0.001$). The mean Michaelis-Menten constant (K_m) were estimated to be 117 mg/L. The fraction of encapsulated CPT-11 released from IHL-305 (F_{Rel}) was estimated to be 0.7 and showed the most inter-individual variability, with IIV for F_{Rel} was estimated to be 153%. The population mean of encapsulation of CPT-11 in the formulation was estimated to be 94.1%. The volume of distribution of released CPT-11 was estimated to be 402 L (IIV 61.3%). The clearance of released CPT-11 was estimated to be 19 L/h (IIV 40.4%).

Active Metabolite Model. The final PK model for encapsulated CPT-11, released CPT-11, and SN-38 was built by fixing PK parameters of encapsulated and released CPT-11 estimated from the final model of encapsulated and released CPT-11. A two-compartment model with linear kinetics was used to describe the data of SN-38. The population mean values of SN-38 for apparent volume of central compartment ($V_{SN-38-1}$), apparent systemic clearance (CL_{SN-38}), apparent volume of peripheral compartment ($V_{SN-38-2}$), and apparent distribution clearance ($CL_{SN-38-d}$) were 108 L (IIV 57.5%), 300.2 L/h (IIV 24.4%), 2433.5 L, and 113.4 L/h (IIV 66.3%), respectively.

Goodness-of-fit plots from the final PK model in all patients are given in **Figure 5.2**. The model adequately describes the PK profile of encapsulated CPT-11. Both the population predicted ($R^2 = 0.90$) and individual predicted ($R^2 = 0.97$) PK data of encapsulated CPT-11 correlated well with the observed data. Although the PK data of released CPT-11 were variable, the population predicted ($R^2 = 0.75$) PK data of released CPT-11 correlated relatively well with the observed data. The individual predicted ($R^2 = 0.94$) PK data of released CPT-11 correlated well with the observed data. The PK data of SN-38 is reasonably but less adequately described by the final model compared to encapsulated and released CPT-11. The observed PK data of SN-38 better correlated with the individual predicted PK data ($R^2 = 0.77$) than population predicted PK data ($R^2 = 0.17$). The observed The Selected individual PK time profiles of encapsulated CPT-11, released CPT-11, and SN-38 are shown in **Figure 5.3**. In general, the observed data of encapsulated CPT-11, released CPT-11and SN-38 were well described by the final model.

D. DISCUSSION

Major advances in the use of liposomes, conjugates, and nanoparticles as vehicles to deliver drugs have occurred the past 10 years (4, 6, 7). Doxil® and albumin stabilized nanoparticle formulation of paclitaxel (Abraxane®) are now FDA approved (8, 9, 31). In addition, there are greater than 200 liposomal and nanoparticle formulations of anticancer agents currently in development (4). This is the first study where population PK modeling was applied to assess the PK of the encapsulated drug, released drug, and its active metabolite after administration of a pegylated liposomal formulation of a camptothecin analogue (26,27,28). Evaluation of the PK disposition of the liposomal encapsulated verses released drug is of the utmost importance because the liposomal encapsulated drug is an inactive prodrug and thus only the released drug is active (1,3).

The inter-individual variability in the disposition of IHL-305 can be explained in part by gender. V_{encap} and $V_{max, encap}$ in male patients is 1.5-fold higher compared with female patients. This data suggest that male patients may have 50% lower exposure and are at risk of having a lower response potential. This gender effect on $V_{max, encap}$ of encapsulated drugs is consistent with previous observations of gender associated variability in clearance of TLI (Optisomal Topotecan), S-CKD602, and Doxil (32, 33). For TLI and S-CKD602, CL was 1.2-fold ($p = 0.14$) and 1.4-fold ($p = 0.009$) lower in female rats compared with male rats, respectively (33). Female patients had lower CL of Doxil ($p < 0.001$), IHL-305 ($p = 0.068$), and SCKD-602 ($p = 0.67$) as compared with male patients overall and also when stratified by age (32). The effect of gender on PK of Doxil was also reported in a population PK analysis of of Doxil (34). The gender effect on V_{encap} has not been reported. The greater V_{encap} in male patients may be explained by the greater blood volume in males compared to females (35).

The gender effect on V_{encap} may also due to the correlation between V_{encap} and $V_{max, encap}$ in the PK model. Overall, these results suggest that gender may be a significant factor affecting the PK disposition of liposomal agents and may play a role in the high PK variability reported in patients treated with liposomal anticancer agents.

Pegylated-liposomal CPT-11 displayed nonlinear PK best described by a one-compartment structural model. The mean values of volume of distribution for encapsulated CPT-11 were 3.22 L for male patients and 2.55 L for female patients, which are very close to plasma volume in humans. The limited volume of distribution of encapsulated CPT-11 is consistent with other liposomal anticancer agents since the size of liposome limited their distribution to the normal tissue (36, 37). Saturation of clearance has been reported for both Doxil® and S-CKD602 and the nonlinear PK of these two drugs have been modeled using Michaelis-Menten kinetics (38-41).

The PK disposition of released CPT-11 was described by a one-compartment model with linear clearance. In contrast, the PK disposition of CPT-11 after administration of nonliposomal CPT-11 was described by two-compartment or three-compartment models with linear clearance in the PK analysis by others. This suggests the PK disposition of released CPT after administration of IHL-305 was primarily dominated by the disposition of the liposome carrier. Published CL values of the total form of non-liposomal CPT-11 are in the range of 12 to 24 L/h/m^2 during short infusions (30 to 90 minutes) (42-44). In our model, CL of the total form of released CPT-11 was estimated to be 19 L/h (10.3 L/h/m^2), which is close but slight lower than previously reported values. Similarly, the steady-state volume of distribution estimate of 402 L (217 L/m^2) for released CPT-11 falls within the range of

reported steady state volume of distribution (377 to 871 L) for non-liposomal CPT-11 (42, 45, 46).

The model prediction for SN-38 was not as accurate as for encapsulated and released CPT-11. This may be related to the highly variable and low concentration levels of SN-38. In addition, the final model of encapsulated CPT-11, released CPT-11 and SN-38 was built sequentially so the model of encapsulated and released CPT-11 drives the model of SN-38. Therefore any error caused by model misspecification of the parent drug model will be carried over and exaggerated in the model of active metabolite.

The model that are developed did not take into account the lactone and carboxylate forms of CPT-11 since only the total (lactone + hydroxy acid) form of the drug were measured in our study. Only the lactone form of CPT-11 has antitumor activity, and they undergo a pH-dependent equilibrium with carboxylate forms. Thus, the model of encapsulated and released CPT-11 can only be used to predict total CPT-11 exposure in the encapsulated and released forms. However, the PK of encapsulated CPT-11 is not affected by this limitation as the drug that remains encapsulated is all in the lactone form because the pH of the core solution is approximately 5.4.

In conclusion, a population PK model was developed for encapsulated and released CPT-11 in patients with advanced solid tumors. The volume of distribution and clearance of encapsulated CPT-11 was influenced by gender. The effect of gender on PK of IHL-305 needs to be further evaluated. This model will not only help to understand the PK of PEGylated liposomal drugs but may also be useful in predicting the PK and optimize dosing of pegylated liposomal agents to achieve a target exposure for a patient with cancer.

E. REFERENCES

1. Zamboni WC. Concept and clinical evaluation of carrier-mediated anticancer agents. Oncologist 2008; 13:248-60.

2. Innocenti F, Kroetz DL, Schuetz E, et al. Comprehensive pharmacogenetic analysis of irinotecan neutropenia and pharmacokinetics. J Clin Oncol 2009; 27:2604-14.

3. Slatter JG, Schaaf LJ, Sams JP, et al. Pharmacokinetics, metabolism, and excretion of irinotecan (CPT-11) following I.V. infusion of [(14)C]CPT-11 in cancer patients. Drug Metab Dispos 2000; 28:423-33.

4. Zamboni WC. Liposomal, nanoparticle, and conjugated formulations of anticancer agents. Clin Cancer Res 2005; 11:8230-4.

5. Xie R, Mathijssen RH, Sparreboom A, Verweij J, Karlsson MO. Clinical pharmacokinetics of irinotecan and its metabolites in relation with diarrhea. Clin Pharmacol Ther 2002; 72:265-75.

6. Papahadjopoulos D, Allen TM, Gabizon A, et al. Sterically stabilized liposomes: improvements in pharmacokinetics and antitumor therapeutic efficacy. Proc Natl Acad Sci U S A 1991; 88:11460-4.

7. Maeda H, Wu J, Sawa T, Matsumura Y, Hori K. Tumor vascular permeability and the EPR effect in macromolecular therapeutics: a review. J Control Release 2000; 65:271-84.

8. Markman M, Gordon AN, McGuire WP, Muggia FM. Liposomal anthracycline treatment for ovarian cancer. Semin Oncol 2004; 31:91-105.

9. Krown SE, Northfelt DW, Osoba D, Stewart JS. Use of liposomal anthracyclines in Kaposi's sarcoma. Semin Oncol 2004; 31:36-52.

10. Zamboni WC, Yoshino K. Formulation and physiological factors affecting the pharmacokinetics and pharmacodynamics of liposomal anticancer agents. Japan DDS 2010; 25:58-70.

11. Zamboni WC, Stewart CF, Thompson J, et al. Relationship between topotecan systemic exposure and tumor response in human neuroblastoma xenografts. J Natl Cancer Inst 1998; 90:505-11.

12. Stewart CF, Zamboni WC, Crom WR, et al. Topoisomerase I interactive drugs in children with cancer. Invest New Drugs 1996; 14:37-47.

13. Kurita A, Furuta T, Kaneda N, al. e. Pharmacokinetics of irinotecan and its metabolites after iv administration of IHL-305, a novel pegylated liposome containing irinotecan, to tumor-bearing mice. the 2007 American Association for Cancer Research–National Cancer Institute–European Organization for Research and Treatment of Cancer AACR-NCI-EORTC Conference; 2007 November 2007; San Francisco, CA; 2007.

14. Takagi A, Matsuzaki T, Furuta T, al e. Antitumor activity of IHL-305, a novel pegylated liposome containing irinotecan, in human xenograft models. the 2007 American Association for Cancer Research–National Cancer Institute–European Organization for Research and Treatment of Cancer AACR-NCI-EORTC Conference; 2007 November 2007; San Francisco, CA; 2007.

15. Zamboni WC, Strychor S, Joseph E, et al. Plasma, tumor, and tissue disposition of STEALTH liposomal CKD-602 (S-CKD602) and nonliposomal CKD-602 in mice bearing A375 human melanoma xenografts. Clin Cancer Res 2007; 13:7217-23.

16. Yu NY, Conway C, Pena RL, Chen JY. STEALTH liposomal CKD-602, a topoisomerase I inhibitor, improves the therapeutic index in human tumor xenograft models. Anticancer Res 2007; 27:2541-5.

17. Zamboni WC, Gajjar AJ, Mandrell TD, et al. A four-hour topotecan infusion achieves cytotoxic exposure throughout the neuraxis in the nonhuman primate model: implications for treatment of children with metastatic medulloblastoma. Clin Cancer Res 1998; 4:2537-44.

18. Allen TM, Hansen C. Pharmacokinetics of stealth versus conventional liposomes: effect of dose. Biochim Biophys Acta 1991; 1068:133-41.

19. Zamboni WC, Maruca LJ, Strychor S, et al. Bidirectional pharmacodynamic interaction between pegylated liposomal CKD-602 (S-CKD602) and monocytes in patients with refractory solid tumors. J Liposome Res.

20. Zamboni WC, Edwards RP, Mountz JM, et al. The Development of Liposomal and Nanoparticle Anticancer Agents: Methods to Evaluate the Encapsulated and Released Drug in Plasma and Tumor and Phenotypic Probes for Pharmacokinetic (PK) and Pharmacodynamic (PD) Disposition. NSTI Nanotechnology; 2007; 2007.

21. Zamboni WC, Maruca LJ, Strychor S, et al. Age and body composition related-effects on the pharmacokinetic disposition of STEALH liposomal CKD-602 (S-CKD602) in patients with advanced solid tumors. 2007; 2007.

22. Sidone BJ, Edwards RP, Zamboni BA, Strychor S, Maruca LJ, Zamboni WC. Evaluation of body surface area (BSA) based dosing, age, and body composition as factors affecting the pharmacokinetic (PK) variability of STEALTH liposomal doxorubicin (Doxil). AACR-NCI-EORTC; 2007; 2007.

23. Zamboni WC, Strychor S, Maruca L, et al. Pharmacokinetic Study of Pegylated Liposomal CKD-602 (S-CKD602) in Patients With Advanced Malignancies. Clin Pharmacol Ther 2009.

24. De Martinis M, Modesti M, Ginaldi L. Phenotypic and functional changes of circulating monocytes and polymorphonuclear leucocytes from elderly persons. Immunol Cell Biol 2004; 82:415-20.

25. Jones SF, Zamboni WC, Burris III HA, et al. Phase I and pharmacokinetic (PK) study of IHL-305 (pegylated liposomal irinotecan) in patients with advanced solid tumors. ASCO; 2009 Jun, 2009; Orlando, FL; 2009.

26. Kurita A, Kaneda N. High-performance liquid chromatographic method for the simultaneous determination of the camptothecin derivative irinotecan hydrochloride, CPT-11, and its metabolites SN-38 and SN-38 glucuronide in rat plasma with a fully automated on-line solid-phase extraction system, PROSPEKT. J Chromatogr B Biomed Sci Appl 1999; 724:335-44.

27. Sheiner LB, Beal SL. Evaluation of methods for estimating population pharmacokinetics parameters. I. Michaelis-Menten model: routine clinical pharmacokinetic data. J Pharmacokinet Biopharm 1980; 8:553-71.

28. Sheiner LB, Rosenberg B, Marathe VV. Estimation of population characteristics of pharmacokinetic parameters from routine clinical data. J Pharmacokinet Biopharm 1977; 5:445-79.

29. Klein CE, Gupta E, Reid JM, et al. Population pharmacokinetic model for irinotecan and two of its metabolites, SN-38 and SN-38 glucuronide. Clin Pharmacol Ther 2002; 72:638-47.

30. Mandema JW, Verotta D, Sheiner LB. Building population pharmacokinetic--pharmacodynamic models. I. Models for covariate effects. J Pharmacokinet Biopharm 1992; 20:511-28.

31. Roy V, LaPlant BR, Gross GG, Bane CL, Palmieri FM. Phase II trial of weekly nab (nanoparticle albumin-bound)-paclitaxel (nab-paclitaxel) (Abraxane) in combination with gemcitabine in patients with metastatic breast cancer (N0531). Ann Oncol 2009; 20:449-53.

32. La-Beck NM, Wu H, Infante JR, et al. The evaluation of gender on the pharmacokinetics (PK) of pegylated liposomal anticancer agents. ASCO Annual Meeting; 2010; 2010. p. e13003.

33. Song G, Wu H, La-Beck N, Zamboni BA, Strychor S, Zamboni WC. Effect of Gender on Pharmacokinetic Disposition of Pegylated Liposomal CKD-602 (S-CKD602) and Optisomal Topotecan (TLI) in Rats. AACR 2009.

34. Zomorodi K, Gupta S. Population Pharmacokinetic Analysis of DOXIL in Adult Patients. AAPS; 1999; 1999.

35. Lee LN. Volume of Blood in A Human; 1998.

36. Allen TM, Cullis PR. Drug delivery systems: entering the mainstream. Science 2004; 303:1818-22.

37. Hilger RA, Richly H, Grubert M, et al. Pharmacokinetics (PK) of a liposomal encapsulated fraction containing doxorubicin and of doxorubicin released from the liposomal

capsule after intravenous infusion of Caelyx/Doxil. Int J Clin Pharmacol Ther 2005; 43:588-9.

38. Zamboni WC, Strychor S, Maruca L, et al. Pharmacokinetic study of pegylated liposomal CKD-602 (S-CKD602) in patients with advanced malignancies. Clin Pharmacol Ther 2009; 86:519-26.

39. Gabizon A, Isacson R, Rosengarten O, Tzemach D, Shmeeda H, Sapir R. An open-label study to evaluate dose and cycle dependence of the pharmacokinetics of pegylated liposomal doxorubicin. Cancer Chemother Pharmacol 2008; 61:695-702.

40. Gabizon A, Shmeeda H, Barenholz Y. Pharmacokinetics of pegylated liposomal Doxorubicin: review of animal and human studies. Clin Pharmacokinet 2003; 42:419-36.

41. Gabizon A, Tzemach D, Mak L, Bronstein M, Horowitz AT. Dose dependency of pharmacokinetics and therapeutic efficacy of pegylated liposomal doxorubicin (DOXIL) in murine models. J Drug Target 2002; 10:539-48.

42. de Jonge MJ, Verweij J, de Bruijn P, et al. Pharmacokinetic, metabolic, and pharmacodynamic profiles in a dose-escalating study of irinotecan and cisplatin. J Clin Oncol 2000; 18:195-203.

43. Kehrer DF, Sparreboom A, Verweij J, et al. Modulation of irinotecan-induced diarrhea by cotreatment with neomycin in cancer patients. Clin Cancer Res 2001; 7:1136-41.

44. Mathijssen RH, van Alphen RJ, Verweij J, et al. Clinical pharmacokinetics and metabolism of irinotecan (CPT-11). Clin Cancer Res 2001; 7:2182-94.

45. Poujol S, Bressolle F, Duffour J, et al. Pharmacokinetics and pharmacodynamics of irinotecan and its metabolites from plasma and saliva data in patients with metastatic digestive cancer receiving Folfiri regimen. Cancer Chemother Pharmacol 2006; 58:292-305.

46. Chabot GG, Abigerges D, Catimel G, et al. Population pharmacokinetics and pharmacodynamics of irinotecan (CPT-11) and active metabolite SN-38 during phase I trials. Ann Oncol 1995; 6:141-51.

Table 5.1.

A summary of Patient Demographics and Covariates Included in the Analysis

Characteristics	Number of patients	Mean ± SD	Median (Range)
Age (years)		60.0 ± 9.4	60 (42– 75)
Body Surface Area (m2)		1.9 ± 0.3	1.9 (1.4 – 2.4)
Body Weight (kg)		76.7 ± 20.4	75.3 (47.1 – 124.5)
Body Mass Index (kg/m2)		27.0 ± 6.8	26.3 (17.2 – 53.6)
Height (cm)		169 ± 10.3	168 (152 – 188)
Ratio of Body Weight to Ideal Body Weight		1.3 ± 0.4	1.2 (0.8 – 2.7)
Sex			
Male	13		
Female	26		
Primary tumor type			
Ovarian Cancer	8		
Breast Cacner	6		
Lung Cancer	6		
Bladder	2		
Head and Neck Squamous	2		
Neuroendocrine Carcinoma	2		
Adenoid cystic, Anus, Cervical, Colon, Gastric, Mediastinal, Metastatic breast, Metastatic prostate, Metastatic carcinoid, Pancreatic, Prosta, Right 4th toe, Uterine	1 patient for each type		

Table 5.2.

Population PK Parameters Obtained From the Final Model for Encapsulated CPT-11, Released CPT-11 and SN-38.

Parameter	Definition	Population Mean RSE[a] (%)	IIV, CV%[b] RSE[a] (%)
V_{Encap} (L)	Volume of distribution for encapsulated		
Female[c]		2.4 (3.9)	22.4 (21)
Male[d]		3.6 (6.1)	
$V_{Release}$ (L)	Volume of distribution for central compartment of released	402 (32)	61.3 (28)
$V_{max, encap}$ (mg/h)	Maximum velocity of encapsulated		40.8 (20)
Female		13.2 (30)	
Male		19.2 (30)	
F_{Rel}	Fraction of encapsulated CPT-11 released from IHL-305	0.7 (63)	153 (53)
K_m (mg/L)	Michaelis-Menten constant	117 (38)	NA[e]
Encapsulation, %	Encapsulation percent of CPT-11 in the formulation	94.1 (34)	NA[e]
CL_{Rel} (L/h)	Systemic clearance for released	19 (7.1)	40.4 (44)
$V_{SN-38-1}$ (L)	Apparent volume of distribution for central compartment of SN-38	108 (NE)	57.5 (24)
$V_{SN-38-2}$ (L)	Apparent volume of distribution for peripheral compartment of SN-38	2433.5 (NE)	NE
CL_{SN-38} (L/h)	Apparent systemic clearance of SN-38	300.2 (10)	24.4 (25)
$CL_{SN-38-d}$ (L/h)	Apparent distribution clearance of SN-38	113.4 (NE)	66.3 (18)
Residual variability			
Proportional error for encapsulated (variability as %)		24.5 % (19)	
Proportional error for released (variability as %)		28.1 % (15)	NA[e]
Proportional error for SN-38 (variability as %)		25.6 % (18)	

[a] Relative standard error (RSE) for estimate.

[b] Coefficient of variation (CV%).

[c] The estimated volume of distribution of encapsulated CPT-11 for female patients.

[d] The estimated volume of distribution of encapsulated CPT-11 for male patients.

[e] Not estimated.

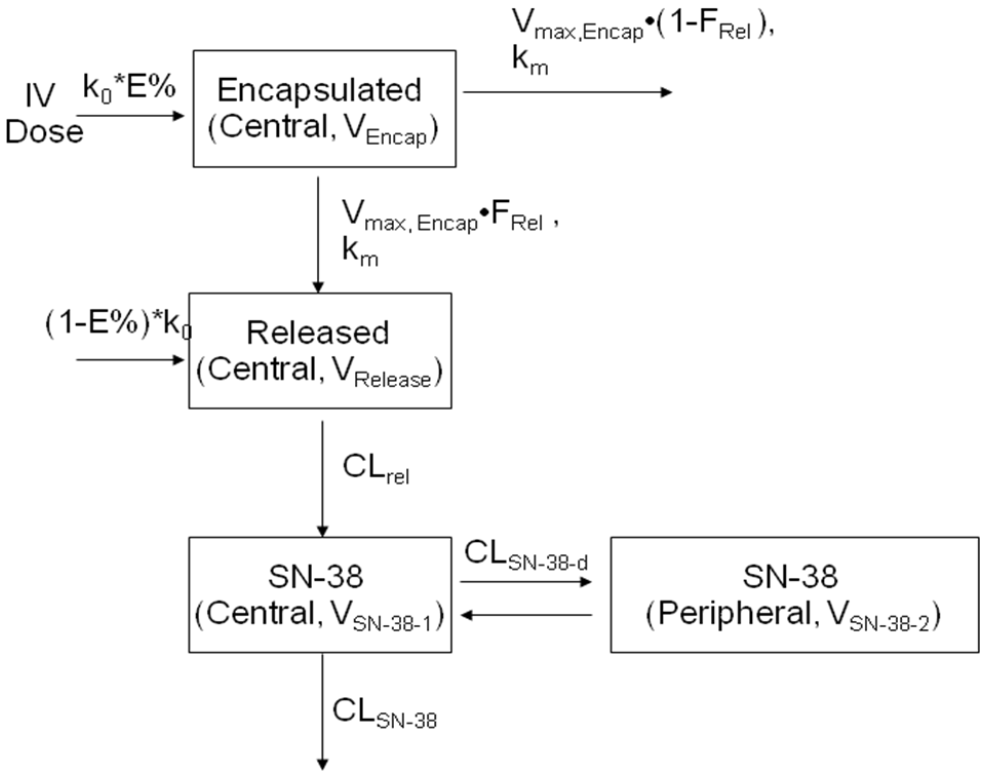

Figure 5.1. The final structural PK model for encapsulated CPT-11, released CPT-11 and SN-38. A fraction of dose which was administered in the form of non-liposomal CPT-11 was included. E% is encapsulation percent of CPT-11 in the formulation.

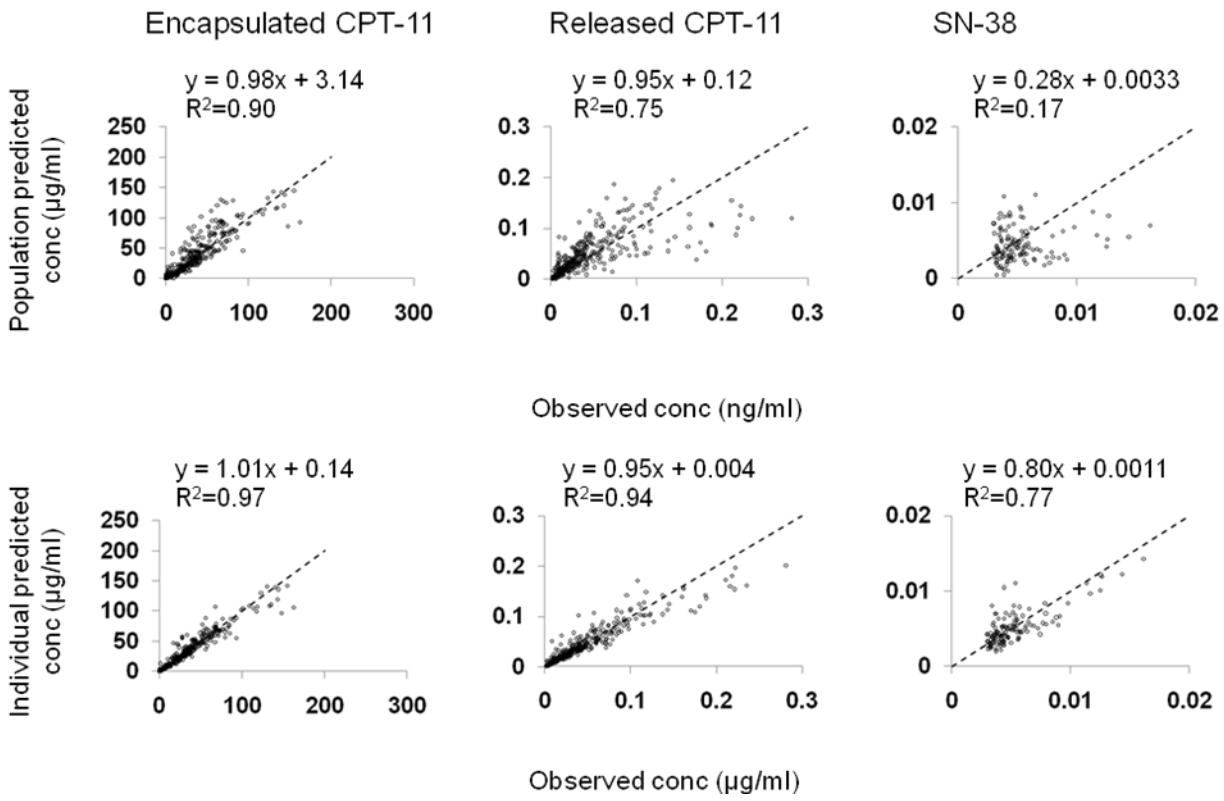

Figure 5.2. Goodness-of-fit plots for the final model of encapsulated CPT-11, released CPT-11, and SN-38. The dashed lines are lines of identity.

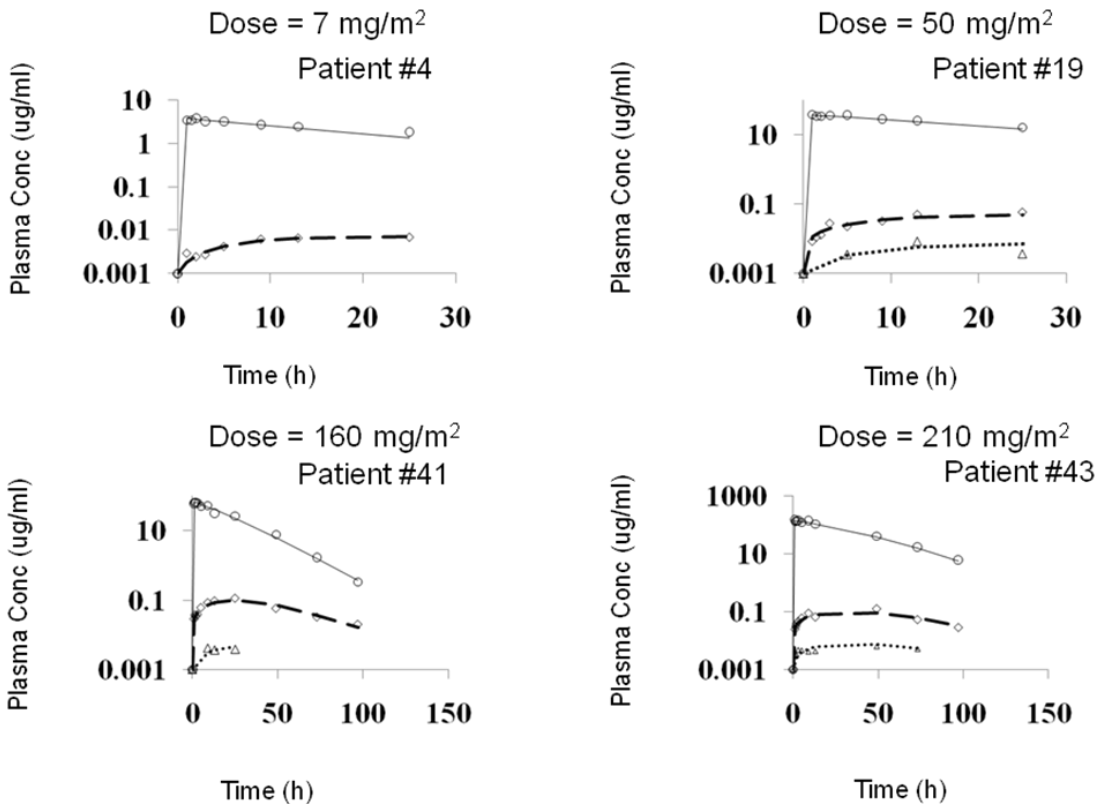

Figures 5.3. Representative individual plots of observed (○) and individual predicted (—) values of plasma concentrations of encapsulated CPT-11, observed (◊) and individual predicted (— —) values of plasma concentrations of released CPT-11, and observed (Δ) and individual predicted (·····) values of plasma concentrations of SN-38 in patients. For the representative patient receiving dose of 7 mg/m^2, there is no detectable concentration of SN-38.

CHAPTER 6

MECHANISM-BASED PHARMACOKINETIC-PHARMACODYNAMIC MODEL CHARACTERIZING BI-DIRECTIONAL INTERACTION BETWEEN PEGYLATED LIPOSOMAL CKD-602 (S-CKD602) AND MONOCYTES IN PATIENTS WITH ADVANCED MALIGNANCIES

A. INTRODUCTION

Liposomes (microparticulate phospholipid vesicles) have been used with growing success as pharmaceutical carriers for anticancer agents. Conventional liposomes are quickly opsonized by plasma proteins, recognized as foreign bodies, and rapidly removed by the mononuclear phagocytic system (MPS) which has also been called the reticuloendothelial system (RES) (1, 2). The development of STEALTH or Polyethylene Glycol (PEG)ylated liposomes was based on the discovery that incorporation of mPEG-lipids into liposomes yields preparations with prolonged plasma exposure and superior tumor delivery compared to conventional liposomes composed of natural phospholipids (3-5). PEGylated liposomal doxorubicin (Doxil®) is approved for the treatment of refractory ovarian cancer, Kaposi sarcoma, and multiple myeloma (6, 7).

S-CKD602 is a PEGylated liposomal formulation of CKD-602, a camptothecin analogue which inhibits topoisomerase I (3, 8, 9). Non-liposomal CKD-602 administered IV at 0.5 mg/m^2/day for 5 consecutive days repeated every 21 days is approved in Korea for the treatment of newly diagnosed small cell lung cancer and relapsed ovarian cancer (10-13). Encapsulation of the CKD-602 in the acidic core of a PEGylated liposome protect the active-lactone form of the drug from being converted to the inactive-hydroxy acid form in the blood and allow for release of the active-lactone form into the tumor over a protracted period of time, which is ideal for a cell cycle-specific drug (3, 14-18). The PEGylated liposomal formulation is expected to have an enhanced therapeutic ratio compared to non-liposomal CKD-602, as well as a more convenient schedule of administration.

The pharmacokinetic (PK) disposition of carrier-mediated agents, such as, nanoparticles, nanosomes, and conjugated agents, is dependent upon the carrier until the drug

is released from the carrier. Unlike traditional anticancer agents which are cleared by the liver and kidneys, the clearance of non-PEGylated and PEGylated liposomes is via the MPS which include monocytes, macrophages and dendritic cells located primarily in the liver and spleen (2). PEGylated liposomes are cleared much slower via MPS compared to non-PEGylated liposomes (4, 19). Uptake of the liposomes or nanoparticles by the MPS usually results in sequestering of the encapsulated drug in the MPS and the sequestered drug in the MPS may cause acute cytotoxicity to the MPS. This toxicity to the MPS in turn decreases clearance of the PEGylated liposomal anticancer agents and alters the pharmacodynamics (PD) of the agents. Thus, there is a bi-directional interaction between PEGylated liposomal anticancer agents and MPS. Since a major portion of the liposomal encapsulated drug molecules are confined primarily to the blood compartment due to their relative large size (20), we have reported that there is a significant and clinically relevant interaction between liposomal agents and MPS cells in the blood circulation (19). This bi-directional interaction between PEGylated liposomal anticancer agents and monocytes is very important in determining the PK and PD of PEGylated liposomal anticancer agents and potentially other nano and conjugated agents.

Clinical PK analysis of Doxil suggests a dose-dependent clearance saturation of clearance when a broad dose range is examined (21). Non-linear clearance was also observed in a phase I PK study of S-CKD602 (22). In addition, Gabizon and colleagues reported that the clearance of sum total (encapsulated + released) doxorubicin decreased by approximately 25 to 50% from cycle 1 to 3 (19, 23). We reported that this reduction in clearance of Doxil® from cycle 1 to cycle 3 was associated with a reduction in pre-cycle monocyte count (19, 24). We have also reported that high % decrease in monocytes was associated with high clearance

of IHL-305 (25). These studies suggest that the dose-dependent and cycle-dependent clearance of PEGylated liposomal anticancer agents may due to the bi-directional interaction between PEGylated liposomal drug and monocytes in blood.

The PK of PEGylated liposomal anticancer agents and Non-PEGylated liposomal anticancer agents in humans have been studied using the population modeling approach (26-31). Conventional compartment models such as one-compartment and two-compartment models were commonly used in these PK studies (26-31). The dose-dependent clearance of PEGylated liposomal anticancer agents was modeled using Michaelis-Menten kinetics (30). The bi-directional interaction between PEGylated liposomal drug and monocytes has not been incorporated in the PK model of these agents.

As monocytes of the MPS play an important role in the PK disposition of liposomes, the monocytopenia after administration of PEGylated liposomal anticancer agents was selected as a PD measure of these agents in this study. Monocytopenia is commonly observed after chemotherapy as a result of myelosuppression and early monocytopenia was reported to be a predictor of neutropenia (32, 33). The results of our prior study suggest that monocytes are more sensitive to S-CKD602 as compared with neutrophils and that the increased sensitivity is related to the liposomal formulation and not the encapsulated CKD-602 (19). Therefore, the monocytopenia after administration of PEGylated liposomal agents have a different mechanism from monocytopenia resulted from treatment with conventional small molecule chemotherapeutic drugs. Incorporation of the bi-directional interaction between PEGylated liposomal formulation and monocytes are important to characterize the PK and PD of these agents.

Although a few physiologically based PD models of chemotherapy-induced anemia, neutropenia, and thrombocytopenia have been developed, PD models of monocytopenia especially as related to nanoparticle PK and PD have not been reported (34-38). As monocytes are derived from the same granulocyte-macrophage progenitor cells as other leukocytes, PD models of leukocytopenia may be applicable to monocytopenia. As we only have relatively sparse PD data of monocytopenia, a semiphysiological model proposed by Friberg et al. for chemotherapy-related myelosuppression was chosen as a standard model to describe monocytopenia after S-CKD602 (34, 35). In this model, the cell maturation associated with myelopoiesis is described by multiple transit compartments with the same rate constant between each compartment to account for the time delay for onset of response (34, 35). In addition, a feedback loop was included to account for rebound of leukocytes typically observed in myelosuppression profiles. This model has been widely applied to various anticancer agents to describe neutropenia, leukocytopenia, and thrombocytopenia because it involves minimum number of parameters (28, 35, 39-42).

The clinical results of the phase I and PK study of S-CKD602 were previously published (43, 44). PK study of S-CKD602 using conventional compartment model have also been published (22). Monocytopenia after chemotherapy are conventionally believed due to myelosuppression. However, it is unclear if the monocytopenia is due to direct cytotoxicity to monocytes in the blood or cytotoxicity to progenitor cells in bone marrow. We believe the bi-directional interaction between PEGylated liposomal anticancer drugs and monocytes are more important to characterize the monocytopenia after these agents and PK of these agents. The objectives of this study were to develop a mechanism-based population PK-PD model to investigate the nature of nonlinear PK of S-CKD602 and to increase our

understanding of the bi-directional interaction between PEGylated liposomal anticancer agents and monocytes in blood of cancer patients.

B. METHODS

Study Design

The PK data were obtained from a phase I study of S-CKD602 in patients with advanced solid tumors (22, 45). The study design and clinical results have been reported elsewhere (22, 45). Forty-five patients (21 males) received S-CKD602 at 0.1 to 2.5 mg/m^2 IV x 1 over approximately 1 hour every 3 weeks. No pre-medications were administered prior to S-CKD602. Written informed consent, approved by the Institutional Review board of the University of Pittsburgh Medical Center, was obtained from all patients prior to study entry. All other eligibility criteria were previously reported (22). Serial plasma samples were obtained prior to drug administration; at the end of the infusion (lasting ~ 1h); and at 3, 5, 7, 24, 48, 72, 96, 168 (day 8), and 336 h (day 15) after the start of the infusion. Total (lactone + hydroxyl acid) concentrations of encapsulated and released CKD-602 in plasma were determined by liquid chromatography-tandem mass spectrometry (46). The lower limit of quantitation (LLQ) of the total form encapsulated and released CKD-602 were 2 and 0.05 ng/mL, respectively. Samples of peripheral blood were collected before dosing on days 7, 14, 21, and 28.

Population PK-PD Analysis

Model Development

We believe that the bi-directional interaction between PEGylated liposomal anticancer agents and monocytes plays the key role in the elimination of PEGylated liposomal anticancer agents and monocytopenia observed in our prior studies (19). We developed a mechanism-based model based on receptor binding kinetics to describe the bi-

directional interaction between the concentration versus time profile of encapsulated CKD-602 and time course of monocytes. We also developed a myelosuppression-based model in absence of the bi-directional interaction to compare with the mechanism-based model. For each kind of model, a variety of model structures were tested. The best model was selected on the basis of smaller values of AIC, better precision of estimates, and superior goodness-of-fit plots (47).

Model I. Myelosuppression-based Model

The PK-PD model of encapsulated CKD-602 and monocytes was built sequentially. One compartment model with Michaelis-Menten kinetics best described the PK data of encapsulated CKD-602 in our previous analysis. The individual PK parameters of encapsulated CKD-602 determined from the best PK model of encapsulated CKD-602 were used in the PD model of monocytes. In the PK modeling part, PK parameters (V_{encap}, V_{max}, and K_m) were estimated for each individual. For the PD modeling of monocytopenia, all of the individual values of the PK parameters were fixed for each patient and the predicted individual encapsulated CKD-602 concentrations-time profiles were used as input functions into this PK-PD model. The PD parameters were simultaneously estimated in the PD modeling part. This sequential modeling approach was selected over a simultaneous PK-PD estimation to expedite the PD modeling by using the existing individual estimates of PK parameters.

A chemotherapy-induced myelosuppression model developed by Friberg et al. was used to describe the monocytopenia after administration of S-CKD602 (**Figure 6.1A**) (35). The model consists of a proliferating compartment (Prol) that represents progenitor cells,

three transit compartments of maturing cells (Transit), and a compartment of circulating monocytes. A negative feedback mechanism $(MONO_0/MONO)^{\gamma}$ from circulating cells on proliferating cells is included to describe the rebound of cells including an overshoot compared to the baseline value ($MONO_0$). The drug concentration in plasma of the central compartment (Conc) is assumed to reduce the proliferation rate by the function E_{Drug}, which was modeled to be an Emax model, [E_{max} x Conc/(EC50 + Conc)]. The differential equations were written as

$$\frac{dA_{Encap}}{dt} = k_0 - \frac{V_{\max} \bullet A_{Encap}}{K_m \bullet V_{Encap} + A_{Encap}} \quad , \quad A_{Encap}(0) = 0,$$

$$C_{Encap} = \frac{A_{Encap}}{V_{Encap}}$$

$$E_{Drug} = \frac{E_{\max} \bullet C_{Encap}}{EC_{50} + C_{Encap}}$$

$$\frac{d\,\mathrm{Prol}}{dt} = k_{prol} \bullet \mathrm{Prol} \bullet (1 - E_{Drug}) \bullet (Mono_0 / Mono)^{\gamma} - k_{tr} \bullet \mathrm{Prol} \quad , \quad \mathrm{Prol}(0) = \mathrm{Mono}_0$$

$$\frac{dTransit1}{dt} = k_{tr} \bullet \mathrm{Prol} - k_{tr} \bullet Transit1 \quad , \quad \mathrm{Transit1}(0) = \mathrm{Mono}_0$$

$$\frac{dTransit2}{dt} = k_{tr} \bullet Transit1 - k_{tr} \bullet Transit2 \quad , \quad \mathrm{Transit2}(0) = \mathrm{Mono}_0$$

$$\frac{dTransit3}{dt} = k_{tr} \bullet Transit2 - k_{tr} \bullet Transit3 \quad , \quad \mathrm{Transit3}(0) = \mathrm{Mono}_0$$

$$\frac{dMono}{dt} = k_{tr} \bullet Transit3 - k_{Mono} \bullet Mono \quad , \quad \mathrm{Mono}(0) = \mathrm{Mono}_0$$

dA_{Encap}/dt is the elimination rate, V_{max} is the maximum elimination rate or maximum velocity, K_m is the concentration at which half-maximum elimination rate is achieved, V_{Encap}

is the volume of distribution, A_{Encap} is encapsulated CKD-602 amount in plasma, C_{Encap} is the plasma concentration of encapsulated CKD-602, k_0 is the infusion rate and k_0 is 0 after stop of infusion, k_{tr} is the transit rate constant, E_{max} is the maximum attainable effect, EC_{50} is the concentration producing 50% of E_{max}, $Mono_0$ is the baseline monocyte count, γ is the feedback constant, k_{tr} is the proliferation rate constant, k_{mono} is the removal rate constant of monocyte, Mono is the monocyte count. The drug concentration in the central compartment (Conc) is assumed to reduce the proliferation rate by the function E_{Drug}, which was modeled using an E_{max} model. In the transit compartments, it is assumed that the only loss of cells is into the next compartment. As the proliferative cells differentiate into more mature cell types, the concentration of cells is maintained by cell division. At steady state, dProl/d t = 0, and therefore $k_{prol} = k_{tr}$. To minimize the number of parameters to be estimated, it was assumed in the modeling that $k_{mono} = k_{tr}$. Thus, the structural model parameters to be estimated were $Mono_0$, k_{tr}, γ, Emax and EC50.

Model II. Mechanism-based PK-PD Model

A mechanism based PK-PD model that incorporates the interaction between PEGylated liposomal anticancer agents and monocytes was developed for S-CKD602 (**Figure 6.1B**). Concentration versus time data of encapsulated CKD-602 in plasma and monocyte count in blood were fit simultaneously by this model. Drug is dosed IV into the systemic circulation (blood compartment) at a zero-order rate (k_0). The distribution of PEGylated liposome is described by a one-compartment model and the PEGylated liposome is eliminated by interacting with monocyte to form liposome-monocyte complex (k_{on}) which represents the phagocytosis of S-CKD602 by the monocyte. PEGylated liposome is also

degraded at a first-order rate (k_{deg}). This represents the elimination of the liposome through routes other than uptake by monocytes. The parameters describing the production and loss of monocytes are k_{in} and k_{out}. The production rate of monocytes k_{in} is equal to k_{out} multiplied by baseline monocyte value. The differential equations were written as

$$\frac{dA_{Encap}}{dt} = k_0 - k_{on} \bullet A_{Encap} \bullet Mono - k_{deg} \bullet A_{Encap} \quad , \; A_{Encap}(0) = 0$$

$$\frac{dMono}{dt} = Mono_0 \bullet k_{out} - k_{out} \bullet Mono - k_{on} \bullet A_{Encap} \bullet Mono / Factor \quad , \; Mono(0) = Mono_0$$

$$C_{Encap} = \frac{A_{Encap}}{V_{Encap}}$$

dA_{Encap}/dt is the elimination rate, A_{Encap} is encapsulated CKD-602 amount in plasma, C_{Encap} is the plasma concentration of encapsulated CKD-602, V_{Encap} is the volume of distribution of encapsulated CKD-602, Mono is the monocyte count, k_{on} is the association rate constant, k_{deg} is the degradation rate constant of S-CKD602, k_{out} is the removal rate constant of monocyte, k_0 is the infusion rate and $k_0 = 0$ after stop of infusion. Since the unit of encapsulated CKD-602 is μg/L and the unit of monocyte count is 10^9/L, the factor is a parameter (Factor) used to bridge the unit gap.

Data Analysis

Encapsulated CKD-602 concentration versus time profile and monocyte count versus time data were analyzed using the nonlinear mixed effects modeling approach as implemented in NONMEM (version 6; University of California, San Francisco, CA) for the mechanistic and myelosuppression based models. The first order conditional estimation

(FOCE) method were used in analyses. S-PLUS 8.0 (Version 8.0, Insightful Corporation, Seattle, Washington) was used for graphical diagnostics.

Mean population PK-PD variables, interindividual variability, and residual error were assessed in the model development (48, 49). Interindividual variability for each PK-PD variable was modeled with an exponential function. Residual error models of the additive, proportional, exponential, and combination methods were evaluated for the best structural PK-PD model. Individual PK-PD variables were obtained by posterior Bayesian estimation (48, 49). Model selection for nonhierarchical models (i.e., linear and nonlinear elimination models) was guided by goodness-of-fit plots (e.g., observed versus predicted plasma concentrations, weighted residuals versus predicted concentrations, and weighted residuals versus time), Akaike information criterion (AIC), and precision of parameter estimates. AIC was calculated as AIC = OFV + 2 x p, where OFV is the NONMEM objective function value and p is the number of PK-PD variables.

C. RESULTS

Patient demographics

Forty-five patients were enrolled on this study from September 29, 2003 to October 17, 2005 at University of Pittsburgh Cancer Institute, Pittsburgh, PA. Plasma concentrations of encapsulated CKD-602 and monocyte counts were obtained from 45 patients. Patient characteristics are listed in **Table 6.1**. The numbers of male and female patients evaluated in the phase I study were 21 and 24, respectively. The mean (median, range) age of the patients was 60.6 years (62 years, 33 to 79 years). A total of 292 plasma concentrations of encapsulated CKD-602 and 123 monocyte counts were used to develop the population PK-PD model. The mean ± SD numbers of concentrations of encapsulated CKD-602 and monocyte counts per patient were 6.5 ± 2.3 and 4.9 ± 2.7, respectively.

Model I. Myelosuppression-based Model

The encapsulated CKD-602 and monocytes were modeled sequentially for all patients. The distribution of residual variability was best described by a proportional error model. The PK and PD parameter estimates obtained from the final model are provided in **Table 6.2**. In the final model, the mean and interindividual variability (IIV, CV%) values for the distribution volume of encapsulated CKD-602 (V_{encap}) was 3.46 L and 78.6%, respectively. The estimated V_{encap} was very close to plasma volume in humans. The mean Michaelis-Menten constant (K_m) was estimated to be 877 μg/L. The maximum velocity (Vmax) of encapsulated CKD-602 was estimated to be 95.5 (IIV 234%) μg/h. The mean transit compartment rate constant (k_{tr}) was estimated to be 0.0774 h^{-1}. The mean maximum inhibition effect was estimated to be 0.64. The inhibition constant (EC_{50}) of S-CKD602 was

estimated to be 355 (IIV 146%) μg/L. The baseline monocyte value was estimated to be 0.605 (IIV 35.5%) $x10^9$/L. The mean feedback constant was estimated to be 0.0955.

Goodness-of-fit plots from the myelosuppression-based PK-PD model in all patients are depicted in **Figure 6.2**. The model adequately describes the PK profile of encapsulated CKD-602. The observed PK data correlated well with the population predicted (R^2 = 0.80) and individual predicted (R^2 = 0.98) data by this model. Although the PD data of monocytes were variable, the observed and model predicted data agreed relatively well. The observed PD data better correlated with the individual predicted PD data (R^2 = 0.83) than population predicted PD data (R^2 = 0.43). The representative individual PK profiles of encapsulated CKD-602 and time course of monocytopenia in patients are shown in **Figure 6.3**. The observed data of encapsulated CKD-602 and monocytes were well described by the myelosuppression-based model.

Model II. Mechanism-based PK-PD Model

The encapsulated CKD-602 and monocytes were modeled simultaneously for all patients. The distribution of residual variability was best described by a proportional plus additive error model. The PK-PD parameter estimates obtained from the final model are provided in **Table 6.3**. The volume of distribution (V_{encap}) was estimated to be 4.1 L (IIV 58.9%). The estimated V_{encap} is close to the plasma volume in humans. The mean association rate constant (k_{on}) was estimated to be 1.9 $L \cdot h^{-1}$. The degradation rate constant (k_{deg}) of S-CKD602 was estimated to be 0.0178 (IIV 50.6%) h^{-1}. The baseline monocyte value was estimated to be 0.671 (IIV 29.9%) $x10^9$/L. The removal rate constant (k_{out}) of monocytes was estimated to be 0.00677 (IIV 3.5%) h^{-1}. The adjusting factor was estimated to be 382 $\mu g/10^9$.

Goodness-of-fit plots from the mechanism-based PK-PD model in all patients are given in **Figure 6.4**. Similar to myelosuppression-based model, the population-predicted and individual-predicted encapsulated CKD-602 concentrations were highly correlated with the observed values and the observed and model predicted data agreed relatively well. The representative individual PK profiles of encapsulated CKD-602 and time course of monocytopenia in patients are shown in **Figure 6.5**. The observed data of encapsulated CKD-602 concentration and monocytes were well described by the mechanism-based model.

D. DISCUSSION

Major advances in the use of liposomes, conjugates, and nanoparticles as vehicles to deliver drugs have occurred the past 10 years (3-5). Doxil® and albumin stabilized nanoparticle formulation of paclitaxel (Abraxane®) are now FDA approved (6, 7, 50). In addition, there are greater than 200 liposomal and nanoparticle formulations of anticancer agents currently in development (3). Despite these fast development, one key hurdle preventing the wider success of liposome-based therapeutics is the complexity in PK and PD of liposomal agents in humans. Evaluation of the relationship of liposomal drug PK and PD and monocytes is of the utmost importance because the nonlinear PK of liposomal drug may be explained by the saturation of MPS and the bi-directional interaction between liposomal drugs and monocytes.

We developed a fully integrated mechanism-based population PK/PD model that described the relationship between PEGylated liposomal anticancer drug and monocyte in cancer patients treated with S-CKD602, a PEGylated liposomal CKD-602. In this model, an irreversible binding of liposomal drug to monocyte was used to account for the bi-directional interaction between PEGylated liposomal anticancer drug and monocyte. This model adequately described the observed clinical data, as illustrated in Figs. 4, 5 and Table 6.3. To our knowledge, this is the first mechanism-based model that includes the bi-directional interaction between PEGylated liposomal anticancer drug and monocytes for PEGylated liposomal anticancer drug in cancer patients.

In the mechanism-based model, the mean value of volume of distribution for encapsulated CKD-602 (V_{encap}) was 4.1 L and is close to plasma volume in humans. The estimated volume of distribution is consistent with our prior PK study of S-CKD602, in

which V_{encap} for patients with nonlinear clearance of encapsulated CKD-602 was estimated to be 2.1 ± 0.7 L/m^2 (22). In addition, the limited volume of distribution of encapsulated CKD-602 is consistent with other liposomal anticancer agents as the size of liposome limited their distribution to the normal tissue (20, 51). The half life of monocytes was estimated to be 102 hours, which is close but longer than the reported half life of monocytes in healthy human (mean 72 hours, range 36 – 104 hours) (52, 53). This discrepancy might be explained by the limited number of PD data and lack of information about removal rate constant in the data. In this model, S-CKD602 was eliminated via uptake by monocytes (as represented by $k_{on} \bullet A_{Encap} \bullet Mono$) and linear degradation (as represented by $k_{deg} \bullet A_{Encap}$). The association rate constant for uptake by monocytes (1.9 L·h^{-1}) is much greater than the estimated degradation rate constant of S-CKD602 (0.0178 h^{-1}). This suggests the importance of the uptake of liposomal drugs by monocyte in blood in determining the elimination of S-CKD602 from the central compartment.

The adjusting factor was introduced to the mechanism-based model to bridge the unit gap between amount of PEGylated liposomal drug and monocyte count. In our study, we have the monocyte absolute count data in unit of number of cells per liter and encapsulated CKD-602 amount in microgram. As the liposome interacts with monocyte via the receptor on the cell surface and the monocyte count is not equal to the concentration of receptors, it is not appropriate to convert the monocyte count data using molar unit. Therefore, we need this adjusting factor to address this issue in the model. We performed modeling on the data with encapsulated CKD-602 amount in microgram and in moles separately. The results from these two different data sets did not show much difference.

The degradation of liposome through route other than uptake by monocytes as represented by k_{deg} was important in the mechanism-based model. We tested the model with and without k_{deg} and deletion of k_{deg} from the final mechanism-based model resulted in an increase in AIC of 86. It is known that the primary accumulation sites of liposomes are liver and spleen and liposomes may be cleared by other phagocytes on sites (eg. Kupffer cells) (54, 55). Therefore, the contribution of other routes is also very important to PK of S-CKD602.

In the myelosuppression-based model, the estimated mean values of volume of distribution for encapsulated CKD-602 (3.46 L) is close to the estimates from mechanism-based model and consistent with other liposomal anticancer. The half-life of monocytes calculated as $0.693/k_{tr}$ was estimated to be 9.0 hours, which is much shorter than the half-life of monocytes estimated from the mechanism-based model and the reported value from literature. This may be due to direct cytotoxicity of liposomes on monocytes in blood. This may also be explained by the different structures between these two models. The myelosuppression-based model incorporated three transit compartments and the rate constant between each compartment was same and equal to the removal rate constant of monocytes from blood circulation. Thus, the offset of the toxic effect on monocyte was counted by three transit compartments in the myelosuppression-based model, whereas, it was counted by one step in the mechanism-based model.

The decrease in monocyte following PEGylated liposomal anticancer agents can be explained by the bi-directional interaction between PEGylated liposomal anticancer agents and monocytes or chemotherapy induced monocytopenia as described in our mechanism-based model and myelosuppression model. We developed a mechanism-based PK-PD model

based on the bi-directional interaction between PEGylated liposomal anticancer agents and monocytes. Meanwhile, to account for chemotherapy induced myelosuppression, we used a myelosuppression-based PK-PD model which has been frequently used to describe neutropenia or leukocytopenia after chemotherapy. Although monocytes and neutrophils have different morphology and functions, both of them are phagocytes and they are derived from the same progenitor cells following similar procedure. To test our hypothesis, we compared the model fit of the mechanism-based and the myelosuppression-based PK-PD model.

The population prediction of PK data obtained from mechanism-based model had a higher correlation with the observed PK data compared to that from myelosuppression-based model. This may suggest that incorporation of bi-directional interaction between PEGylated liposomal anticancer agents and monocytes in the model helped to explain the interindividual variability in the PK of S-CKD602. Although the individual prediction of PK data from mechanism-based model was more accurate than that from myelosuppression-based model, the population prediction of PK data from mechanism-based model was lower than the observed PK data at higher concentration level. This may suggest that the degradation of S-CKD602 through other routes was saturated at high concentration levels. Overall, both of these two models adequately described the PK data.

Both of the mechanism-based and myelosuppression-based PK-PD models described the observed PD data of monocytopenia relatively well. This suggests that both the chemotherapy induced myelosuppression and the bi-directional interaction between PEGylated liposomal anticancer agents and monocytes are important to describe the PD profile of monocytes after administration of S-CKD602. However, these two models

predicted two different time courses of monocyte count change after administration of S-CKD602. The myelosuppression-based model predicted a day of nadir around the observed day of nadir whereas the mechanism-based model predicted an earlier day of nadir compared to the observed. As no monocyte count was collected at the earlier time after administration of S-CKD602, the exact monocyte profile at earlier time points needs to be determined in future studies. PD profile of monocytes reached nadir at 2 days after administration of liposomal alendonate in rats (56). The half-life of monocytes in rats is about 2 days, which is similar to the reported half-life of monocytes in human (52, 53). The PD profile of monocytopenia after administration of liposomal alendonate suggested that the day of monocyte nadir after administration of S-CKD602 may be earlier than the observed value (8.6 ± 3.3 days). Thus, cytotoxic effects in blood and in bone marrow explain the decrease in monocytes after administration of PEGylated liposomal anticancer agents.

The individual predicted value of monocyte counts from myelosuppression-based model showed higher correlation with observed monocyte counts compared to mechanism-based model. The mechanism-based model overestimated monocyte count at lower monocyte count and underestimated monocyte count at higher monocyte count compared to myelosuppression-based model. This may be explained by the absence of feedback loop in the mechanism-based model. We tested the myelosuppression-based model without the feedback loop which produced a more serious overestimation monocyte count at lower monocyte count and underestimation of monocyte count at higher monocyte count than mechanism-based model (data not shown). The feedback loop was incorporated in myelosuppression-based model to describe leukocytopenia and neutropenia because it is known that the proliferation rate of progenitor cells can be affected by endogenous growth

factors and cytokines and that circulating neutrophil counts and the growth factor G-CSF levels are inversely related (35, 57, 58). No feedback mechanism has been reported for monocytes. The better PD fit of myelosuppression-based model suggest that feedback loop may be applicable for monocytes. However, the addition of feedback loop to the developed mechanism-based model did not improve the PD fits.

In conclusion, a mechanism-based PK-PD model was developed for encapsulated CKD-602 and monocyte counts in patients with advanced solid tumors. Comparison of this model and the myelosuppression-based model helped to explain PK and PD of PEGylated liposomal anticancer agents. The developed mechanism-based PK-PD model may be useful in predicting the PK and optimize dosing of pegylated liposomal agents to achieve a target exposure for each patient with malignant diseases. This model could also be used to describe the bi-directional interaction between PK and monocytes for other nanoparticle and conjugated anticancer agents as a method to profile and classify these agents.

E. REFERENCES

1. Drummond DC, Meyer O, Hong K, Kirpotin DB, Papahadjopoulos D. Optimizing liposomes for delivery of chemotherapeutic agents to solid tumors. Pharmacol Rev 1999; 51:691-743.

2. Allen TM, Hansen C. Pharmacokinetics of stealth versus conventional liposomes: effect of dose. Biochim Biophys Acta 1991; 1068:133-41.

3. Zamboni WC. Liposomal, nanoparticle, and conjugated formulations of anticancer agents. Clin Cancer Res 2005; 11:8230-4.

4. Papahadjopoulos D, Allen TM, Gabizon A, et al. Sterically stabilized liposomes: improvements in pharmacokinetics and antitumor therapeutic efficacy. Proc Natl Acad Sci U S A 1991; 88:11460-4.

5. Maeda H, Wu J, Sawa T, Matsumura Y, Hori K. Tumor vascular permeability and the EPR effect in macromolecular therapeutics: a review. J Control Release 2000; 65:271-84.

6. Markman M, Gordon AN, McGuire WP, Muggia FM. Liposomal anthracycline treatment for ovarian cancer. Semin Oncol 2004; 31:91-105.

7. Krown SE, Northfelt DW, Osoba D, Stewart JS. Use of liposomal anthracyclines in Kaposi's sarcoma. Semin Oncol 2004; 31:36-52.

8. Zamboni WC, Friedland DM, Ramalingam S, et al. Relationship between the plasma and tumor disposition of STEALTH liposomal CKD-602 and macrophages/dendritic cells (MDC) in mice bearing human tumor xenografts. American Association for Cancer Research; 2006; 2006. p. 1280.

9. Zamboni WC, Strychor S, Joseph E, et al. Plasma and tumor disposition of STEALTH Liposomal CKD-602 (S-CKD602) and non-liposomal CKD-602, a camptothecin analogue, in mice bearing A375 human melanoma xenograft. . American Association for Cancer Research; 2006 Nov; 2006. p. 3064.

10. Crul M. CKD-602. Chong Kun Dang. Curr Opin Investig Drugs 2003; 4:1455-9.

11. Lee JH, Lee JM, Lim KH, et al. Preclinical and phase I clinical studies with Ckd-602, a novel camptothecin derivative. Ann N Y Acad Sci 2000; 922:324-5.

12. Yu NY, Conway C, Pena RL, Chen JY. STEALTH liposomal CKD-602, a topoisomerase I inhibitor, improves the therapeutic index in human tumor xenograft models. Anticancer Res 2007; 27:2541-5.

13. Lee DH, Kim SW, Suh C, et al. Belotecan, new camptothecin analogue, is active in patients with small-cell lung cancer: results of a multicenter early phase II study. Ann Oncol 2008; 19:123-7.

14. Zamboni WC. Concept and clinical evaluation of carrier-mediated anticancer agents. Oncologist 2008; 13:248-60.

15. Innocenti F, Kroetz DL, Schuetz E, et al. Comprehensive pharmacogenetic analysis of irinotecan neutropenia and pharmacokinetics. J Clin Oncol 2009; 27:2604-14.

16. Slatter JG, Schaaf LJ, Sams JP, et al. Pharmacokinetics, metabolism, and excretion of irinotecan (CPT-11) following I.V. infusion of [(14)C]CPT-11 in cancer patients. Drug Metab Dispos 2000; 28:423-33.

17. Zamboni WC, Stewart CF, Thompson J, et al. Relationship between topotecan systemic exposure and tumor response in human neuroblastoma xenografts. J Natl Cancer Inst 1998; 90:505-11.

18. Stewart CF, Zamboni WC, Crom WR, et al. Topoisomerase I interactive drugs in children with cancer. Invest New Drugs 1996; 14:37-47.

19. Zamboni WC, Maruca LJ, Strychor S, et al. Bidirectional pharmacodynamic interaction between pegylated liposomal CKD-602 (S-CKD602) and monocytes in patients with refractory solid tumors. J Liposome Res.

20. Allen TM, Cullis PR. Drug delivery systems: entering the mainstream. Science 2004; 303:1818-22.

21. Gabizon A, Tzemach D, Mak L, Bronstein M, Horowitz AT. Dose dependency of pharmacokinetics and therapeutic efficacy of pegylated liposomal doxorubicin (DOXIL) in murine models. J Drug Target 2002; 10:539-48.

22. Zamboni WC, Strychor S, Maruca L, et al. Pharmacokinetic study of pegylated liposomal CKD-602 (S-CKD602) in patients with advanced malignancies. Clin Pharmacol Ther 2009; 86:519-26.

23. Gabizon A, Isacson R, Rosengarten O, Tzemach D, Shmeeda H, Sapir R. An open-label study to evaluate dose and cycle dependence of the pharmacokinetics of pegylated liposomal doxorubicin. Cancer Chemother Pharmacol 2008; 61:695-702.

24. La-Beck NM, Zamboni BA, Tzemach D, et al. Evaluation of the relationship between patient factors and the reduction in clearance of pegylated liposomal doxorubicin. ASCO Annual Meeting; 2009 Dec 15; 2009. p. abstr 2548.

25. Wu H, Infante JR, Jones SF, et al. Factors affecting the pharmacokinetics (PK) and pharmacodynamics (PD) of PEGylated liposomal irinotecan (IHL-305) in patients with advanced solid tumors AACR-NCI-EORTC; 2009; 2009.

26. Hempel G, Reinhardt D, Creutzig U, Boos J. Population pharmacokinetics of liposomal daunorubicin in children. Br J Clin Pharmacol 2003; 56:370-7.

27. Hong Y, Shaw PJ, Nath CE, et al. Population pharmacokinetics of liposomal amphotericin B in pediatric patients with malignant diseases. Antimicrob Agents Chemother 2006; 50:935-42.

28. Fetterly GJ, Grasela TH, Sherman JW, et al. Pharmacokinetic/pharmacodynamic modeling and simulation of neutropenia during phase I development of liposome-entrapped paclitaxel. Clin Cancer Res 2008; 14:5856-63.

29. Amantea MA, Forrest A, Northfelt DW, Mamelok R. Population pharmacokinetics and pharmacodynamics of pegylated-liposomal doxorubicin in patients with AIDS-related Kaposi's sarcoma. Clin Pharmacol Ther 1997; 61:301-11.

30. Zomorodi K, Gupta S. Population Pharmacokinetic Analysis of DOXIL in Adult Patients. AAPS; 1999; 1999.

31. Marina NM, Cochrane D, Harney E, et al. Dose escalation and pharmacokinetics of pegylated liposomal doxorubicin (Doxil) in children with solid tumors: a pediatric oncology group study. Clin Cancer Res 2002; 8:413-8.

32. Kondo M, Oshita F, Kato Y, Yamada K, Nomura I, Noda K. Early monocytopenia after chemotherapy as a risk factor for neutropenia. Am J Clin Oncol 1999; 22:103-5.

33. Oshita F, Yamada K, Nomura I, Tanaka G, Ikehara M, Noda K. Prophylactic administration of granulocyte colony-stimulating factor when monocytopenia appears lessens neutropenia caused by chemotherapy for lung cancer. Am J Clin Oncol 2000; 23:278-82.

34. Friberg LE, Freijs A, Sandstrom M, Karlsson MO. Semiphysiological model for the time course of leukocytes after varying schedules of 5-fluorouracil in rats. J Pharmacol Exp Ther 2000; 295:734-40.

35. Friberg LE, Henningsson A, Maas H, Nguyen L, Karlsson MO. Model of chemotherapy-induced myelosuppression with parameter consistency across drugs. J Clin Oncol 2002; 20:4713-21.

36. Minami H, Sasaki Y, Saijo N, et al. Indirect-response model for the time course of leukopenia with anticancer drugs. Clin Pharmacol Ther 1998; 64:511-21.

37. Krzyzanski W, Jusko WJ. Multiple-pool cell lifespan model of hematologic effects of anticancer agents. J Pharmacokinet Pharmacodyn 2002; 29:311-37.

38. Woo S, Krzyzanski W, Jusko WJ. Pharmacodynamic model for chemotherapy-induced anemia in rats. Cancer Chemother Pharmacol 2008; 62:123-33.

39. Kloft C, Wallin J, Henningsson A, Chatelut E, Karlsson MO. Population pharmacokinetic-pharmacodynamic model for neutropenia with patient subgroup identification: comparison across anticancer drugs. Clin Cancer Res 2006; 12:5481-90.

40. Leger F, Loos WJ, Bugat R, et al. Mechanism-based models for topotecan-induced neutropenia. Clin Pharmacol Ther 2004; 76:567-78.

41. Latz JE, Karlsson MO, Rusthoven JJ, Ghosh A, Johnson RD. A semimechanistic-physiologic population pharmacokinetic/pharmacodynamic model for neutropenia following pemetrexed therapy. Cancer Chemother Pharmacol 2006; 57:412-26.

42. van Kesteren C, Zandvliet AS, Karlsson MO, et al. Semi-physiological model describing the hematological toxicity of the anti-cancer agent indisulam. Invest New Drugs 2005; 23:225-34.

43. Wonganan P, Zamboni WC, Strychor S, Dekker JD, Croyle MA. Drug-virus interaction: effect of administration of recombinant adenoviruses on the pharmacokinetics of docetaxel in a rat model. Cancer Gene Ther 2009; 16:405-14.

44. Zamboni WC, Strychor S, Maruca L, et al. Pharmacokinetic Study of Pegylated Liposomal CKD-602 (S-CKD602) in Patients With Advanced Malignancies. Clin Pharmacol Ther 2009.

45. Zamboni WC, Ramalingam S, Friedland DM, et al. Phase I and pharmacokinetic study of pegylated liposomal CKD-602 in patients with advanced malignancies. Clin Cancer Res 2009; 15:1466-72.

46. Zamboni WC, Strychor S, Joseph E, et al. Plasma, tumor, and tissue disposition of STEALTH liposomal CKD-602 (S-CKD602) and nonliposomal CKD-602 in mice bearing A375 human melanoma xenografts. Clin Cancer Res 2007; 13:7217-23.

47. Bonate PL. Pharmacokinetic-Pharmacodynamic Modeling and Simulation 1ed: Springer Science and Business Media, Inc; 2005.

48. Sheiner LB, Beal SL. Evaluation of methods for estimating population pharmacokinetics parameters. I. Michaelis-Menten model: routine clinical pharmacokinetic data. J Pharmacokinet Biopharm 1980; 8:553-71.

49. Sheiner LB, Rosenberg B, Marathe VV. Estimation of population characteristics of pharmacokinetic parameters from routine clinical data. J Pharmacokinet Biopharm 1977; 5:445-79.

50. Roy V, LaPlant BR, Gross GG, Bane CL, Palmieri FM. Phase II trial of weekly nab (nanoparticle albumin-bound)-paclitaxel (nab-paclitaxel) (Abraxane) in combination with gemcitabine in patients with metastatic breast cancer (N0531). Ann Oncol 2009; 20:449-53.

51. Hilger RA, Richly H, Grubert M, et al. Pharmacokinetics (PK) of a liposomal encapsulated fraction containing doxorubicin and of doxorubicin released from the liposomal capsule after intravenous infusion of Caelyx/Doxil. Int J Clin Pharmacol Ther 2005; 43:588-9.

52. Jain NC. Essentials of Veterinary Hematology. 1 ed: Williams & Wilkins, Media, PA 19063; 1993.

53. Whitelaw DM. Observations on human monocyte kinetics after pulse labeling. Cell Tissue Kinet 1972; 5:311-7.

54. Koning GA, Morselt HW, Kamps JA, Scherphof GL. Uptake and intracellular processing of PEG-liposomes and PEG-immunoliposomes by kupffer cells in vitro 1 *. J Liposome Res 2001; 11:195-209.

55. Van Rooijen N, Sanders A. Kupffer cell depletion by liposome-delivered drugs: comparative activity of intracellular clodronate, propamidine, and ethylenediaminetetraacetic acid. Hepatology 1996; 23:1239-43.

56. Haber E, Afergan E, Epstein H, et al. Route of administration-dependent anti-inflammatory effect of liposomal alendronate. J Control Release.

57. Takatani H, Soda H, Fukuda M, et al. Levels of recombinant human granulocyte colony-stimulating factor in serum are inversely correlated with circulating neutrophil counts. Antimicrob Agents Chemother 1996; 40:988-91.

58. Hoffbrand AV, Lewis SM, Tuddenham E. Postgraduate Haematology. 4 ed: Oxford, United Kingdom, Butterworth-Heinemann; 1999.

Table 6.1.

A summary of Patient Demographics

Characteristics	Number of patients	Mean ± SD	Median (Range)
Age (years)		60.6 ± 12.2	62 (33.– 79)
Body Surface Area (m2)		1.91 ± 0.30	1.86 (1.36 – 2.76)
Body Weight (kg)		78.7 ± 21.4	75.5 (44.0 – 148)
Body Mass Index (kg/m2)		27.4 ± 5.60	26.7 (18.8 – 45.7)
Creatinine Clearance (ml/min)		98.4 ± 46.6	84.7 (33.2 – 277)
Height (cm)		169 ± 11.9	170 (142 – 196)
Ratio of Body Weight to Ideal Body Weight		1.27 ± 0.28	1.22 (0.83 – 2.13)
Sex			
Male	24		
Female	21		
Primary tumor type			
Colorectal Adenocarcinoma	17		
Ovarian Cancer	5		
Sarcoma	5		
Non-Small Cell Lung Cancer	4		
Pancreatic Adenocarcinoma	3		
Hepatocellular Carcinoma	2		
Prostate Carcinoma	2		
Esophageal, Metastatic Breast, Mesothelioma, Renal Cell Carcinoma, Thyroid, Appendix, Unknown Primary	1 patient for each type		
Patients with Tumors in liver	26		
Patients without tumors in liver	19		

Table 6.2.

Population PK-PD Parameters Obtained From the Myelosuppression-Based Model for Encapsulated CKD-602 and Monocytes.

Parameter	Definition	Population Mean RSE[a] (%)	IIV, CV%[b] RSE[a] (%)
V_{Encap} (L)	Volume of distribution for encapsulated CKD-602	3.46 (7.8)	70.9 (43)
V_{max} (μg/h)	Maximum velocity of encapsulated CKD-602	95.5 (31)	234 (34)
k_m (μg/L)	Michaelis-Menten constant	877 (21)	NE (NA)
$Mono_0$ (10^9/L)	Baseline monocyte count	0.605 (14)	35.5 (43)
k_{tr} (1/h)	Transit rate constant	0.0774 (7.7)	NE (NA)
E_{max}	Maximum inhibition	0.64 (31)	NE (NA)
EC_{50} (μg/L)	Inhibition constant	355 (60)	146 (80)
γ	Feedback constant	0.0955 (12)	NE (NA)
Residual variability			
Proportional error (variability as %)			
Encapsulated CKD-602		13.3 % (52)	NA[c]
Monocytes		37.3% (36)	NA[c]
Additive error			
Encapsulated CKD-602 (μg/L)		8.66 (54)	NA[c]
Monocytes (10^9/L)		NE (NA)	NA[c]

[a] Relative standard error for estimate.

[b] Coefficient of variation.

c Not estimated.

Table 6.3.

Population PK-PD Parameters Obtained From the Mechanism-Based Model for Encapsulated CKD-602 and Monocytes.

Parameter	Definition	Population Mean RSE[a] (%)	IIV, CV%[b] RSE[a] (%)
V_{Encap} (L)	Volume of distribution for encapsulated CKD-602	4.10 (11)	58.9 (35)
k_{on} (L/h)	Association rate constant	1.9 (47)	16.9 (75)
k_{deg} (1/h)	Degradation rate constant of S-CKD602	0.0178 (28)	50.6 (42)
$Mono_0$ (10^9/L)	Baseline monocyte count	0.671 (7.7)	29.9 (45)
k_{out} (1/h)	Removal rate constant of monocyte	0.00677 (18)	3.5 (195)
Factor (μg/10^9)	Adjusting factor	382 (34)	99.3 (89)
Residual variability			
Proportional error (variability as %)			
Encapsulated CKD-602		19.3 % (45)	NA[c]
Monocytes		10.2 % (48)	NA[c]
Additive error			
Encapsulated CKD-602 (μg/L)		9.02 (42)	NA[c]
Monocytes (10^9/L)		0.0471 (30)	NA[c]

[a] Relative standard error for estimate.

[b] Coefficient of variation.

c Not estimated.

Figure 6.1A

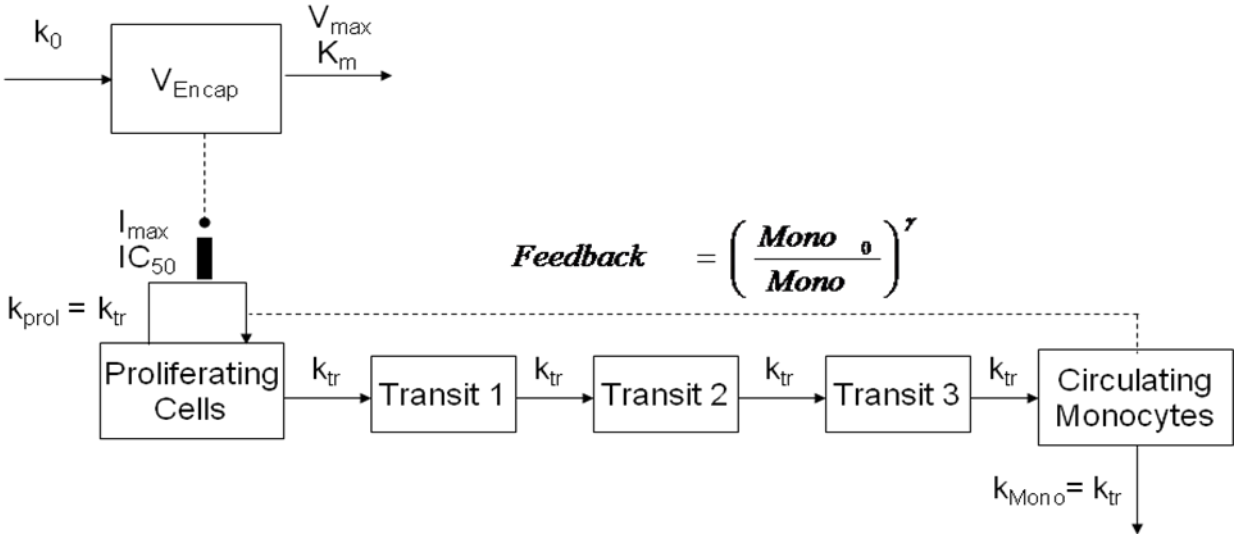

Figure 6.1B

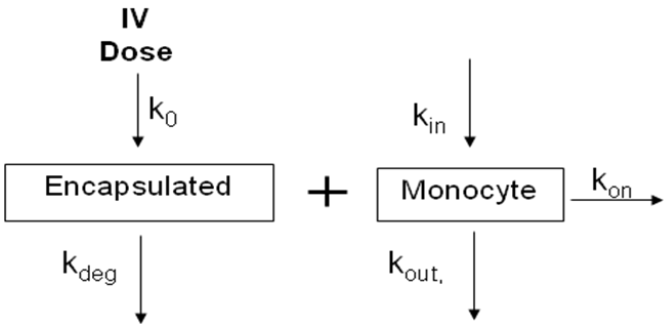

Figure 6.1. The myelosuppression-based PK-PD model for (A) and the mechanism-based PK-PD model (B) for encapsulated CKD-602 and monocytes.

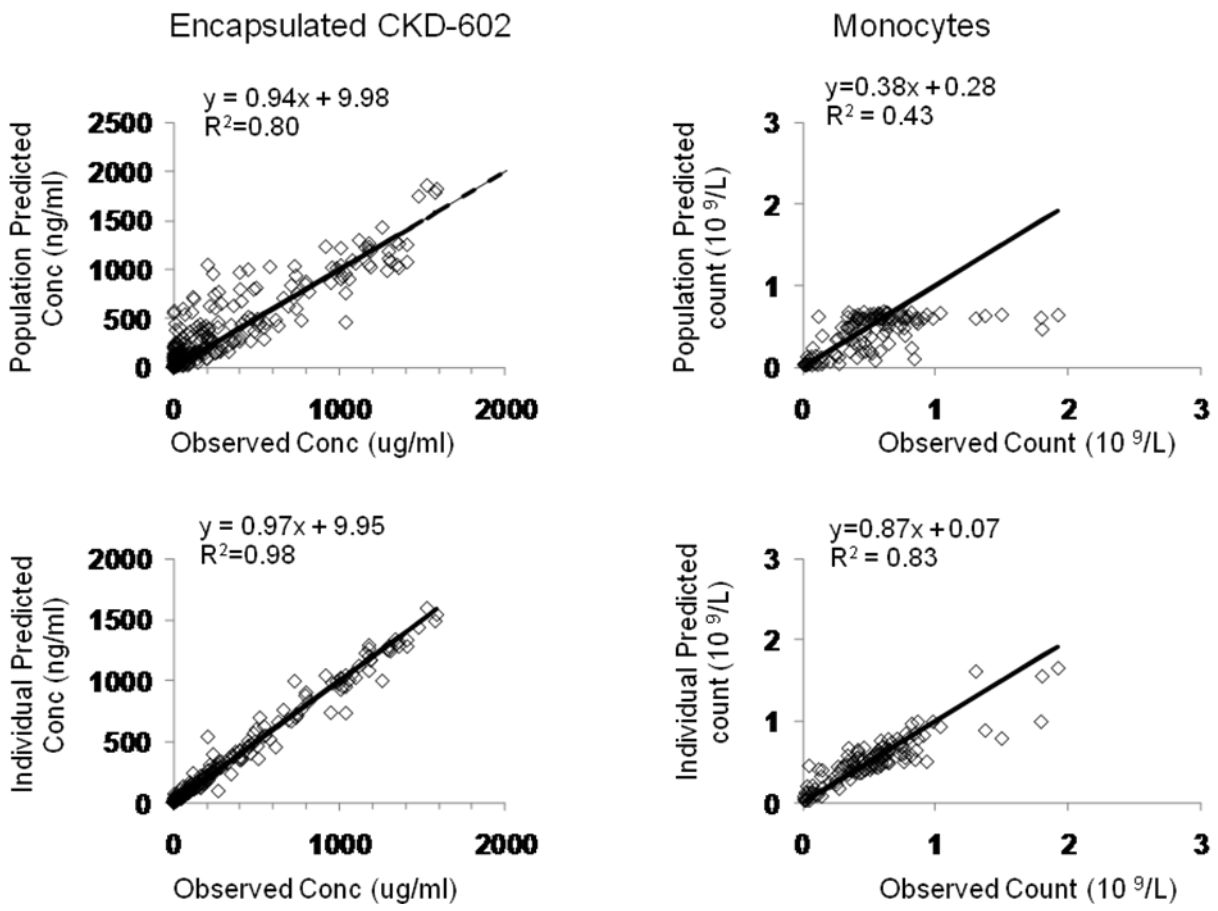

Figure 6.2. Goodness-of-fit plots for the myelosuppression-based model of encapsulated CKD-602 and monocytes. The solid lines are lines of identity.

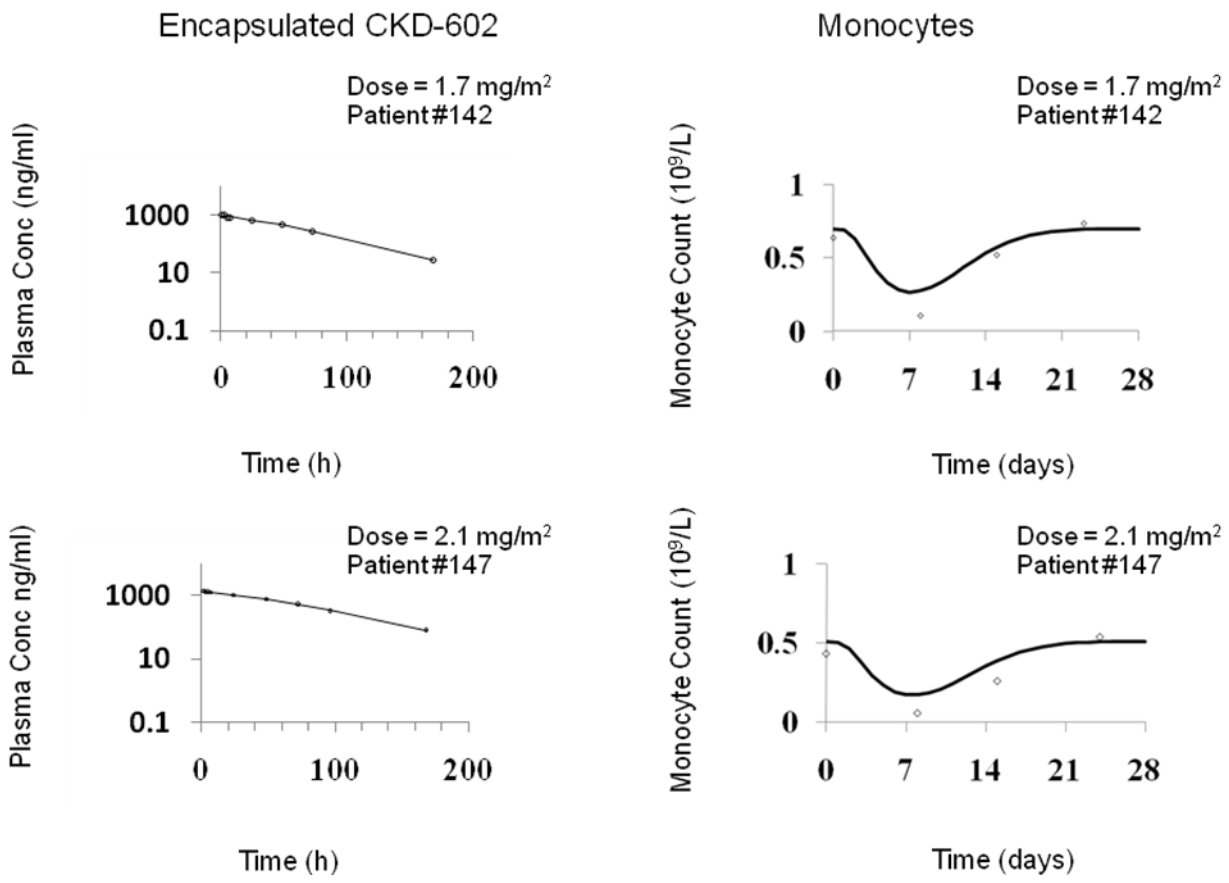

Figure 6.3. Representative individual plots of observed (○) and individual predicted (—) values from myelosuppression-based model for the plasma concentrations of encapsulated CKD-602 and monocyte count in all patients.

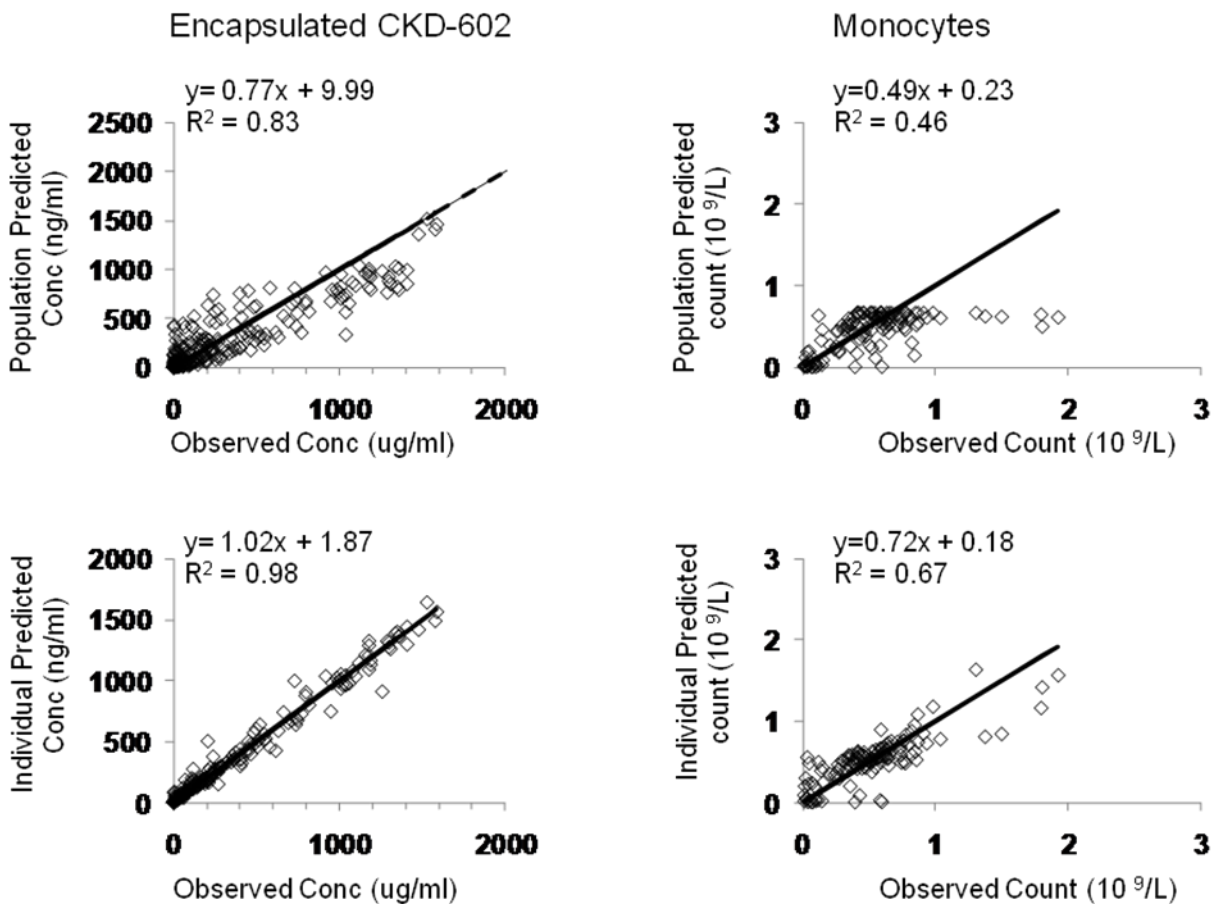

Figure 6.4. Goodness-of-fit plots for the mechanism-based model of encapsulated CKD-602 and monocytes. The solid lines are lines of identity.

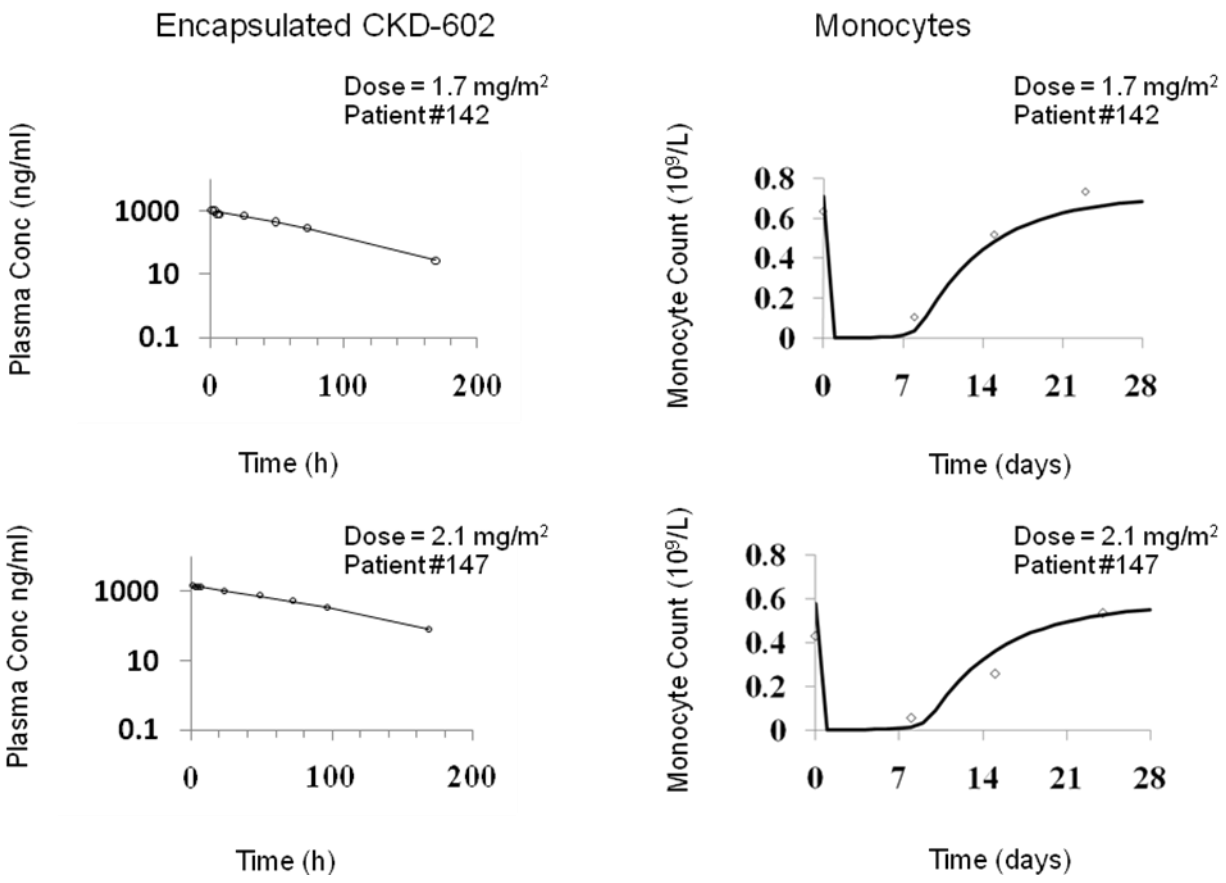

Figure 6.5. Representative individual plots of observed (○) and individual predicted (—) values from mechanism-based model for the plasma concentrations of encapsulated CKD-602 and monocyte counts in all patients.

CHAPTER 7

MECHANISM-BASED PHARMACOKINETIC-PHARMACODYNAMIC MODEL CHARACTERIZING BI-DIRECTIONAL INTERACTION BETWEEN PEGYLATED LIPOSOMAL CPT-11 (IHL-305) AND MONOCYTES IN PATIENTS WITH ADVANCED MALIGNANCIES

A. INTRODUCTION

Liposomes (microparticulate phospholipid vesicles) have been used with growing success as pharmaceutical carriers for anticancer agents. Conventional liposomes are quickly opsonized by plasma proteins, recognized as foreign bodies, and rapidly removed by the mononuclear phagocytic system (MPS) which has also been called the reticuloendothelial system (RES) (1, 2). The development of STEALTH or Polyethylene Glycol (PEG)ylated liposomes was based on the discovery that incorporation of mPEG-lipids into liposomes yields preparations with prolonged plasma exposure and superior tumor delivery compared to conventional liposomes composed of natural phospholipids (3-5). PEGylated liposomal doxorubicin (Doxil®) is approved for the treatment of refractory ovarian cancer, Kaposi sarcoma, and multiple myeloma (6, 7).

IHL-305 is a PEGylated liposomal formulation of irinotecan (CPT-11), a camptothecin analogue which inhibits topoisomerase I and has been approved for the treatment of metastatic colorectal cancer (3, 8-10). The PEGylated liposomal formulation consists of phospholipids covalently bound to polyethylene glycol (PEG) only on the outside of the lipid bilayer. CPT-11 is a prodrug that requires activation to the active metabolite, 7-ethyl-10-hydroxy-camptothecin (SN-38), which is approximately 100- to 1000-fold more active than the parent drug. SN-38 is further conjugated to form an inactive glucuronide (SN-38G) by uridine diphosphate glucuronosyltransferases (UGTs), primarily the UGT1A1 isoform. Other identified CPT-11 metabolites are 7-ethyl-10-[4-N-(5-aminopentanoic acid)-1-piperidino]-carbonyloxycamptothecin (APC) and 7-ethyl-10-[4-amino-1-piperidino]-carbonyloxycamptothecin (NPC) (10, 11).

The PEGylated liposomes of Doxil and IHL-305 were made using two different methods. The PEGylated liposome of Doxil was made by adding the PEG lipid before the process of liposomal formation which results PEG tether being projected on both the inside and outside of liposome. The PEGylated liposome of IHL-305 is made by adding the PEG lipids after the process of liposomal formation which results in PEG tether only being localized on the outer leaflet (12). Encapsulation of the CPT-11 allow for release of the active-lactone form into the tumor over a protracted period of time, which is ideal for a cell cycle-specific drug (3, 8-10, 13, 14).

The pharmacokinetic (PK) disposition of carrier-mediated agents, such as, nanoparticles, nanosomes, and conjugated agents, is dependent upon the carrier until the drug is released from the carrier. Unlike traditional anticancer agents which are cleared by the liver and kidneys, the clearance of non-PEGylated and PEGylated liposomes is via MPS which include monocytes, macrophages and dendritic cells located primarily in the liver and spleen (2). PEGylated liposomes are cleared much slower via MPS compared to non-PEGylated liposomes (4, 15). Uptake of the liposomes or nanoparticles by the MPS usually results in sequestering of the encapsulated drug in the MPS and the sequestered drug in the MPS may cause acute cytotoxicity to the MPS. This toxicity to the MPS in turn decreases clearance of the PEGylated liposomal anticancer agents and alters the PK and pharmacodynamics (PD) of PEGylated liposomal anticancer agents. Thus, there is a bi-directional interaction between PEGylated liposomal anticancer agents and MPS. Since a major portion of the liposomal encapsulated drug molecules are confined primarily to the blood compartment due to their relative large size (16), we have reported that there is a significant and clinically relevant interaction between liposomal agents and MPS cells in the

blood circulation (15). This bi-directional interaction between PEGylated liposomal anticancer agents and monocytes is very important in determining the PK and PD of PEGylated liposomal anticancer agents and potentially other nano and conjugated agents.

Clinical PK analysis of Doxil suggests a dose-dependent clearance saturation of clearance when a broad dose range is examined (17). Non-linear clearance was also observed in a phase I PK study of S-CKD602 (18). In addition, Gabizon and colleagues reported that the clearance of sum total (encapsulated + released) doxorubicin decreased by approximately 25 to 50% from cycle 1 to 3 (15, 19). We reported that this reduction in clearance of Doxil® from cycle 1 to cycle 3 was associated with a reduction in pre-cycle monocyte count (20). We have also reported that high % decrease in monocytes was associated with high clearance of IHL-305 (21). These studies suggest that the dose-dependent and cycle-dependent clearance of PEGylated liposomal anticancer agents may due to the bi-directional interaction between PEGylated liposomal drug and monocytes in blood.

The PK of PEGylated liposomal anticancer agents and Non-PEGylated liposomal anticancer agents in humans have been studied using the population modeling approach (22-27). Conventional compartment models such as one-compartment and two-compartment models were commonly used in these PK studies (22-27). The dose-dependent clearance of PEGylated liposomal anticancer agents was modeled using Michaelis-Menten kinetics (26). Mechanistic models based on physiology and pharmacology generally are more reliable for prediction of PK and PD than empirical models. Mechanistic PD models have been reported for neutropenia (28, 29). However, to date, mechanism-based models have not been developed for the PK and PD of PEGylated liposomal anticancer agents.

As monocytes of the MPS play an important role in the PK disposition of liposomes, the monocytopenia after administration of PEGylated liposomal anticancer agents was selected as a PD measure of these agents in this study. Monocytopenia is commonly observed after chemotherapy as a result of myelosuppression and early monocytopenia was reported to be a predictor of neutropenia (30, 31). The results of our prior study suggest that monocytes are more sensitive to S-CKD602 as compared with neutrophils and that the increased sensitivity is related to the liposomal formulation and not the encapsulated CKD-602 (15). Therefore, the monocytopenia after administration of PEGylated liposomal agents have a different mechanism from monocytopenia resulted from treatment with conventional small molecule chemotherapeutic drugs. Incorporation of the bi-directional interaction between PEGylated liposomal formulation and monocytes are important to characterize the PK and PD of these agents.

Although a few physiologically based PD models of chemotherapy-induced anemia, neutropenia, and thrombocytopenia have been developed, PD models of monocytopenia especially as related to nanoparticle PK and PD have not been reported (28, 32-35). As monocytes are derived from the same granulocyte-macrophage progenitor cells as other leukocytes, PD models of leukocytopenia may be applicable to monocytopenia. As we only have relatively sparse PD data of monocytopenia, a semiphysiological model proposed by Friberg et al. for chemotherapy-related myelosuppression was chosen as a standard model to describe monocytopenia after IHL-305 (28, 32). In this model, the cell maturation associated with myelopoiesis is described by multiple transit compartments with the same rate constant between each compartment to account for the time delay for onset of response (28, 32). In addition, a feedback loop was included to account for rebound of leukocytes typically

observed in myelosuppression profiles. This model has been widely applied to various anticancer agents to describe neutropenia, leukocytopenia, and thrombocytopenia because it involves minimum number of parameters (24, 28, 36-39).

The clinical results of the phase I study and limited PK results were previously published (40). The PK variability of IHL-305 is associated with linear and non-linear clearance (21). Monocytopenia after chemotherapy are conventionally believed due to myelosuppression. However, it is unclear if the monocytopenia is due to direct cytotoxicity to monocytes in the blood or cytotoxicity to progenitor cells in bone marrow. We believe the bi-directional interaction between PEGylated liposomal anticancer drugs and monocytes are more important to characterize the monocytopenia after these agents and PK of these agents. The objectives of this study were to develop a mechanism-based population PK-PD model to investigate the nature of nonlinear PK of IHL-305 and to increase our understanding of the bi-directional interaction between PEGylated liposomal anticancer agents and monocytes in blood of cancer patients.

B. METHODS

Study Design

The PK data were obtained from a phase I study of IHL-305 in patients with advanced solid tumors (40). The study design and clinical results have been reported elsewhere (40). Thirty-nine patients (13 males) received IHL-305 at 3.5 to 210 mg/m^2 IV x 1 over approximately 1 hour every 4 weeks. Prior to administration of the study drug, patients were premedicated with ondansetron (or other 5-HT3 inhibitor should circumstances require) and dexamethasone, according to each institution's standard of care. Written informed consent, approved by the Institutional Review board of the Sarah Cannon Research Institute and Vanderbilt University Medical Center, was obtained from all patients prior to study entry. Serial plasma samples were obtained at the following times: prior to administration, at end of the infusion (approximately 1 h), and at 1.5 h , 2 h , 3 h , 5 h , 9 h , 13 h, and 25 h after the start of the infusion for patients treated at < 67 mg/m^2 and the first three patients treated at 67 mg/m^2. Additional samples at 49 h, 73 h, 97 h, 169 h (day 7), 192 h (day 8), and 216 h (day 9) after the start of the infusion were also collected for the last three patients treated at 67 mg/m^2 and patients treated at > 67 mg/m^2. Total (lactone + hydroxyl acid) concentrations of sum total CPT-11, released CPT-11 and SN-38 in plasma were determined by a high-performance liquid chromatography (HPLC) as previously described (41). The lower limit of quantitation (LLQ) of the total form sum total CPT-11, released CPT-11 and SN-38 were 100, 2 and 2 ng/mL, respectively. Encapsulated CPT-11 was calculated by substracting the released CPT-11 concentration from sum total CPT-11 concentration at each time point. Complete blood counts were obtained weekly and as medically indicated.

Model Development

We believe that the bi-directional interaction between PEGylated liposomal anticancer agents and monocytes plays the key role in the elimination of PEGylated liposomal anticancer agents and monocytopenia observed in our prior studies (15). We developed a mechanism-based model based on receptor binding kinetics to describe the bi-directional interaction between the concentration versus time profile of encapsulated CPT-11 and time course of monocytes. We also developed a myelosuppression-based model in absence of the bi-directional interaction to compare with the mechanism-based model. For each kind of model, a variety of model structures were tested. The best model was selected on the basis of smaller values of AIC, better precision of estimates, and superior goodness-of-fit plots (42).

Model I. Myelosuppression-based Model

The PK-PD model of encapsulated CPT-11 and monocytes was built sequentially. One compartment model with Michaelis-Menten kinetics best described the PK data of encapsulated CPT-11 in our previous analysis. The individual PK parameters of encapsulated CPT-11 determined from the best PK model of encapsulated CPT-11 were used in the PD model of monocytes. In the PK modeling part, PK parameters (V_{encap}, V_{max}, and K_m) were estimated for each individual. For the PD modeling of monocytopenia, all of the individual values of the PK parameters were fixed for each patient and the predicted individual encapsulated CPT-11 concentrations-time profiles were used as input functions into this PK-PD model. The PD parameters were simultaneously estimated in the PD modeling part. This

sequential modeling approach was selected over a simultaneous PK-PD estimation to expedite the PD modeling by using the existing individual estimates of PK parameters.

A chemotherapy-induced myelosuppression model developed by Friberg et al. was used to describe the monocytopenia after administration of IHL-305 (**Figure 7.1A**) (28). The model consists of a proliferating compartment (Prol) that represents progenitor cells, three transit compartments of maturing cells (Transit), and a compartment of circulating monocytes. A negative feedback mechanism $(MONO_0/MONO)^{\gamma}$ from circulating cells on proliferating cells is included to describe the rebound of cells including an overshoot compared to the baseline value ($MONO_0$). The drug concentration in the central compartment (Conc) is assumed to reduce the proliferation rate by the function E_{Drug}, which was modeled to be an Emax model, [E_{max} x Conc/(EC50 + Conc)]. The differential equations were written as

$$\frac{dA_{Encap}}{dt} = k_0 - \frac{V_{\max} \bullet A_{Encap}}{K_m \bullet V_{Encap} + A_{Encap}} \quad , \quad A_{Encap}(0) = 0,$$

$$C_{Encap} = \frac{A_{Encap}}{V_{Encap}}$$

$$E_{Drug} = \frac{E_{\max} \bullet C_{Encap}}{EC_{50} + C_{Encap}}$$

$$\frac{d\,\mathrm{Prol}}{dt} = k_{prol} \bullet \mathrm{Prol} \bullet (1 - E_{Drug}) \bullet (Mono_0 / Mono)^{\gamma} - k_{tr} \bullet \mathrm{Prol} \quad , \quad \mathrm{Prol}(0) = \mathrm{Mono}_0$$

$$\frac{dTransit1}{dt} = k_{tr} \bullet \mathrm{Prol} - k_{tr} \bullet Transit1 \quad , \quad \mathrm{Transit1}(0) = \mathrm{Mono}_0$$

$$\frac{dTransit2}{dt} = k_{tr} \bullet Transit1 - k_{tr} \bullet Transit2 \quad , \quad \mathrm{Transit2}(0) = \mathrm{Mono}_0$$

$$\frac{dTransit3}{dt} = k_{tr} \bullet Transit2 - k_{tr} \bullet Transit3 \quad , \ \text{Transit3}(0) = \text{Mono}_0$$

$$\frac{dMono}{dt} = k_{tr} \bullet Transit3 - k_{Mono} \bullet Mono \quad , \ \text{Mono}(0) = \text{Mono}_0$$

dA_{Encap}/dt is the elimination rate, V_{max} is the maximum elimination rate or maximum velocity, K_m is the concentration at which half-maximum elimination rate is achieved, V_{Encap} is the volume of distribution, A_{Encap} is the encapsulated CPT-11 amount in plasma, C_{Encap} is the plasma concentration of encapsulated CPT-11, k_0 is the infusion rate and k_0 is 0 after stop of infusion, k_{tr} is the transit rate constant, E_{max} is the maximum attainable effect, EC_{50} is the concentration producing 50% of E_{max}, $Mono_0$ is the baseline monocyte count, γ is the feedback constant, k_{tr} is the proliferation rate constant, k_{mono} is the removal rate constant of monocyte, Mono is the monocyte count. The drug concentration in the central compartment (Conc) is assumed to reduce the proliferation rate by the function E_{Drug}, which was modeled using an E_{max} model. In the transit compartments, it is assumed that the only loss of cells is into the next compartment. As the proliferative cells differentiate into more mature cell types, the concentration of cells is maintained by cell division. At steady state, dProl/d t = 0, and therefore $k_{prol} = k_{tr}$. To minimize the number of parameters to be estimated, it was assumed in the modeling that $k_{mono} = k_{tr}$. Thus, the structural model parameters to be estimated were $Mono_0$, k_{tr}, γ, Emax and EC50.

Model II. Mechanism-based PK-PD Model

A mechanism based PK-PD model that incorporates the interaction between PEGylated liposomal anticancer agents and monocytes was developed for IHL-305 (**Figure 7.1B**). Concentration versus time data of encapsulated CPT-11 in plasma and monocyte

count in blood were fit simultaneously by this model. Drug is dosed IV into the systemic circulation (blood compartment) at a zero-order rate (k_0). The distribution of PEGylated liposome is described by a one-compartment model and the PEGylated liposome is eliminated by interacting with monocyte to form liposome-monocyte complex (k_{on}) which represents the phagocytosis of IHL-305 by the monocyte. PEGylated liposome is also degraded at a first-order rate (k_{deg}). This represents the elimination of the liposome through routes other than uptake by monocytes. The parameters describing the production and loss of monocytes are k_{in} and k_{out}. The production rate of monocytes k_{in} is equal to k_{out} multiplied by baseline monocyte value. The differential equations were written as

$$\frac{dA_{Encap}}{dt} = k_0 - k_{on} \bullet A_{Encap} \bullet Mono - k_{deg} \bullet A_{Encap} \quad , \; A_{Encap}(0) = 0$$

$$\frac{dMono}{dt} = Mono_0 \bullet k_{out} - k_{out} \bullet Mono - k_{on} \bullet A_{Encap} \bullet Mono / Factor \quad , \; Mono(0) = Mono_0$$

$$C_{Encap} = \frac{A_{Encap}}{V_{Encap}}$$

dA_{Encap}/dt is the elimination rate, A_{Encap} is encapsulated CPT-11 amount in plasma, C_{Encap} is the plasma concentration of encapsulated CPT-11, V_{Encap} is the volume of distribution of encapsulated CPT-11, Mono is the monocyte count, k_{on} is the association rate constant, k_{deg} is the degradation rate constant of IHL-305, k_{out} is the removal rate constant of monocyte, k_0 is the infusion rate and k_0 is 0 after stop of infusion. Since the unit of encapsulated CPT-11 is mg/L and the unit of monocyte count is 10^9/L, factor is a parameter used to bridge the unit gap.

Data Analysis

Encapsulated CPT-11 concentration versus time profile and monocyte count versus time data were analyzed using the nonlinear mixed effects modeling approach as implemented in NONMEM (version 6; University of California, San Francisco, CA) for the mechanistic and myelosuppression based models. The first order conditional estimation (FOCE) method were used in analyses. S-PLUS 8.0 (Version 8.0, Insightful Corporation, Seattle, Washington) was used for graphical diagnostics.

Mean population PK-PD variables, interindividual variability, and residual error were assessed in the model development (43, 44). Interindividual variability for each PK-PD variable was modeled with an exponential function. Residual error models of the additive, proportional, exponential, and combination methods were evaluated for the best structural PK-PD model. Individual PK-PD variables were obtained by posterior Bayesian estimation (43, 44). Model selection for nonhierarchical models (i.e., linear and nonlinear elimination models) was guided by goodness-of-fit plots (e.g., observed versus predicted plasma concentrations, weighted residuals versus predicted concentrations, and weighted residuals versus time), Akaike information criterion (AIC), and precision of parameter estimates. AIC was calculated as AIC = OFV + 2 x p, where OFV is the NONMEM objective function value and p is the number of PK-PD variables.

C. RESULTS

Patient demographics

Forty-two patients were enrolled on this study from 14 December 2006 to 15 December 2008 at Sarah Cannon Research Institute and Vanderbilt University Medical Center, Nashville, TN. Plasma concentrations of encapsulated CPT-11 and monocyte counts were obtained from 39 patients. Patient characteristics are listed in **Table 7.1**. The numbers of male and female patients evaluated in the phase I study were 13 and 26, respectively. The mean (median, range) age of the patients was 59.3 years (60 years, 41 to 75 years). A total of 392 plasma concentrations of encapsulated CPT-11 and 95 monocytes count were used to develop the population PK model. The mean ± SD numbers of concentrations of encapsulated CPT-11 and monocyte counts per patient were 10.1 ± 1.5 and 4.5 ± 1.6, respectively.

Model I. Myelosuppression-based Model

The encapsulated CPT-11 and monocytes were modeled sequentially for all patients. The distribution of residual variability was best described by a proportional plus additive error model. The PK and PD parameter estimates obtained from the final model are provided in **Table 7.2**. In the final model, the mean and interindividual variability (IIV, CV%) values for the distribution volume of encapsulated CPT-11 (V_{encap}) was 2.93 L and 27.9%, respectively. The estimated V_{encap} was very close to the plasma volume in humans. The mean Michaelis-Menten constant (K_m) was estimated to be 103 mg/L. The maximum velocity (Vmax) of encapsulated CPT-11 was estimated to be 14.2 (IIV 41.8%) mg/h. The mean transit compartment rate constant (k_{tr}) was estimated to be 0.0628 h^{-1}. The mean

maximum inhibition effect was estimated to be 0.95. The inhibition constant (EC_{50}) of IHL-305 was estimated to be 21.3 (IIV 54%) mg/L. The baseline monocyte value was estimated to be 0.564 (IIV 34.9%) $x10^9$/L. The mean feedback constant was estimated to be 0.319.

Goodness-of-fit plots from the myelosuppression-based PK-PD model in all patients are depicted in **Figure 7.2**. The model adequately describes the PK profile of encapsulated CPT-11. The observed PK data correlated well with the population predicted ($R^2 = 0.76$) and individual predicted ($R^2 = 0.93$) data by this model. Although the PD data of monocytes were variable, the observed and model predicted data agreed relatively well. The observed PD data better correlated with the individual predicted PD data ($R^2 = 0.86$) than population predicted PD data ($R^2 = 0.07$). The representative individual PK profiles of encapsulated CPT-11 and time course of monocytopenia in patients are shown in **Figure 7.3**. The observed data of encapsulated CPT-11 and monocytes were well described by the myelosuppression-based model.

Model II. Mechanism-based PK-PD Model

The encapsulated CPT-11 and monocytes were modeled simultaneously for all patients. The distribution of residual variability was best described by a proportional plus additive error model. The PK-PD parameter estimates obtained from the final model are provided in **Table 7.3**. The volume of distribution (V_{encap}) was estimated to be 2.86 L (IIV 27.4%). The estimated V_{encap} was close to the plasma volume in humans. The mean association rate constant (k_{on}) was estimated to be 0.00001 $L \cdot h^{-1}$. The degradation rate constant (k_{deg}) of IHL-305 was estimated to be 0.0389 (IIV 23%) h^{-1}. The baseline monocyte value was estimated to be 0.619 (IIV 33.8%) $x10^9$/L. The removal rate constant (k_{out}) of

monocytes was estimated to be 0.00487 (IIV 54.6%) h^{-1}. The adjusting factor was estimated to be 0.0358 mg·L/10^9.

Goodness-of-fit plots from the mechanism-based PK-PD model in all patients are depicted in **Figure 7.4**. The mechanism-based model adequately describes the PK profile of encapsulated CPT-11. The observed PK data correlated well with the population predicted (R^2 = 0.77) and individual predicted (R^2 = 0.94) data by this model. Although the PD data of monocytes were variable, the observed and model predicted data agreed relatively well. The observed PD data better correlated with the individual predicted PD data (R^2 = 0.86) than population predicted PD data (R^2 = 0.07). The representative individual PK profiles of encapsulated CPT-11 and time course of monocytopenia are shown in **Figure 7.5**. The observed data of encapsulated CPT-11 and monocytes were well described by the mechanism-based model.

D. DISCUSSION

Major advances in the use of liposomes, conjugates, and nanoparticles as vehicles to deliver drugs have occurred the past 10 years (3-5). Doxil® and albumin stabilized nanoparticle formulation of paclitaxel (Abraxane®) are now FDA approved (6, 7, 45). In addition, there are greater than 200 liposomal and nanoparticle formulations of anticancer agents currently in development (3). Despite these fast developments, one key hurdle preventing the wider success of liposome-based therapeutics is the complexity in PK and PD of liposomal agents in humans. Evaluation of the relationship of liposomal drug PK and PD and monocytes is of the utmost importance because the nonlinear PK of liposomal drug may be explained by the saturation of MPS and the bi-directional interaction between liposomal drugs and monocytes.

We developed a fully integrated mechanism-based population PK/PD model that described the relationship between PEGylated liposomal anticancer drug and monocyte in cancer patients treated with IHL-305, a PEGylated liposomal CPT-11. In this model, an irreversible binding of liposomal drug to monocyte was used to account for the bi-directional interaction between PEGylated liposomal anticancer drug and monocyte. This model adequately described the observed clinical data, as illustrated in **Figs. 4, 5** and **Table 7.3**. To our knowledge, this is the first mechanism-based model that includes the bi-directional interaction between PEGylated liposomal anticancer drug and monocytes for PEGylated liposomal anticancer drug in cancer patients.

In the mechanism-based model, the mean value of volume of distribution for encapsulated CPT-11 was 2.86 L and is close to plasma volume in humans. The estimated volume of distribution is consistent with our prior population PK study of S-CKD602, in

which the volume of distribution of encapsulated CKD-602 was estimated to be 3.63 L (46). In addition, the limited volume of distribution of encapsulated CPT-11 is consistent with other liposomal anticancer agents since the size of liposome limited their distribution to the normal tissue (16, 47). The half life of monocytes was estimated to be 142 hours. The reported half life of monocytes in healthy human (mean 72 hours, range 36 – 104 hours) (48, 49). This discrepancy might be explained by the limited number of PD data and lack of information about removal rate constant in the data. In this model, IHL-305 was eliminated via uptake by monocytes (as represented by $k_{on} \bullet A_{Encap} \bullet Mono$) and linear degradation as represented by ($k_{deg} \bullet A_{Encap}$). The association rate constant (k_{on} = 0.00001 $L \cdot h^{-1}$) is much lower than the estimated degradation rate constant of IHL-305 (k_{deg} = 0.0389 h^{-1}). This data suggested that the irreversible binding of monocytes and IHL-305 contribute less than linear degradation to the elimination of IHL-305. The toxicity of the sequestered CPT-11 to monocytes may be less than other liposomal anticancer agents such as S-CKD-602 as CPT-11 is a prodrug. In this case, the contribution of IHL-305 to the decrease of monocytes may be modest. In addition, the binding of IHL-305 and monocytes may be more reversible than irreversible for monocytes. However, due to the limited data points, we were unable to fit the data using a reversible binding kinetics.

The adjusting factor was introduced to the mechanism-based model to bridge the unit gap between amount of PEGylated liposomal drug and monocyte count. In our study, we have the monocyte absolute count data in unit of number of cells per liter and encapsulated CPT-11 amount in microgram. As liposome interacts with monocyte via the receptor on the cell surface, and the monocyte count is not equal to the concentration of receptors, it is not appropriate to convert the monocyte count data using molar unit. Therefore, we need this

adjusting factor to address this issue in the model. We performed modeling on the data with encapsulated CPT-11 amount in microgram and in molar separately. And the results from these two different data sets did not show much difference.

The degradation of liposome through route other than uptake by monocytes as represented by k_{deg} was important in the mechanism-based model. We tested the model with and without k_{deg} and deletion of k_{deg} from the final mechanism-based model resulted in an increase in AIC of 34. It is known that the primary accumulation sites of liposomes are liver and spleen and liposomes may be cleared by other phagocytes on sites (eg. Kupffer cells) (50, 51). Therefore, the contribution of other routes is also very important to PK of IHL-305.

In the myelosuppression-based model, the estimated mean values of volume of distribution for encapsulated CPT-11 (2.93 L) is close to the estimates from mechanism-based model and consistent with other liposomal anticancer. The half-life of monocytes calculated as $0.693/k_{tr}$ was estimated to be 11.0 hours, which is much shorter than the half-life of monocytes estimated from the mechanism-based model and the reported value from literature. This may be due to direct cytotoxicity of liposomes on monocytes in blood. This may also be explained by the different structures between these two models. The myelosuppression-based model incorporated three transit compartments and the rate constant between each compartment was same and equal to the removal rate constant of monocytes from blood circulation. Thus, the offset of the toxic effect on monocyte was counted by three transit compartments in the myelosuppression-based model, whereas, it was counted by one step in the mechanism-based model.

The correlations between the population and individual predicted and observed PK data is slightly better in mechanism-based model compared to myelosuppression-based

model. This may suggest that incorporation of bi-directional interaction between PEGylated liposomal anticancer agents and monocytes in the model helped to explain the interindividual variability in the PK of S-CKD602. In addition, this is consistent with our findings in developing mechanism-based model for S-CKD602.

Both of the mechanism-based and myelosuppression-based PK-PD models described the change of monocyte counts over the dosing period relatively well. This suggested that both the chemotherapy induced myelosuppression and the bi-directional interaction between PEGylated liposomal anticancer agents and monocytes are important to describe the PD profile of monocytes after administration of IHL-305. Although the correlation between model predicted and observed PD data of these two models were comparable, the prediction of PD data from myelosuppression-based model was more accurate than that from mechanism-based model. The mechanism-based model overestimated monocyte count at lower monocyte count and underestimated monocyte count at higher monocyte count compared to myelosuppression-based model. This may be explained by the absence of feedback loop in the mechanism-based model. The feedback loop was incorporated in myelosuppression-based model to describe leukocytopenia and neutropenia because it is known that the proliferation rate of progenitor cells can be affected by endogenous growth factors and cytokines and that circulating neutrophil counts and the growth factor G-CSF levels are inversely related (28, 52, 53). No feedback mechanism has been reported for monocytes. The better PD fit of myelosuppression-based model suggest that feedback loop may be applicable for monocytes. However, the addition of feedback loop to the developed mechanism-based model did not improve the PD fits.

Although the myelosuppression-based model described the PD data relatively well, the individual prediction of monocyte counts from this model showed a fluctuating curve of monocyte change. This fluctuation of monocyte counts after administration of IHL-305 is related to the feedback constant. The fluctuation of monocyte can be reduced by fixing the feedback constant at low value. Deletion of this feedback constant from the myelosuppression model can delete the fluctuation of monocyte counts but also produces a worse model.

The mechanism-based and myelosuppression-based models predicted two different time courses of monocyte count change after administration of IHL-305. The myelosuppression-based model predicted a day of nadir around the observed day of nadir whereas the mechanism-based model predicted an earlier day of nadir compared to the observed. As no monocyte count was collected at the earlier time after administration of IHL-305, the exact monocyte profile at earlier time points needs to be determined in future studies. PD profile of monocytes reached nadir at 2 days after administration of liposomal alendonate in rats (54). The half-life of monocytes in rats is about 2 days, which is similar to the reported half-life of monocytes in human (48, 49). The PD profile of monocytopenia after administration of liposomal alendonate suggested that the day of monocyte nadir after administration of IHL-305 may be earlier than the observed value (11.2 ± 6.1 days). Thus, cytotoxic effects in blood and in bone marrow explain the decrease in monocytes after administration of PEGylated liposomal anticancer agents.

In conclusion, a mechanism-based PK-PD model was developed for encapsulated CPT-11 and monocyte counts in patients with advanced solid tumors. Comparison of this model and the myelosuppression-based model helped to explain PK and PD of PEGylated

liposomal anticancer agents. The developed mechanism-based PK-PD model may be useful in predicting the PK and optimize dosing of pegylated liposomal agents to achieve a target exposure for a patient with malignant diseases. This model could also be used to describe the bi-directional interaction between PK and monocytes for other nanoparticle and conjugated anticancer agents as a method to profile and classify these agents.

E. REFERENCES

1. Drummond DC, Meyer O, Hong K, Kirpotin DB, Papahadjopoulos D. Optimizing liposomes for delivery of chemotherapeutic agents to solid tumors. Pharmacol Rev 1999; 51:691-743.

2. Allen TM, Hansen C. Pharmacokinetics of stealth versus conventional liposomes: effect of dose. Biochim Biophys Acta 1991; 1068:133-41.

3. Zamboni WC. Liposomal, nanoparticle, and conjugated formulations of anticancer agents. Clin Cancer Res 2005; 11:8230-4.

4. Papahadjopoulos D, Allen TM, Gabizon A, et al. Sterically stabilized liposomes: improvements in pharmacokinetics and antitumor therapeutic efficacy. Proc Natl Acad Sci U S A 1991; 88:11460-4.

5. Maeda H, Wu J, Sawa T, Matsumura Y, Hori K. Tumor vascular permeability and the EPR effect in macromolecular therapeutics: a review. J Control Release 2000; 65:271-84.

6. Markman M, Gordon AN, McGuire WP, Muggia FM. Liposomal anthracycline treatment for ovarian cancer. Semin Oncol 2004; 31:91-105.

7. Krown SE, Northfelt DW, Osoba D, Stewart JS. Use of liposomal anthracyclines in Kaposi's sarcoma. Semin Oncol 2004; 31:36-52.

8. Zamboni WC. Concept and clinical evaluation of carrier-mediated anticancer agents. Oncologist 2008; 13:248-60.

9. Innocenti F, Kroetz DL, Schuetz E, et al. Comprehensive pharmacogenetic analysis of irinotecan neutropenia and pharmacokinetics. J Clin Oncol 2009; 27:2604-14.

10. Slatter JG, Schaaf LJ, Sams JP, et al. Pharmacokinetics, metabolism, and excretion of irinotecan (CPT-11) following I.V. infusion of [(14)C]CPT-11 in cancer patients. Drug Metab Dispos 2000; 28:423-33.

11. Xie R, Mathijssen RH, Sparreboom A, Verweij J, Karlsson MO. Clinical pharmacokinetics of irinotecan and its metabolites in relation with diarrhea. Clin Pharmacol Ther 2002; 72:265-75.

12. Zamboni WC, Yoshino K. Formulation and physiological factors affecting the pharmacokinetics and pharmacodynamics of liposomal anticancer agents. Japan DDS 2010; 25:58-70.

13. Zamboni WC, Stewart CF, Thompson J, et al. Relationship between topotecan systemic exposure and tumor response in human neuroblastoma xenografts. J Natl Cancer Inst 1998; 90:505-11.

14. Stewart CF, Zamboni WC, Crom WR, et al. Topoisomerase I interactive drugs in children with cancer. Invest New Drugs 1996; 14:37-47.

15. Zamboni WC, Maruca LJ, Strychor S, et al. Bidirectional pharmacodynamic interaction between pegylated liposomal CKD-602 (S-CKD602) and monocytes in patients with refractory solid tumors. J Liposome Res.

16. Allen TM, Cullis PR. Drug delivery systems: entering the mainstream. Science 2004; 303:1818-22.

17. Gabizon A, Tzemach D, Mak L, Bronstein M, Horowitz AT. Dose dependency of pharmacokinetics and therapeutic efficacy of pegylated liposomal doxorubicin (DOXIL) in murine models. J Drug Target 2002; 10:539-48.

18. Zamboni WC, Strychor S, Maruca L, et al. Pharmacokinetic study of pegylated liposomal CKD-602 (S-CKD602) in patients with advanced malignancies. Clin Pharmacol Ther 2009; 86:519-26.

19. Gabizon A, Isacson R, Rosengarten O, Tzemach D, Shmeeda H, Sapir R. An open-label study to evaluate dose and cycle dependence of the pharmacokinetics of pegylated liposomal doxorubicin. Cancer Chemother Pharmacol 2008; 61:695-702.

20. La-Beck NM, Zamboni BA, Tzemach D, et al. Evaluation of the relationship between patient factors and the reduction in clearance of pegylated liposomal doxorubicin. ASCO Annual Meeting; 2009 Dec 15; 2009. p. abstr 2548.

21. Wu H, Infante JR, Jones SF, et al. Factors affecting the pharmacokinetics (PK) and pharmacodynamics (PD) of PEGylated liposomal irinotecan (IHL-305) in patients with advanced solid tumors AACR-NCI-EORTC; 2009; 2009.

22. Hempel G, Reinhardt D, Creutzig U, Boos J. Population pharmacokinetics of liposomal daunorubicin in children. Br J Clin Pharmacol 2003; 56:370-7.

23. Hong Y, Shaw PJ, Nath CE, et al. Population pharmacokinetics of liposomal amphotericin B in pediatric patients with malignant diseases. Antimicrob Agents Chemother 2006; 50:935-42.

24. Fetterly GJ, Grasela TH, Sherman JW, et al. Pharmacokinetic/pharmacodynamic modeling and simulation of neutropenia during phase I development of liposome-entrapped paclitaxel. Clin Cancer Res 2008; 14:5856-63.

25. Amantea MA, Forrest A, Northfelt DW, Mamelok R. Population pharmacokinetics and pharmacodynamics of pegylated-liposomal doxorubicin in patients with AIDS-related Kaposi's sarcoma. Clin Pharmacol Ther 1997; 61:301-11.

26. Zomorodi K, Gupta S. Population Pharmacokinetic Analysis of DOXIL in Adult Patients. AAPS; 1999; 1999.

27. Marina NM, Cochrane D, Harney E, et al. Dose escalation and pharmacokinetics of pegylated liposomal doxorubicin (Doxil) in children with solid tumors: a pediatric oncology group study. Clin Cancer Res 2002; 8:413-8.

28. Friberg LE, Henningsson A, Maas H, Nguyen L, Karlsson MO. Model of chemotherapy-induced myelosuppression with parameter consistency across drugs. J Clin Oncol 2002; 20:4713-21.

29. Zamboni WC, D'Argenio DZ, Stewart CF, et al. Pharmacodynamic model of topotecan-induced time course of neutropenia. Clin Cancer Res 2001; 7:2301-8.

30. Kondo M, Oshita F, Kato Y, Yamada K, Nomura I, Noda K. Early monocytopenia after chemotherapy as a risk factor for neutropenia. Am J Clin Oncol 1999; 22:103-5.

31. Oshita F, Yamada K, Nomura I, Tanaka G, Ikehara M, Noda K. Prophylactic administration of granulocyte colony-stimulating factor when monocytopenia appears lessens neutropenia caused by chemotherapy for lung cancer. Am J Clin Oncol 2000; 23:278-82.

32. Friberg LE, Freijs A, Sandstrom M, Karlsson MO. Semiphysiological model for the time course of leukocytes after varying schedules of 5-fluorouracil in rats. J Pharmacol Exp Ther 2000; 295:734-40.

33. Minami H, Sasaki Y, Saijo N, et al. Indirect-response model for the time course of leukopenia with anticancer drugs. Clin Pharmacol Ther 1998; 64:511-21.

34. Krzyzanski W, Jusko WJ. Multiple-pool cell lifespan model of hematologic effects of anticancer agents. J Pharmacokinet Pharmacodyn 2002; 29:311-37.

35. Woo S, Krzyzanski W, Jusko WJ. Pharmacodynamic model for chemotherapy-induced anemia in rats. Cancer Chemother Pharmacol 2008; 62:123-33.

36. Kloft C, Wallin J, Henningsson A, Chatelut E, Karlsson MO. Population pharmacokinetic-pharmacodynamic model for neutropenia with patient subgroup identification: comparison across anticancer drugs. Clin Cancer Res 2006; 12:5481-90.

37. Leger F, Loos WJ, Bugat R, et al. Mechanism-based models for topotecan-induced neutropenia. Clin Pharmacol Ther 2004; 76:567-78.

38. Latz JE, Karlsson MO, Rusthoven JJ, Ghosh A, Johnson RD. A semimechanistic-physiologic population pharmacokinetic/pharmacodynamic model for neutropenia following pemetrexed therapy. Cancer Chemother Pharmacol 2006; 57:412-26.

39. van Kesteren C, Zandvliet AS, Karlsson MO, et al. Semi-physiological model describing the hematological toxicity of the anti-cancer agent indisulam. Invest New Drugs 2005; 23:225-34.

40. Jones SF, Zamboni WC, Burris III HA, et al. Phase I and pharmacokinetic (PK) study of IHL-305 (pegylated liposomal irinotecan) in patients with advanced solid tumors. ASCO; 2009 Jun, 2009; Orlando, FL; 2009.

41. Kurita A, Kaneda N. High-performance liquid chromatographic method for the simultaneous determination of the camptothecin derivative irinotecan hydrochloride, CPT-11, and its metabolites SN-38 and SN-38 glucuronide in rat plasma with a fully automated on-line solid-phase extraction system, PROSPEKT. J Chromatogr B Biomed Sci Appl 1999; 724:335-44.

42. Bonate PL. Pharmacokinetic-Pharmacodynamic Modeling and Simulation 1ed: Springer Science and Business Media, Inc; 2005.

43. Sheiner LB, Beal SL. Evaluation of methods for estimating population pharmacokinetics parameters. I. Michaelis-Menten model: routine clinical pharmacokinetic data. J Pharmacokinet Biopharm 1980; 8:553-71.

44. Sheiner LB, Rosenberg B, Marathe VV. Estimation of population characteristics of pharmacokinetic parameters from routine clinical data. J Pharmacokinet Biopharm 1977; 5:445-79.

45. Roy V, LaPlant BR, Gross GG, Bane CL, Palmieri FM. Phase II trial of weekly nab (nanoparticle albumin-bound)-paclitaxel (nab-paclitaxel) (Abraxane) in combination with gemcitabine in patients with metastatic breast cancer (N0531). Ann Oncol 2009; 20:449-53.

46. Wu H, Ramanathan RK, Strychor S, et al. Population Pharmacokinetics of PEGylated Liposomal CKD-602 (S-CKD602) in Patients with Advanced Malignancies. ASCO; 2009; 2009.

47. Hilger RA, Richly H, Grubert M, et al. Pharmacokinetics (PK) of a liposomal encapsulated fraction containing doxorubicin and of doxorubicin released from the liposomal capsule after intravenous infusion of Caelyx/Doxil. Int J Clin Pharmacol Ther 2005; 43:588-9.

48. Jain NC. Essentials of Veterinary Hematology. 1 ed: Williams & Wilkins, Media, PA 19063; 1993.

49. Whitelaw DM. Observations on human monocyte kinetics after pulse labeling. Cell Tissue Kinet 1972; 5:311-7.

50. Koning GA, Morselt HW, Kamps JA, Scherphof GL. Uptake and intracellular processing of PEG-liposomes and PEG-immunoliposomes by kupffer cells in vitro 1 *. J Liposome Res 2001; 11:195-209.

51. Van Rooijen N, Sanders A. Kupffer cell depletion by liposome-delivered drugs: comparative activity of intracellular clodronate, propamidine, and ethylenediaminetetraacetic acid. Hepatology 1996; 23:1239-43.

52. Takatani H, Soda H, Fukuda M, et al. Levels of recombinant human granulocyte colony-stimulating factor in serum are inversely correlated with circulating neutrophil counts. Antimicrob Agents Chemother 1996; 40:988-91.

53. Hoffbrand AV, Lewis SM, Tuddenham E. Postgraduate Haematology. 4 ed: Oxford, United Kingdom, Butterworth-Heinemann; 1999.

54. Haber E, Afergan E, Epstein H, et al. Route of administration-dependent anti-inflammatory effect of liposomal alendronate. J Control Release.

Table 7.1.

A summary of Patient Demographics

Characteristics	Number of patients	Mean ± SD	Median (Range)
Age (years)		60.0 ± 9.4	60 (42– 75)
Body Surface Area (m2)		1.88 ± 0.28	1.85 (1.41 – 2.39)
Body Weight (kg)		76.7 ± 20.4	75.3 (47.1 – 124.5)
Body Mass Index (kg/m2)		27.0 ± 6.8	26.3 (17.2 – 53.6)
Height (cm)		169 ± 10.3	168 (152 – 188)
Ratio of Body Weight to Ideal Body Weight		1.26 ± 0.36	1.16 (0.81 – 2.74)
Sex			
Male	13		
Female	26		
Primary tumor type			
Ovarian Cancer	8		
Breast Cancer	6		
Lung Cancer	6		
Bladder	2		
Head and Neck Squamous	2		
Neuroendocrine Carcinoma	2		
Adenoid cystic, Anus, Cervical, Colon, Gastric, Mediastinal, Metastatic breast, Metastatic prostate, Metastatic carcinoid, Pancreatic, Prosta, Right 4th toe, Uterine	1 patient for each type		

Table 7.2.

Population PK-PD Parameters Obtained From the Myelosuppression-based Model for Encapsulated CPT-11 and Monocytes.

Parameter	Definition	Population Mean RSE[a] (%)	IIV, CV%[b] RSE[a] (%)
V_{Encap} (L)	Volume of distribution for encapsulated CPT-11	2.93 (5.0)	27.9 (25)
V_{max} (mg/h)	Maximum velocity of encapsulated CPT-11	14.2 (38)	41.8 (20)
k_m (mg/L)	Michaelis-Menten constant	103 (48)	NE (NA)
Baseline (10^9/L)	Baseline monocyte count	0.564 (7.4)	34.9 (64)
k_{tr} (1/h)	Transit rate constant	0.0628 (1.5)	NE (NA)
E_{max}	Maximum inhibition	0.95 (7.6)	NE (NA)
EC_{50} (mg/L)	Inhibition constant	21.3 (1)	54 (220)
γ	Feedback constant	0.319 (3.7)	NE (NA)
Residual variability			
Proportional error (variability as %)			
Encapsulated CPT-11		22.2 % (23)	NA[c]
Monocytes		21.4% (5.5)	NA[c]
Additive error			
Encapsulated CPT-11 (mg/L)		0.199 (177)	NA[c]
Monocytes (10^9/L)		0.00322 (52)	NA[c]

[a] Relative standard error for estimate.

[b] Coefficient of variation.

c Not estimated.

Table 7.3.

Population PK-PD Parameters Obtained From the Mechanism-based Model for Encapsulated CPT-11 and Monocytes.

Parameter	Definition	Population Mean RSE[a] (%)	IIV, CV%[b] RSE[a] (%)
V_{Encap} (L)	Volume of distribution for encapsulated CPT-11	2.86 (4.5)	27.4 (24)
k_{on} (L/h)	Association rate constant	0.00001 (30)	NE (NA)
k_{deg} (1/h)	Degradation rate constant of IHL-305	0.0389 (5.1)	23.0 (36)
Baseline (10^9/L)	Baseline monocyte count	0.619 (7.2)	33.8 (59)
k_{out} (1/h)	Removal rate constant of monocyte	0.00487 (27)	54.6 (91)
Factor ($\mu g \cdot L/10^9$)	Adjusting factor	0.0358 (5.7)	NE (NA)
Residual variability			
Proportional error (variability as %)			
Encapsulated CPT-11		22.1 % (26)	NA[c]
Monocytes		22.4% (155)	NA[c]
Additive error			
Encapsulated CPT-11 (mg/L)		0.484 (51)	NA[c]
Monocytes (10^9/L)		0.00352 (110)	NA[c]

[a] Relative standard error for estimate.

[b] Coefficient of variation.

c Not estimated.

Figure 7.1A

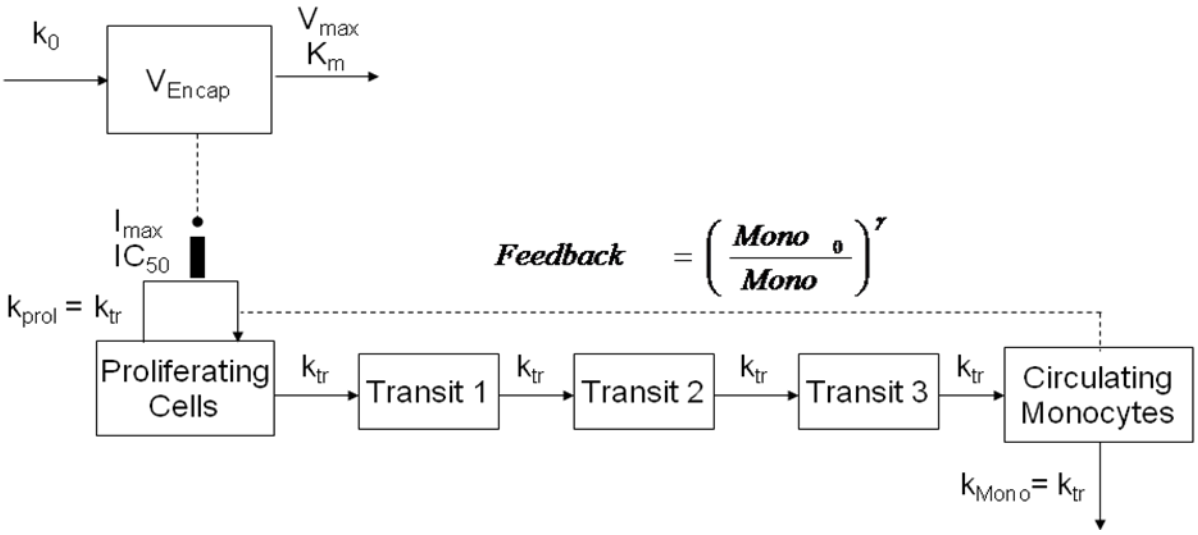

Figure 7.1B

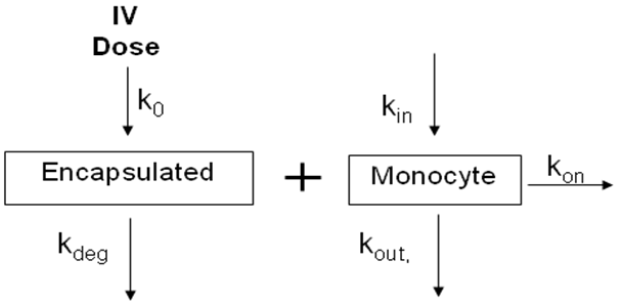

Figure 7.1. The myelosuppression-based PK-PD model for (A) and the mechanism-based PK-PD model (B) for encapsulated CPT-11 and monocytes.

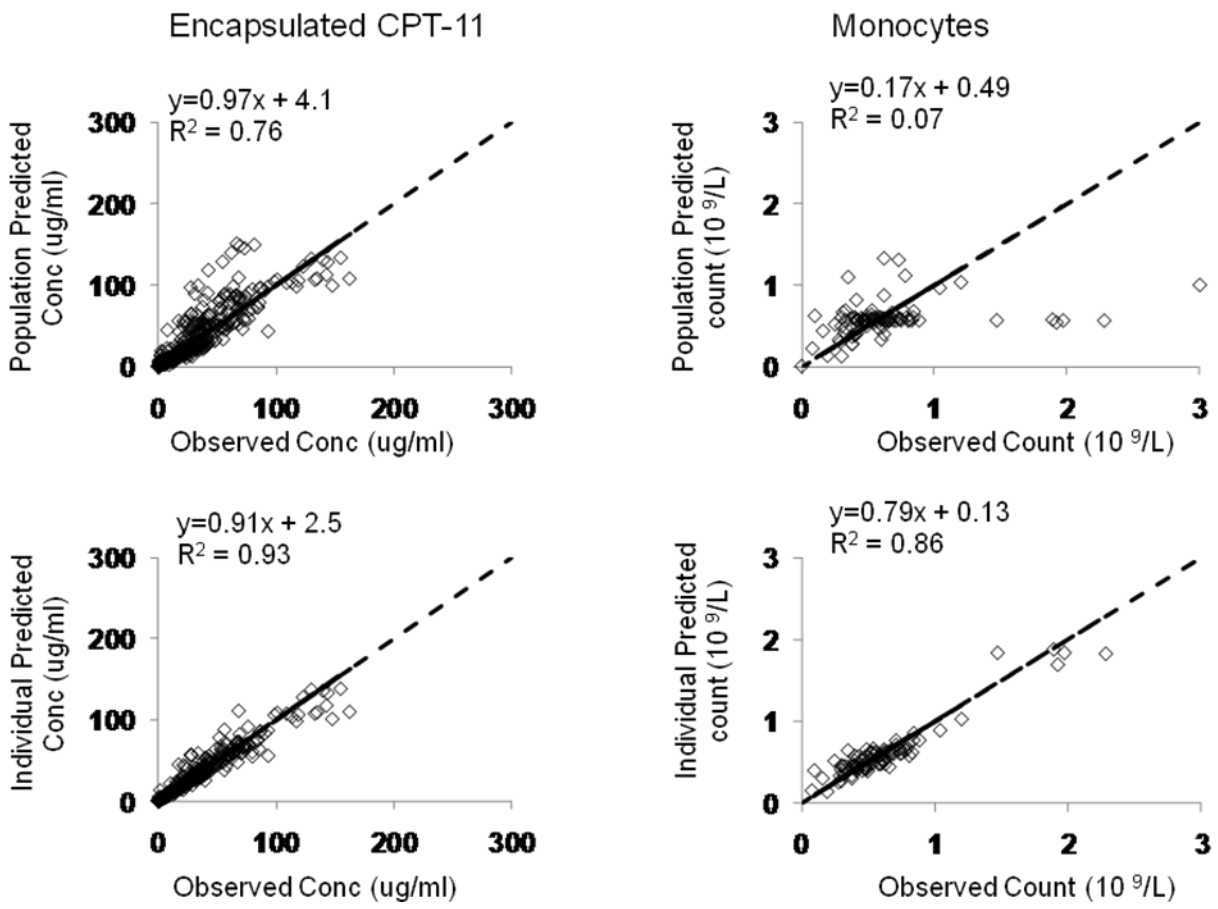

Figure 7.2. Goodness-of-fit plots for the myelosuppression-based model of encapsulated CPT-11 and monocytes. The dashed lines are lines of identity.

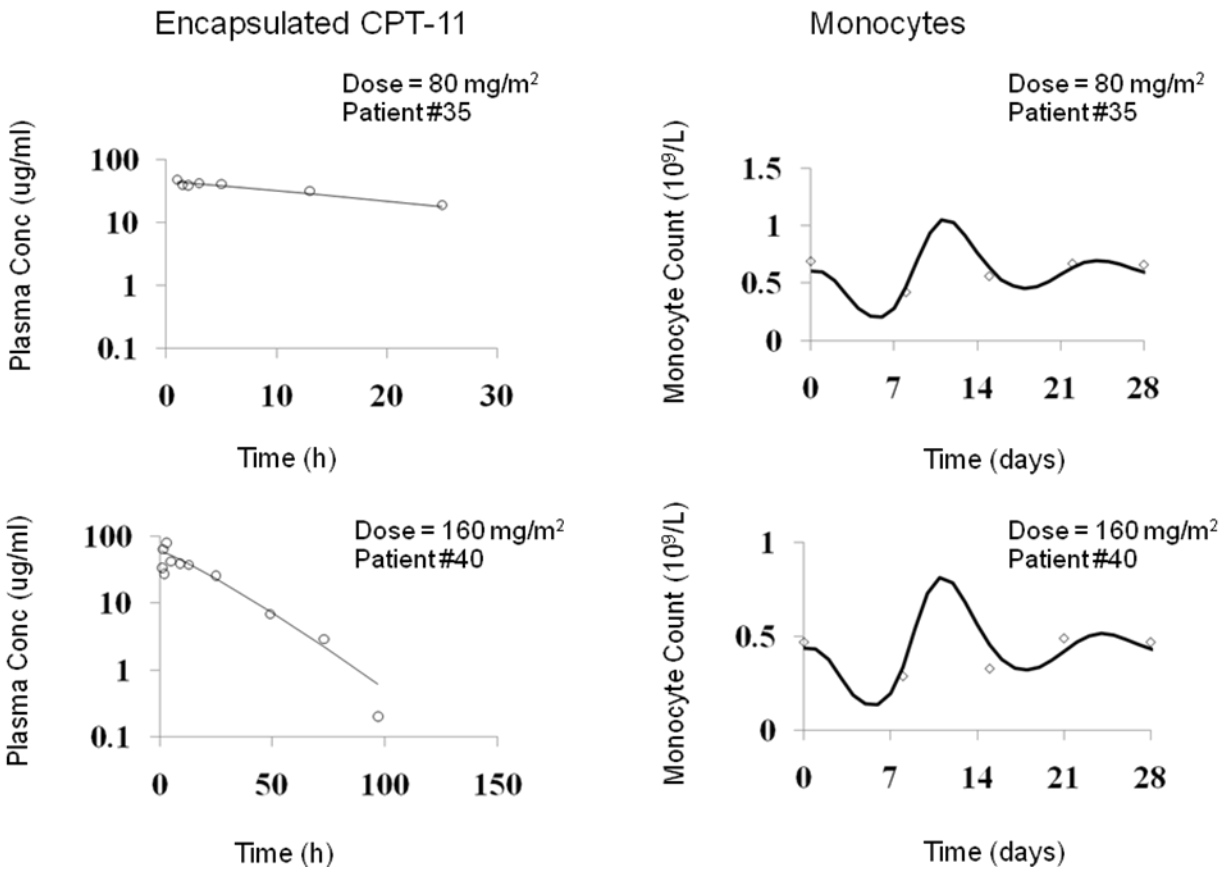

Figures 7.3. Representative individual plots of observed (○) and individual predicted (—) values from myelosuppression-based model for the plasma concentrations of encapsulated CPT-11 and monocyte count in all patients.

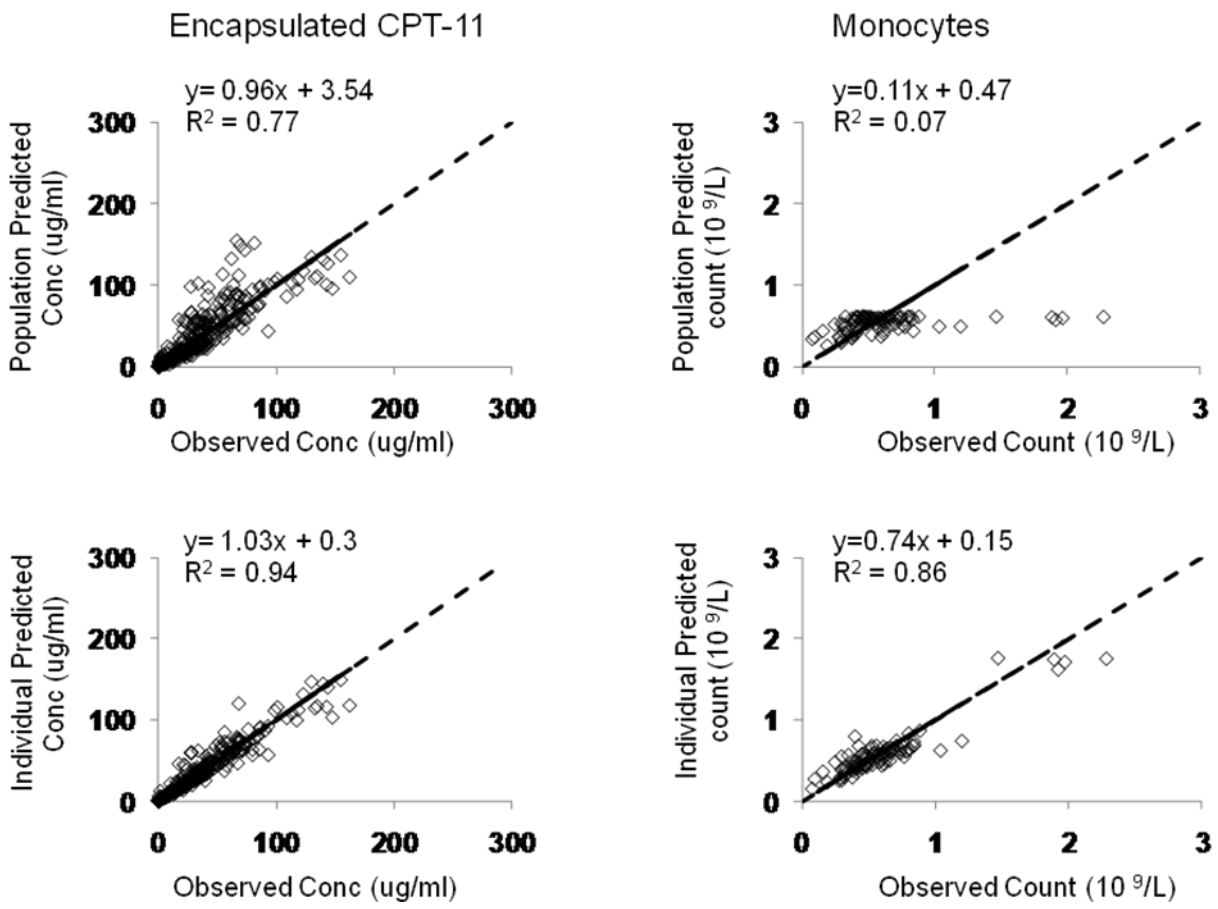

Figure 7.4. Goodness-of-fit plots for the mechanism-based model of encapsulated CPT-11 and monocytes. The dashed lines are lines of identity.

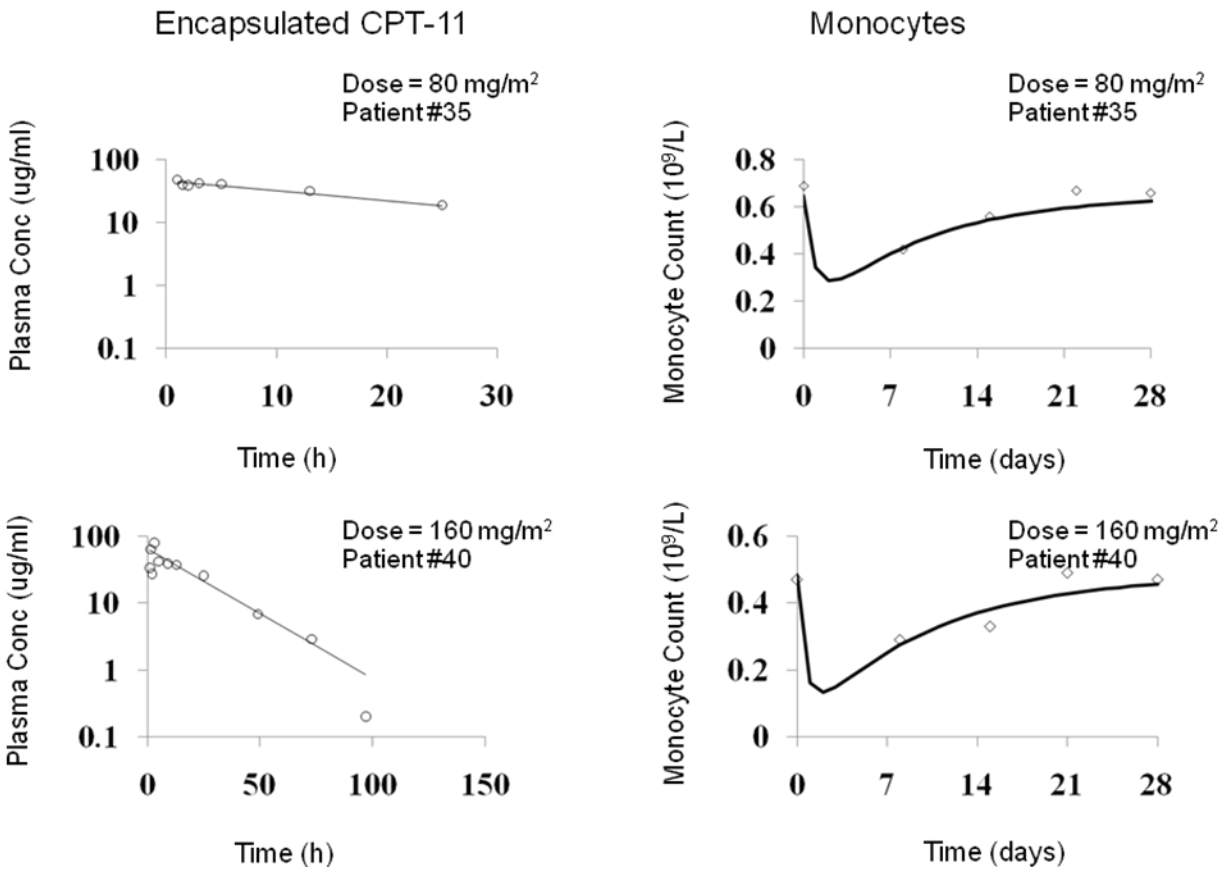

Figures 7.5. Representative individual plots of observed (○) and individual predicted (—) values from mechanism-based model for the plasma concentrations of encapsulated CPT-11 and monocyte counts in all patients.

CHAPTER 8

MECHANISM-BASED PHARMACOKINETIC-PHARMACODYNAMIC MODEL CHARACTERIZING BI-DIRECTIONAL INTERACTION BETWEEN LIPOSOME MEMBRANE LIPIDS AND MONOCYTES IN PATIENTS WITH ADVANCED MALIGNANCIES

A. INTRODUCTION

Liposomes (microparticulate phospholipid vesicles) have been used with growing success as pharmaceutical carriers for anticancer agents. Conventional liposomes are quickly opsonized by plasma proteins, recognized as foreign bodies, and rapidly removed by the mononuclear phagocytic system (MPS) which has also been called the reticuloendothelial system (RES) (1, 2). The development of STEALTH or Polyethylene Glycol (PEG)ylated liposomes was based on the discovery that incorporation of mPEG-lipids into liposomes yields preparations with prolonged plasma exposure and superior tumor delivery compared to conventional liposomes composed of natural phospholipids (3-5).

The PEGylated liposomal anticancer agents have demonstrated a superior antitumor activity and reduced toxicity compared to conventional liposomal and nonliposomal drugs in both preclinical studies and clinical studies. PEGylated liposomal doxorubicin (Doxil®) is approved for the treatment of refractory ovarian cancer, Kaposi sarcoma, and multiple myeloma (6, 7). However, nonlinear and highly variable pharmacokinetic (PK) property of the PEGylated liposomal anticancer agents was observed in clinic studies. Saturation of clearance was reported for both Doxil® and S-CKD602 and cycle dependent PK was reported for Doxil® (8-11). In addition, high interpatient variability in the PK of PEGylated liposomal CKD-602 (S-CKD602) and other liposomal agents has been reported (12). There was a 100-fold range at lower dose and a 10-fold to 20-fold range at higher dose in encapsulated CKD-602 AUC (12).

The complicated PK of PEGylated liposomal anticancer agents was believed to be related to the PK of liposomal carrier. The PK disposition of carrier-mediated agents, such as, nanoparticles, nanosomes, and conjugated agents, is dependent upon the carrier until the

drug is released from the carrier. Unlike traditional anticancer agents which are cleared by the liver and kidneys, the clearance of non-PEGylated and PEGylated liposomes is via the MPS which include monocytes, macrophages and dendritic cells located primarily in the liver and spleen (2). PEGylated liposomes are cleared much slower via MPS compared to non-PEGylated liposomes (4, 13). Uptake of the liposomes or nanoparticles by the MPS usually results in sequestering of the liposome membrane lipids and encapsulated drug in the MPS and the sequestered drug and/or the liposome membrane lipids in the MPS may cause acute cytotoxicity to the MPS. This toxicity to the MPS in turn decreases clearance of the PEGylated liposomal anticancer agents and alters the pharmacodynamics (PD) of the agents. Thus, there is a bi-directional interaction between PEGylated liposomal anticancer agents and MPS. Since a major portion of the liposomal encapsulated drug molecules are confined primarily to the blood compartment due to their relative large size, we have reported that there is a significant and clinically relevant interaction between liposomal agents and MPS cells in the blood circulation (13, 14). This bi-directional interaction between PEGylated liposomal anticancer agents and monocytes is very important in determining the PK and PD of PEGylated liposomal anticancer agents and potentially other nano and conjugated agents.

We have developed a mechanism-based population PK-PD model that included the bi-directional interaction between PEGylated liposomal anticancer agents and monocytes for PEGylated liposomal CKD602 (S-CKD602) and PEGylated liposomal CPT-11 (IHL-305). As the liposome membrane lipids may also contribute to the toxicity of PEGylated liposomal anticancer agents to monocytes, we developed a population PK-PD model for the liposome membrane lipids based on the previously developed mechanism-based PK-PD model. The liposome PK and PD data were obtained by pooling the PK and PD data of S-CKD602 and

IHL-305. In this pooled data set, the lipid concentrations were calculated using the encapsulated drug concentration according to the drug-to-lipid ratio of S-CKD602 and IHL-305. The pooled data allow a more accurate estimation of the PK and PD parameters due to the larger data sets.

The PEGylated liposomes of S-CKD602 and IHL-305 were made using two different methods. The PEGylated liposome of S-CKD602 was made by adding the PEG lipid before the process of liposomal formation which results in PEG tether being projected on both the inside and outside of liposome. The PEGylated liposome of IHL-305 is made by adding the PEG lipids after the process of liposomal formation which results in PEG tether being only localized on the outer leaflet (15).

The objectives of this study were to evaluate the relationship of PEGylated liposome membrane lipids PK and PD and monocytes and to increase our understanding of the bi-directional interaction between PEGylated liposomal anticancer agents and monocytes in blood of cancer patients.

B. METHODS

Study Design

The PK and PD data of this study was pooled from two separate phase I studies of S-CKD602 and IHL-305. The concentrations of liposome membrane lipids were calculated according to the drug-to-lipid ratio of S-CKD602 and IHL-305. The drug-to-lipid ratios of S-CKD602 and IHL-305 were 1:8.9, and 1:4, respectively.

The PK and PD data of S-CKD602 were obtained from a phase I study of S-CKD602 in patients with advanced solid tumors (8, 12). The study design and clinical results have been reported elsewhere (8, 12). Forty-five patients (21 males) received S-CKD602 at 0.1 to 2.5 mg/m^2 IV x 1 over approximately 1 hour every 3 weeks. No pre-medications were administered prior to S-CKD602. Written informed consent, approved by the Institutional Review board of the University of Pittsburgh Medical Center, was obtained from all patients prior to study entry. All other eligibility criteria were previously reported (8). Serial plasma samples were obtained prior to drug administration; at the end of the infusion (lasting ~ 1h); and at 3, 5, 7, 24, 48, 72, 96, 168 (day 8), and 336 h (day 15) after the start of the infusion. Total (lactone + hydroxyl acid) concentrations of encapsulated CKD-602 in plasma were determined by liquid chromatography-tandem mass spectrometry (16). The lower limit of quantitation (LLQ) of the total form encapsulated CKD-602 was 2 ng/mL. Samples of peripheral blood were collected before dosing on days 7, 14, 21, and 28.

The PK and PD data of IHL-305 were obtained from a phase I study of IHL-305 in patients with advanced solid tumors (17). The study design and clinical results have been reported elsewhere (17). Thirty-nine patients (13 males) received IHL-305 at 3.5 to 210 mg/m^2 IV x 1 over approximately 1 hour every 4 weeks. Prior to administration of the study

drug, patients were premedicated with ondansetron (or other 5-HT3 inhibitor should circumstances require) and dexamethasone, according to each institution's standard of care. Written informed consent, approved by the Institutional Review board of the Sarah Cannon Research Institute and Vanderbilt University Medical Center, was obtained from all patients prior to study entry. Serial plasma samples were obtained at the following times: prior to administration, at end of the infusion (approximately 1 h), and at 1.5 h , 2 h , 3 h , 5 h , 9 h , 13 h, and 25 h after the start of the infusion for patients treated at < 67 mg/m^2 and the first three patients treated at 67 mg/m^2. Additional samples at 49 h, 73 h, 97 h, 169 h (day 7), 192 h (day 8), and 216 h (day 9) after the start of the infusion were also collected for patients treated at > 67 mg/m^2 and the last three patients treated at 67 mg/m^2. Total (lactone + hydroxyl acid) concentrations of sum total CPT-11, released CPT-11 in plasma were determined by a specific liquid chromatographic tandem mass spectrometry assay (LC-MS/MS) as previously described (18). Encapsulated CPT-11 was calculated by substracting the released CPT-11 concentration from sum total CPT-11 concentration at each time point. The lower limit of quantitation (LLQ) of the total form sum total CPT-11 and released CPT-11 were 100 and 2 ng/mL, respectively. Complete blood counts were obtained weekly and as medically indicated.

Population PK-PD Analysis

We believe that the bi-directional interaction between PEGylated liposomal anticancer agents and monocytes plays the key role in the elimination of PEGylated liposomal anticancer agents and monocytopenia observed in our prior studies (13). In this study, we used the previously developed mechanism model that incorporated the bi-

directional interaction to describe the pooled PK and PD data of S-CKD602 and IHL-305. The pooled PK and PD data were analyzed using the nonlinear mixed effects modeling approach as implemented in NONMEM (version 6; University of California, San Francisco, CA) for the mechanism-based model. The first order conditional estimation (FOCE) method were used in analyses. S-PLUS 8.0 (Version 8.0, Insightful Corporation, Seattle, Washington) was used for graphical diagnostics.

Mean population PK-PD variables, interindividual variability (IIV), and residual error were assessed in the model development (19, 20). IIV for each PK-PD variable was modeled with an exponential function. Residual error models of the additive, proportional, exponential, and combination methods were evaluated for the best structural PK-PD model. Individual PK-PD variables were obtained by posterior Bayesian estimation (19, 20).

As the PK data were pooled plasma concentrations of liposome membrane lipids from two different PEGylated liposomal drugs, the drug type as potential covariates were tested for their influence on the drug-related parameters (V, k_{on}, k_{deg}, Factor). The system-related parameters ($Mono_0$, k_{out}) were assumed to be independent of drug. General patient characteristics were not evaluated in this study. The covariate model building was a stepwise process. A screen for drug type as covariates on drug-related parameters was done using S-PLUS 8.0 (Version 8.0, Insightful Corporation, Seattle, Washington). The potential significant covariates selected from screen were introduced into the covariate model and assessed in the population PK models. A significant covariate was selected to be retained in the final model if addition of the covariate resulted in a decrease in OFV >3.875 ($P < 0.05$) during the forward full covariate model building, and removal of the covariate resulted in an increase in OFV >10.828 ($P < 0.001$) during the stepwise backward model reduction (21). In

addition, the increase in precision of the variable estimate (% relative SE of prediction) and reduction in inter-individual (IIV) were used as another indicator of the improvement of the goodness of fit.

Mechanism-based PK-PD Model

A mechanism based PK-PD model that incorporates the interaction between PEGylated liposomal anticancer agents and monocytes has been previously developed for S-CKD602 and IHL-305 (**Figure 8.1**). Concentration versus time data of liposome membrane lipids in plasma and monocyte count in blood were fit simultaneously by this model. Drug is dosed IV into the systemic circulation (blood compartment) at a zero-order rate (k_0). The distribution of PEGylated liposome membrane lipids is described by a one-compartment model and the PEGylated liposome membrane lipids is eliminated by interacting with monocyte to form liposome-monocyte complex (k_{on}) which represents the phagocytosis of PEGylated liposome by the monocyte. The liposome-monocyte complex may then be degraded. This represents the degradation or catabolism of the liposome within the monocyte. PEGylated liposome membrane lipids is also degraded at a first-order rate (k_{deg}). The parameters describing the production and loss of monocytes are k_{in} and k_{out}. The production rate of monocytes k_{in} is calculated as k_{out} multiplied by baseline monocyte value. The differential equations were written as

$$\frac{dA_{lipids}}{dt} = k_0 - k_{on} \bullet A_{lipids} \bullet Mono - k_{deg} \bullet A_{lipids} \quad , \; A_{lipids}(0) = 0$$

$$\frac{dMono}{dt} = Mono_0 \bullet k_{out} - k_{out} \bullet Mono - k_{on} \bullet A_{lipids} \bullet Mono / Factor \quad , \; Mono(0) = Mono_0$$

$$C_{lipids} = \frac{A_{lipids}}{V_{lipids}}$$

dA_{lipids}/dt is the elimination rate, A_{lipids} is liposome membrane lipids amount in plasma, C_{lipids} is the plasma concentration of liposome membrane lipids, V_{lipids} is the volume of distribution of liposome membrane lipids, Mono is the monocyte count, k_0 is the infusion rate and $k_0 = 0$ after stop of infusion. Since the unit of liposome membrane lipids is mg/L and the unit of monocyte count is 10^9/L, the factor is a parameter used to bridge the unit gap.

C. RESULTS

Patient demographics

The summary of patients demographic data have been listed in Chapter 4 and Chapter 5.

Mechanism-based PK-PD Model

The liposome membrane lipids and monocytes were modeled simultaneously for all patients. The distribution of residual variability was best described by a proportional plus additive error model. The PK-PD parameter estimates obtained from the final model are provided in **Table 8.1**. During the covariate screen, drug type was identified as a significant covariate for the association rate constant (k_{on}) and the adjusting factor. The k_{on} for liposome membrane lipids of S-CKD602 and for IHL-305 were estimated to be 0.175 (IIV 283%) $L \cdot h^{-1}$ and 0.0001 (IIV 283%) $L \cdot h^{-1}$, respectively. The inclusion of drug type as a covariate in the final model decreased the IIV of the k_{on} by 50%. The adjusting factors for liposome membrane lipids of S-CKD602 and for IHL-305 were estimated to be 8.14 (IIV 56%) $\mu g/10^9$ and 0.393 (IIV 56%) $\mu g/10^9$, respectively. The inclusion of drug type as a covariate in the final model decreased the IIV of the adjusting factor by 66%. The volume of distribution (V_{lipids}) was estimated to be 3.35 L (IIV 34.1%). The estimated V_{lipids} is close to the plasma volume in humans. The degradation rate constant (k_{deg}) was estimated to be 0.0326 (IIV 48.1%) h^{-1}. The baseline monocyte value was estimated to be 0.60 (IIV 35.6%) $x10^9/L$. The degradation rate constant (k_{out}) of monocytes was estimated to be 0.00774 (IIV 46.9%) h^{-1}.

Goodness-of-fit plots from the mechanism-based PK-PD model in all patients are given in **Figure 8.2**. The model adequately describes the PK profile of liposome membrane

lipids. Both the population predicted (R^2 = 0.82) and individual predicted (R^2 = 0.95) PK profile correlated well with the observed PK profile. Although the PD data of monocytes were variable, the observed and model predicted data agreed relatively well. The observed PD data better correlated with the individual predicted PD data (R^2 = 0.79) than population predicted PD data (R^2 = 0.22). The representative individual PK time profiles of liposome membrane lipids and monocytes in patients after administration of S-CKD602 and IHL-305, respectively, are shown in **Figure 8.3A and 8.3B**. The observed data of liposome membrane lipids concentration and monocytes were well described by the mechanism-based model.

D. DISCUSSION

The bi-directional interaction between PEGylated liposomal anticancer agents and monocytes plays the key role in the elimination of PEGylated liposomal anticancer agents and monocytopenia observed in our prior studies (13). The bi-directional interaction between PEGylated liposomal anticancer agents and monocytes have been evaluated via a mechanism-based PK-PD model assuming the encapsulated drug is toxic to the monocyte. In this study, the bi-directional interaction between PEGylated liposome membrane lipids and monocytes was evaluated to test if PEGylated liposome membrane lipids alone can explain the toxicity of these agents to monocyte.

The inter-individual variability in the PK and PD of liposome membrane lipids can be explained in part by the encapsulated drug. The elimination of PEGylated liposome membrane lipids via uptake by monocyte is reflected by the association rate constant (k_{on}). The k_{on} of S-CKD602 is 1750-fold higher compared with IHL-305. In addition, k_{on} of S-CKD602 is 5.4-fold higher than $k_{deg,}$ whereas, k_{on} of IHL-305 is 326-fold lower than k_{deg}. This data suggest that the bi-directional interaction between PEGylated liposomes and monocytes may be more important to the elimination of S-CKD602 compared with IHL-305. The cytotoxicity effect of PEGylated liposomal anticancer agents on monocytes is reflected by the ratio of k_{on} to the adjusting factor. The ratio of k_{on} to the adjusting factor of S-CKD602 (0.021) is 84-fold higher compared with IHL-305 (0.00025). This data is consistent with previous observations of higher ratio of % decrease of monocytes to neutrophils in S-CKD602 compared to IHL-305. These results may be due to CPT-11 being less potent than CKD-602 or due to the different liposomal formulations used in each product.

The model predicted PD profiles of S-CKD602 and IHL-305 were different. The nadir of monocytes after S-CKD602 last longer compared to IHL-305. The doses and concentration levels of liposome membrane lipids in IHL-305 were much higher compared to that of S-CKD602. These results suggest that liposome membrane lipids or liposomal carrier of S-CKD602 are more toxic than that of IHL-305. However, this difference may also be related to the encapsulated drugs in these two PEGylated liposomal drugs as CKD-602 is more potent than CPT-11. Therefore, liposome membrane lipids in PEGylated liposomal anticancer agents alone may not account for all the toxicity of these agents to monocytes.

In the mechanism-based model, the mean value of volume of distribution for liposome membrane lipids was 3.35 L, which is close to plasma volume in humans. The volume of distribution for liposome membrane lipids reflected the distribution of PEGylated liposomes in human and the estimated volume of distribution is consistent with our prior population PK study of S-CKD602 and IHL-305 (22). In addition, the limited volume of distribution of liposome membrane lipids is consistent with other liposomal anticancer agents since the size of liposomes limits their distribution to the normal tissue (14, 23). The estimated half life of monocytes (89 hours) is within the range of the reported half life of monocytes in healthy human (mean 72 hours, range 36 – 104 hours) (24, 25).

In conclusion, a mechanism-based PK-PD model was developed for a pooled liposome membrane lipids and monocyte data of S-CKD602 and IHL-305 in patients with advanced solid tumors. S-CKD602 and IHL-305 were found to have different interactions with monocyte. The mechanism-based PK-PD model that was developed can be used to assess factors influencing the PK and PD of PEGylated liposomal drugs.

E. REFERENCES

1. Drummond DC, Meyer O, Hong K, Kirpotin DB, Papahadjopoulos D. Optimizing liposomes for delivery of chemotherapeutic agents to solid tumors. Pharmacol Rev 1999; 51:691-743.

2. Allen TM, Hansen C. Pharmacokinetics of stealth versus conventional liposomes: effect of dose. Biochim Biophys Acta 1991; 1068:133-41.

3. Zamboni WC. Liposomal, nanoparticle, and conjugated formulations of anticancer agents. Clin Cancer Res 2005; 11:8230-4.

4. Papahadjopoulos D, Allen TM, Gabizon A, et al. Sterically stabilized liposomes: improvements in pharmacokinetics and antitumor therapeutic efficacy. Proc Natl Acad Sci U S A 1991; 88:11460-4.

5. Maeda H, Wu J, Sawa T, Matsumura Y, Hori K. Tumor vascular permeability and the EPR effect in macromolecular therapeutics: a review. J Control Release 2000; 65:271-84.

6. Markman M, Gordon AN, McGuire WP, Muggia FM. Liposomal anthracycline treatment for ovarian cancer. Semin Oncol 2004; 31:91-105.

7. Krown SE, Northfelt DW, Osoba D, Stewart JS. Use of liposomal anthracyclines in Kaposi's sarcoma. Semin Oncol 2004; 31:36-52.

8. Zamboni WC, Strychor S, Maruca L, et al. Pharmacokinetic study of pegylated liposomal CKD-602 (S-CKD602) in patients with advanced malignancies. Clin Pharmacol Ther 2009; 86:519-26.

9. Gabizon A, Isacson R, Rosengarten O, Tzemach D, Shmeeda H, Sapir R. An open-label study to evaluate dose and cycle dependence of the pharmacokinetics of pegylated liposomal doxorubicin. Cancer Chemother Pharmacol 2008; 61:695-702.

10. Gabizon A, Shmeeda H, Barenholz Y. Pharmacokinetics of pegylated liposomal Doxorubicin: review of animal and human studies. Clin Pharmacokinet 2003; 42:419-36.

11. Gabizon A, Tzemach D, Mak L, Bronstein M, Horowitz AT. Dose dependency of pharmacokinetics and therapeutic efficacy of pegylated liposomal doxorubicin (DOXIL) in murine models. J Drug Target 2002; 10:539-48.

12. Zamboni WC, Ramalingam S, Friedland DM, et al. Phase I and pharmacokinetic study of pegylated liposomal CKD-602 in patients with advanced malignancies. Clin Cancer Res 2009; 15:1466-72.

13. Zamboni WC, Maruca LJ, Strychor S, et al. Bidirectional pharmacodynamic interaction between pegylated liposomal CKD-602 (S-CKD602) and monocytes in patients with refractory solid tumors. J Liposome Res.

14. Allen TM, Cullis PR. Drug delivery systems: entering the mainstream. Science 2004; 303:1818-22.

15. Zamboni WC, Strychor S, Joseph E, et al. Plasma, tumor, and tissue disposition of STEALTH liposomal CKD-602 (S-CKD602) and nonliposomal CKD-602 in mice bearing A375 human melanoma xenografts. Clin Cancer Res 2007; 13:7217-23.

16. Jones SF, Zamboni WC, Burris III HA, et al. Phase I and pharmacokinetic (PK) study of IHL-305 (pegylated liposomal irinotecan) in patients with advanced solid tumors. ASCO; 2009 Jun, 2009; Orlando, FL; 2009.

17. Kurita A, Kaneda N. High-performance liquid chromatographic method for the simultaneous determination of the camptothecin derivative irinotecan hydrochloride, CPT-11, and its metabolites SN-38 and SN-38 glucuronide in rat plasma with a fully automated on-line solid-phase extraction system, PROSPEKT. J Chromatogr B Biomed Sci Appl 1999; 724:335-44.

18. Sheiner LB, Beal SL. Evaluation of methods for estimating population pharmacokinetics parameters. I. Michaelis-Menten model: routine clinical pharmacokinetic data. J Pharmacokinet Biopharm 1980; 8:553-71.

19. Sheiner LB, Rosenberg B, Marathe VV. Estimation of population characteristics of pharmacokinetic parameters from routine clinical data. J Pharmacokinet Biopharm 1977; 5:445-79.

20. Mandema JW, Verotta D, Sheiner LB. Building population pharmacokinetic--pharmacodynamic models. I. Models for covariate effects. J Pharmacokinet Biopharm 1992; 20:511-28.

21. Roy V, LaPlant BR, Gross GG, Bane CL, Palmieri FM. Phase II trial of weekly nab (nanoparticle albumin-bound)-paclitaxel (nab-paclitaxel) (Abraxane) in combination with gemcitabine in patients with metastatic breast cancer (N0531). Ann Oncol 2009; 20:449-53.

22. Wu H, Ramanathan RK, Strychor S, et al. Population Pharmacokinetics of PEGylated Liposomal CKD-602 (S-CKD602) in Patients with Advanced Malignancies. ASCO; 2009; 2009.

23. Hilger RA, Richly H, Grubert M, et al. Pharmacokinetics (PK) of a liposomal encapsulated fraction containing doxorubicin and of doxorubicin released from the liposomal capsule after intravenous infusion of Caelyx/Doxil. Int J Clin Pharmacol Ther 2005; 43:588-9.

24. Jain NC. Essentials of Veterinary Hematology. 1 ed: Williams & Wilkins, Media, PA 19063; 1993.

25. Whitelaw DM. Observations on human monocyte kinetics after pulse labeling. Cell Tissue Kinet 1972; 5:311-7.

Table 8.1.

Population PK-PD Parameters Obtained From the Mechanism-Based Model for Liposome Membrane Lipids and Monocytes.

Parameter	Definition	Population Mean RSE[a] (%)	IIV, CV%[b] RSE[a] (%)
V_{lipids} (L)	Volume of distribution for liposome membrane lipids	3.35 (11)	34.1 (25)
k_{on} (L/h)	Association rate constant		
S-CKD602		0.175 (47)	283 (NA)
IHL-305		0.0001 (53)	
k_{deg} (1/h)	Degradation rate constant of PEGylated liposome	0.0326 (35)	48.1 (45)
$Mono_0$ (10^9/L)	Baseline monocyte count	0.60 (7.1)	35.6 (40)
k_{out} (1/h)	Degradation rate constant of monocyte	0.00774 (15)	46.9 (110)
Factor ($\mu g/10^9$)	Adjusting factor		
S-CKD602		8.14 (55)	56 (94)
IHL-305		0.393 (67)	
Residual variability			
Proportional error (variability as %)			
Liposome membrane lipids		24.0 % (54)	NA[c]
Monocytes		2.0 % (85)	NA[c]
Additive error			
Liposome membrane lipids (mg/L)		0.0538 (43)	NA[c]
Monocytes (10^9/L)		0.0157 (52)	NA[c]

[a] Relative standard error for estimate.

[b] Coefficient of variation.

c Not estimated.

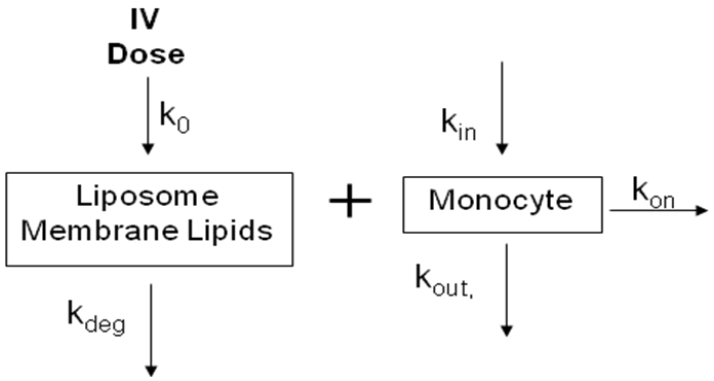

Figure 8.1. The mechanism-based PK-PD model for liposome membrane lipids and monocytes.

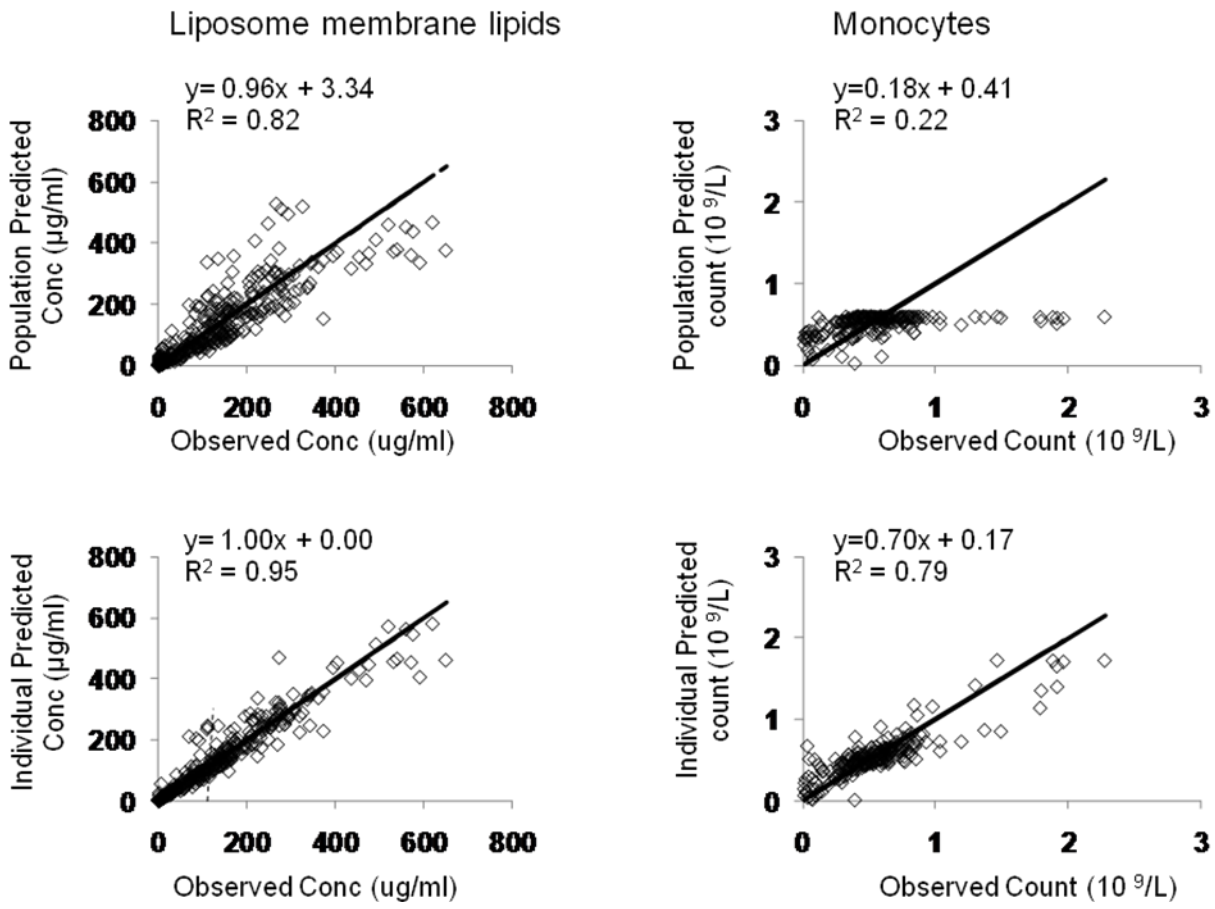

Figure 8.2. Goodness-of-fit plots for the mechanism-based model of liposome membrane lipids and monocytes. The solid lines are lines of identity.

Figure 8.3A

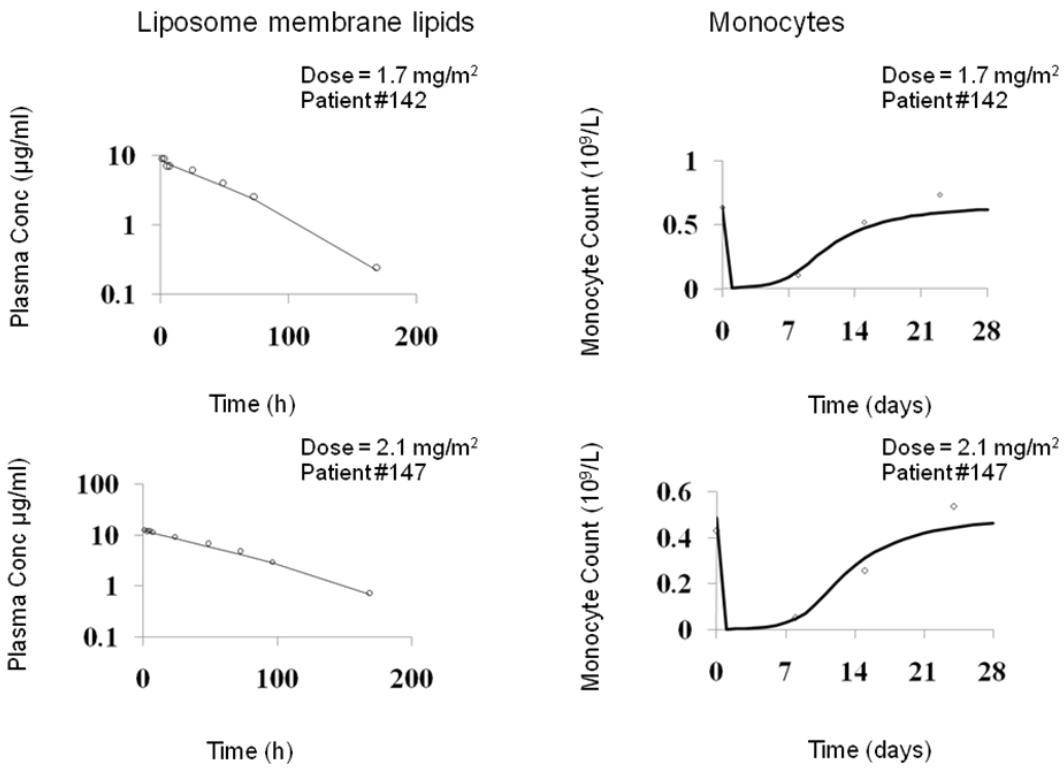
Liposome membrane lipids
Monocytes
Dose = 1.7 mg/m2
Patient #142
Plasma Conc (µg/ml)
10
1
0.1
0
100
200
Time (h)
Monocyte Count (10⁹/L)
1
0.5
0
0
7
14
21
28
Time (days)
Dose = 2.1 mg/m2
Patient #147
Plasma Conc µg/ml)
100
10
1
0.1
0
100
200
Time (h)
Monocyte Count (10⁹/L)
0.6
0.4
0.2
0
0
7
14
21
28
Time (days)

Figure 8.3B

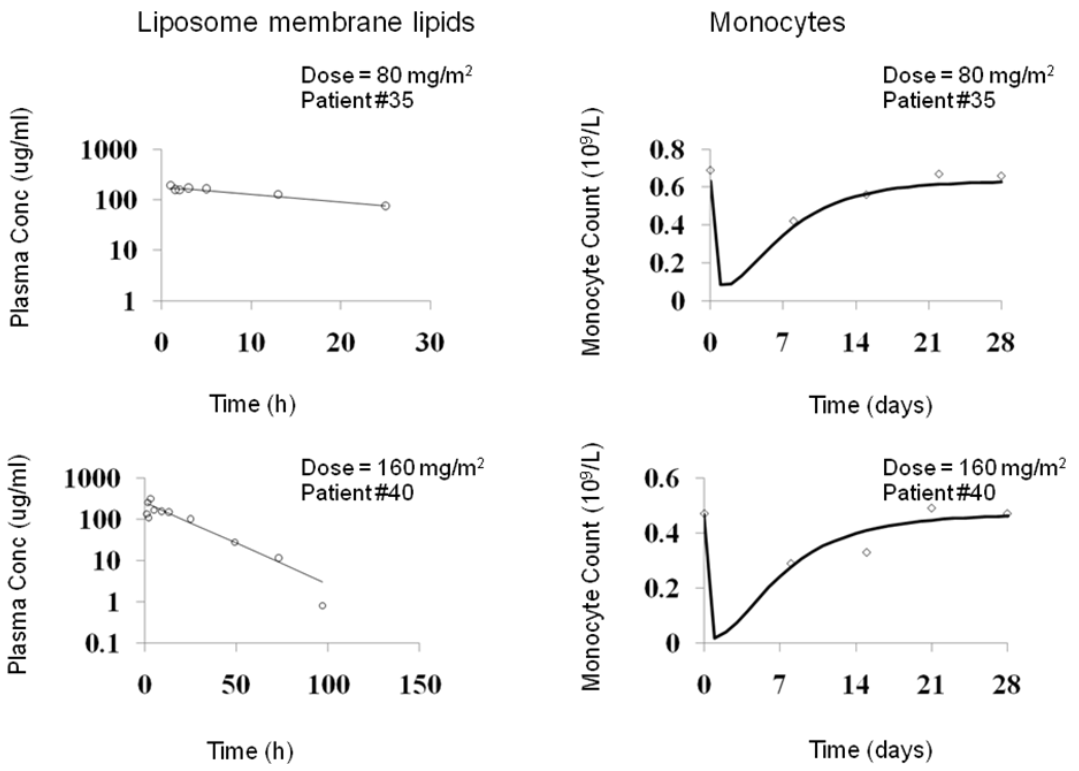

Figure 8.3. Representative individual plots of observed (○) and individual predicted (—) values from mechanism-based model for the plasma concentrations of liposome membrane lipids and monocyte counts in all patients after administration of S-CKD602 (A) and IHL-305 (B).

CHAPTER 9

CONCLUSION

General PK Properties of Pegylated Liposomal Anticancer Agents

Targeted therapies are a major focus of cancer research today (1). With recent advances of technology, liposomal-based drug delivery system is designed to address drug PK and PD properties such as circulation half-lives, permeability, biodistribution and targeting specificity. PEGylated liposomal doxorubicin (Doxil®) is a successful application of this system. PEGylated liposomal anticancer agents have their unique PK and PD properties related to the liposomal carrier. Evaluation of the PK disposition of the liposomal encapsulated verses released drug is of the utmost importance because the liposomal encapsulated drug is an inactive prodrug and thus only the released drug is active (2, 3).

Pegylated liposomal anticancer agents have a distinct PK profile characterized by a prolonged circulation time and a reduced volume of distribution. IHL-305 is a PEGylated liposomal formulation of irinotecan (CPT-11). The prolonged plasma exposure of released CPT-11 over 1 week after administration of IHL-305 is consistent with PEGylated liposomes and provides extended exposure compared with non-liposomal CPT-11 (2-5). The PK profile of released CPT-11 and its active metabolite SN-38 paralleled with the PK profile of sumtotal CPT-11. This observation is consistent with our previous observation of paralled PK profiles of released and encapsulated CKD-602 in plasma in a phase I PK study of S-CKD602 (6). These observations suggest that the release of agents from PEGylated liposomal anticancer agents can be the rate determining step for removal of released agent and the metabolites from the system.

The PK disposition of IHL-305 is consistent with the PEGylated concept (2, 7-10). The volume of distribution of encapsulated CPT-11 estimated from the population PK analysis for female and male patients were 2.4 L and 3.6 L, respectively. The volume of

distribution of encapsulated CKD-602 estimated from the population PK analysis was 3.63 L. Compared to non-liposomal CPT-11 (377 to 871 L) and CKD-602 (range of V_{ss}, 31 to 87 L), the distribution of encapsulated CPT-11 and CKD-602 were significantly reduced (11-14). The limited volume of distribution of encapsulated CPT-11 and CKD-602 is consistent with other liposomal anticancer agents and is based on their limited distribution to the normal tissue (15).

Besides prolonged exposure and reduced volume of distribution, we found that the variability of IHL-305 PK was associated with non-linear clearance of IHL-305. Saturation of clearance has been reported for both Doxil® and S-CKD602 and the nonlinear PKs of these two drugs have been modeled using Michaelis-Menten kinetics (6, 16-18). The nonlinear clearance of sum total CPT-11 after administration of IHL-305 and other nanoparticle agents may be related to the saturation in the clearance capacity of the RES/MPS.

As only the released drug is active, the PK disposition of the liposomal encapsulated verses released drug was evaluated for IHL-305 through noncompartmental and compartmental PK analysis (2, 3). The release drug concentrations and AUC are much lower compared with the sum total or encapsulated drug for both S-CKD602 and IHL-305. The ratio of released CPT-11 AUC to sum total CPT-11 AUC ranged from 0.001 to 0.01. This data suggests that most of the CPT-11 remains encapsulated in the plasma after administration of IHL-305. These results are also consistent with previous studies of IHL-305 in mice (19, 20). The mean ratio of SN-38 AUC to released CPT-11 AUC and APC AUC to released CPT-11 AUC after administration of IHL-305 ranged from 0.02 to 0.06 and from 0.09 to 0.55, respectively. This values are similar to that after administration of non-

liposomal CPT-11 (21, 22). After a single dose of IHL-305 at the MTD of 160 mg/m^2, the plasma exposure of CPT-11 and SN-38 were similar to that of non-liposomal CPT-11 at the MTD of 150 mg/m^2(21, 22). This data suggest that the PK of the released CPT-11 after administration of IHL-305 is consistent with that after administration of non-liposomal CPT-11. In chapter 5, the volume of distribution and clearance of released CPT-11 estimated from population PK analysis were also comparable to that of non-liposomal CPT-11. All these data suggest that once the drug is released from the carrier, the PK disposition of the drug will be the same as after administration of the non-carrier form of the drug.

The inter-patient variability in the PK disposition of sum total and released CPT-11 after administration of IHL-305 is lower than that of sum total and released CKD-602 after administration of S-CKD602. At the MTD of IHL-305 (160 mg/m^2), there was a 2.7-fold range in sum total CPT-11 AUC and 4-fold range in released CPT-11 AUC. At the MTD of of S-CKD602 (2.1 mg/m^2), there was a 13-fold range in encapsulated CKD-602 AUC and 17-fold range in released CKD-602 AUC (23). The encapsulated CKD-602 AUC was similar to the sum total AUC at all doses (23). Additionally, there is greater PK variability in released CPT-11 compared with sum total CPT-11, whereas, there is smaller PK variability in released CKD-602 compared with sum total CKD-602. The difference in the PK between IHL-305 and S-CKD602 may be related to the difference in liposomal formulations and pegylation between these two agents. There was also a poor relationship between the dose of IHL-305 and the AUC of released CPT-11. A poor relationship between the dose of S-CKD602 and the AUC of released CKD-602 has also been reported (23). Overall, the high inter-patient variability in the PK disposition of IHL-305 and S-CKD602 is consistent with other liposomal anticancer agents (5, 26-28).

Patient Factors Affecting the PK and PD of PEGylated Liposomal Anticancer Agents

Patient factors associated with the high inter-patient PK variability of S-CKD602 were evaluated in this study using population-based PK modeling approach. Age, body composition, saturable clearance, and prior PLD therapy were previously identified as important factors on the PK disposition of S-CKD602 using individual-based PK modeling approach (6). In the population PK analysis of S-CKD602, we found that the clearance of encapsulated CKD-602 was influenced by presence of tumor in liver. V_{max} in patients with tumor(s) in the liver is 1.5-fold higher compared with patients without tumor(s) in the liver. Most studies show a decrease in clearance of small molecule drugs in patients with tumors in the liver (24-26). This is the first study reporting an increased clearance of drug in patients with tumor involvement in the liver. The exact mechanism of this phenomenon is unknown. However, recruitment of various populations of phagocytic cells (monocytes, macrophages and dendritic cells) of the MPS is involved in the immune response against tumor cell deposits in liver (27, 28). Since liposomes are mainly cleared by MPS and liver is an important functional site of MPS, the increased clearance of encapsulated CKD-602 may due to enhanced MPS activity in patients with tumor in the liver.

Age was also identified as a significant covariate on the release rate of CKD-602 from S-CKD602. In patients with linear clearance of encapsulated CKD-602, patients ≥ 60 years of age have a reduced release rate of CKD-602 from S-CKD602 compared with patients < 60 years. This is consistent with our prior studies which showed that a reduced clearance of the liposomal encapsulated form of S-CKD-602 in patients ≥ 60 years of age and that the release of drug from liposome is related to clearance of liposome.(29, 30) Aging

related decrease in the function of monocytes may account for the reduced clearance of liposomal agents (9, 31).

Patient factors associated with inter-patient PK variability of IHL-305 were evaluated in this study using individual-based and population-based PK modeling approach. In the individual-based PK modeling approach, the relationship between patient demographic data and the PK parameters estimated for each individual patient were analyzed. In the population-based PK modeling approach, patient factors were evaluated by covariate analysis. For IHL-305, we found that clearance of total and encapsulated CPT-11 was lower in female patients compared to male patients using both model-independent (1.7-fold lower) and model-dependent (1.5-fold lower) approach. This gender effect on PK of encapsulated drugs is consistent with previous observations of gender associated variability in clearance of TLI (Optisomal Topotecan), S-CKD602, and Doxil (32, 33) in rats and patients. For TLI and S-CKD602, CL was 1.2-fold ($p = 0.14$) and 1.4-fold ($p = 0.009$) lower in female rats compared with male rats, respectively (33). Female patients had lower CL of Doxil ($p < 0.001$), IHL-305 ($p = 0.068$), and S-CKD602 ($p = 0.67$) as compared with male patients overall and also when stratified by age (32). The effect of gender on PK of Doxil was also reported in a population PK analysis of of Doxil (34). Gender-related differences in monocyte function may account for the differences in clearance of liposomal agents. In the population PK analysis of IHL-305, V_{encap} in male patients was found to be 1.5-fold higher compared with female patients. The gender effect on V_{encap} has not been reported. The greater V_{encap} in male patients may be explained by the greater blood volume in males compared to females (35). The gender effect on V_{encap} may also due to the correlation between V_{encap} and $V_{max, encap}$ in the PK model. These results indicate that gender is an

influential factor on the PK disposition of liposomal agents. The influence of gender needs to be investigated further.

Body composition was also associated with PK of IHL-305. Patients < 60 years of age with a lean body composition have an increased plasma exposure of IHL-305. The relationship between body composition and plasma exposure of IHL-305 in patients is consistent with our prior studies of S-CKD602 which showed that patients with a lean body composition have a higher plasma exposure of S-CKD602 (9).

Patient factors associated with inter-patient PD variability of IHL-305 were evaluated in this study using individual-based PK modeling approach. The % decrease in monocytes at nadir and the % decrease in neutrophils at nadir was used as PD measures of IHL-305. There was an inverse relationship between patients age and % decrease in monocytes after IHL-305 with younger patients having a higher % decrease in monocytes. This is consistant with our study of S-CKD602, indicating that an age related decrease in the function of monocytes may account for the reduced uptake and clearance of PEGylated liposomes and cytotoxicity to the monocytes (36). Additionally, monocytes are more sensitive to IHL-305 as compared with neutrophils in our study. This is consistant with our previous study that the increased sensitivity is related to the liposomal formulation and not the encapsulated drug (36). The overall difference in monocyte and neutrophil sensitivity to IHL-305 is less than reported for S-CKD602. This may be associated with CPT-11 being less potent than CKD-602 or due to the different liposomal formulations used in each product.

Besides the factors affecting PK and PD of IHL-305, we also found the % decrease in monocytes as a PD measure was significantly correlated with clearance of sum total CPT-11 where patients with a higher % decrease in monocytes at nadir have an increased clearance of

sum total CPT-11. The relationship between changes in monocytes and the PK disposition of IHL-305 suggests that the monocytes engulf liposomal anticancer agents via their phagocytic function as part of the MPS which causes the release of drug from the liposome and cytotoxicity to the monocytes (37). Therefore, evaluation of the relationship of liposomal drug PK and PD and monocytes is of the utmost importance because the nonlinear PK of liposomal drug may be explained by the saturation of MPS and the bi-directional interaction between liposomal drugs and monocytes.

Mechanism-based PK-PD Model

We developed a fully integrated mechanism-based population PK/PD model that described the relationship between PEGylated liposomal anticancer drug and monocytes in patients with advanced solid tumor treated with S-CKD602 or IHL-305. In this model, an irreversible binding of liposomal drug to monocyte was used to account for the bi-directional interaction between PEGylated liposomal anticancer drug and monocyte. This model adequately described the observed clinical data of S-CKD602 and IHL-305, as illustrated in Figs. 6.4, 6.5, 7.4, 7.5, Tables 6.3, and 7.3. To our knowledge, this is the first mechanism-based model that includes the bi-directional interaction between PEGylated liposomal anticancer drug and monocytes for PEGylated liposomal anticancer drug in cancer patients. This model was also applied to describe the relationship between liposome membrane lipids and monocytes in combined patient data from S-CKD602 and IHL-305.

Monocytopenia after chemotherapy is conventionally believed to be due to myelosuppression in bone marrow. However, it is unclear if the monocytopenia after PEGylated liposomal anticancer agents is due to direct cytotoxicity to monocytes in the

blood or cytotoxicity to progenitor cells in bone marrow. We believe the bi-directional interaction between PEGylated liposomal anticancer drugs and monocytes are important to characterize the monocytopenia and PK of these agents. Therefore, besides the mechanism-based PK-PD model, we also used a myelosuppression-based PK-PD model which has been frequently used to describe neutropenia or leukocytopenia after chemotherapy to describe the monocytopenia after S-CKD602 and IHL-305. Comparison of the mechanism-based model and the myelosuppression-based model were used to test our hypothesis.

The common PK-PD parameters between the mechanism-based model and myelosuppression-based model were volume of distribution of encapsulated drug, monocyte baseline value, and removal rate constant for monocyte. The mean values of volume of distribution for encapsulated CKD-602 (4.1 L) and CPT-11 (2.86 L) estimated from the mechanism-based model and encapsulated CKD-602 (3.46 L) and CPT-11 (2.93 L) estimated from the myelosuppression-based model are consistent with results from conventional PK compartmental models. These values are also close to plasma volume in humans. The half life of monocytes estimated from the mechanism-based model using S-CKD602 (102 hours) and IHL-305 (142 hours) PK-PD data is longer than the half life of monocytes estimated from the myelosuppression-based model using S-CKD602 (9 hours) and IHL-305 (11 hours) PK-PD data. Furthermore, the half-life of monocyte estimated from the mechanism-based model was more close to the reported half life of monocytes in healthy human (mean 72 hours, range 36 – 104 hours) compared to the myelosuppression-based model (38, 39). This may be explained by the different structures used in the two models. The myelosuppression-based model incorporated three transit compartments and the rate constant between each compartment was same and equal to the removal rate constant of monocytes from blood

circulation. Thus, the offset of the toxic effect on monocyte was counted by three transit compartments in the myelosuppression-based model, whereas, it was counted by one step in the mechanism-based model. The monocyte baseline values estimated from the mechanism-based model of S-CKD602 ($Mono_0$ = 0.671 x 10^9/L) and IHL-305 ($Mono_0$ = 0.619 x 10^9/L) and the myelosuppression-based model of S-CKD602 ($Mono_0$ = 0.605 x 10^9/L) and IHL-305 ($Mono_0$ = 0.564 x 10^9/L) were approximately same as the observed median of monocyte baseline value of S-CKD602 ($Mono_0$ = 0.645 x 10^9/L) and IHL-305 ($Mono_0$ = 0.620 x 10^9/L).

In the mechanism-based model, encapsulated drug was eliminated via uptake by monocytes (as represented by $k_{on} \bullet A_{Encap} \bullet Mono$) and linear degradation (as represented by $k_{deg} \bullet A_{Encap}$). For S-CKD602, the association rate constant for uptake by monocytes (k_{on} = 1.9 $L \cdot h^{-1}$) is much greater than the estimated degradation rate constant of S-CKD602 (k_{deg} = 0.0178 h^{-1}). For IHL-305, the association rate constant (k_{on} = 0.00001 $L \cdot h^{-1}$) is much lower than the estimated degradation rate constant of IHL-305 (k_{deg} = 0.0389 h^{-1}). This data suggested that the irreversible interaction between S-CKD602 and monocyte contribute more than the linear degradation to the elimination of S-CKD602, whereas, the irreversible binding of monocytes and IHL-305 contribute less than linear degradation to the elimination of IHL-305. This may be due to CPT-11 being less potent than CKD-602 and the toxicity of sequestered CPT-11 to monocytes may be less than other anticancer agents encapsulated in liposome such as CKD-602. In this case, the contribution of IHL-305 to the decrease of monocytes may be modest. In addition, the interaction between IHL-305 and monocytes may be likely reversible than irreversible for monocytes. Due to the limited data points, we were not able to fit the data using a reversible binding kinetics model. However, the bi-directional

interaction between PEGylated liposomal anticancer agents and monocytes plays a more important role in the PK and PD of S-CKD602.

In the mechanism-based model, the degradation of liposome through route other than uptake by monocytes (as represented by k_{deg}) was important in the mechanism-based model for S-CKD602 and IHL-305 data. We tested the model with and without k_{deg} and deletion of k_{deg} from the final mechanism-based model of S-CKD602 and IHL-305 resulted in an increase in AIC of 86 and 34, respectively. It is known that the primary accumulation sites of liposomes are liver and spleen. Therefore, liposomes may also be cleared by phagocytes in liver and spleen (40, 41). Therefore, the contribution of other routes is also very important to PK of S-CKD602.

The model predictions of PK data were comparable between the mechanism-based and myelosuppression-based model for both S-CKD602 and IHL-305. The observed PK data correlated better with the predicted data from the mechanism-based model than that from the myelosuppression-based model. This may suggest that incorporation of bi-directional interaction between PEGylated liposomal anticancer agents and monocytes in the model helped to explain the interindividual variability in the PK of S-CKD602 and IHL-305.

The mechanism-based and myelosuppression-based PK-PD models both described the observed PD data of monocytopenia relatively well. However, these two models predicted two different time courses of monocyte count change after administration of S-CKD602. The myelosuppression-based model predicted a day of nadir around the observed day of nadir whereas the mechanism-based model predicted an earlier nadir compared to the observed nadir. As no monocyte count was collected at the earlier time after administration of S-CKD602, the exact monocyte profile at earlier time points needs to be determined in

future studies. PD profile of monocytes reached nadir at 2 days after administration of liposomal alendonate in rats (42). The half-life of monocytes in rats is about 2 days, which is similar to the reported half-life of monocytes in human (38, 39). The PD profile of monocytopenia after administration of liposomal alendonate suggested that the day of monocyte nadir after administration of S-CKD602 may be earlier than the observed value (8.6 ± 3.3 days). Thus, cytotoxic effects in blood and in bone marrow may explain the decrease in monocytes after administration of PEGylated liposomal anticancer agents.

For S-CKD602, the individual predicted value of monocyte counts from myelosuppression-based model showed higher correlation with observed monocyte counts compared to mechanism-based model. For both S-CKD602 and IHL-305, the mechanism-based model overestimated monocyte count at lower monocyte count and underestimated monocyte count at higher monocyte count compared to myelosuppression-based model. This may be explained by the absence of feedback loop in the mechanism-based model. We tested the myelosuppression-based model without the feedback loop which produced a more serious overestimation monocyte count at lower monocyte count and underestimation of monocyte count at higher monocyte count than mechanism-based model (data not shown). The feedback loop was incorporated in myelosuppression-based model to describe leukocytopenia and neutropenia because it is known that the proliferation rate of progenitor cells can be affected by endogenous growth factors and cytokines and that circulating neutrophil counts and the growth factor G-CSF levels are inversely related (43-45). No feedback mechanism has been reported for monocytes. The better PD fit of myelosuppression-based model suggest that feedback loop may be applicable for monocytes.

However, the addition of feedback loop to the developed mechanism-based model did not improve the PD fits.

We also developed a mechanism-based population PK-PD model for PEGylated liposome membrane lipids based on the mechanism-based model for S-CKD602 and IHL-305. In this model we evaluated the bi-directional interaction between PEGylated liposome membrane lipids and monocytes. A pooled liposome membrane lipids and monocyte data of S-CKD602 and IHL-305 were used in this model development. We found that the inter-individual variability in the PK and PD of liposome membrane lipids can be explained in part by the encapsulated drug. The results suggested that S-CKD602 and IHL-305 have different interactions with monocytes. In addition, the bi-directional interaction between PEGylated liposomes and monocytes may be more important to the elimination of PEGylated liposome and decrease of monocyte after administration of S-CKD602. This may be due to CPT-11 being less potent than CKD-602 or due to the different liposomal formulations used in each product. Therefore, lipids in PEGylated liposomal anticancer agents alone may not account for all the toxicity of these agents to monocytes.

In summary, the PK of S-CKD602 and IHL-305 were evaluated by noncompartmental, individual-based and population-based compartmental PK analysis. The patients factors identified through these analyses may also help to explain inter-patient variability of other nanoparticle and conjugated anticancer agents. The descriptive population PK model of encapsulated drug and released drug for S-CKD602 and IHL-305 may be used as the base to develop a population PK model for other PEGylated liposomal anticancer agents. Comparison of this model and the myelosuppression-based model helped to explain PK and PD of PEGylated liposomal anticancer agents. The developed mechanism-based PK-

PD model may be useful in predicting the PK and PD and optimize dosing of pegylated liposomal agents to achieve a target exposure for each patient with malignant diseases. The mechanism-based model developed for S-CKD602 and IHL-305 could also be used to describe the bi-directional interaction between PK and monocytes for other nanoparticle and conjugated anticancer agents as a method to profile and classify these agents.

Future Direction

We found that age, body composition, gender, monocyte function, and tumor in liver were patient factors affecting the PK and PD of S-CKD602 and/or IHL-305. Among these factors, monocyte function and tumor in liver was the first time being identified as factors affecting PK of liposomal drugs. The clinical importance of these factors especially monocyte function and tumor in liver needs to be further investigated for S-CKD602, IHL-305 and other liposomal and nanoparticle anticancer agents.

Considering the potential myelosuppression effect of released anticancer drug, further developments to the mechanism-based model include incorporating the myelosuppression effect from released CKD-602. In addition, the PK and PD of PEGylated liposomal anticancer drugs are associated with high interpatient variability, including covariate effects in the mechanism-based model will increase the predicting potential in clinical situations and help to optimize treatment for individuals.

As this is the first model that incorporated the bi-direcitonal interaction between PEGylated liposomal anticancer drugs and monocyte, validation of the model structure with additional data will be desired so this model can be used for simulation of clinical trials. An external model evaluation will be necessary to show that this model allows reasonable extrapolation beyond the data used to develop the model. PK/PD data from a study of a novel

biweekly dosage regimen of IHL-305 (referred to as study 2) will be used as validation dataset.

Considering the nonlinear and high variability in the PK and PD of PEGylated liposomal anticancer agents, simulation based on a validated PK-PD model can predict PK/PD profiles of PEGylated liposomal anticancer agents under various dosage regimens and would be very useful in guiding the search for the optimal dose and regimen. We are specifically interested in comparing the differences between shorter, more intense schedules and longer, more fractionated schedules, administered the same dose intensity and how these issues change the PK and PD of liposomal agents.

REFERENCE

1. Wang J, Sui M, Fan W. Nanoparticles for tumor targeted therapies and their pharmacokinetics. Curr Drug Metab; 11:129-41.

2. Zamboni WC. Liposomal, nanoparticle, and conjugated formulations of anticancer agents. Clin Cancer Res 2005; 11:8230-4.

3. Zamboni WC. Concept and clinical evaluation of carrier-mediated anticancer agents. Oncologist 2008; 13:248-60.

4. Innocenti F, Kroetz DL, Schuetz E, et al. Comprehensive pharmacogenetic analysis of irinotecan neutropenia and pharmacokinetics. J Clin Oncol 2009; 27:2604-14.

5. Slatter JG, Schaaf LJ, Sams JP, et al. Pharmacokinetics, metabolism, and excretion of irinotecan (CPT-11) following I.V. infusion of [(14)C]CPT-11 in cancer patients. Drug Metab Dispos 2000; 28:423-33.

6. Zamboni WC, Strychor S, Maruca L, et al. Pharmacokinetic study of pegylated liposomal CKD-602 (S-CKD602) in patients with advanced malignancies. Clin Pharmacol Ther 2009; 86:519-26.

7. Papahadjopoulos D, Allen TM, Gabizon A, et al. Sterically stabilized liposomes: improvements in pharmacokinetics and antitumor therapeutic efficacy. Proc Natl Acad Sci U S A 1991; 88:11460-4.

8. Maeda H, Wu J, Sawa T, Matsumura Y, Hori K. Tumor vascular permeability and the EPR effect in macromolecular therapeutics: a review. J Control Release 2000; 65:271-84.

9. Zamboni WC, Strychor S, Maruca L, et al. Pharmacokinetic Study of Pegylated Liposomal CKD-602 (S-CKD602) in Patients With Advanced Malignancies. Clin Pharmacol Ther 2009.

10. Zamboni WC, Strychor S, Joseph E, et al. Plasma, tumor, and tissue disposition of STEALTH liposomal CKD-602 (S-CKD602) and nonliposomal CKD-602 in mice bearing A375 human melanoma xenografts. Clin Cancer Res 2007; 13:7217-23.

11. Poujol S, Bressolle F, Duffour J, et al. Pharmacokinetics and pharmacodynamics of irinotecan and its metabolites from plasma and saliva data in patients with metastatic digestive cancer receiving Folfiri regimen. Cancer Chemother Pharmacol 2006; 58:292-305.

12. Chabot GG, Abigerges D, Catimel G, et al. Population pharmacokinetics and pharmacodynamics of irinotecan (CPT-11) and active metabolite SN-38 during phase I trials. Ann Oncol 1995; 6:141-51.

13. de Jonge MJ, Verweij J, de Bruijn P, et al. Pharmacokinetic, metabolic, and pharmacodynamic profiles in a dose-escalating study of irinotecan and cisplatin. J Clin Oncol 2000; 18:195-203.

14. Lee DH, Kim SW, Bae KS, et al. A phase I and pharmacologic study of belotecan in combination with cisplatin in patients with previously untreated extensive-stage disease small cell lung cancer. Clin Cancer Res 2007; 13:6182-6.

15. Allen TM, Cullis PR. Drug delivery systems: entering the mainstream. Science 2004; 303:1818-22.

16. Gabizon A, Isacson R, Rosengarten O, Tzemach D, Shmeeda H, Sapir R. An open-label study to evaluate dose and cycle dependence of the pharmacokinetics of pegylated liposomal doxorubicin. Cancer Chemother Pharmacol 2008; 61:695-702.

17. Gabizon A, Shmeeda H, Barenholz Y. Pharmacokinetics of pegylated liposomal Doxorubicin: review of animal and human studies. Clin Pharmacokinet 2003; 42:419-36.

18. Gabizon A, Tzemach D, Mak L, Bronstein M, Horowitz AT. Dose dependency of pharmacokinetics and therapeutic efficacy of pegylated liposomal doxorubicin (DOXIL) in murine models. J Drug Target 2002; 10:539-48.

19. Takagi A, Matsuzaki T, Furuta T, al e. Antitumor activity of IHL-305, a novel pegylated liposome containing irinotecan, in human xenograft models. the 2007 American Association for Cancer Research–National Cancer Institute–European Organization for Research and Treatment of Cancer AACR-NCI-EORTC Conference; 2007 November 2007; San Francisco, CA; 2007.

20. Kurita A, Furuta T, Kaneda N, al. e. Pharmacokinetics of irinotecan and its metabolites after iv administration of IHL-305, a novel pegylated liposome containing irinotecan, to tumor-bearing mice. the 2007 American Association for Cancer Research–National Cancer Institute–European Organization for Research and Treatment of Cancer AACR-NCI-EORTC Conference; 2007 November 2007; San Francisco, CA; 2007.

21. Rothenberg ML, Kuhn JG, Burris HA, 3rd, et al. Phase I and pharmacokinetic trial of weekly CPT-11. J Clin Oncol 1993; 11:2194-204.

22. Rothenberg ML, Kuhn JG, Schaaf LJ, et al. Phase I dose-finding and pharmacokinetic trial of irinotecan (CPT-11) administered every two weeks. Ann Oncol 2001; 12:1631-41.

23. Zamboni WC, Ramalingam S, Friedland DM, et al. Phase I and pharmacokinetic study of pegylated liposomal CKD-602 in patients with advanced malignancies. Clin Cancer Res 2009; 15:1466-72.

24. Robieux I, Sorio R, Borsatti E, et al. Pharmacokinetics of vinorelbine in patients with liver metastases. Clin Pharmacol Ther 1996; 59:32-40.

25. Twelves CJ, O'Reilly SM, Coleman RE, Richards MA, Rubens RD. Weekly epirubicin for breast cancer with liver metastases and abnormal liver biochemistry. Br J Cancer 1989; 60:938-41.

26. Wilson WH, Berg SL, Bryant G, et al. Paclitaxel in doxorubicin-refractory or mitoxantrone-refractory breast cancer: a phase I/II trial of 96-hour infusion. J Clin Oncol 1994; 12:1621-9.

27. Heuff G, van der Ende MB, Boutkan H, et al. Macrophage populations in different stages of induced hepatic metastases in rats: an immunohistochemical analysis. Scand J Immunol 1993; 38:10-6.

28. Gulubova M, Manolova I, Cirovski G, Sivrev D. Recruitment of dendritic cells in human liver with metastases. Clin Exp Metastasis 2008; 25:777-85.

29. Zamboni WC, Maruca LJ, Strychor S, et al. Age and body composition related-effects on the pharmacokinetic disposition of STEALH liposomal CKD-602 (S-CKD602) in patients with advanced solid tumors. 2007; 2007.

30. Sidone BJ, Edwards RP, Zamboni BA, Strychor S, Maruca LJ, Zamboni WC. Evaluation of body surface area (BSA) based dosing, age, and body composition as factors affecting the pharmacokinetic (PK) variability of STEALTH liposomal doxorubicin (Doxil). AACR-NCI-EORTC; 2007; 2007.

31. De Martinis M, Modesti M, Ginaldi L. Phenotypic and functional changes of circulating monocytes and polymorphonuclear leucocytes from elderly persons. Immunol Cell Biol 2004; 82:415-20.

32. La-Beck NM, Wu H, Infante JR, et al. The evaluation of gender on the pharmacokinetics (PK) of pegylated liposomal anticancer agents. ASCO Annual Meeting; 2010; 2010. p. e13003.

33. Song G, Wu H, La-Beck N, Zamboni BA, Strychor S, Zamboni WC. Effect of Gender on Pharmacokinetic Disposition of Pegylated Liposomal CKD-602 (S-CKD602) and Optisomal Topotecan (TLI) in Rats. AACR 2009.

34. Zomorodi K, Gupta S. Population Pharmacokinetic Analysis of DOXIL in Adult Patients. AAPS; 1999; 1999.

35. Lee LN. Volume of Blood in A Human; 1998.

36. Zamboni WC, Maruca LJ, Strychor S, et al. Bi-Directional Pharmacodynamic Interaction between STEALTH Liposomal CKD-602 (S-CKD602) and Monocytes in Patients with Refractory Solid Tumors. Clin Cancer Res; Submitted.

37. Zamboni WC, Eiseman JE, Strychor S, et al. Relationship between the plasma and tumor disposition of STEALTH liposomal CKD-602 and macrophages/dendritic cells (MDC) in mice bearing human tumor xenografts. AACR; 2006; 2006. p. 5449.

38. Jain NC. Essentials of Veterinary Hematology. 1 ed: Williams & Wilkins, Media, PA 19063; 1993.

39. Whitelaw DM. Observations on human monocyte kinetics after pulse labeling. Cell Tissue Kinet 1972; 5:311-7.

40. Koning GA, Morselt HW, Kamps JA, Scherphof GL. Uptake and intracellular processing of PEG-liposomes and PEG-immunoliposomes by kupffer cells in vitro 1 *. J Liposome Res 2001; 11:195-209.

41. Van Rooijen N, Sanders A. Kupffer cell depletion by liposome-delivered drugs: comparative activity of intracellular clodronate, propamidine, and ethylenediaminetetraacetic acid. Hepatology 1996; 23:1239-43.

42. Haber E, Afergan E, Epstein H, et al. Route of administration-dependent anti-inflammatory effect of liposomal alendronate. J Control Release.

43. Friberg LE, Henningsson A, Maas H, Nguyen L, Karlsson MO. Model of chemotherapy-induced myelosuppression with parameter consistency across drugs. J Clin Oncol 2002; 20:4713-21.

44. Takatani H, Soda H, Fukuda M, et al. Levels of recombinant human granulocyte colony-stimulating factor in serum are inversely correlated with circulating neutrophil counts. Antimicrob Agents Chemother 1996; 40:988-91.

45. Hoffbrand AV, Lewis SM, Tuddenham E. Postgraduate Haematology. 4 ed: Oxford, United Kingdom, Butterworth-Heinemann; 1999.